

Geometric modeling of heterogeneous cellular structures with functionally graded parameters

Nikita Letov
(Никита Николаевич Летов)



Department of Mechanical Engineering
McGill University
Montréal, Québec, Canada

November 2023

PIGRAPH

Highly organized research is guaranteed to produce nothing new.

— Frank Herbert (1920 – 1986), DUNE

ACKNOWLEDGEMENTS

First and foremost, I would like to express my deepest gratitude to my supervisor, Professor Yaoyao Fiona Zhao, for her unwavering support, guidance, and encouragement throughout my Ph.D. journey. Her expertise and insights have been invaluable to the success of this research.

I deeply appreciate everyone at Axya Inc. and Mitacs for allowing me to grow professionally and enhance my research skills. Their support has played a significant role in my academic journey, and I am grateful for their trust in my abilities. You are amazing and I am glad I was able to be a part of your success just as you were able to be a part of mine.

I am grateful for the opportunity to work alongside the talented and dedicated Additive Design and Manufacturing Lab members. My heartfelt thanks go to Bogdan Bogachov, Josh Campbell, Yuzheng Chen, Yuzheng Chen, Guoying Dong, Randy El Haddad, Zhenyang Gao, Xiaoyi Guan, Samuel Iyengar, Lingchen Kong, Jinghao Li, Yi Fan Li, Yuan Liu, Zhibo Luo, Wenbo Min, Negin Moslemi, Thomas Page, Shubham Bacharam Raut, Arnaud Ridard, Andrei Mircea Romascanu, Mutahar Safdar, Manuel Sage, Shivangi Sarabhai, Siyuan Sun, Yunlong Tang, Pavan Tejaswi Velivela, Jiarui Xie, Sheng Yang, Chonghui Zhang, and Ying Zhang. I have not only learned a great deal from working with you all but have also enjoyed the camaraderie and fun times we have shared, including the memorable moments spent together outside the lab. Indeed, there have been difficulties on our path that would not be possible to overcome without occasional releases.

I would like to extend special thanks to my childhood friend Artyom Smirnov, who has been a source of inspiration and support throughout my life. Our bond has endured the passage of time, and I am grateful for your unwavering friendship.

My heartfelt appreciation goes to my dear friends in Russia, who have been a constant

source of support and encouragement with their goofs and gaffs throughout my journey. Your friendship means the world to me, even from afar on the other side of this crazy world we live in, and I eagerly look forward to the day when we can reunite. Special thanks to my friends with whom we went through our undergraduate years at Bauman Moscow State Technical University: Alexey Atanov, Sergey Chausov, Zakhar Dmitriev, Kirill Dobrynin, Artem Elin, Sergey Koltunov, Oleg Naumov, Georgy Plischenko, Andrey Semyonkin, and Kim Tregubov. Thank you all for keeping me sane with your insanity.

Thank you to the friends I made at the Skolkovo Institute of Science and Technology: Alexey Boyko, Dmitry Ermachenkov, Alexander Morozov, Andrey Sartison, Oleg Sudakov, and many others. You are all brilliant, and it has been eternally enjoyable for me to spend time with you. I also extend deep gratitude to Professor Clemént Fortin, my Master's thesis supervisor, for laying the foundational stones of research rigor and passion that guided me through this Ph.D. journey.

I express my heartfelt appreciation for my beloved feline companions, Antonina and Valentina. Their comforting cuddles, not without occasional bites and scratches, have brought immeasurable joy and stress relief to my life during my time as a graduate student.

I thank my parents for their unwavering support and encouragement throughout this journey. You have always been there for me, and I am deeply grateful for your love and understanding.

Finally, I would like to express my boundless love and appreciation to my enchanting Anastasia, who has illuminated even the darkest moments of this journey with her radiant presence. Your unwavering love, compassion, and support have filled my heart with courage and inspiration. I am forever grateful.

Thank you all for being a part of my journey. Merci à tous d'avoir fait partie de mon voyage. Спасибо вам всем за то, что были частью моего пути.

STATEMENT OF ORIGINALITY

This thesis, composed of six chapters, includes an introduction, a literature review, a proposed geometric modeling approach, its implementation, case studies, and a conclusion. It is written within the Additive Design and Manufacturing Lab (ADML)¹ at McGill University's Faculty of Engineering. The author claims the originality of the main ideas and research results reported in this thesis. The major contributions of this thesis are:

- **Lattice-function representation (LF-rep):** An extension of the function representation (F-rep) method, formulated specifically for the advanced geometric modeling of cellular structures. This new approach derives from a critical review of the existing research and identifies the gaps and potential directions in the realm of cellular structure modeling.
- **Skeletal graphs independence:** An innovative methodology where skeletal graphs are delineated distinctly from other geometric parameters. This separation enhances modeling adaptability, ensuring a dynamic and flexible design process.
- **Parameter customization:** Moving beyond the traditional emphasis on thickness parametrization, the introduction of modifiable cross-section shapes and truncation increases the flexibility of cellular structure design. This development amplifies the potential of cellular structures by enhancing customization and adaptability.
- **Versatile application:** Whether the need is for stochastic, conformal, or multi-topology structures, the applicability of LF-rep remains. A suite of case studies further underscores its efficacy, validating the theoretical background of the method and illuminating its transformative potential across various engineering domains, including

¹<https://adml.lab.mcgill.ca>

the design and optimization of gas turbines.

This thesis and its related published manuscripts were conducted as part of a Ph.D. study under the supervision of Prof. Yaoyao Fiona Zhao of ADML. The literature review presented in Chapter 2 was conducted in collaboration with Yuan Li, Guolei Zheng, Pavan Tejaswi Velivela, and Siyuan Sun. The case studies in Chapter 5 were performed in collaboration with Pavan Tejaswi Velivela, Shivangi Sarabhai, and Lingchen Kong of ADML, as well as Mitch Kibsey and Fabian Sanchez from Siemens Energy Canada Limited. The following works related to this thesis have been published:

1. Letov, N., and Y. F. Zhao, 2021: Volumetric cells: A framework for a bio-inspired geometric modelling method to support heterogeneous lattice structures. *Proceedings of the Design Society: DESIGN Conference*, Dubrovnik, Croatia, Cambridge University Press, Vol. 1, 295–304, doi:[10.1017/dsd.2020.164](https://doi.org/10.1017/dsd.2020.164).
2. Liu, Y., G. Zheng, N. Letov, and Y. F. Zhao, 2021: A survey of modeling and optimization methods for multi-scale heterogeneous lattice structures. *Journal of Mechanical Design*, **143** (4), 040 803, doi:[10.1115/1.4047917](https://doi.org/10.1115/1.4047917).
3. Letov, N., P. T. Velivela, S. Sun, and Y. F. Zhao, 2021: Challenges and opportunities in geometric modeling of complex bio-inspired three-dimensional objects designed for additive manufacturing. *Journal of Mechanical Design*, **143** (12), 121 705, doi:[10.1115/1.4051720](https://doi.org/10.1115/1.4051720).
4. Velivela, P. T., N. Letov, Y. Liu, and Y. F. Zhao, 2021: Application of Domain Integrated Design methodology for bio-inspired design-a case study of suture pin design. *Proceedings of the Design Society: DESIGN Conference*, Dubrovnik, Croatia, Cambridge University Press, Vol. 1, 487–496, doi:[10.1017/pds.2021.49](https://doi.org/10.1017/pds.2021.49).

-
5. Letov, N., and Y. F. Zhao, 2022: A geometric modelling framework to support the design of heterogeneous lattice structures with non-linearly varying geometry. *Journal of Computational Design and Engineering*, **9** (5), 1565–1584, doi:[10.1093/jcde/qwac076](https://doi.org/10.1093/jcde/qwac076).
 6. Letov, N., 2022: jalovisko/LatticeQuery: (0.1LQ). Zenodo, [Repository], doi:[10.5281/zenodo.6959068](https://doi.org/10.5281/zenodo.6959068).
 7. Gao, Z., H. Wang, N. Letov, Y. F. Zhao, X. Zhang, Y. Wu, C. L. A. Leung, and H. Wang, 2023: Data-driven design of biometric composite metamaterials with extremely recoverable and ultrahigh specific energy absorption. *Composites Part B: Engineering*, **251**, 110 468, doi:[10.1016/j.compositesb.2022.110468](https://doi.org/10.1016/j.compositesb.2022.110468)
 8. Sarabhai, S., N. Letov, M. Kibsey, F. Sanchez, and Y. F. Zhao, 2023: Understanding the flow and thermal characteristics of non-stochastic strut-based and surface-based lattice structures. *Materials & Design*, **227**, 111 787, doi:[10.1016/j.matdes.2023.111787](https://doi.org/10.1016/j.matdes.2023.111787).
 9. Letov, N., and Y. F. Zhao, 2023: Beam-based lattice topology transition with function representation. *Journal of Mechanical Design*, **145** (1), 011 704, doi:[10.1115/1.4055950](https://doi.org/10.1115/1.4055950).
 10. Letov, N., and Y. F. Zhao, 2023: Geometric modelling of heterogeneous lattice structures through function representation with LatticeQuery. *Proceedings of the Design Society: International Conference on Engineering Design (ICED23)*, Bordeaux, France, Cambridge University Press, Vol. 3, 2045-2054, doi:[10.1017/pds.2023.205](https://doi.org/10.1017/pds.2023.205).
 11. Velivila, P. T., N. Letov, L. Kong, and Y. F. Zhao, 2023: A case study of multifunctional non-pneumatic tire design for the validation of meta-level design parameter in

Domain Integrated Design (DID) method. *Proceedings of the Design Society: International Conference on Engineering Design (ICED23)*, Bordeaux, France, Cambridge University Press, Vol. 3, 39-48, doi:[10.1017/pds.2023.5](https://doi.org/10.1017/pds.2023.5).

ABSTRACT

Geometric modeling has been an essential component of the design process since the advent of computer-aided design (CAD) systems. It plays a crucial role in computer-aided engineering (CAE) and topology optimization which rely on efficient and versatile modeling techniques. In recent years, additive manufacturing (AM) has emerged as a groundbreaking technology, offering unprecedented design freedom by enabling the creation of complex cellular structures that are challenging to produce using conventional methods. Cellular structures have significant potential for lightweight, high-strength, and customizable products across various industries, including aerospace, automotive, and biomedical.

However, the geometric modeling of heterogeneous cellular structures remains substantially limited, resulting in a situation where manufacturing capabilities outpace geometric modeling capabilities. This disparity hinders the full realization of the potential of AM technology. Although there have been advancements in modeling heterogeneous cellular structures, a review of the relevant literature revealed critical limitations of the existing approaches, including their inability to model non-linear variations, a restricted number of controllable geometric parameters, and the exclusive focus on thickness parametrization.

Moreover, the underdevelopment of free and open-source software (FOSS) for engineering, particularly in the AM domain, has further constrained the widespread adoption and exploration of novel methodologies. This gap in accessible software tools limits the growth and innovation of the field, reducing the potential benefits of AM technologies.

This work presents a novel geometric modeling methodology based on function representation (F-rep) principles, termed as lattice-function representation (LF-rep), to address these limitations and bridge the gap between manufacturing and modeling capabilities. The proposed approach goes beyond typical cellular structure thickness parametrization,

enabling the control of a broader range of geometric parameters through mathematical functions. This offers higher precision and customization in creating complex cellular structures that can be conformal, stochastic, or exhibit multiple topologies.

Furthermore, the proposed approach supports a more extensive range of heterogeneous features than other existing solutions, making it suitable for various applications across different industries. To validate the effectiveness and feasibility of the proposed methodology and address the lack of FOSS tools, a free and open-source software prototype implementing the approach has been developed. Using the proposed F-rep method, this prototype empowers users to generate and manipulate heterogeneous cellular structures.

Several use cases are analyzed to demonstrate the applicability and benefits of the proposed approach in different scenarios, including lightweight structural components, energy-absorbing materials, and biomedical implants. These use cases underscore the potential of the presented methodology to revolutionize the design and manufacturing processes for cellular structures, fostering new possibilities in the AM industry and promoting the growth of FOSS tools for engineering.

RÉSUMÉ

La modélisation géométrique est un élément essentiel du processus de conception depuis l'apparition des systèmes de conception assistée par ordinateur (CAO). Elle joue un rôle crucial dans l'ingénierie assistée par ordinateur (IAO) et l'optimisation topologique qui reposent sur des techniques de modélisation efficaces et polyvalentes. Ces dernières années, la fabrication additive (AM) a émergé comme une technologie révolutionnaire, offrant une liberté de conception sans précédent en permettant la création de structures cellulaires complexes qui seraient difficiles à produire avec des méthodes conventionnelles. Les structures cellulaires présentent un potentiel important pour des produits légers, résistants et personnalisables dans diverses industries, notamment l'aérospatial, l'automobile et le biomédical.

Cependant, la modélisation géométrique des structures cellulaires hétérogènes reste considérablement limitée, ce qui entraîne une situation où les capacités de fabrication dépassent les capacités de modélisation géométrique. Ce déséquilibre entrave la pleine réalisation du potentiel de la technologie AM. Bien qu'il y ait eu des progrès dans la modélisation des structures cellulaires hétérogènes, une revue de la littérature pertinente a révélé des limites critiques des approches existantes, notamment leur incapacité à modéliser les variations non linéaires, un nombre restreint de paramètres géométriques contrôlables et une attention exclusive portée à la paramétrisation de l'épaisseur.

De plus, le sous-développement des logiciels libres et open source (FOSS) pour l'ingénierie, en particulier dans le domaine de l'AM, a encore limité l'adoption généralisée et l'exploration de nouvelles méthodologies. Cette lacune dans les outils logiciels accessibles limite la croissance et l'innovation du domaine, réduisant les avantages potentiels des technologies AM.

Ce travail présente une nouvelle méthodologie de modélisation géométrique basée sur la représentation fonctionnelle (F-rep) pour surmonter ces limitations et combler l'écart entre

les capacités de fabrication et de modélisation. L'approche proposée, nommée comme la représentation de fonction de réseau (LF-rep), va au-delà de la paramétrisation d'épaisseur typique des structures cellulaires, permettant le contrôle d'une gamme plus large de paramètres géométriques grâce à des fonctions mathématiques. Cela offre une précision et une personnalisation accrues dans la création de structures cellulaires complexes pouvant être conformes, stochastiques ou présenter plusieurs topologies.

En outre, l'approche proposée prend en charge un éventail plus large de caractéristiques hétérogènes que les autres solutions existantes, la rendant adaptée à diverses applications dans différentes industries. Pour valider l'efficacité et la faisabilité de la méthodologie proposée et pallier le manque d'outils FOSS, un prototype de logiciel libre et open source mettant en œuvre l'approche a été développé. En utilisant la méthode F-rep proposée, ce prototype permet aux utilisateurs de générer et de manipuler des structures cellulaires hétérogènes.

Plusieurs cas d'utilisation sont analysés pour démontrer l'applicabilité et les avantages de l'approche proposée dans différents scénarios, y compris les composants structuraux légers, les matériaux absorbant l'énergie et les implants biomédicaux. Ces cas d'utilisation soulignent le potentiel de la méthodologie présentée pour révolutionner les processus de conception et de fabrication des structures cellulaires, favorisant de nouvelles possibilités dans l'industrie de l'AM et promouvant la croissance des outils FOSS pour l'ingénierie.

Contents

1	Introduction	1
1.1	Background	1
1.1.1	A brief history of cellular structures in engineering applications	2
1.1.2	Additive manufacturing capabilities for cellular structures	8
1.1.3	Geometric modeling of cellular structures	12
1.2	Dissertation outline	16
2	Literature review	20
2.1	Current status of geometric modeling	21
2.1.1	Surface modeling	22
2.1.2	Volumetric modeling	30
2.1.3	Hybrid modeling	37
2.1.4	Function representation concepts and their application in geometric modeling of cellular structures	38
2.1.5	Multi-scale modeling	42
2.2	Challenges in geometric modeling of complex structures	44
2.3	Challenges in the geometric modeling of heterogeneous cellular structures	46
2.3.1	Challenges associated with surface modeling to model heterogeneous cellular structures	53

2.3.2	Challenges associated with volumetric modeling to model heterogeneous cellular structures	55
2.3.3	Challenges associated with hybrid modeling to model heterogeneous cellular structures	56
2.4	Existing software tools for the geometric modeling of cellular structures	57
2.4.1	Surface modeling-based software tools	58
2.4.2	Volumetric modeling-based software tools	60
2.4.3	Hybrid modeling-based software tools	61
2.4.4	Comparison of tools for cellular structure modeling	63
2.4.5	Graphical user interface of software packages for the geometric modeling of cellular structures	65
2.5	Research objectives	65
3	Proposed geometric modeling framework	68
3.1	Functional definition of cellular topologies	72
3.1.1	Beam-based topologies	72
3.1.2	Surface-based topologies	76
3.2	Functional variation of geometric parameters	78
3.3	Cellular structures with multiple topologies	85
3.3.1	Beam-based cellular structures with multiple topologies	87
3.3.2	Surface-based cellular structures with multiple topologies	94
3.4	Stochastic cellular structures	96
3.5	Conformal cellular structures	99
3.5.1	Surface conformality	100
3.5.2	Volume conformality	102

4 Implementation	104
4.1 Functional definition of cellular topologies	107
4.1.1 Beam-based topologies	107
4.1.2 Surface-based topologies	109
4.2 Functional variation of geometric parameters	111
4.3 Cellular structures with multiple topologies	117
4.3.1 Beam-based cellular structures with multiple topologies	117
4.3.2 Surface-based cellular structures with multiple topologies	121
4.4 Stochastic cellular structure	122
4.5 Conformal cellular structures	124
4.5.1 Surface conformality	126
4.5.2 Volume conformality	127
4.6 LatticeQuery – the implemented FOSS tool	129
4.6.1 Architecture	129
4.6.2 Usage	131
4.7 Computational performance	133
4.8 Implementation summary	137
5 Case studies	138
5.1 Geometric modeling of cellular structures to estimate their flow and thermal characteristics	139
5.1.1 Geometric, flow, and thermal properties of cellular structures	140
5.1.2 Existing experimental results	142
5.1.3 Methods	143
5.1.4 Results	145

5.2	Multifunctional non-pneumatic tire design	149
5.2.1	Ideation and conceptual design	149
5.2.2	Results	152
5.3	Printed cellular structures modeled with the proposed approach	154
6	Conclusion and future directions	157
Bibliography	160
Appendices	190
Appendix A	Case study of a bio-inspired geometric modeling framework	191

List of Figures

1.1	(a) Branches of a conifer tree and (b) the roof of the Kiyomizu-dera temple in Kyoto, Japan follow the pattern of (c) the brachistochrone curve – an optimal curve of fastest descent – to prevent rainfall water from staying on them (Letov et al., 2021)	3
1.2	(a) The intricate skeleton of glass sponge of the Venus' flower basket (<i>Euplectella aspergillum</i>), (b) the Eiffel Tower in Paris (Jones et al., 2009), (c) bio-inspired structure and honeycomb structures, and (d) the compression versus displacement curves for three bio-inspired structures (Li et al., 2020b).	4
1.3	(a) A honeycomb structure (Thane, 2007) and (b) the cross-sectional view of a composite rotor blade (Garinis et al., 2012)	6
1.4	(a) Lightweight plates used in automotive industry (Rosenthal et al., 2019), (b) a wrench with a Voronoi-Monte Carlo structure for enhanced energy absorption (Liu et al., 2019), and (c) a pelvic implant for bone ingrowth (Park et al., 2022a)	7
1.5	Classification chart for cellular structures designs (McGregor et al., 2021)	8
1.6	Various ways to parametrize heterogeneous cellular structures	9
1.7	Additive manufacturing processes. Adapted from Wong and Hernandez (2012).	10

1.8 Examples of cellular structures that can be printed with AM: (a) a Voronoi topology, (b) a body-centered cubic (BCC) topology, and (c) a metal-printed simple cubic topology (Letov and Zhao, 2022)	11
1.9 A printed example of a heterogeneous cellular structure with multiple topologies and a varying beam thickness (Leonardi et al., 2019)	12
1.10 Committed lifecycle cost versus time (Hamelin et al., 2010)	13
2.1 Two closed two-manifolds: (a) an oriented two-manifold of genus $g = 1$ (torus) $\mathbb{T} = M_1^2$ and (b) a non-oriented two-manifold of genus $g = 2$ (Klein's bottle) N_2^2 (Hatcher, 2001)	23
2.2 Model complexity in regions with high curvature affects the computation of rendering of a surface mesh (Chen and Bishop, 1997)	24
2.3 A mesh convergence study used to find an optimal number of elements sufficient to estimate values of a parameter – friction factor in this case (Sarabhai et al., 2023)	25
2.4 An example of a single triangular mesh element in STL format (Letov et al., 2021)	26
2.5 A mesh of non-convex geometry (Letov et al., 2021)	33
2.6 A torus is constructed using five solids of revolution in volumetric representation modeling (Wassermann et al., 2020)	34
2.7 (a) A transformation \mathcal{N} of a cubic finite element to a new shape and (b) the geometric modeling of a structure with different stages of refinement with iso-geometric finite elements (Burkhart et al., 2010)	35
2.8 Triangular mesh and voxel methods for representing original geometry representations. Adapted from (Schnös et al., 2021).	37

2.9	A homogeneous cellular structure with the simple cubic topology generated with HyperFun (Letov and Zhao, 2022)	41
2.10	(a) A code snippet of a HyperFun program that generates a gyroid surface and (b) the resulting model (Letov et al., 2021)	42
2.11	Reducing the complexity of a 3D model by adjusting its level of detail, which directly corresponds to the number of polygons required for rendering (Luebke et al., 2003)	43
2.12	Levels of detail associated with Boolean operations in feature-based CAD (Borrmann et al., 2015)	43
2.13	(a) The Young's modulus–density and (b) the strength–density chart for engineering materials, including woods (Gibson, 2012)	45
2.14	The conceptual sketch of a gecko-inspired surface that sticks to the implant surface (Velivila, 2018)	47
2.15	Two conceptual designs inspired by an ant's claw (Velivila, 2018)	48
2.16	Skin texture (Li et al., 2022a)	50
2.17	Two scutoids (a) shown transparent separately and (b) shown opaque and transitioning one into another (Gómez-Gálvez et al., 2018)	51
2.18	Tire designs with different lattice topologies, which include (a) bare design space, (b) grid lattice, (c) X lattice, and (d) vintiles lattice modeled with Intralattice (Kurtz, 2009)	59
3.1	The sequential mapping of the function T that defines the topology and the function P that defines the geometric parameters of a heterogeneous cellular structure (Letov and Zhao, 2022)	70
3.2	A BCC unit cell described by Equation 3.6 (Letov and Zhao, 2022)	74

3.3 An FCC unit cell described by Equation 3.10. The thicker lines correspond to the beams located in the visible faces of the arbitrary cube with the side u . The edges of the arbitrary cube are represented as dotted lines. The nodes are represented as circles (Letov and Zhao, 2023a)	75
3.4 Various beam-based topologies inspired by the cubic crystal system supported by the developed approach: (a) simple cubic, (b) BCC, (c) FCC, (d) S-FCC, (e) BCCz, (f) FCCz, (g) S-FCCz, (h) FBCC, (i) S-FBCC, and (j) S-FBCCz (Letov and Zhao, 2022)	78
3.5 Additional beam-based topologies supported by the developed approach: (a) diamond, (b) rhombicuboctahedron, and (c) truncated cube (Letov and Zhao, 2022)	82
3.6 A gyroid surface described by Equation 3.12 (Letov and Zhao, 2022) . . .	83
3.7 Various TPMS-based topologies supported by the developed approach: (a) gyroid, (b) Schwarz P surface, and (c) Schwarz D surface (Letov and Zhao, 2022)	84
3.8 (a) A side view on a single column of a heterogeneous cellular structure with Schwarz P topology with linearly varying thickness in the z -direction, and (b) the linear function P that corresponds to the thickness of the TPMS-based structure vs. the z coordinate (Letov and Zhao, 2022)	85
3.9 An example of a cellular structure with multiple topologies that are inspired by topology optimization (Liu et al., 2020b)	86
3.10 A schematic of a cellular structure with multiple topologies (Liu et al., 2020a)	88
3.11 A diagram of two topologies transitioning in a plane (Letov and Zhao, 2023a)	91
3.12 A skeletal graph of the truncated cube topology with the unit cell size u and the truncation τ (Letov and Zhao, 2023a)	93

3.13	The transition region $T_{1\#2}$ in the gap δ between topologies T_1 and T_2	95
3.14	Voronoi cellular structures with various α which defines the ratio between the maximal and minimal beam thicknesses (Do et al., 2021)	97
3.15	The edge $\epsilon_{i,j}$ between vertices w_i and w_j of a graph Γ	98
3.16	A transformation of the design space $\mathcal{N} : \mathbf{X} = (x, y, z) \rightarrow \mathbf{X}_\Phi = (\xi, \zeta, \eta)$ where \mathbf{X}_Φ is Cartesian with respect to the surface Φ . The skeletal graph of the cellular structure is used to maintain the topology while achieving surface conformality. Φ is considered the middle surface of the cellular structure that infills the volume with the thickness h .	101
3.17	(a) A trimmed cellular structure based on the skeletal graph, (b) the cellular structure with a net-skin, and (c) the net-skin (Aremu et al., 2017)	103
4.1	(a) An isometric view on a heterogeneous cellular structure with Schwarz P topology with linearly varying thickness generated with the proposed approach, (b) a side view on its single column in the z -direction, and (c) the linear function P that corresponds to the thickness of the TPMS-based structure vs. the z coordinate (Letov and Zhao, 2022)	113
4.2	(a) An isometric view on a heterogeneous cellular structure with BCC topology with non-linearly varying thickness generated with the proposed approach, (b) a side view on its single column in the x -direction, and (c) the parabolic function P that corresponds to the thickness of the TPMS-based structure vs. the x coordinate (Letov and Zhao, 2022)	114

4.3 (a) An isometric view on a heterogeneous cellular structure with Schwarz P topology with non-linearly varying thickness generated with the proposed approach, (b) a side view on its single column in the z -direction, and (c) the sine function P that corresponds to the thickness of the TPMS-based structure vs. the z coordinate (Letov and Zhao, 2022)	115
4.4 A heterogeneous cellular structure with the FCC topology with varying thickness and beam cross-section (Letov and Zhao, 2022)	116
4.5 Cross-sections of a beam in shapes of (a) a square with rounded corners and (b) a circle (Letov and Zhao, 2022)	117
4.6 The transition between the FCC topology with the cubic unit cell to the BCC topology with the cuboid unit cell along the transition plane \mathcal{P} . Note that the BCC topology is rotated 45° (Letov and Zhao, 2023a)	119
4.7 A heterogeneous cellular structure with the topology based on a truncated cube with the truncation parameter τ varying along the z -axis. The topology converges to the simple cubic at the bottom, and the cuboctahedron topology shifted to half of the unit cell size at the top. The thickness of the beams is linearly varying along the x -axis (Letov and Zhao, 2023a)	120
4.8 A heterogeneous cellular structure with the topology based on a rhombicuboctahedron with the truncation parameter τ varying along the z -axis. The topology converges to the simple cubic at the bottom and the octahedron topology at the top. The thickness of the beams is linearly varying along the x -axis (Letov and Zhao, 2023a)	122
4.9 A wireframe transition between skeletal graphs of a gyroid and a Schwarz P topologies	123

4.10	Surface-based cellular structure transition between the gyroid and Schwarz P topologies. The thickness of the structure varies vertically	124
4.11	A stochastic Voronoi infill of a human femur bone	125
4.12	Stochastic Voronoi structures that conform to random polyhedrons	125
4.13	A cellular structure with varying thickness conforming to a surface	127
4.14	(a) An isometric and (b) a profile view on a conformal heterogeneous cellular tire design modeled with the beam thickness increase further away from the wheel axle (Letov and Zhao, 2022)	129
4.15	The high-level software architecture of the LatticeQuery library (Letov and Zhao, 2023b)	130
4.16	The low-level software architecture of the LatticeQuery library (Letov and Zhao, 2023b)	131
4.17	The main window of the software prototype that embeds LatticeQuery (Letov and Zhao, 2023b)	131
4.18	A use-case showing the cellular structure transition with the proposed approach: (a)The orientation of topologies for the manufacturability performance test and (b) the resulting print with a zoomed-in view on the topology transition region. In the zoomed-in view, the transition planes are marked with dotted lines, and the instances of the FCC and BCC unit cells are marked with dashed lines (Letov and Zhao, 2023a).	136
5.1	The statistics on the use of different topologies in the literature (Sarabhai et al., 2023)	143
5.2	The simulation setting and planes chosen for sensitivity analysis (Sarabhai et al., 2023)	145

5.3	A_L/V_S ratio vs. \varnothing_{AP} of strut-based and surface-based cellular structures (Sarabhai et al., 2023)	146
5.4	Dependency of the heat transfer variation $Q/\Delta T$ on the available surface area per unit total volume A_L/V_S for (a) $Re = 1.8 \cdot 10^3$, (b) $Re = 30.0 \cdot 10^3$, and (c) $Re = 292.0 \cdot 10^3$ (Sarabhai et al., 2023)	147
5.5	A flow and thermal property chart illustrating the distribution of the heat transfer coefficient h and the friction factor ratio f/f_0 for various Reynolds numbers, topologies, and thicknesses (Sarabhai et al., 2023)	148
5.6	The initial conceptual designs that were produced in the ideation process (Velivela et al., 2023)	150
5.7	A single column is split into three regions with different porosities (Velivela et al., 2023)	151
5.8	The simulation results show the magnitude of elongation for (a) the woodpecker- and (b) the pomelo-inspired tire designs (Velivela et al., 2023)	153
5.9	Diverse cellular structures created using the proposed approach: (a) Rotated FCC topology in Ti-6Al-4V alloy, (b) Gyroid cellular structure, (c) Heterogeneous tire concept with simple cubic topology and increasing thickness towards the outer edge, and (d) Cellular structure with varying thickness conforming to a surface. All structures except (a) are printed with Formlabs BioMed Amber Resin (Formlabs Inc., 2020a) using the Formlabs Form 2 (Formlabs Inc., 2018) SLA 3D printer.	155
A.1	Representation of the geometrical model \mathbb{S}	193
A.2	The long axis rule observed in cell division process of the embryos of sea urchin (<i>Echinoidea</i>) (Minc et al., 2011)	194

A.3	The flowchart of the combined bio-inspired algorithm for geometric modeling (Letov and Zhao, 2021)	196
A.4	(a) LAR, (b) the S/V ratio minimization, (c) the combined method, and (d) the modified combined algorithms applied as discretization methods to a circular cross-section for $k_{\max} = 4$ iterations. Long axes are shown as dotted lines (Letov and Zhao, 2021).	197
A.5	(a) LAR, (b) the S/V ratio minimization, (c) the combined method, and (d) the modified combined algorithms applied as discretization methods to a square cross-section with a circular hole in its middle for $k_{\max} = 4$ iterations. Long axes are shown as dotted lines (Letov and Zhao, 2021).	198
A.6	A heterogeneous lattice structure with the graded beam thickness modeled with volumetric cells	199

List of Tables

2.1	Comparison of features and capabilities of cellular structure modeling tools	64
3.1	Various beam-based topologies inspired by the cubic crystal system supported by the developed approach.	77
3.2	The diamond topology supported by the developed approach.	79
3.3	Rhombicuboctahedron topology supported by the developed approach.	80
3.4	Truncated cube topology supported by the developed approach.	81
3.5	Various TPMS-based topologies supported by the developed approach.	82
4.1	The performance metrics of the modeling with the proposed approach.	134
A.1	Performance metrics comparing the voxel, Rhinoceros 3D, and volumetric cell models.	200

List of Acronyms

2D	two-dimensional
3D	three-dimensional
ADML	Additive Design and Manufacturing Lab
AM	additive manufacturing
ASCII	American Standard Code for Information Interchange
B-rep	boundary representation
B-spline	boundary spline
BCC	body-centered cubic
BCCz	body-centered cubic with additional four z -direction oriented beam
CAD	computer-aided design
CAE	computer-aided engineering
CAM	computer-aided manufacturing
CFD	computational fluid dynamics
CPU	central processing unit
CSG	constructive solid geometry

DFMA	design for additive manufacturing
DID	Domain Integrated Design
EBM	electron beam melting
F-rep	function representation
FBCC	face- and body-centered cubic
FCC	face-centered cubic
FCCz	FCC with additional four z -direction oriented beams
FCN	fully convolutional network
FDM	fused deposition modeling
FEA	finite element analysis
FEM	finite element modeling
FOSS	free and open-source software
FPS	frames-per-second
FVM	finite volume method
GMK	geometric modelling kernel
GPU	graphical processing unit
GUI	graphical user interface
IGA	isogeometric analysis
IGES	Initial Graphics Exchange Specification
LAR	long axis rule
LENS	laminated engineered net shaping
LF-rep	lattice-function representation
LOD	level of detail

LSM	level-set method
MBD	model-based definition
MBSE	model-based systems engineering
MDI	multi-document interface
MVP	minimal viable product
NURBS	non-uniform rational basis spline
OCCT	Open Cascade Technology
OOP	object-oriented programming
OS	operating system
PC	personal computer
RAM	random-access memory
RBF	radial basis function
S-FBCC	self-supporting face- and body-centered cubic without horizontal beam
S-FBCCz	self-supporting face- and body-centered cubic without horizontal beam with additional four z -direction oriented beams
S-FCC	self-supporting face-centered cubic without horizontal beam
S-FCCz	self-supporting face-centered cubic without horizontal beam with additional four z -direction oriented beams
Schwarz D	Schwarz ‘diamond’
Schwarz P	Schwarz ‘primitive’

SLS	selective laser sintering
SSD	solid-state drive
SST	shear stress transport
STEP	Standard for the Exchange of Product
STL	stereolithography
TPMS	triply periodic minimal surface
V-rep	volumetric representation

List of Symbols

The following is a list of the most important symbols used in the thesis. Where relevant, boldface is used to denote vectors or matrices. Their measuring units follow the description of some of the symbols in the International System of Units in square brackets where applicable.

Symbols

\emptyset_{AP}	apparent porosity [-]
Γ	skeletal graph of a cellular structure
Δ	cross-section shape function
ΔP	pressure loss [Pa]
ΔT	temperature difference between the solid surface and the surrounding fluid [K]
ϵ_{ij}	edge between vertices w_i and w_j
ρ	density [kg/m ³]
ρ'	relative density [-]
ρ_f	fluid density [kg/m ³]
σ	perpendicular surface

τ	truncation in topologies [m]
ϕ	porosity [%]
B	Bézier curve
$C(t)$	trimming curve of a surface
c	centroid
d	hydraulic diameter [m]
$F(\mathbf{X})$	function that defines the shape of a solid body in function representation
f	friction factor [-]
g	genus of a manifold
h	heat transfer coefficient [$\text{W}/(\text{m}^2 \text{K})$]
L	long axis
M_g^d	orientable d -dimensional manifold with the genus g
Ma	Mach number [-]
N_g^d	non-orientable d -dimensional manifold with the genus g
P	parameter-defining function
\mathcal{P}	transition plane between different topologies
Q	heat transfer rate [W]
Re	Reynolds number [-]
S	surface area [m^2]
$S(u(t), v(t))$	non-uniform rational basis splines surface defined by the knot vectors $u(t)$ and $v(t)$
\mathbb{S}	solid body
\mathbb{T}	torus

T	topology-defining function
t	lattice thickness [m]
u	unit cell size [m]
V	volume [m^3]
v	finite volumetric element
\hat{v}	mean flow velocity of the fluid [m/s]
w_i	i -th vertex of a graph
\mathbf{X}	design space in the real-valued space \mathbb{R}^3

Chapter 1

Introduction

It's the job that's never started as takes longest
to finish.

John Ronald Reuel Tolkien (1892 – 1973),

THE LORD OF THE RINGS

1.1 Background

In recent years, the maturation of additive manufacturing (AM) technologies has opened up new possibilities for designing and producing complex, lightweight, and high-strength materials. One such area of interest is the creation and manipulation of cellular structures, which offer unique properties and applications across various industries, including aerospace, automotive, and biomedical engineering. Cellular structures, characterized by their repeating patterns and interconnected units, have been studied and utilized for centuries. However, the advent of AM has enabled unprecedented design freedom and the potential to manufacture structures with intricate geometries and graded properties, such as heterogeneous cellular structures.

This thesis delves into the geometric modeling of heterogeneous cellular structures, emphasizing functionally graded parameters. The research seeks to address the limitations of current geometric modeling approaches, which hinder many potentials of AM technologies, and to develop a novel methodology based on function representation (F-rep) to overcome these limitations. The dissertation also discusses the current state of free and open-source software (FOSS) tools for engineering and their impact on growth and innovation in the AM industry. By presenting a software prototype implementing the proposed F-rep methodology, this work aims to advance geometric modeling techniques for cellular structures and the broader adoption of FOSS tools in the engineering domain.

1.1.1 A brief history of cellular structures in engineering applications

Ever since the early days of humankind, nature has been an immense source of inspiration when it comes to designing and inventing ([Li et al., 2019](#)). For example, more than 2000 years ago, people in Asia noticed that some trees, such as European spruce (*Picea abies*) illustrated in Fig. 1.1a, have their branches shaped in a way that raindrops slide along them fast. Rainfall water does not hold on them for long ([Weiskittel et al., 2009](#)). As there was a need to prevent roof leakage, it is believed that this idea was adapted to the roof-building process and can be traced up to pagoda roofs illustrated in Fig. 1.1b, which are common in China, Korea, Japan, and other regions of Asia ([Moffett et al., 2003; Lutfi, 2018](#)). The intuition of the ancient people led them to the right solution, as this shape appeared to be a so-called brachistochrone curve—an optimal curve of fastest descent and thus does not let water stay on roofs for long ([Ashby et al., 1975](#)). Figure 1.1c shows a plot of a brachistochrone curve and the specific time required to travel along it, as well as plots of a circular arc, a parabola, and a straight line for comparison. While not a cellular structure, the brachistochrone curve illustrates how nature has inspired functional design throughout

history, which can also be applied to studying cellular structures. The history of design is full of other examples of bio-inspiration.

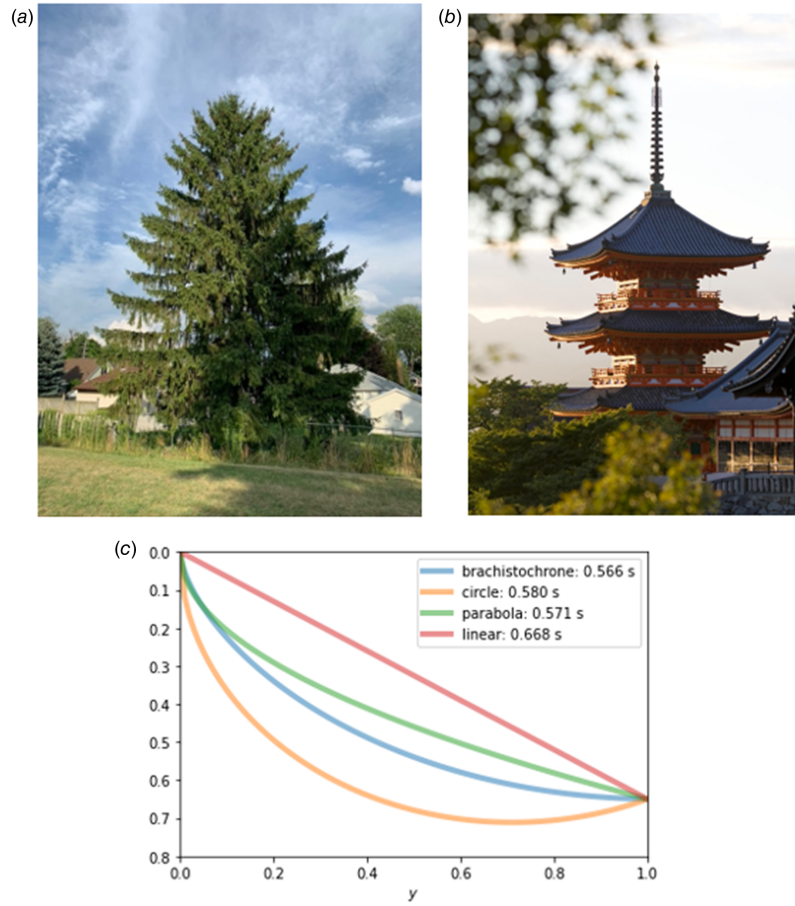


Figure 1.1 (a) Branches of a conifer tree and (b) the roof of the Kiyomizudera temple in Kyoto, Japan follow the pattern of (c) the brachistochrone curve – an optimal curve of fastest descent – to prevent rainfall water from staying on them ([Letov et al., 2021](#))

Another example is a glass sponge structure of Venus' flower basket (*Euplectella aspergillum*) with complex hierarchical structures, which inspires some modern architectures in the world, such as the Swiss Re Tower in London, United Kingdom, and the Eiffel Tower in Paris, France, shown in Fig. 1.2b. The intricate skeleton of a glass sponge is shown in Fig. 1.2a. The structure is strong and flexible, even though it is made of fragile glass. The

reason is that the glass sponge has complex hierarchical and lightweight structures from nanometer to macroscopic length scales. This multiscale heterogeneous cellular structure overcomes the brittleness of the glass material, which helps it achieve lightweight combined with high strength (Li et al., 2020b). This naturally occurring cellular structure found in the glass sponge is a prime example of nature's ability to create lightweight and strong structures, which can be harnessed in engineering applications.

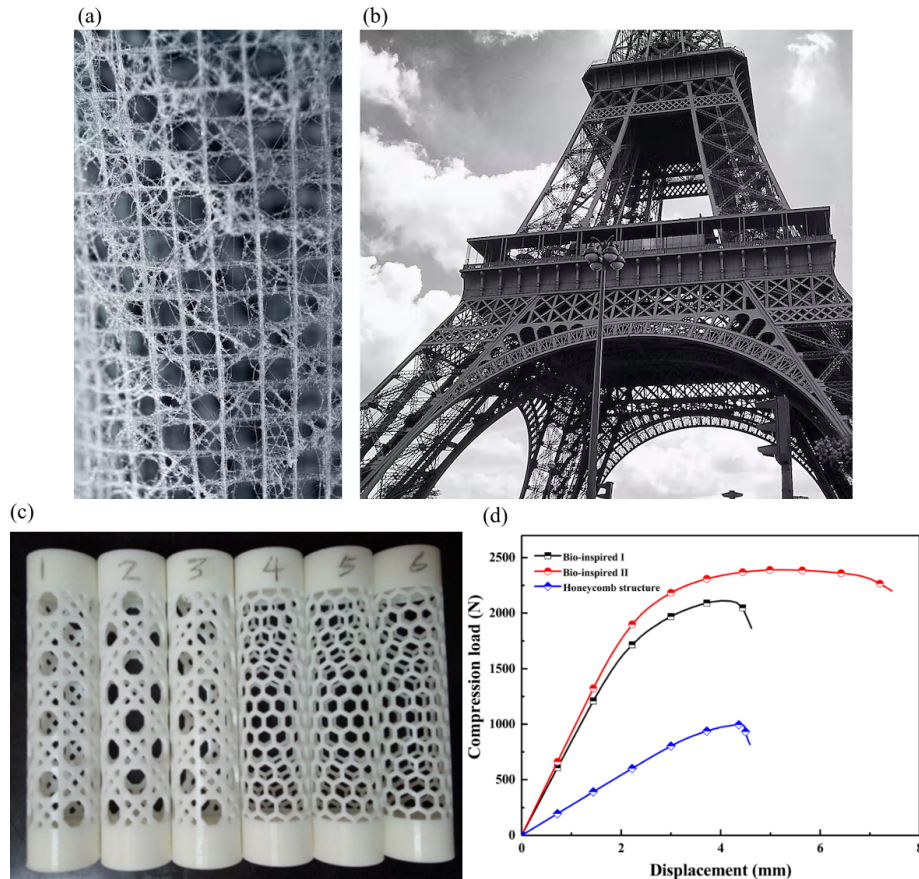


Figure 1.2 (a) The intricate skeleton of glass sponge of the Venus' flower basket (*Euplectella aspergillum*), (b) the Eiffel Tower in Paris (Jones et al., 2009), (c) bio-inspired structure and honeycomb structures, and (d) the compression versus displacement curves for three bio-inspired structures (Li et al., 2020b).

This lightweight structure of the glass sponge also inspired engineering designs of tube-

shaped and thin-walled structures, such as the bio-inspired and honeycomb lightweight structures produced by AM, as shown in Fig. 1.2c. These two structures have been tested through finite element modeling (FEM) analysis to compare the difference between their structural properties under a specific compression condition. As seen in the compression-displacement curve of different structures shown in Fig. 1.2d, the honeycomb structure was not able to provide superior structural compression-bearing characteristics and low lightweight compared to the bio-inspired structures I and II, which indicates that the structure inspired from glass sponge performs better on the compression, bending, and torsion capacity. The lightweight structure inspired by glass sponge can be widely used in industry sectors that require low weight and high reliability, such as the aerospace and automotive industries.

Another similar example would be the aircraft structure inspired by the honeycomb structure. The honeycomb illustrated in Fig. 1.3a comprises hexagonal cellular structures, which provide the most stable containment using the least amount of material (Bar-Cohen, 2005). The honeycomb structure is a perfect example of a naturally occurring cellular structure widely adopted in engineering design for its exceptional properties, such as strength-to-weight ratio. A cross-section of a rotor blade is presented in Fig. 1.3b, which is composed of various composite materials to produce a lightweight and strong rotor blade. The rotor blade incorporates the honeycomb structure because it should be strong enough to provide the lifting force for the helicopter along with the adjustments of the angles of its blades while being as light as possible (Bar-Cohen, 2005). The bonding of the environmentally friendly Nomex honeycomb core and metal skin also allows the designer to form desirable shapes into blades, increasing the performance in beam strength (Kerrick, 2011).

Heterogeneous cellular structures, in which material properties or geometric parameters vary across the structure, offer several advantages over their homogeneous counterparts,

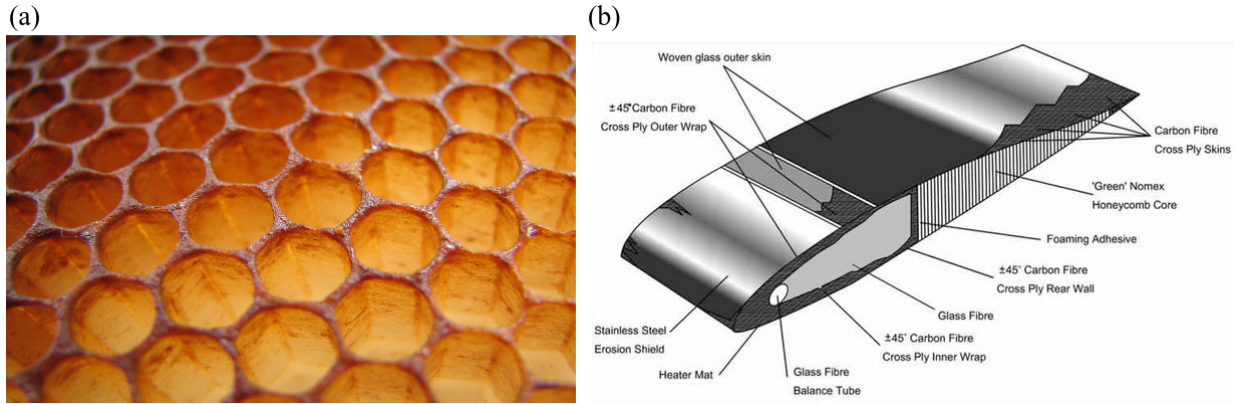


Figure 1.3 (a) A honeycomb structure ([Thane, 2007](#)) and (b) the cross-sectional view of a composite rotor blade ([Garinis et al., 2012](#))

particularly in scenarios where a combination of properties is desired or when a specific performance requirement must be met. For example, heterogeneous structures can be designed to exhibit spatially varying stiffness, strength, or energy absorption properties, allowing them to be tailored to specific loading conditions or functional requirements ([Arabnejad Khanoki and Pasini, 2012; Wang et al., 2016](#)). In contrast, homogeneous structures with uniform material properties and geometric parameters may not provide the same adaptability or performance optimization level.

AM-fabricated cellular structures have applications in many other industry sectors, such as automotive (Fig. 1.4a), engineering (Fig. 1.4b), and medical (Fig. 1.4c). In the aerospace industry, heterogeneous structures can provide an optimal strength-to-weight ratio crucial for reducing fuel consumption and enhancing structural performance ([Liu et al., 2018](#)). In the biomedical field, graded cellular structures can mimic the properties of natural bone, resulting in improved osseointegration and load-bearing capacity of implants ([Arabnejad Khanoki and Pasini, 2012](#)).

Cellular structures can be classified variously, as shown in Fig. 1.5. For example, they can be classified as homogeneous and heterogeneous. The cellular structure properties vary

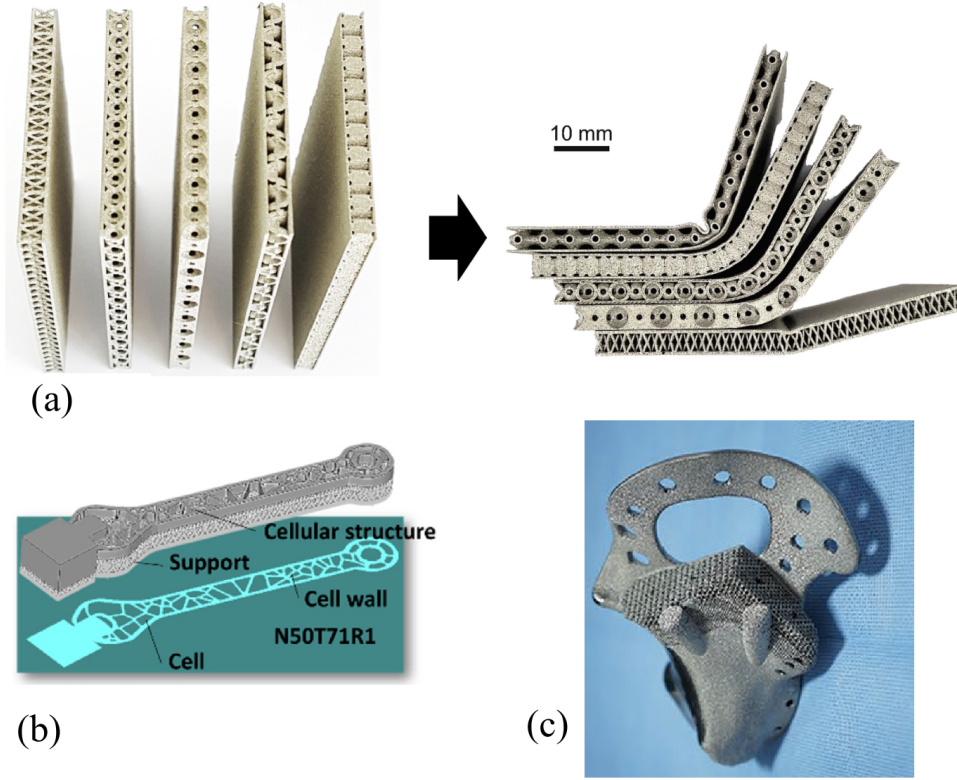


Figure 1.4 (a) Lightweight plates used in automotive industry ([Rosenthal et al., 2019](#)), (b) a wrench with a Voronoi-Monte Carlo structure for enhanced energy absorption ([Liu et al., 2019](#)), and (c) a pelvic implant for bone ingrowth ([Park et al., 2022a](#))

over the entire structure in a heterogeneous structure, while these parameters stay constant in a homogeneous cellular structure ([Tang and Zhao, 2016](#)).

Figure 1.6 illustrates different research directions on heterogeneous cellular structures in a diagram. Cellular structures can be heterogeneous in their geometry and material. The geometry can be made heterogeneous by varying parameters and topology.

In summary, nature has been a rich source of inspiration for designing and developing cellular structures throughout history. From the brachistochrone curve to the glass sponge and honeycomb structures, these naturally occurring patterns have provided valuable insights into creating lightweight and strong structures. This historical context lays the

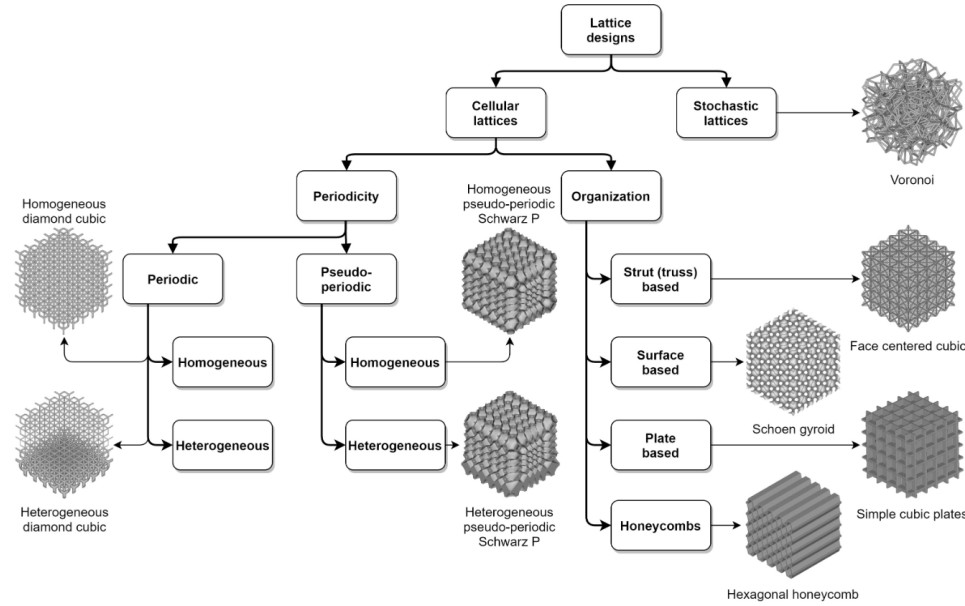


Figure 1.5 Classification chart for cellular structures designs ([McGregor et al., 2021](#))

foundation for exploring the challenges and advancements in the additive manufacturing and geometric modeling of cellular structures, as discussed in the following subsections.

This historical context lays the foundation for exploring the challenges and advancements in the AM and geometric modeling of cellular structures. Heterogeneous cellular structures, in particular, offer even more complex and versatile design possibilities due to the variations in parameters and topology. The following subsections will discuss the challenges and advancements in modeling and manufacturing these heterogeneous cellular structures.

1.1.2 Additive manufacturing capabilities for cellular structures

This section discusses the strong relationship between AM and cellular structures, highlighting how AM has revolutionized the fabrication of cellular structures with its unique capabilities. Understanding this connection is crucial for exploring the challenges and

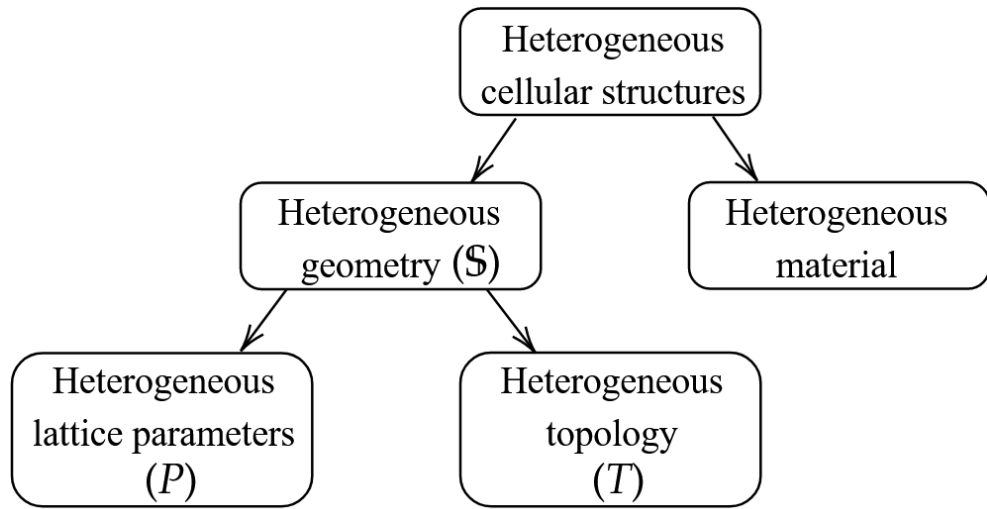


Figure 1.6 Various ways to parametrize heterogeneous cellular structures

advancements in modeling and manufacturing cellular structures presented in this dissertation.

Figure 1.7 presents a comprehensive overview of various AM processes that will be discussed in more detail. This figure, adapted from Wong and Hernandez (2012), categorizes these processes into three groups: liquid-based, solid-based, and powder-based. The selected processes represent the most significant historical methods and hold great potential for the future of the industry. Included in this review are stereolithography (STL), Poly-jet, fused deposition modeling (FDM), laminated object manufacturing (LOM), 3D printing (3DP), Prometal, selective laser sintering (SLS), laminated engineered net shaping (LENS), and electron beam melting (EBM). Among these, liquid- and powder-based processes show greater promise than solid-based processes, with LOM being the most prevalent solid-based process currently in use (Wong and Hernandez, 2012).

AM has been pushing the limits of design freedom since its introduction (Yang et al., 2015b; Yang and Zhao, 2015; Bikas et al., 2016). This work defines AM as “the process of joining materials to make objects from 3D model data, usually layer upon layer, as opposed

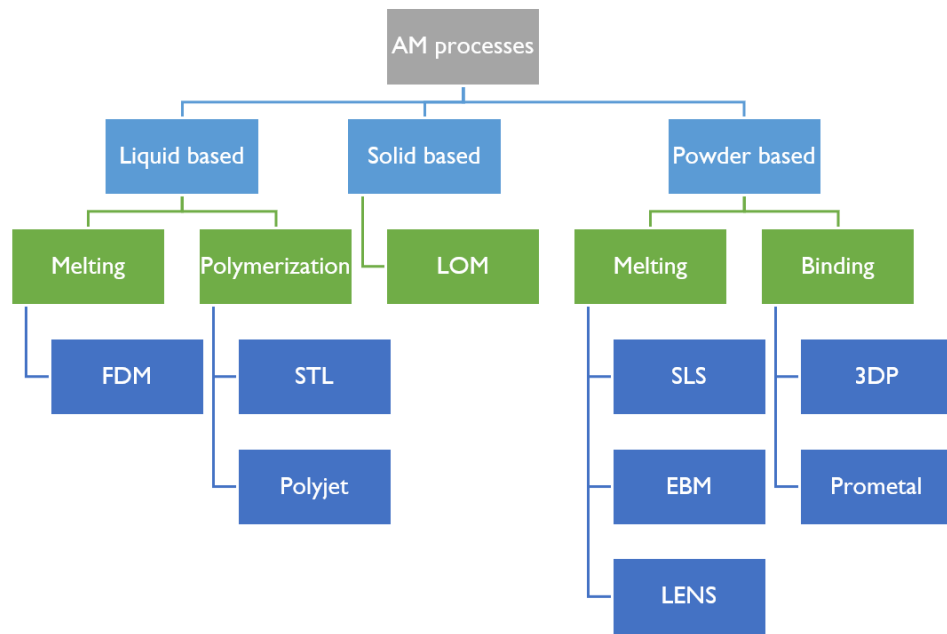


Figure 1.7 Additive manufacturing processes. Adapted from Wong and Hernandez (2012).

to subtractive manufacturing methodologies” ([ASTM F2792-12](#)). AM allows much higher geometric complexity than the more conventional manufacturing methods ([Jared et al., 2017](#)). The increased complexity that AM can fabricate is mainly associated with the additive nature of this technology. AM fuses or solidifies material at desired places ([Zhang and Liou, 2021](#)). AM does not require extra tooling and can build parts with complexity unachievable by conventional manufacturing methods ([Chu et al., 2008](#)). One of the key benefits of AM for cellular structures is its ability to produce highly complex and intricate shapes that would be challenging or impossible to create using traditional manufacturing methods, making it an ideal choice for producing lightweight and high-strength cellular structures.

The unique capabilities of AM have led to the realization of complex cellular structures, which were previously unachievable with traditional manufacturing methods. Figure 1.8

illustrates a few examples of cellular structures produced by AM. An example of a heterogeneous cellular structure is shown in Fig. 1.9, which shows a cellular structure that consists of multiple topologies. Cellular structures have found their industrial applications in various sectors such as aerospace, medicine, and construction (Balzannikov et al., 2016; Azarov et al., 2019; Wang and Tamijani, 2022). AM enables the fabrication of heterogeneous cellular structures, which combine multiple sets of geometric properties in different regions of a single structure. These structures can be tailored to possess unique properties, such as a reduced mass or a negative Poisson ratio (Savio et al., 2017; Mohammadi et al., 2020). Heterogeneous cellular structures can enhance mechanical properties like stress and strain in specific directions, making them suitable for applications that require varying load distribution throughout different regions (Leonardi et al., 2019; Zhang et al., 2021). These structures have found their application in biomedicine (Yang et al., 2021), dentistry (Javaid et al., 2019), vibration management (Matlack et al., 2016), bridge construction (Koltunov and Koroleva, 2021), heat exchange (Kim and Yoo, 2020), and more.

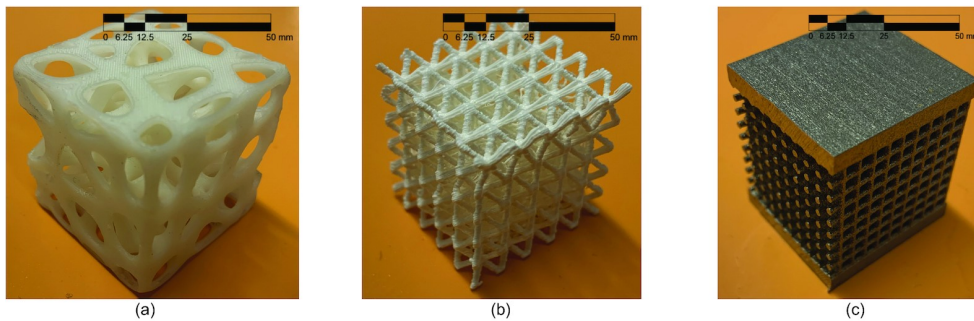


Figure 1.8 Examples of cellular structures that can be printed with AM: (a) a Voronoi topology, (b) a body-centered cubic (BCC) topology, and (c) a metal-printed simple cubic topology (Letov and Zhao, 2022)

Cellular structures can be seen in all of these applications. Numerous research domains are utilized in AM: computational optimization, geometric modeling, structural simulation, material science, and other domains (Wohlers and Gornet, 2014; Taufik and Jain, 2016).

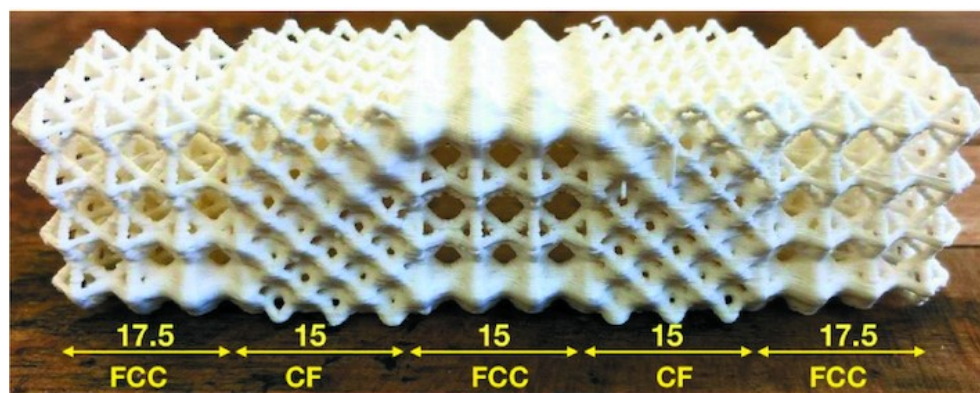


Figure 1.9 A printed example of a heterogeneous cellular structure with multiple topologies and a varying beam thickness ([Leonardi et al., 2019](#))

Even though these domains use different software tools, methodologies, and approaches, they cannot be considered separately. For example, computational optimization can be applied not only to weight reduction but to parts consolidation as well. The geometric modeling tool for AM must support the representation of these multi-domain computer-aided analyses and further optimization and simulation.

In summary, the advent of additive manufacturing has dramatically expanded the possibilities for designing and fabricating cellular structures with unprecedented complexity and functionality. The unique capabilities of AM have made it possible to create heterogeneous cellular structures with tailored mechanical properties, enabling their use in a wide range of applications, from aerospace to biomedicine. The following subsection explores the role of geometric modeling techniques in supporting the design and MA fabrication of cellular structures.

1.1.3 Geometric modeling of cellular structures

Since the introduction of the first computer-aided design (CAD) software packages, engineers and designers have been intensively using solid geometric modeling. Geometric

modeling in engineering is applied as early as the conceptual design stage, and the geometric model is used throughout the product development lifecycle. The conceptual stage of a product lifecycle is one of the most crucial ones. It is the first or early phase of the design process where designers and engineers explore ideas for the project using various tools such as drawings, physical models, and 3D renderings of basic, preliminary ideas ([Fortin et al., 2017](#)). The conceptual design phase is about generating several design concepts that are then compared and contrasted to the product design specifications and ultimately the problem the product is trying to solve ([Menshenin et al., 2020](#)). The importance of the conceptual design stage lies in the fact that it determines 70% of the development cost, unit cost, performance, and usability ([Hamelin et al., 2010](#)). 70% percent of the success of a product is determined in the conceptual design phase, as illustrated in Fig. 1.10.

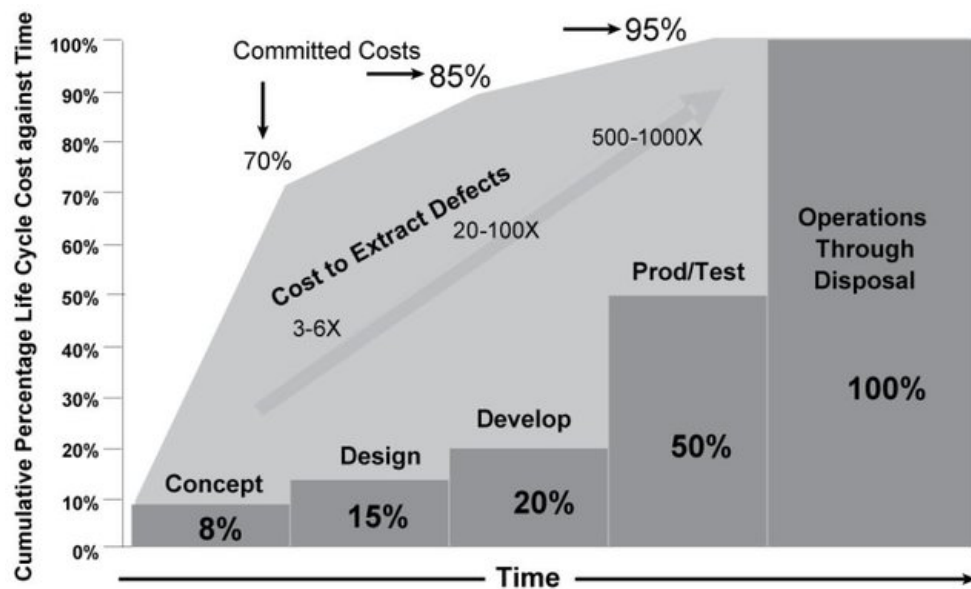


Figure 1.10 Committed lifecycle cost versus time ([Hamelin et al., 2010](#))

Geometric modeling tools allow for the creation of 3D models that can be used to detect potential design issues and find solutions. These tools are often parametric and

allow for rapid and interactive control of shapes, which is essential in developing a product (Haimes and Drela, 2012). Geometric modeling can enhance model-based systems engineering (MBSE) (Letov, 2018; Menshenin et al., 2020). The integration of system models with geometric models can provide a more comprehensive view of the system and help to identify potential issues (Bajaj et al., 2016). Model-based definition (MBD) starts with streamlining the engineering product definition process to use 3D CAD geometry models and associated data sets.

While conventional geometric modeling has proved useful for engineering design, it failed to meet the demands of AM techniques. Existing CAD software packages and their geometric modeling kernels (GMKs) cannot handle the significantly increased complexity that bio-inspired designs typically create. They are also challenged to model the complex structures that AM technology can easily fabricate, such as heterogeneous cellular structures. In other words, there is a research gap between manufacturing capacity and geometric modeling capabilities (Doubrovski et al., 2015; Letov et al., 2021).

Current geometric modeling techniques tend to fail in supporting AM due to AM technology's increased design freedom, which can support the high geometric complexity of manufactured parts. Since geometric modeling is based on classical topology and geometry, the higher the geometric complexity, the harder it is to model it (Edalat and Lieutier, 2002), especially when the geometry is bio-inspired and does not follow the typical design rules (Kou and Tan, 2007). This complexity cannot be supported by explicit modeling mainly due to the enormous amount of Boolean operations required to design a single geometrically complex part (Rosen, 2007), such as cellular structures and bio-inspired structures seen in Fig. 1.2c (Dimas and Buehler, 2014; Panda, 2015). It has been identified that there is no sufficient geometric modeling tool that would be able to represent complex heterogeneous cellular structures (Tang and Zhao, 2016). This lack of a proper tool forms

a research gap yet to be filled (Letov et al., 2021).

In this work, a geometric model is considered to be complex if (1) it is more difficult to model it with Boolean descriptive modeling rather than with parametric modeling, or (2) it is not possible to support 30 frames-per-second (FPS) frame rate performance on an average computer used in engineering. Additionally, a machine is considered average if it can provide at least 16 GB of random-access memory (RAM), a graphical processing unit (GPU) with at least 6 GB of video memory, a solid-state drive (SSD), and a 64-bit central processing unit (CPU) with a clock signal frequency of 3.3 GHz. These system requirements are identified according to the recommended system requirements for SolidWorks (Dassault Systèmes SE, 2006) and Rhinoceros 3D (Robert McNeel & Associates, 2020a) software packages, which are extensively used for 3D modeling (Dassault Systèmes SE, 2020; Robert McNeel & Associates, 2020b). The threshold of 30 FPS is chosen as it is proven to be sufficient for convenient work and observations (Kamaci and Altunbasak, 2003).

Topology optimization is a powerful computational method that aims to optimize material distribution within a given design space, subject to certain constraints and objectives, to achieve the best possible performance for a specific application. The method has gained significant attention over the past few decades due to its ability to generate highly efficient and innovative designs for various engineering applications, from structural components to heat exchangers and acoustic devices (Bendsøe and Sigmund, 2013).

One of the main advantages of topology optimization is that it can automatically identify the most effective material distribution to minimize weight, maximize stiffness, or achieve other desired performance criteria without the need for explicit geometric modeling (Sigmund, 1997). This is particularly useful for applications where the optimal design may be highly complex or counterintuitive and where traditional design approaches may struggle to identify the best solution. However, the resulting designs from topology optimization are

often highly intricate and may require further explicit geometric modeling and refinement to ensure manufacturability and to meet other practical requirements ([Jihong et al., 2021](#)).

Furthermore, explicit geometric modeling is essential for successfully integrating topology-optimized designs into the broader engineering design process. This includes model validation, design evaluation, and incorporating manufacturing constraints and requirements ([Jihong et al., 2021](#)). By developing advanced explicit geometric modeling techniques and tools, it is possible to improve the overall efficiency and effectiveness of the design process, bridging the gap between the idealized solutions generated by topology optimization and the practical realities of engineering design and manufacturing. In other words, no implicit modeling method can be developed without a proper explicit modeling method at its core. With this in mind, this research focuses on more explicit geometric modeling methods and aims to contribute to this field.

This thesis introduces a novel methodology based on function representation (F-rep) for the geometric modeling of heterogeneous cellular structures and its implementation in a software prototype. The software prototype is packaged in a library called LatticeQuery. The methodology is simplified to be used as a collection of simplified functions, which can generate a heterogeneous cellular structure based on the function arguments. The library presented in this thesis aims to provide flexible methods that reduce the amount of user input to provide a desired heterogeneous cellular structure.

1.2 Dissertation outline

The structure of the remaining portions of the thesis is as follows:

Chapter 2:

Chapter 2 presents a comprehensive literature review on geometric modeling, particularly focusing on its application to cellular structures. The chapter explores various aspects of geometric modeling, such as surface, volumetric, hybrid, and multi-scale modeling, and examines bio-inspired geometric modeling approaches. It also discusses the challenges in the geometric modeling of heterogeneous cellular structures, existing techniques for modeling cellular structures, and the role of multiple topologies in cellular structures. Additionally, the chapter covers the graphical user interface of software packages for modeling cellular structures and function representation concepts applied to geometric modeling.

Chapter 3:

Chapter 3 presents the proposed geometric modeling method based on the function representation approach for the geometric modeling of heterogeneous cellular structures. The chapter introduces a novel geometric description to represent various cellular topologies. It then discusses a method for varying geometric parameters in a non-linear manner, enabling greater control and flexibility in designing cellular structures. The chapter further explores the creation of cellular structures with multiple topologies, demonstrating the versatility of the proposed method. It also delves into the generation of stochastic cellular structures, showcasing the ability of the approach to produce random and unique configurations. Finally, the chapter examines conformal cellular structures, illustrating how the proposed method can effectively adapt to complex and varying surface geometries, thereby offering a comprehensive solution for designing heterogeneous cellular structures.

Chapter 4:

Chapter 4 details the practical aspects of the proposed geometric modeling method introduced in Chapter 3. The chapter begins by providing functional definitions of cellular topologies, including beam- and surface-based topologies. It then discusses the functional variation of geometric parameters essential for designing complex heterogeneous cellular structures. The chapter further explores the generation of cellular structures with multiple topologies, illustrating the implementation process for both beam- and surface-based cellular structures. It also covers the modeling of stochastic cellular structures, emphasizing the implementation of randomness and uniqueness in design. The chapter then delves into the implementation of conformal cellular structures, addressing both surface conformality and volume conformality aspects. Subsequently, the chapter introduces LatticeQuery, an open-source software developed to support the proposed method, describing its architecture and usage. Finally, the chapter assesses the computational performance of the proposed method, highlighting its efficiency and effectiveness in designing heterogeneous cellular structures.

Chapter 5:

Chapter 5 demonstrates the practical applications of the proposed geometric modeling method to real-life scenarios.

The first case study focuses on the use of the proposed method to model cellular structures used to estimate their flow and thermal characteristics, showcasing the utility of the method in solving real-world engineering problems. The chapter begins by discussing geometric, flow, and thermal properties of cellular structures, setting the context for the case study. It then reviews existing experimental results, highlighting the importance of

accurate geometric modeling in understanding the performance of cellular structures. The chapter describes the methods to apply the proposed geometric modeling approach to the case study. Finally, the chapter presents the results obtained from the case study, emphasizing the effectiveness and accuracy of the proposed method in capturing the complex behavior of cellular structures and estimating their flow and thermal characteristics.

The second case study explores the multifunctional non-pneumatic tire design. The ideation and conceptual design process are discussed, illustrating how the proposed geometric modeling method can be applied in the early design stages to develop innovative solutions. The results of this case study are presented, showcasing the potential of the proposed method to create novel and effective designs in the context of non-pneumatic tire engineering. Together, these case studies provide examples of the versatility and practicality of the proposed geometric modeling method in addressing complex design challenges.

Chapter 6:

Chapter 6 summarizes the dissertation's main contributions and discusses the limitation of this work and the future research needed in this area.

Chapter 2

Literature review

We penetrated deeper and deeper into the heart
of darkness.

Joseph Conrad (1875 – 1924),
HEART OF DARKNESS

This chapter presents a comprehensive literature review on the current state of geometric modeling, focusing on techniques used for bio-inspired designs, geometrically complex structures, and cellular structures. This review serves as a foundation for understanding the challenges and research gaps in the field, which will inform the development of a novel methodology and software prototype for the geometric modeling of heterogeneous cellular structures in additive manufacturing in this research.

The rest of this chapter is organized as follows. Section 2.1 delves into the current status of geometric modeling, covering surface modeling, volumetric modeling, hybrid modeling, and multi-scale modeling. In Section 2.2, the geometric modeling of geometrically complex structures is discussed, followed by Section 2.3, which highlights the challenges in the geometric modeling of heterogeneous cellular structures. Section 2.4 explores existing

techniques and tools for the geometric modeling of cellular structures, including surface, volumetric, and hybrid modeling approaches. Finally, Section 2.5 presents the research objectives of this thesis that are based on the performed literature review.

2.1 Current status of geometric modeling

Modern engineering software, including CAD, computer-aided manufacturing (CAM), and computer-aided engineering (CAE) applications, relies on a GMK at its core, supplemented by various other tools (Letov, 2018). GMKs are responsible for creating numerical representations of geometries using mathematical methods (C3D Labs, 2020). The geometric modeling of intricate bio-inspired structures poses significant challenges, predominantly concerning the definition of bounding shapes and the computational optimization of a GMK (X. Gu et al., 2016; Savio et al., 2018). The mathematical foundations of GMKs encompass linear algebra, topology, mathematical logic, graph theory, and more (Gardan, 2014; Golovanov, 2014), which are translated into code to display geometric information on a screen.

Efficient GMK development relies on programming techniques offering high-level functionality (Ushakov, 2018). As the development process typically involves a large team of software developers and mathematicians working over several years, it becomes extremely challenging for smaller teams to create a GMK (Schnitger Corporation, 2012).

GMKs share similarities with 3D graphics software packages used in the movie and video game industries (Felbrich et al., 2018). Both represent 3D models on screen and simulate their behavior. However, while GMK-based 3D models are solid models with material properties, 3D graphics models primarily possess geometric and visual properties. Despite their differences, the two types of software have overlapping features that could

potentially be adopted by one another to enhance quality.

In this research, 3D objects are defined according to the functional representation (F-rep) methodology, where a 3D object is described by a real-valued function $F(\mathbf{X})$ such that $F(\mathbf{X}) \leq 0$ represents the object, $F(\mathbf{X}) = 0$ its surface, and $F(\mathbf{X}) > 0$ the rest of the design space (Pasko et al., 1995). This notation is chosen for defining 3D objects in this research because of its flexibility, compactness, support for constructive operations, ability to represent implicit surfaces, analytical properties, and adaptability to multi-scale modeling. To visualize these objects, most CAD software packages use GMKs in conjunction with parametric modeling kernels that support Boolean operations and geometric constraints (Golovanov, 2014).

CAD tools generally employ surface or volumetric modeling to represent the geometry of solid bodies in CAD files. In this section, general concepts of geometric modeling are introduced. Sections 2.1.1 and 2.1.2 below provide a comprehensive overview of these two approaches to geometric modeling. Hybrid modeling methods are covered in Section 2.1.3. Section 2.1.4 introduces function representation concepts and their application to geometric modeling. Section 2.1.5 describes techniques to support multi-scale geometric modeling.

2.1.1 Surface modeling

This section discusses the topological aspects of geometric modeling and the limitations of conventional modeling techniques like polygonal meshes, boundary representation (B-rep), constructive solid geometry (CSG), isogeometric analysis (IGA), and subdivision surfaces in handling these complexities. Recent advancements and alternative methods in the field of geometric modeling are also explored, which may offer improved performance and accuracy for modeling complex structures

Topologically, the surface of a geometrically complicated part such as a cellular structure

is a closed-oriented two-manifold M_g^2 of a significantly large non-zero genus ($g \gg 0$). In topology, a closed two-manifold is a connected surface that exists in 3D. They are oriented if there is no path from one side of a surface to another, as seen in Fig. 2.1a. Non-oriented manifolds such as Klein's bottle in Fig. 2.1b cannot exist and be manufactured in reality and thus are not considered for modeling. Only orientable two-manifolds are considered in this work because only a solid body bounded by an orientable two-manifold without intersections is manufacturable. A single simple unit grid has genus $g = 5$, meaning that it has many curvatures and details on its micro-scale (Letov and Zhao, 2021).

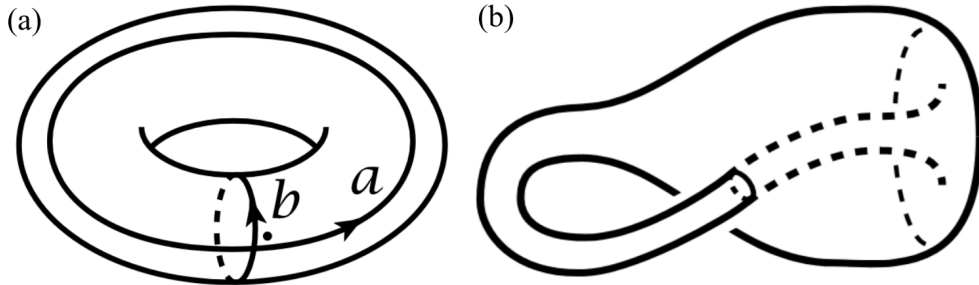


Figure 2.1 Two closed two-manifolds: (a) an oriented two-manifold of genus $g = 1$ (torus) $\mathbb{T} = M_1^2$ and (b) a non-oriented two-manifold of genus $g = 2$ (Klein's bottle) N_2^2 (Hatcher, 2001)

Polygonal meshes begin to fail when complex geometric objects are modeled with them, such as heterogeneous cellular structures. One of the most popular non-proprietary CAD file formats – stereolithography (STL) – utilizes polygonal representation (Braun et al., 2021). In polygon surface mesh, the number of finite elements rises exponentially with model complexity. It severely impacts the modeling of complex shapes due to its high computational cost, as seen in Fig. 2.2 (Cutanda et al., 2001).

Note that mindlessly increasing the number of nodes stops showing any improvement at some point, and critical non-plane areas typically require smaller element sizes (Ghavidel et al., 2018). Moreover, smaller finite elements increase calculation time and introduce

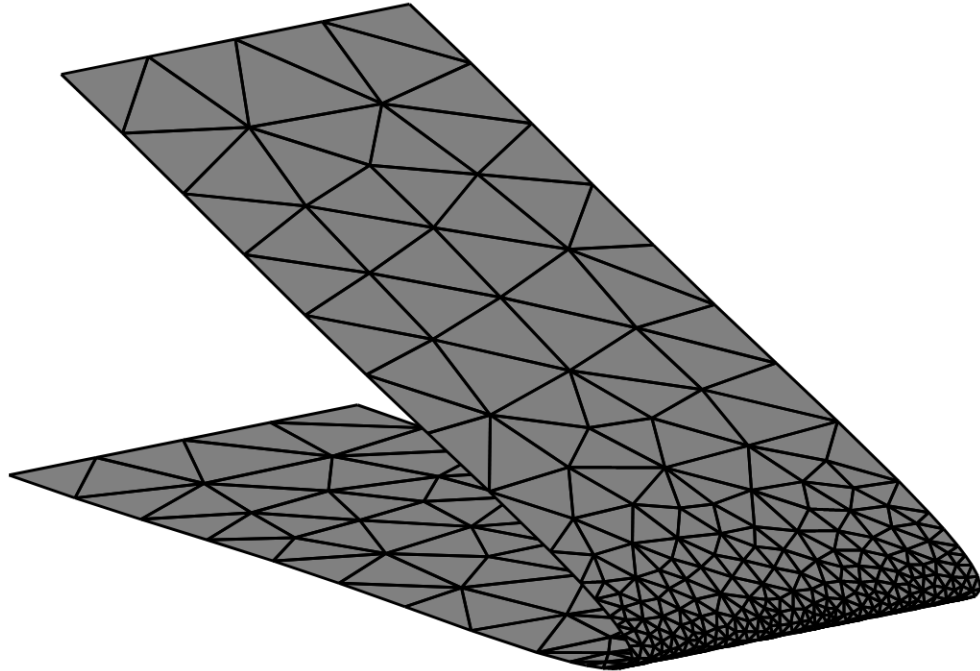


Figure 2.2 Model complexity in regions with high curvature affects the computation of rendering of a surface mesh ([Chen and Bishop, 1997](#))

errors in geometry representation, as seen in Fig. 2.3. A mesh convergence study is usually applied in such cases to obtain an optimal number of elements ([Sarabhai et al., 2023](#)).

The so-called influencing points of the increased complexity of the mesh require the mesh edges to be orthogonal to the surface boundary for increased performance and decreased error-proneness ([Gillebaart et al., 2016](#)). Note that in Fig. 2.2, the mesh becomes denser when nearing the influencing points, located in this case near the surface boundaries and at non-planar surfaces. This requires extra calculations, which slows the mesh generation and the corresponding modeling process. The interpolation based on radial basis functions (RBFs) attempts to improve the performance of these operations significantly ([Kedward et al., 2017](#)). However, this approach was initially designed for 2D mesh generation and still requires specific improvements to be widely used in 3D. For example, it has been found that RBF interpolation may fail when it is applied to a closed-oriented surface, such as an

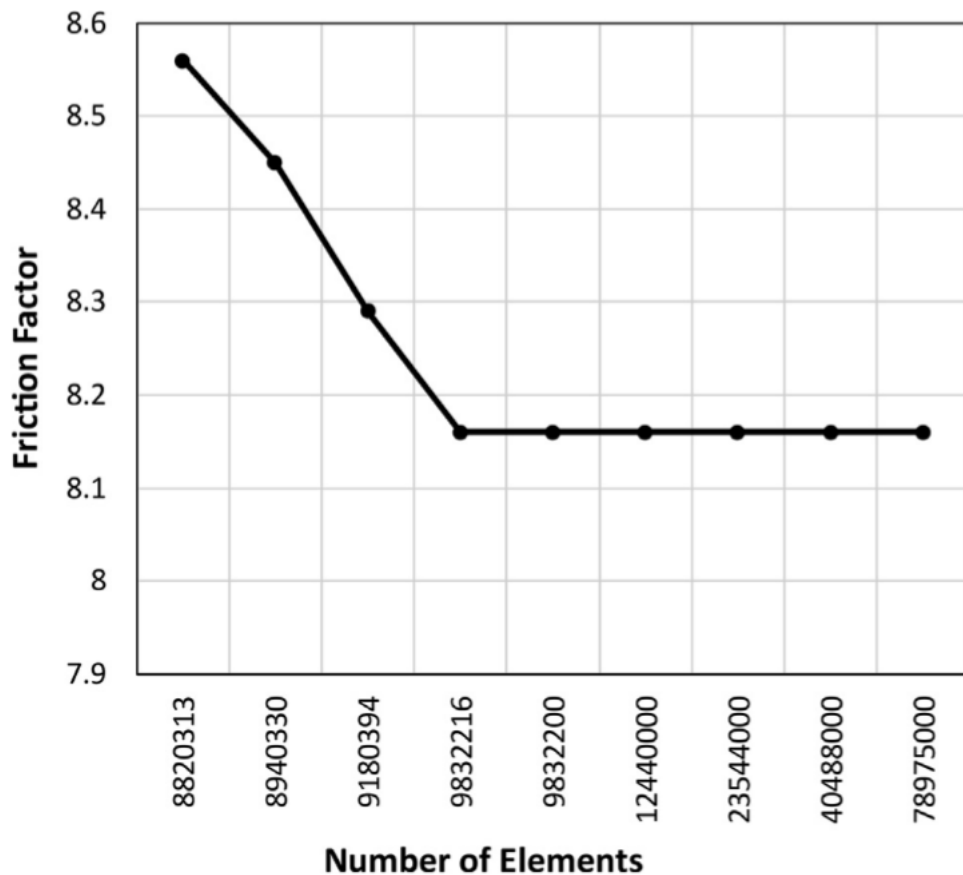


Figure 2.3 A mesh convergence study used to find an optimal number of elements sufficient to estimate values of a parameter – friction factor in this case ([Sarabhai et al., 2023](#))

entire cylindrical surface. The reason for this is the failure to detect the influencing points in a completely symmetrical and closed surface, as every point is influential in this case. The possible solution for it lies in applying hybrid methods that introduce parallelization to the process, but even then, it requires top-tier CPU capabilities ([Zhong et al., 2020](#)).

Mesh modeling assumes that a solid model is defined by tiny finite elements (often triangular), each of which can be defined by vertices and the position and orientation of the element in the design space. For example, Fig. 2.4 shows an example of a triangular finite element defined in an American Standard Code for Information Interchange (ASCII)

STL file by its normal vector and vertices.

```

facet normal 0.95105690250522623
  0.30901580574003779 -0
  outer loop
    vertex 14.842915534973145
    11.243449211120605 -5
    vertex 14.648882865905762
    11.840622901916504 -5
    vertex 14.648882865905762
    11.840622901916504 0
  endloop
endfacet

```

Figure 2.4 An example of a single triangular mesh element in STL format ([Letov et al., 2021](#))

Most modeling techniques used in GMKs involve surfaces that bind the solid model. The most popular modeling techniques are boundary representation (B-rep) and constructive solid geometry (CSG). These techniques often utilize polygonal meshes, which operate in a trade-off between quality and performance. It is not trivial to balance the trade-off when modeling complex geometric objects such as heterogeneous cellular structures, which often results in a high computation time and decreased quality of models due to errors ([Cutanda et al., 2001](#); [Letov et al., 2021](#)).

B-rep techniques have evolved rapidly and incorporated into major GMKs such as Parasolid ([Siemens Digital Industries Software, 2018](#)) and Open Cascade Technology (OCCT) ([Open Cascade S.A.S.U., 2018](#)). B-rep allows the modeling of solids made by revolution, extrusion, chamfering, and other operations with solids common in modern CAD in addition to Boolean operations used prior to B-rep ([Stroud, 2006](#)). For example, a torus in B-rep can be defined as a circle given by

$$\rho^2 - 2\rho R \cos(\theta) + R^2 = r^2, \quad (2.1)$$

where (ρ, θ) are the polar coordinates, r is the radius of the circle and, consequently, of the torus tube, and R is the distance between the origin and the center of the circle and, consequently, between the center of the torus and the center of its tube. Polar coordinates are favorable in the representation of circles and curves in B-rep due to decreased computation time ([Sánchez-Reyes, 1995](#)). This circle then revolved around the z -axis of the design space.

B-rep suffers from the same inability to model highly complicated geometries such as the ones in Fig. 1.2, for example. The reason for this is the lack of parametrization and the need of numerous operations to achieve the modeling of even a simple homogeneous cellular structure. The overall performance of B-rep methods can be improved by, for example, hybrid B-rep methods ([Song and Cohen, 2019](#)) and optimizing boundary spline (B-spline) functions ([Wang and Qian, 2014](#); [Sasaki et al., 2017](#)). However, the number of operations limits this optimization, and efforts are needed to model geometrically complex structures. Even if functions are getting more straightforward, the number of functions needed to define a complex structure can be overwhelming. Moreover, the surface-to-volume ratios (S/V) of the multi-scale and cellular structures can be thousands of times larger than the CAD models encountered in conventional design, which poses a big issue for modeling tools based on B-rep.

Non-uniform rational basis splines (NURBS) and their extension to surface modeling were introduced to mitigate difficulties associated with the modeling of complex structures and are used widely in B-rep ([Rogers, 2001](#)). NURBS surfaces and their trimming allow interpolation of the desired shape by points with simplicity. The Initial Graphics Exchange Specification (IGES) and the Standard for the Exchange of Product (STEP) are popular CAD file formats utilizing NURBS. However, trimming a NURBS surface $S(u(t), v(t))$ with a trimming curve $C(t)$ is not always possible, as it is not always possible to retrieve the knot

vectors $u(t)$ and $v(t)$ for every parameter t ([Schmidt et al., 2012](#)). Moreover, attempting to define an enormous amount of entirely different NURBS surfaces for geometrically complex shapes makes the design process too tedious for an engineering designer.

While B-rep does not operate with meshes, the mesh representation is still used for representing and rendering 3D models on screen. For example, even when a circle is defined in the design space, it still looks like a polygon with several vertices enough to be seen as a circle. Therefore, a particular conversion from B-rep to mesh is required to allow the rendering of the model. This straightforward process has been extensively discussed in the literature ([Boender et al., 1994](#); [Brunet et al., 2000](#)). Spline-based B-rep is precise enough for conventional engineering design. However, as AM allowed more design freedom, more complicated shapes became manufacturable. There appears to be a trade-off between having a higher quality of geometry and having a more complex geometry. Note that the inverse problem is not straightforward and encounters issues often associated with this type of problem, mostly related to the need to develop a feature recognition algorithm ([Raja, 2019](#); [Ben Makhoul et al., 2019](#)). Some techniques explicitly allow the rendering of shapes with curvature, and the development of these techniques significantly contributed toward research on function representation (F-rep) since these shapes often require an explicit function that controls its curves ([Martin et al., 2000](#); [Raviv and Elber, 2001](#)).

The CSG technique can be applied to define boundary conditions of the design space of a cellular structure ([Wang et al., 2021](#)). However, this thesis does not focus on defining boundary conditions. At the same time, the CSG technique is not well suited for the geometric modeling of periodic structures ([Loh et al., 2018](#)).

Isogeometric analysis (IGA) is a computational approach that was introduced to bridge the gap between CAD and finite element analysis (FEA) ([Hughes et al., 2005](#)). The main idea behind IGA is to utilize the same mathematical basis for both geometry representa-

tion and analysis. This allows for seamless integration of the design and analysis phases, eliminating the need for mesh generation and simplifying the overall process. In conventional FEA, the geometry of the model is often represented using NURBS or other spline-based techniques, while the analysis relies on piecewise polynomial basis functions such as Lagrange or Hermite polynomials. This discrepancy between geometric and analysis representations requires a mesh generation step, which can be time-consuming and prone to errors, especially for complex geometries. IGA, on the other hand, employs NURBS or other compatible basis functions for both geometry representation and analysis. This approach provides several advantages over traditional FEA, including improved accuracy, elimination of mesh generation, and enhanced integration with CAD tools ([Cottrell et al., 2009](#)). Despite its advantages, IGA also has some limitations. One challenge is the increased computational cost associated with higher-order basis functions. However, ongoing research aims to develop efficient algorithms and computational techniques to address this issue ([Cazzani et al., 2016](#)).

Subdivision surfaces are a powerful mathematical technique in computer graphics, CAD, and geometric modeling. Subdivision surfaces are a geometric modeling technique that recursively refines an initial coarse polygonal mesh into a smooth and more detailed surface by applying iterative subdivision rules, resulting in a continuous and visually appealing representation of complex shapes. Subdivision surfaces have since become popular for modeling complex, smooth, and organic shapes ([Catmull and Clark, 1978](#)). This approach allows for precise control over the surface's shape and smoothness, making it suitable for modeling complex geometries. There are various types of subdivision schemes, such as the Catmull-Clark scheme for quadrilateral meshes ([Catmull and Clark, 1978](#)), Loop's scheme for triangular meshes ([Loop, 1987](#)), and Doo-Sabin scheme for polygonal meshes ([Doo and Sabin, 1978](#)). Each scheme has its own set of subdivision rules and properties, catering to

different applications and requirements. Some advantages of subdivision surfaces include compact representation, local control, adaptive refinement, and compatibility with existing modeling techniques (DeRose et al., 1998). However, disadvantages of subdivision surfaces include increased computational complexity with each iteration (Peters and Reif, 1997), difficulty in handling sharp features or creases (Halstead et al., 1993), and the potential for undesirable artifacts or surface distortions (Warren and Weimer, 2002). Subdivision surfaces have been widely used in various applications, including computer animation, video games, and CAD systems. With their ability to efficiently represent smooth and complex shapes and compatibility with other modeling techniques, subdivision surfaces have become a valuable tool in geometric modeling.

2.1.2 Volumetric modeling

The volumetric modeling approach, contrarily to the surface modeling approach, models not only the surface $F(\mathbf{X}) = 0$ but the whole internal structure $F(\mathbf{X}) \geq 0$ as well. Modeling of the internal structure enables better control over the geometric model since trimming and Boolean operations are less computationally expensive as there is no need to generate a boundary surface (Aremu et al., 2017). Furthermore, volumetric modeling is particularly useful in applications where internal material properties or stress distribution matter, such as in medical imaging (Ritter et al., 2011), fluid dynamics (Ashgriz and Mostaghimi, 2002), or structural analysis (Loh and Choong, 2013). Such flexibility, however, often comes at the cost of higher computation time to generate volumetric models.

Voxel modeling has been used for eliminating high-frequency details of the object ever since the introduction of voxels (He et al., 1995; Nooruddin and Turk, 2003), which is essential for modeling complex structures such as bio-inspired ones. Moreover, voxels have an advantage in downsampling and acquiring real-world data (Laine and Karras, 2010).

Moreover, there is no need for voxels smaller than the resolution of a 3D printer as they would not be manufacturable (Telea and Jalba, 2011). Voxelized models support the same Boolean operations as the mesh models (Aremu et al., 2017). A significant advantage of voxel modeling for AM lies in straightforward machine learning applications, such as the prediction of model printability (Gobert et al., 2018).

In voxel modeling, voxels typically have a cubic shape (Strand, 2004) with some non-cubic approximations such as the ones produced by the marching cubes algorithm (Lorensen and Cline, 1987; Newman and Yi, 2006). Having the same element tessellated in the design space results in an inaccurate representation of curvatures in case of insufficient voxel density. On the other hand, having significantly high voxel density results in high computational cost. Applying the level-set method (LSM) allows considering a voxelized 3D design space as a set of 2D layers, which improves the computational complexity from $O(n^3)$ to the still highly demanding $O(n^2)$ (Adalsteinsson and Sethian, 1995).

Applying voxelization as it is without any additional optimization is still computationally expensive (Kauker et al., 2016). One of the most popular voxel-based simplification methods involves using sparse voxel octrees, which are based on generating multi-scale voxels which could be visible or invisible depending on the resolution, size of the screen, and point of view (Laine and Karras, 2010). This approach applied to large voxel models can result in up to six times increased efficiency (Marcus, 2017).

Another common volumetric modeling approach is the finite volume method (FVM) which generates volumetric mesh similar to surface mesh but with the whole solid body discretized rather than just the surface. As a result, the body is subdivided into polyhedrons, not polygons (Rom and Brakhage, 2011). However, this approach has disadvantages similar to surface mesh: computation of curvatures is nontrivial due to their geometric complexity, and the computational expenses rise exponentially with the increase of com-

plexity.

Note that unit elements in existing geometry discretization techniques are typically convex, whether they are finite elements or voxels. Convex unit elements require less computation, but it is required to have more unit elements to model strongly non-convex shapes, such as bio-inspired cellular structures. This requirement implies a proper meshing algorithm that considers convexity and curvature and affects meshed models' quality, especially those requiring multi-scale modeling ([Fuchs et al., 2010](#)). Thus, there is a need to identify whether non-convex unit elements such as the one sketched in Fig. 2.5 could be used for the geometric modeling of non-convex geometries. Combining two convex finite elements into one non-convex would result in a computationally less efficient finite element and reduce the total number of finite elements, introducing a trade-off between these two parameters. One of the potential benefits of using non-convex unit elements in volumetric modeling is the ability to represent more complex and intricate shapes with fewer elements, as they can better conform to the underlying geometry ([Bronstein et al., 2017](#)). This can lead to more efficient representations in terms of memory and computation, particularly for models with highly non-convex features or irregularities. Moreover, non-convex unit elements can potentially provide higher accuracy in capturing the object's geometry, as they can match the object's natural shape more closely compared to convex elements ([Bronstein et al., 2017](#)).

However, there are also drawbacks associated with using non-convex unit elements. One of the primary challenges is that they can be more computationally expensive to process, as the algorithms for intersection, containment, and other geometric operations are often more complex for non-convex shapes ([De Berg et al., 2008](#)). Furthermore, non-convex unit elements can lead to difficulty in generating stable and accurate finite element simulations. The numerical integration and shape functions for non-convex elements can

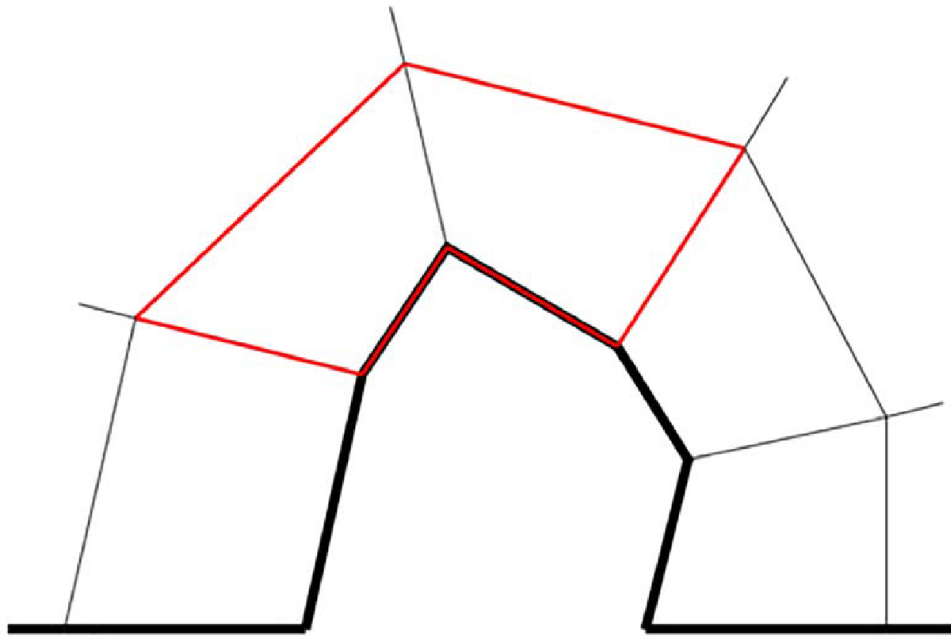


Figure 2.5 A mesh of non-convex geometry ([Letov et al., 2021](#))

be more challenging to compute and may exhibit poorer convergence properties ([Milbrandt and Pick, 2008](#)).

In recent years, there has been growing interest in exploring non-convex unit elements in various applications, such as geometric deep learning. For example, the work of [Bronstein et al. \(2017\)](#) focuses on leveraging non-convex elements to capture complex, non-Euclidean structures in various data domains, including 3D shapes, graphs, and manifolds. By incorporating non-convex unit elements into their learning framework, it is possible to develop more expressive and flexible models that can better handle the challenges associated with geometric data.

Volumetric representation (V-rep) modeling is another recently introduced volumetric modeling technique ([Massarwi and Elber, 2016](#)). It utilizes elliptic partial differential equations and modifies the design space to have various unit volumes that handle extreme

geometric complexity. The approach is superior to B-rep modeling in terms of geometric complexity handling (Wassermann et al., 2020) and is more adaptable for simulation purposes (Antolin et al., 2019). However, it suffers from an issue like B-rep: while in B-rep, two surfaces collide by an edge or a group of edges, and in V-rep, two volumes collide by a surface or a group of surfaces since surfaces are, in general, more computational than edges (Massarwi et al., 2019). This can dramatically increase the computational expenses in cases with many unit volumes. Evidence shows that a hybrid B-rep approach can be applied to V-rep to increase its performance (Song and Cohen, 2019). The torus used as an example in the previous section can be represented in V-rep as a union of five solids of revolution, as seen in Fig. 2.6. Note that the “core” of the torus is required to be a separate solid to avoid convergence of the other four solids to zero.

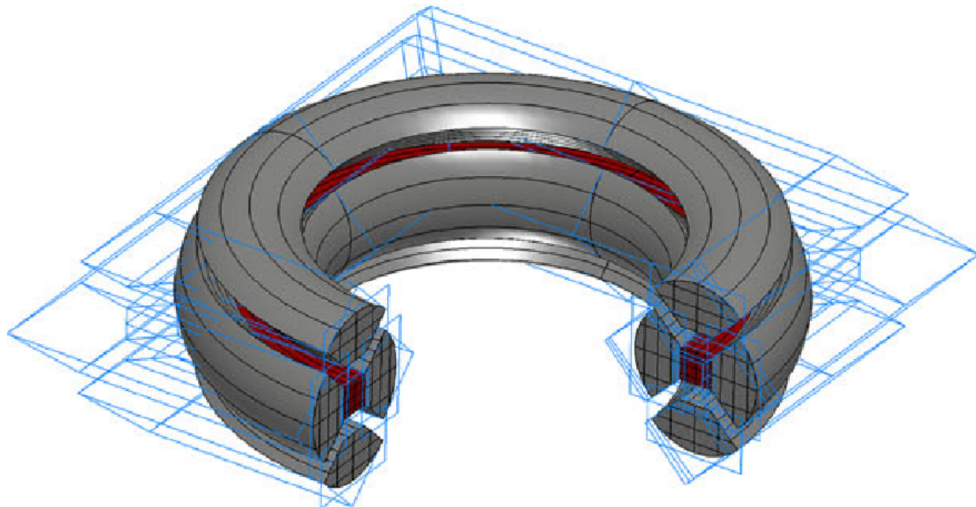


Figure 2.6 A torus is constructed using five solids of revolution in volumetric representation modeling (Wassermann et al., 2020)

Volumetric modeling with iso-geometric finite elements utilizes finite cubic elements that are transformed to fit the desired model better by, for example, moving vertices of the default cube to new positions as illustrated in Fig. 2.7a. Such effect is achieved, in this

example, by an affine shear and scale transformation $\mathcal{N} : \Gamma \mapsto \mathbf{X}$ that transforms a cube in the $\Gamma = (\xi, \zeta, \eta)$ coordinates to the $\mathbf{X} = (x, y, z)$ coordinates of the real design space. The resulting model consists of numerous iso-geometric finite elements, as shown in Fig. 2.7b. However, this method inherits drawbacks of polygonal-based and voxel modelings. These disadvantages include, for example, having irregularities at regions with high curvature. Even though the variety of shapes is larger than having only one type of voxel, the finite elements are still limited to having six faces.

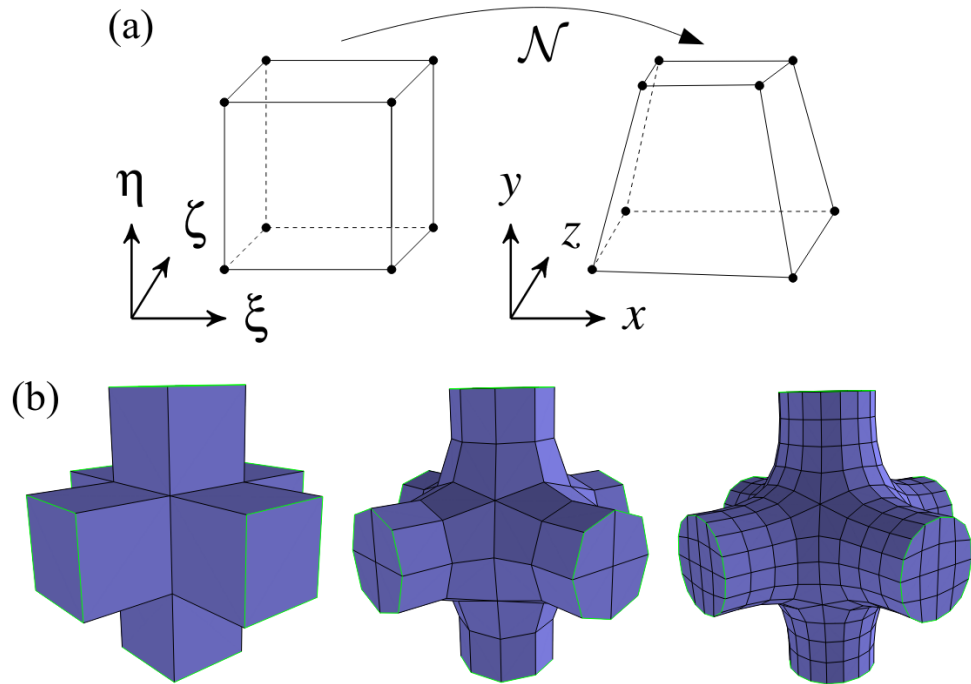


Figure 2.7 (a) A transformation \mathcal{N} of a cubic finite element to a new shape and (b) the geometric modeling of a structure with different stages of refinement with iso-geometric finite elements (Burkhart et al., 2010)

The described drawbacks of voxel modeling suggest modifying volumetric modeling techniques to fit better the rising demand for a geometric modeling approach that could support more complicated geometry. Using non-cuboid voxels, which often find their use in computer graphics rather than in geometric CAD modeling, improves the performance

but introduces significant distortion to the model they are applied to. However, there is evidence that using a variety of unit volumes in a single model can dramatically improve the performance and quality of the model. The IRIT¹ modeling environment (Eggli et al., 1997) does this by allowing the modeling of so-called VModels with non-conventional unit volumes, which allows storing 3D data in much smaller sized IRT² files native to the IRIT modeling environment (Hahmann et al., 2012).

Overall, one of the main challenges associated with volumetric modeling is the increased memory and computational resources required compared to surface models. Since volumetric models represent not only the surface but also the internal structure of an object, they often require more storage space and processing power (Gavryushkina, 2021). For example, Fig. 2.8 shows that the amount of voxels needed to represent an original geometry is significantly larger than the number of triangular mesh elements. In contrast, the curvatures are represented less accurately with voxels. A single triangular mesh element requires three vertices and a normal vector defined. A single voxel is defined by its coordinates and a binary mask. This can make volumetric modeling less suitable for certain applications, particularly those with limited computational resources or tight performance constraints, such as real-time rendering or interactive applications (Aremu et al., 2017).

Another challenge is the conversion between surface and volumetric representations. This conversion process can be complex and may introduce errors or artifacts, especially when dealing with complex geometries or intricate internal structures. Ensuring that the generated volumetric model maintains the essential characteristics of the original surface model can be challenging and may require sophisticated algorithms and techniques (Noorud-din and Turk, 2003; Strand, 2004).

¹Named after the wife of its creator Gershon Elber – Irit

²Short for IRIT



Figure 2.8 Triangular mesh and voxel methods for representing original geometry representations. Adapted from ([Schnös et al., 2021](#)).

Moreover, voxel-based representations, commonly used in volumetric modeling, can suffer from aliasing artifacts and a loss of fine details when the voxel resolution is insufficient. A higher voxel resolution is needed to capture high-frequency details, increasing the memory and computational requirements. This trade-off between accuracy and performance is a common challenge in volumetric modeling applications ([He et al., 1995](#); [Laine and Karras, 2010](#)).

2.1.3 Hybrid modeling

The respective benefits of surface-based and volumetric geometric modeling approaches have led to the development of hybrid modeling techniques that aim to capitalize on the strengths of both methods. Surface-based methods, well-established in the AM process, offer significant ease of manipulation when working with geometry. In contrast, volumetric methods, particularly voxel-based models, provide greater computational flexibility by facilitating operations with 3D matrices ([Wang et al., 2005](#); [Tang et al., 2019](#)).

The development of hybrid modeling techniques has involved various approaches, such as integrating voxel-based models with surface representations or combining different volumetric and surface-based models within a single framework ([Wang et al., 2005](#)). For

example, the work of Wang et al. (2005) presents a hybrid modeling method that constructs volumetric models from surface representations, enabling the efficient manipulation of complex geometries and facilitating Boolean operations. Another example is the work of Tang et al. (2019), which introduces a hybrid mesh representation that combines surface-based and volumetric meshes hybrid models that incorporate surface-based and volumetric elements to improve the efficiency and quality of 3D shape processing and analysis.

However, hybrid modeling techniques are not without limitations, as they inherit constraints from the original geometric modeling frameworks, such as limited parametrization. These limitations encompass the inability to model non-linear variation of geometric parameters and the restricted amount of controllable parameters (Letov and Zhao, 2022).

2.1.4 Function representation concepts and their application in geometric modeling of cellular structures

Function representation, here onwards referred to as F-rep, is a mathematical approach used in geometric modeling and computer graphics for the representation and manipulation of geometric objects (Pasko et al., 1995). This method describes a shape or object by defining an implicit function, which assigns a scalar value to each point in the 3D space. The object's surface is represented by the zero set of the implicit function, i.e., the set of points in space where the function value is equal to zero (Bloomenthal et al., 1997).

F-rep offers several advantages over other geometric modeling techniques, such as the ability to represent complex shapes, seamless blending of objects, and smooth transitions between different geometric features (Pasko et al., 1995). Moreover, F-rep can handle both solids and surfaces, allowing for efficient representation of complex and heterogeneous structures (Pasko and Adzhiev, 2004).

In F-rep, a solid is considered to be defined by its defining real-valued function F as

follows:

$$F(\mathbf{X}) \geq 0, \quad (2.2)$$

where $\mathbf{X} = (x, y, z) \subset \mathbb{R}^3$ is the design space, such that $F(\mathbf{X}) \geq 0$ is the solid itself, with $F(\mathbf{X}) = 0$ being the surface of the solid, and $F(\mathbf{X}) < 0$ is the rest of the design space (Pasko et al., 1995). Note that the design space \mathbf{X} is not limited by existence in the 3D Euclidean space E^3 , as printing of non-Euclidean geometry is a topic of interest in AM nowadays (Zurlo and Truskinovsky, 2017; Mensch et al., 2021).

Even though F-rep existed before the rise of AM, using real functions for representing solid models demonstrated advantages in providing higher design freedom compared to the conventional Boolean methods of modeling (Shapiro, 1994). Modern F-rep methods also allow the modeling of both explicit and implicit functions. In this thesis, a function $F : \mathbb{R}^n \mapsto \mathbb{R}$ is called explicit if an expression defines F . This expression is a relation solved for one of its independent variables, for example, $F(x) := x^2 + 2x + 1$. A function $F : \mathbb{R}^n \mapsto \mathbb{R}$ is called implicit if F is defined by a relation not solved for one of its independent variables, for example, $x^3 F^3(x) = F(x) + 2x$.

Comparing $F(\mathbf{X})$ with 0 in F-rep allows the modeling of implicit surfaces bounding the solid body without calculations needed to convert them into explicit surfaces. For example, a solid torus \mathbb{T}_S is implicitly defined by

$$\mathbb{T}_S(x, y, z) : -F(\mathbf{X}) = \left(\sqrt{x^2 + y^2} - R \right)^2 + z^2 - r^2 \leq 0, \quad (2.3)$$

where x , y , and z are the Cartesian coordinates, R is the radius from the center of the hole to the center of the torus, and r is the radius of the tube.

The torus \mathbb{T} can be explicitly defined by its standard form derived from solving $F(\mathbf{X}) =$

0 for z :

$$\mathbb{T}(x, y, z) : z = \pm \sqrt{r^2 - R^2 + 2R\sqrt{x^2 + y^2} - x^2 - y^2}. \quad (2.4)$$

Equation 2.4 requires additional calculations to derive it from the standard form in Equation 2.3. While solving $F(\mathbf{X}) = 0$ for the torus \mathbb{T} results in Equation 2.4, solving $F(\mathbf{X}) \geq 0$ for the solid torus \mathbb{T}_S requires more conditions that need to be taken into account. Moreover, there are cases when an explicit form of the function cannot be achieved, such as the functions defined by $x^2y^2 = (x + y)^3 - \sqrt{xy}$ and $x\sqrt{\cos(xy)} = e^y$. Thus, using implicit functions as an input is a significant advantage of F-rep, which amplifies further because cellular structures can be defined as a set of functions.

Initially, implicit surfaces used in F-rep had limited support for R -functions, sweeping, and other operations that are common for conventional CAD systems. F-rep methods use non-trivial solutions to this issue to mitigate this limited support, such as moving solids (Sourin and Pasko, 1996). The R -function support drastically increases the flexibility of geometric modeling by allowing a complete definition of geometry with the terms of real analysis (Shapiro, 2007). Naturally, such a viable tool is now found to be supported by most of the F-rep geometric modeling approaches.

Still, there are certain disadvantages to using the F-rep modeling. Defining a geometrically complex structure, such as a heterogeneous cellular structure, is complicated by the necessity of defining rules by which lattice parameters or topology vary throughout the structure in a set of mathematical functions. The review of related literature identified that such a process could be arduous for an engineering designer and that there is no tool so far that would simplify this design process significantly enough, while it is clear that AM could benefit from such a tool (Liu et al., 2017). Moreover, the function by which a geometrical shape is formed is not clearly defined in some cases, such as in the bio-inspired

design ([Letov et al., 2021](#)).

It was shown that F-rep is applicable to the geometric modeling of cellular structures, as their geometry can be defined simply by periodic functions ([Pasko et al., 2011](#)). For example, HyperFun – an F-rep programming language – can model a simple homogeneous cellular structure illustrated in Fig. 2.9 in a simple loop ([Pasko et al., 1999](#)). Note that this representation is simplistic as nodes are not modeled, and the cellular structure is homogeneous. Also, note that HyperFun used to be open-source but is not publicly available anymore ([Adzhieva et al., 2020](#)). The ability to render periodic structures and mathematically well-defined Boolean operations between functions allowed F-rep to find its application for modeling heterogeneous cellular structures ([Alkebsi et al., 2021](#); [Wang and Tamjani, 2022](#)).

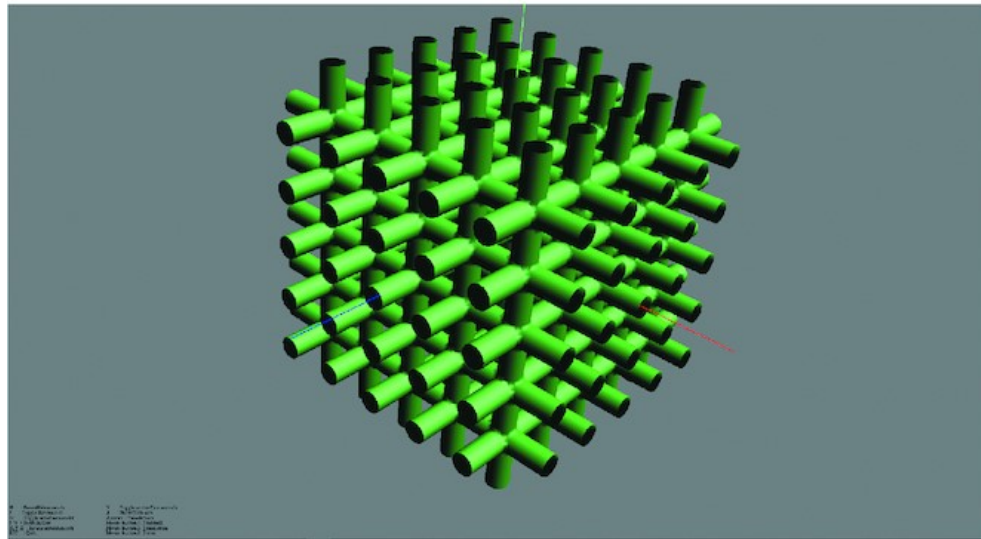


Figure 2.9 A homogeneous cellular structure with the simple cubic topology generated with HyperFun ([Letov and Zhao, 2022](#))

While modeling a TPMS is not complicated in F-rep, as can be seen in the example with HyperFun in Fig. 2.10a, the resulting structure in Fig. 2.10b is a TPMS with no thickness and thus cannot be manufactured. F-rep requires additional effort to derive equations

needed to derive a solid structure based on a TPMS. In this example, the model is set to $F(\mathbf{X})$, which defines the boundary surface $F(\mathbf{X}) = 0$ in 3D Cartesian coordinates.

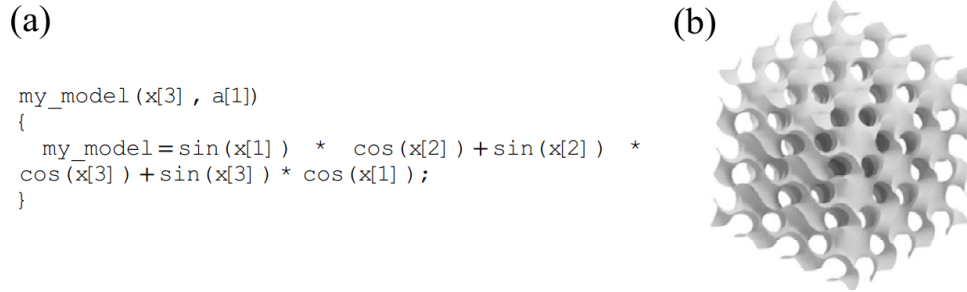


Figure 2.10 (a) A code snippet of a HyperFun program that generates a gyroid surface and (b) the resulting model ([Letov et al., 2021](#))

2.1.5 Multi-scale modeling

Geometric modeling of complex structures often involves addressing various challenges, including incorporating multi-scale modeling support, particularly for bio-inspired structures ([Chen et al., 2017](#)). These structures often require sufficient and accurate visual information at both meso- and macro-scales to be effectively represented ([Rawson et al., 2015](#)).

In geometric modeling and computer graphics, the level of detail (LOD) is widely applied to reduce computational costs by adjusting the model's complexity according to the required level of detail. This involves decreasing or increasing the number of details in the model based on the desired LOD. Figure 2.11 illustrates how the complexity of the Stanford bunny's surface mesh model changes with the number of polygons ([Luebke et al., 2003](#)). Higher LODs correspond to more detailed renderings.

Typically, LOD is manually or automatically associated with CAD features, as shown in Fig. 2.12. However, bio-inspired structures are often designed using parametric modeling

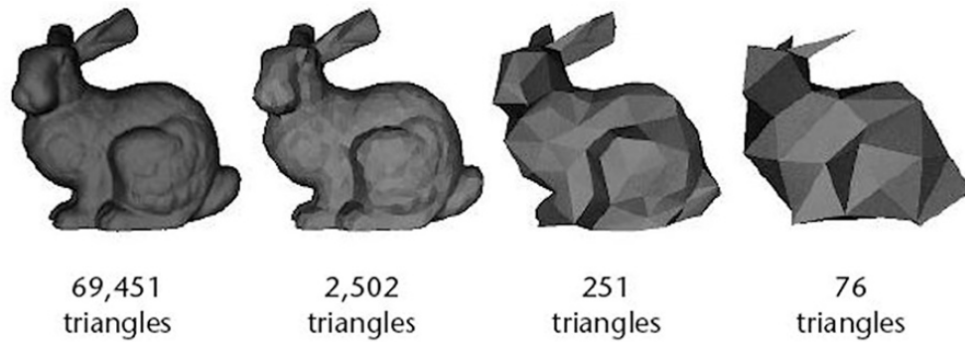


Figure 2.11 Reducing the complexity of a 3D model by adjusting its level of detail, which directly corresponds to the number of polygons required for rendering (Luebke et al., 2003)

techniques rather than feature-based approaches, leading to ambiguity in determining the features corresponding to each LOD.

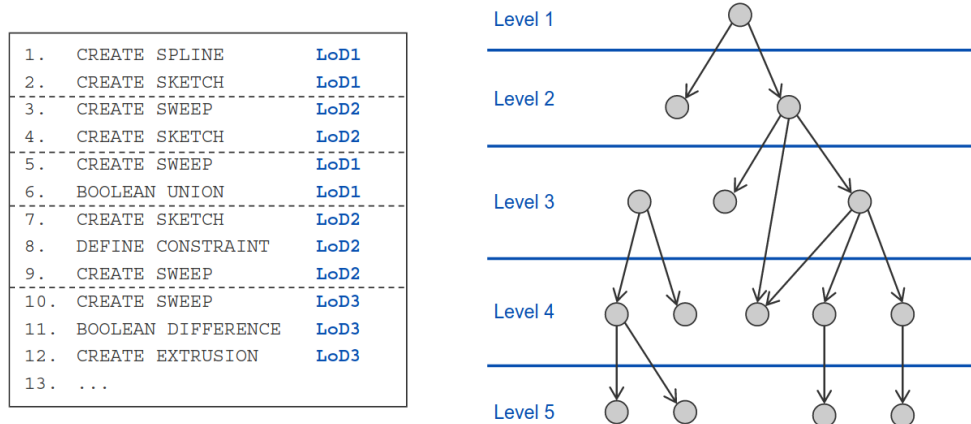


Figure 2.12 Levels of detail associated with Boolean operations in feature-based CAD (Borrman et al., 2015)

Interestingly, the challenge of LOD ambiguity is not limited to bio-inspired structure modeling but also arises in other research areas, such as geoinformatics and medicine. For example, in geoinformatics, researchers may need to consider 3D scans of large archaeological sites, like the Maya civilization, from various LODs ranging from an entire city (LOD0) to intricate column ornament details (LOD3) (Agugiaro et al., 2011). Similarly, in

medicine, a multi-scale geometric modeling approach is necessary for accurately modeling a human heart, where even minor defects can have significant consequences (Rawson et al., 2015; Sacks et al., 2017).

Despite the potential benefits of multi-scale modeling, current voxelization methods are not adaptive due to difficulties in clustering voxels (Weiler et al., 2000). This limitation forms a research gap due to the absence of an appropriate adaptive voxelization algorithm for geometric modeling. An effective adaptive voxelization approach would enable automatic changes in voxel size based on the user's point of view and the corresponding LOD. Existing methods struggle to represent critical features of a part on a larger scale using voxels (Seemann et al., 2016) and become inefficient on smaller scales (Kauker et al., 2016). Key challenges in this area include determining which features should be associated with LODs, recognizing and classifying these features, and identifying the appropriate voxel size for accurate representation.

2.2 Challenges in geometric modeling of complex structures

The bio-inspired design has gained significant attention in recent years due to its potential for creating innovative, sustainable, and efficient solutions to various engineering challenges. However, the inherent complexity of biological structures often poses challenges in the geometric modeling of these designs. This section of the thesis will discuss some of the primary challenges and limitations of geometric modeling to support the bio-inspired design.

Designers frequently encounter difficulties when attempting to create micro-structures that mimic the features of animals or plants, particularly during the conceptual development phase when sketching ideas (Velivila et al., 2021).

One of the main challenges in the geometric modeling of bio-inspired designs is the

intricate and often hierarchical organization of biological structures. These structures are characterized by multi-scale features, which can be challenging to replicate in a computational model ([Wen et al., 2014](#)). Biological structures often exhibit unique structural properties, such as anisotropy, heterogeneity, and graded properties, which are challenging to model and replicate in engineering materials ([Gibson, 2012](#)). For example, it can be seen from Fig. 2.13 that wooden materials can be replicated only by foam materials which are typically difficult to control and only in certain conditions. Due to the complexity and multi-scale nature of biological structures, geometric modeling of bio-inspired designs can demand significant computational resources, which may not be readily available or accessible to all designers ([Fang et al., 2017](#)). The successful geometric modeling of bio-inspired designs should consider the limitations of manufacturing processes, such as additive manufacturing or traditional machining techniques, which might not be capable of producing the intricate features of bio-inspired designs ([Stratakis et al., 2020](#)).

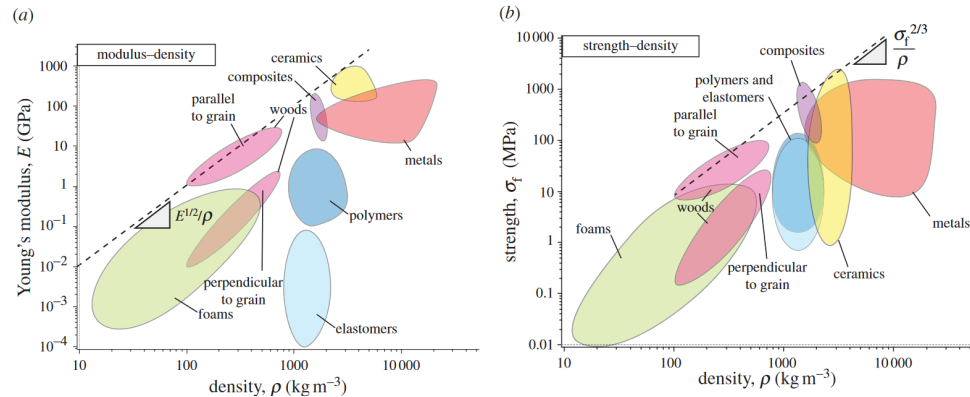


Figure 2.13 (a) The Young's modulus–density and (b) the strength–density chart for engineering materials, including woods ([Gibson, 2012](#))

Consequently, designers often simplify the design by redefining the concept and seeking inspiration from other animals or organisms ([Federle et al., 2002](#); [Song et al., 2016](#)). One example of such design simplification is the following design case study of a dental implant

masking cap. In this case study, an initial surface concept inspired by the feet of a gecko (*Gekkota*) in Fig. 2.14 was transitioned to a simpler design inspired by the claw of a common black ant (*Lasius niger*) in Fig. 2.15 due to modeling and fabrication challenges (Huang et al., 2010; Velivila, 2018). The initial gecko-inspired concept aimed to provide a sticky surface for dental implants during chemical etching. However, designing the setae (micro-hair) of the gecko's feet proved challenging, as was the fabrication process. Inspired by an ant's claw, the final design is significantly less complex than the initial bio-inspired concept but serves its intended function sufficiently.

This case study is just one example of how bio-inspired designs can be affected by geometric modeling and manufacturing limitations. Other examples include bio-inspired cellular structures resulting from topology optimization, which often require advanced graphics processing capabilities and highly capable geometric modeling tools (Alsheghri et al., 2021).

2.3 Challenges in the geometric modeling of heterogeneous cellular structures

Cellular structures, a subset of bio-inspired structures in this research, are inspired by the intricate formations found in nature, such as the hexagonal matrix of honeycombs, the complex patterns of spider webs, or the porous structures of bones. These structures, although complex, have been increasingly manufactured via AM techniques due to its advancements in the past two decades (Dong et al., 2017). Cellular structures offer unique properties, such as optimal performance-to-weight ratio, variable elasticity, and water absorption or resistance, which are not typically seen in conventionally manufactured parts (Frulloni et al., 2007; Martínez et al., 2016; Schumacher et al., 2015).

Geometric parameters like the cross-section of the lattice beam or the truncation of

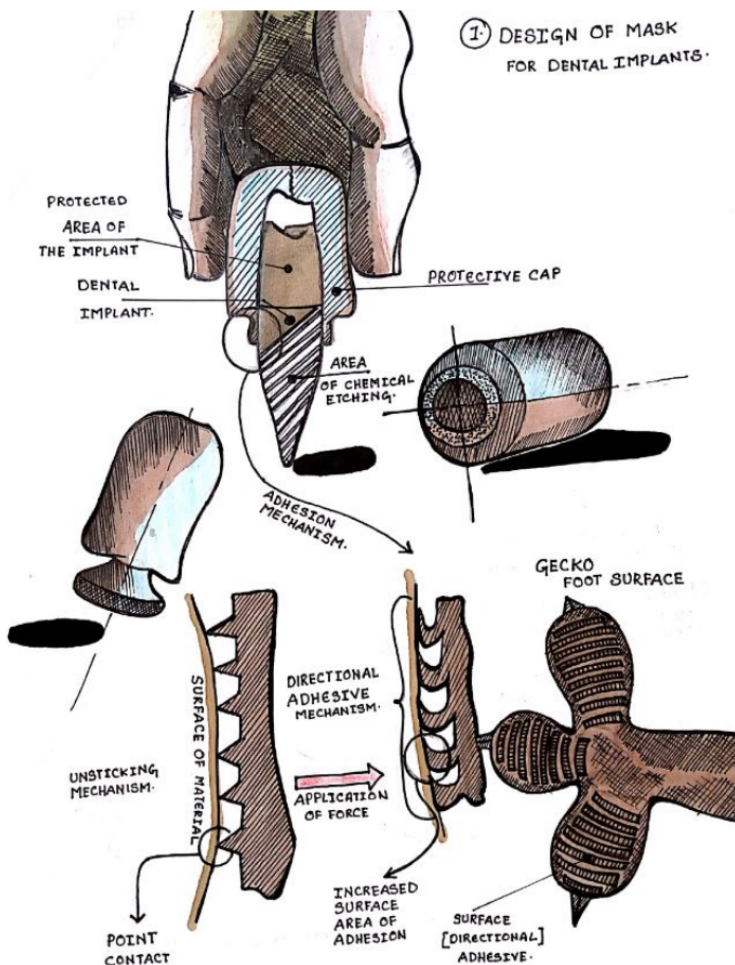


Figure 2.14 The conceptual sketch of a gecko-inspired surface that sticks to the implant surface ([Velivila, 2018](#))

some topologies may vary across the structure, contributing to a different kind of heterogeneous lattice. While these parameters are not commonly studied in AM, they have seen extensive use in other industries, such as construction, where I-beams offer optimal bending properties ([Kloft et al., 2023](#)). Moreover, truncated cube topologies can mitigate node stress concentration, depending on the truncation size ([Hedayati et al., 2016](#)). Currently, geometric modeling techniques for such optimized structures are yet to be developed ([Letov and Zhao, 2022, 2023a](#)).

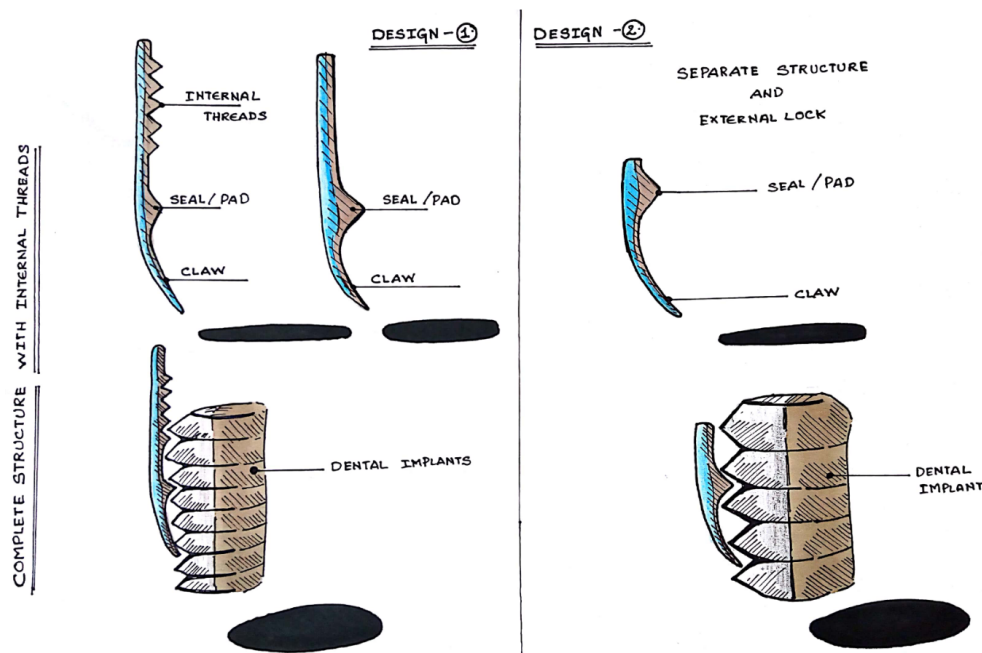


Figure 2.15 Two conceptual designs inspired by an ant's claw ([Velivila, 2018](#))

Bio-inspired cellular structures, which are primarily heterogeneous, can mimic complex geometric shapes found in nature and offer a wider range of design possibilities ([Zheng, 2019](#)). They are primarily used in specialized cases where unique biological properties are needed ([Hancock et al., 2012; Liu et al., 2014](#)). For example, a heterogeneous sponge-like cellular structure can make a part ultra-lightweight while maintaining strength and energy absorption ([An and Fan, 2016](#)).

Geometric modeling of homogeneous cellular structures is well-documented ([Kucewicz et al., 2018](#)). However, the modeling of heterogeneous cellular structures is more complex due to their semi-periodic nature. Modeling these structures requires various techniques to capture features of different sizes and shapes, such as nodes and struts ([Leonardi et al., 2019](#)). This complexity often leads to substituting these models with homogenized versions or 2D cross-sectional analogs, neither of which provide accurate information about a

heterogeneous object ([Tang et al., 2019](#)).

Traditional CAD systems present challenges when designing cellular structures. The primary issue lies in the difficulty of describing cellular structures using Boolean operations, akin to the challenge of associating LODs to CAD features ([Liu et al., 2021b](#)). Creating heterogeneous cellular structures with descriptive CAD systems is even more challenging due to their inherent complexity. The geometric modeling of heterogeneous cellular structures often requires large amounts of computational resources due to the intricate and variable nature of these structures. The increased complexity may lead to longer processing times, negatively impacting the overall design and manufacturing process. High-performance computing and parallel processing techniques can help address this issue by reducing the computational time required for modeling and analysis ([Abueidda et al., 2017](#)), but they are not readily accessible to average design engineers.

Heterogeneous cellular structures often consist of numerous interconnected elements, such as struts and nodes, which can lead to significant memory requirements when modeled and analyzed. Efficient memory management techniques and data compression strategies are crucial for handling the large-scale data associated with these structures.

Accurate and efficient mesh generation is critical for modeling heterogeneous cellular structures. It directly impacts the quality of the resulting FEA and computational fluid dynamics (CFD) simulations. Automatic mesh generation and optimization techniques that can adapt to the complex geometry of these structures are essential for ensuring accurate and efficient simulations ([Aage et al., 2017](#)).

Heterogeneous cellular structures often exhibit multi-scale properties, with features ranging from macroscopic to microscopic scales. As discussed in Section [2.1.5](#), this necessitates the development of multi-scale modeling techniques that can capture the geometric and mechanical behavior of these structures at different scales while maintaining compu-

tational efficiency. Due to the variability in heterogeneous cellular structures, adaptive modeling techniques that can automatically adjust the model's resolution and parameters based on the desired level of detail and computational resources available are essential for efficient geometric modeling.

It has been proposed that since bio-inspired structures are challenging to model, a potential method to model such structures could be bio-inspired as well ([Letov and Zhao, 2021](#)). Indeed, discretization plays a crucial role in both geometric modeling and the structure of living organisms. In geometric modeling, discretization allows for control over mesh size and density, which in turn influences the quality and complexity of the model. Similarly, living organisms comprise small building blocks called cells ([Letov and Zhao, 2021](#)). One example of discretization in nature is the tessellation of the epidermis, the upper layer of human skin, as shown in Fig. 2.16. This discretization resembles the triangular mesh used in geometric modeling.

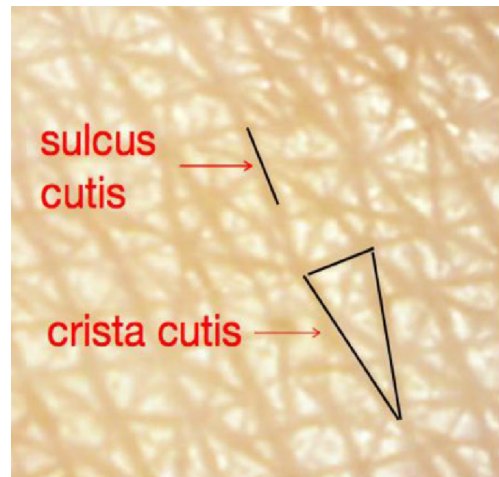


Figure 2.16 Skin texture ([Li et al., 2022a](#))

Recent research has started exploring bio-inspiration for modeling and simulating complex structures, analogous to how deep neural networks are inspired by neuron activity in

the brain ([Ivakhnenco and Lapa, 1967](#)). For example, [Dimas and Buehler \(2014\)](#) proposed a novel modeling technique for bio-inspired composites, which focuses on simulating 2D cross-sections of the composite. [Fantini et al. \(2016\)](#) developed a method for designing bio-inspired structures based on Voronoi lattices.

Considering discretization in nature, examining living organisms with easily analyzable structures, such as humans, is essential. The evolutionary process has led to the development of optimal shapes and structures in living organisms over billions of years. One such example is the scutoid cells, which are 3D solids bounded by two polygons lying in parallel surfaces (not necessarily planar) and with vertices interconnected either by curves or by Y-shaped connections, as seen in Fig. 2.17 ([Gómez-Gálvez et al., 2018](#)). However, bio-inspired algorithms or techniques for geometric modeling have yet to be developed.

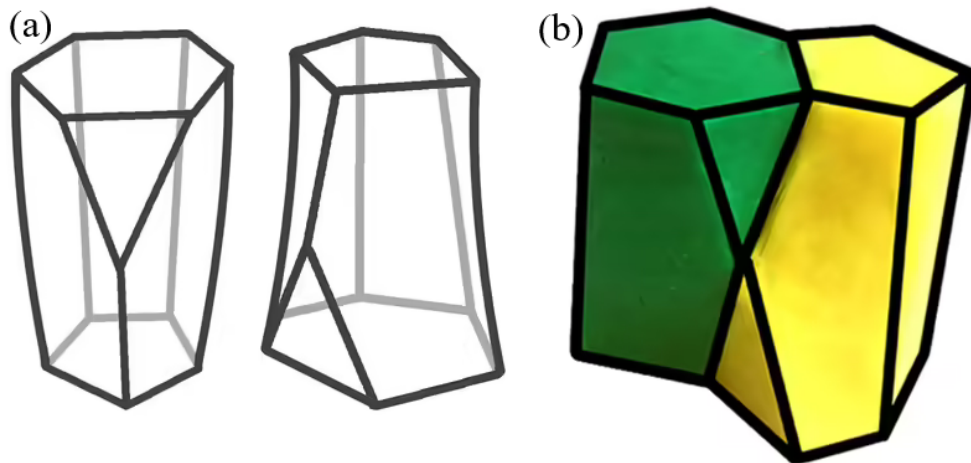


Figure 2.17 Two scutoids (a) shown transparent separately and (b) shown opaque and transitioning one into another ([Gómez-Gálvez et al., 2018](#))

Surface mesh modeling mimics discretization in a manner similar to how human skin consists of skin cells but does not model the interior. Voxels typically discretize a design space into cubes, while cell geometry is not necessarily cubic ([Savio et al., 2018](#)). Although non-cubic voxels, such as body-centered cubic (BCC) and face-centered cubic (FCC) vox-

els, have been investigated, they have not demonstrated significant advantages over cubic voxels ([Strand, 2004](#)). Sparse voxel octree techniques enable modeling with voxels of different sizes ([Laine and Karras, 2010](#)); however, the cubic shape of voxels remains unchanged, limiting the variety of shapes that can be represented.

Given that bio-inspired structures originate from nature, it is crucial to be able to model a variety of shapes. Both mesh and voxel modeling face computational and accuracy-related challenges when applied to complex geometric objects. Consequently, for bio-inspired geometric modeling, other bio-inspired geometry classes should be considered ([Schulz, 2009](#)).

In nature, numerous shapes and sizes of cells together converge into a living body. These parameters are defined by the cell division process, which in turn is defined by genetics and external conditions. Thus, it is required to consider the cell division process in more detail.

Appendix A presents a detailed case study demonstrating the practical implementation of a bio-inspired geometric modeling approach. This approach leverages the long axis rule (LAR) and surface-to-volume ratio (SVR) minimization techniques to create a more efficient and adaptive solution than traditional modeling methods. However, there are several limitations to this approach. First, the LAR method can generate a high level of inconsistency between volumetric cells and a large variety of shapes. Second, the SVR method may lead to volumetric cells that do not fit the framework, as they correspond to 2-manifolds of genus higher than 0. Additionally, the manual combination of the LAR and SVR methods may not result in an optimal solution. Typically, the development of such an approach requires a substantial team of programmers and mathematicians working together, which can be resource-intensive and time-consuming. Overall, while the bio-inspired geometric modeling approach offers promising improvements over traditional methods, it still faces significant challenges that need to be addressed outside of the scope of this thesis.

2.3.1 Challenges associated with surface modeling to model heterogeneous cellular structures

Applying surface modeling techniques like the polygonal mesh, B-rep, CSG, IGA, and subdivision surfaces to design complex structures comes with unique challenges related to accurately representing intricate geometries, managing computational demands, and ensuring efficient mesh generation.

Polygonal mesh often represents 3D objects using interconnected polygons (usually triangles or quadrilaterals). Creating a high-quality polygonal mesh can be challenging for complex structures with intricate details. The mesh must accurately capture the geometry while minimizing the number of polygons used ([Botsch and Kobbelt, 2004](#)). Additionally, the mesh quality directly impacts the results of FEA and CFD simulations ([Hirt and Nichols, 1981](#)). Bio-inspired structures often exhibit intricate and irregular geometric features. Representing these features using standard surface modeling techniques can be difficult and time-consuming, as these techniques may struggle to capture the high level of detail and organic nature of the geometry.

B-rep models use a combination of vertices, edges, and faces to define the boundaries of 3D objects. Complex structures with organic shapes, intricate details, or multiple interconnected components can be challenging to model and manipulate using B-rep due to its reliance on precise topological relationships ([Lee and Lee, 2001](#)). Maintaining a consistent and accurate topology becomes increasingly challenging as the complexity of the structure increases.

CSG models represent 3D objects using a combination of primitive shapes and Boolean operations. Designing complex structures with CSG can be challenging due to the limitations of Boolean operations, which may not adequately capture the intricate details

and relationships present in the structure ([Liu et al., 2021b](#)). Creating and modifying complex structures in CSG often requires manual input and manipulation, which can be time-consuming and error-prone ([Rossignac and Requicha, 1986](#)).

IGA unifies the geometric representation of a structure with its analysis using the same mathematical basis, such as NURBS or T-splines. While IGA provides a more accurate representation of complex structures, it can also increase computational complexity and demands, especially when dealing with large-scale structures or intricate details ([Cottrell et al., 2009](#)). Additionally, IGA requires specialized knowledge and expertise to properly implement and use, which may not be readily available to average design engineers ([Bazilevs et al., 2010](#)).

Subdivision surfaces enable the creation of smooth and organic shapes by recursively refining an initial coarse mesh. While this technique is well-suited for modeling complex, organic shapes, it can be computationally expensive for large-scale structures or those with intricate details ([Stam, 1998](#)). Additionally, controlling the local and global properties of the generated surfaces can be challenging, as it often requires manual input and fine-tuning ([Zorin et al., 1997](#)).

Bio-inspired, homogeneous, and heterogeneous cellular structures often exhibit intricate and irregular geometric features. Representing these features using standard surface modeling techniques can be difficult and time-consuming. These techniques may struggle to capture the high level of detail and organic nature of the geometry ([Vaxman et al., 2016](#)). Such structures may have features at multiple scales, ranging from macroscopic to microscopic. Traditional surface modeling techniques may not efficiently handle multi-scale modeling, which is necessary to accurately represent the geometric and mechanical behavior of these structures at different scales. Designing these structures using surface modeling techniques can be computationally intensive, especially for models with a high

level of detail and complexity. This may increase processing times, negatively impacting the overall design and manufacturing process ([Botsch and Kobbelt, 2004](#)).

Overall, while surface modeling techniques offer powerful tools for designing complex structures, they also present challenges related to accurately capturing intricate geometries, managing computational demands, and ensuring efficient mesh generation. Overcoming these challenges requires a deep understanding of the specific technique and the development of novel approaches that address the unique requirements of complex structures ([Liu et al., 2021b](#)).

2.3.2 Challenges associated with volumetric modeling to model heterogeneous cellular structures

Applying volumetric modeling techniques such as voxels, V-rep, and FVM to design complex structures presents several challenges. Complex structures may have intricate and irregular geometric features. Volumetric modeling techniques can struggle with capturing these features accurately, leading to approximations and potential loss of geometric fidelity. This can be especially problematic in applications where high precision is crucial ([Batty et al., 2007](#)). Bio-inspired and heterogeneous cellular structures often have intricate and irregular geometric features.

Volumetric modeling techniques, such as voxel-based approaches, often consume large amounts of memory due to the discretization of the entire volume, leading to significant storage and computational costs. This can be a limitation when working with complex structures such as bio-inspired and heterogeneous cellular structures, especially at high resolutions ([Laine and Karras, 2010](#)).

Bio-inspired and cellular structures often require fine discretization to capture intricate details. However, volumetric techniques such as voxel-based representations can suffer from

scalability issues, as the number of elements increases rapidly with finer discretization, resulting in memory and computational challenges ([Roettger et al., 2003](#)).

Generating high-quality meshes for FEA or computational fluid dynamics (CFD) simulations from volumetric models can be challenging, especially for bio-inspired and heterogeneous cellular structures with intricate geometries and topologies. Ensuring accurate simulation results requires careful mesh generation and processing ([Hirt and Nichols, 1981](#)). Complex structures often have intricate and irregular geometric features, which may not be easily represented using a single modeling technique. Hybrid approaches aim to capture these features more accurately by combining different methods, but this can lead to increased complexity in the overall modeling process and may introduce new challenges in terms of geometric fidelity.

2.3.3 Challenges associated with hybrid modeling to model heterogeneous cellular structures

Applying hybrid geometric modeling techniques to design complex structures presents several challenges, as these techniques aim to combine the advantages of various modeling approaches. Integrating these different techniques seamlessly can be challenging, as they may have distinct data structures, mathematical foundations, and computational requirements ([Shapiro, 2002](#)).

Developing efficient data structures and algorithms for handling these different techniques can be challenging, as it requires careful consideration of memory consumption, processing times, and scalability. Generating high-quality meshes from hybrid models for FEA or CFD simulations can be challenging, especially for bio-inspired and heterogeneous cellular structures with intricate geometries and topologies. Ensuring accurate simulation results requires careful mesh generation and processing, which the presence of multiple

modeling techniques may further complicate.

2.4 Existing software tools for the geometric modeling of cellular structures

As the AM industry has expressed growing interest in modeling heterogeneous cellular structures, various software tools have emerged due to academic research and CAD providers' efforts.

Generally, a prevalent issue among many cellular structure modeling and CAD tools is their predominant support for the Microsoft Windows OS. This limitation stems from the fact that most GMKs, responsible for mathematical computations and rendering, have been developed specifically for Windows. GMKs depend heavily on GPUs for parallel computing, and Windows offers time-tested proprietary GPU drivers. However, Apple macOS has recently introduced the M1 CPU, which can handle parallel computing in a manner similar to a GPU ([Becker et al., 2021](#)). Furthermore, Linux provides greater customization potential and can easily support proprietary GPU drivers while maintaining lower OS performance than Windows. As macOS and Linux are based on the Unix OS family, developing cross-platform software tools between these systems becomes more accessible. Consequently, it is possible to expect more cross-platform geometric modeling tools in the future.

Open-source geometric modeling tools have demonstrated their ability to improve the design experience for AM ([Letov and Zhao, 2023b](#)). However, the literature review reveals a general lack of free and open-source (FOSS) applications in engineering and, more specifically, design in AM ([Junk and Kuen, 2016](#)). This scarcity of FOSS applications results in a shortage of lean, agile, and accessible engineering design tools ([Brasseur, 2018](#)).

This section delves into software packages for the geometric modeling of heterogeneous cellular structures. Section 2.4.1 discusses the use of surface modeling software tools to create cellular structures and their limitations. Section 2.4.2 highlights the advantages of tools that use voxel-based modeling for heterogeneous cellular structures and the use of these tools for extracting geometry from computer tomography scans. Section 2.4.3 discusses tools that use surface and volume modeling methods for a more comprehensive approach to designing complex, bio-inspired cellular structures. Section 2.4.4 provides a comparative analysis of various tools and their capabilities in modeling cellular structures, showcasing their strengths and limitations. Finally, the graphical user interface of software packages for the geometric modeling of cellular structures is discussed in Section 2.4.5.

2.4.1 Surface modeling-based software tools

Surface modeling is a vital approach in cellular structure modeling, and several tools have been developed to facilitate this process. For instance, Autodesk Netfabb ([Autodesk Inc., 2017](#)) requires users to provide a design space or select one from standard types. Users then select a topology from a substantial list, which includes beam-based and triply periodic minimal surfaces (TPMS). However, user customization of this list is not possible. Autodesk Netfabb also permits the application of a linear gradient field to the design space, which varies the thickness of the cellular structure. However, this gradient does not allow changes to other cellular parameters and only supports linear variations.

Sulis Lattice ([Gen3D Ltd., 2019](#)) is another tool for modeling cellular structures. It allows importing a CAD model to be used as a design space for lattice generation. Like Autodesk Netfabb, Sulis Lattice also provides a list of topologies and enables adding a linear gradient distribution of thickness. Nonetheless, it does not support non-linear thickness distribution or variation of parameters beyond beam or surface thickness.

Rhinoceros 3D ([Robert McNeel & Associates, 2020a](#)) offers more versatility in modeling heterogeneous cellular structures. As a parametric CAD tool, it allows fine-tuning of geometric parameters and the scripting of designs with embedded Python support ([Gao et al., 2023](#)). Within Rhinoceros 3D, Grasshopper 3D ([Davidson, 2009](#)) provides visual scripting of parametric models and support for custom plugins that can aid cellular design. Intralattice ([Kurtz, 2009](#)), developed as a part of research efforts preceding this work, is one such plugin that can model cellular structures with custom topologies. However, Intralattice's capabilities are limited to modeling conformal cellular structures, which strive to fit a custom design space. For example, the tire design shown in Fig. 2.18 has the design space filled with a conformal cellular, which can be considered homogeneous in cylindrical coordinates. Intralattice does not support heterogeneity in other geometric cellular parameters.

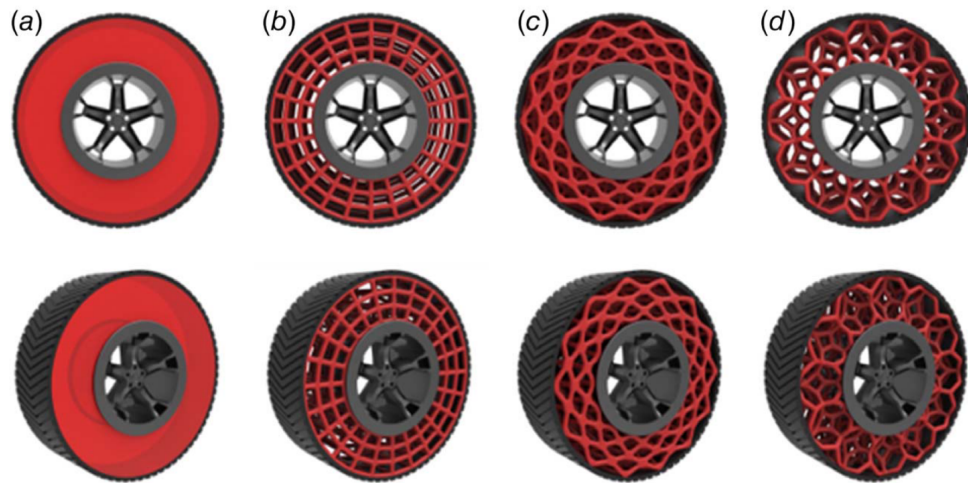


Figure 2.18 Tire designs with different lattice topologies, which include (a) bare design space, (b) grid lattice, (c) X lattice, and (d) vintiles lattice modeled with Intralattice ([Kurtz, 2009](#))

Crystallon ([F EQUALS F LLC., 2019](#)), another plugin for Rhinoceros 3D, allows conformal cellular modeling with a topology chosen from a list of available ones ([Letov et al., 2021](#)). Like Intralattice, Crystallon does not support the modeling of heterogeneous cellular

structures. However, literature reports a case where Intralattice and Crystallon were used in the same cellular generation project ([García-Dominguez et al., 2020](#)). Intralattice was preferred for defining topologies due to its ease, while Crystallon was better at generating nodes. To address the limitations of Intralattice and Crystallon, Dendro ([ECR Labs, 2018](#)), another plugin for Grasshopper 3D, was developed. Dendro uses voxel modeling techniques provided by OpenVDB ([Academy Software Foundation, 2012](#)) to model linearly heterogeneous cellular structures. However, it does not support non-linear heterogeneity.

2.4.2 Volumetric modeling-based software tools

Voxel-based modeling is increasingly popular due to its potential applications in heterogeneous cellular structure modeling. Selecting the appropriate voxel size for conventional manufacturing can be ambiguous, particularly for solid models with significant variations in the radius of curvature. However, in AM, the voxel size does not need to exceed the tolerance of a 3D printer, as a higher voxel resolution would not be manufacturable ([Letov et al., 2021](#)). Assigning material in the voxelized model of a multi-material cellular structure is straightforward, as each voxel can be designated a different material ([Liu et al., 2022](#)).

An alternative approach to obtaining volumetric CAD models of heterogeneous cellular structures and other bio-inspired structures is exporting geometry from computer tomography scans. Tools such as Materialise Mimics [Materialise NV. \(2012\)](#) and Dragonfly ([Object Research Systems, 2018](#)) can retrieve these models. Materialise Mimics can segment imported medical images, which can then be converted into solid models and filled with a cellular structure using the Materialise 3-matic tool. Similarly, the output solid models in Dragonfly can be subjected to various manipulations. For instance, a porous bone structure can be visualized as a graph with all the nodes and links extracted ([Reznikov et al.,](#)

2020). These tools offer a unique perspective on understanding biological structures and are often employed in AM for prosthetic parts. It is important to note that while biological structures are typically heterogeneous, existing tools frequently lack precise control over the geometric parameters of heterogeneous cellular structures (Letov and Zhao, 2021).

2.4.3 Hybrid modeling-based software tools

Implicit modeling approaches offer significant advantages when applied to the geometric modeling of heterogeneous cellular structures. Explicit modeling techniques require individually modeling each beam or surface region of a cellular structure. In contrast, implicit modeling techniques provide high-level functions that simplify complex geometry definition by bundling lower-level functions (Nguyen et al., 2021).

nTopology (nTopology, Inc., 2017), a popular heterogeneous cellular modeling tool, allows users to define topologies as skeletal graphs, which can be thickened to obtain the desired solid cellular structure model. This approach is based on voxelizing the space around the skeletal graph and adding or removing layers of voxels to adjust the thickness (nTopology, Inc., 2017). In addition to linear thickness variation, nTopology introduces topology optimization to control thickness based on estimated stresses. Topology optimization can be considered an implicit geometric modeling method due to limited user input and control over geometric parameters (Hamri et al., 2010).

Randomized cellular structures such as the Voronoi scaffold illustrated in Fig. 1.8a often require specialized approaches. For example, consider a Voronoi scaffold with no unit cells in common sense. Designing a Voronoi scaffold requires setting general geometric parameters of the cellular structure rather than the geometric parameters of each unit cell. These parameters include the number of Voronoi seeds and the size of pores (Fantini et al., 2016). Such randomized structures often appear in nature. At the same time, beam-

based cellular structures are not common in nature, and an advanced surface modeling approach is usually required to mimic bio-inspired geometry appropriately. It is possible, for example, to apply randomized geometric modeling approaches based on TPMS to mimic bone tissue ([Shi et al., 2018](#)).

Some of the existing tools support implicit modeling to a certain extent. Implicit modeling enables the definition of geometry based on implicit mathematical functions. Implicit functions extend the design freedom of a geometric modeling tool by, for example, minimizing the user input and are the only practical way to model TPMS structures. In particular, topology optimization supported by nTopology is characterized as implicit modeling. Topology optimization adjusts the geometric parameters of each unit cell according to a field function. This field function is commonly obtained through a CAE simulation. Topology optimization is currently limited by optimizing the thickness of a cellular structure which in some cases is not a sole parameter of a topology. The truncated cube topology, for example, requires the truncation parameter to be fully defined.

Moreover, the design freedom is limited by the results of the optimization process. Other adjustments must be manually introduced in the resulting solid model, often to each relevant unit cell. This thesis mainly focuses on geometric modeling methods not based on optimization.

MATLAB ([The MathWorks, Inc., 2008](#)) is another powerful tool that finds applications in mathematical and geometric simulations. Moreover, MATLAB is extendable by add-ons. For example, MSLattice ([Al-Ketan and Abu Al-Rub, 2021](#)) allows the modeling of various TPMS-based cellular structures. It also supports the modeling of a transition between two different topologies. Another example is FLatt Pack ([Maskery et al., 2022](#)) which allows their modeling of simple TPMS-based homogeneous cellular structures and even their export to the STL file format. Both tools support modeling conformal cellular

structures in cylindrical and spherical coordinates. FLatt Pack supports a homogeneous cellular structure infill within an imported STL file. Both tools do not support the STEP file format export as of now. Both tools are also limited to the modeling of TPMS-based cellular structures only. However, FLatt Pack considers the body-centered cubic (BCC) topology as an extreme case of a gyroid topology. FLatt Pack and MSLattice define the TPMS topologies by their corresponding implicit functions. FLatt Pack voxelizes the unit cell design space according to that implicit function and can approximate the triangular mesh for export to STL.

2.4.4 Comparison of tools for cellular structure modeling

This subsection has made a comparison to provide a clearer understanding of the capabilities and features of various tools for cellular structure modeling. The comparison encompasses custom topology support, linear and non-linear gradient application, parametric design capabilities, customizable heterogeneity, and platform compatibility.

Autodesk Netfabb and Sulis Lattice offer limited custom topology support and linear gradient application but lack non-linear gradient and parametric design capabilities. They also do not support customizable heterogeneity and are limited to the Windows platform.

Rhinoceros 3D and Grasshopper provide more comprehensive support for custom topologies, linear and non-linear gradients, and parametric design. However, the customizable heterogeneity in these tools is limited. They are compatible with both Windows and macOS platforms. Intralattice and Crystallon, plugins for Grasshopper, offer similar features with varying levels of heterogeneity support.

Dendro, another plugin for Grasshopper 3D, does not support custom topologies but allows for linear gradient application, parametric design, and limited customizable heterogeneity. It is also compatible with both Windows and macOS platforms.

nTopology, a more recent tool, offers robust support for custom topologies, linear and non-linear gradients, parametric design, and customizable heterogeneity, making it a strong option for advanced cellular structure modeling. However, it is currently limited to the Windows platform. Furthermore, heterogeneity of parameters other than lattice thickness remains unachieved.

Table 2.1 compares the features and capabilities of various tools for modeling cellular structures. It highlights the differences in custom topology support, linear and non-linear gradient application, parametric design capabilities, customizable heterogeneity, and platform compatibility. In conclusion, the choice of a tool for modeling cellular structures depends on the specific requirements of a project. While some tools offer more features and capabilities than others, it is essential to evaluate the suitability of a tool based on the particular demands of the design and manufacturing process.

Table 2.1 Comparison of features and capabilities of cellular structure modeling tools

Tool	Custom topology	Linear gradient	Non-linear gradient	Parametric design	Heterogeneity
Autodesk Netfabb	Limited	Yes	No	No	No
Sulis Lattice	Limited	Yes	No	No	No
Rhinoceros 3D	Yes	Yes	Yes	Yes	Limited
Intralattice	Yes	Yes	No	Yes	Limited
Crystallon	Yes	Yes	No	Yes	Limited
Dendro	No	Yes	No	Yes	Limited
nTopology	Yes	Yes	Yes	Yes	Limited

2.4.5 Graphical user interface of software packages for the geometric modeling of cellular structures

Heterogeneous cellular structures require a substantial number of parameters to be defined. Tools such as Autodesk Netfabb provide a graphical user interface (GUI) similar to a conventional feature-based CAD package, which increases interactivity but negatively impacts the design intent when designing complex geometry ([Mathur et al., 2020](#)). On the other hand, the previously mentioned plugins for Rhinoceros 3D support the geometric modeling of cellular structures through Grasshopper 3D, which introduces a visual programming language (VPL) to describe the geometry as a dataflow diagram. The GUI of nTopology allows the user to design cellular structures with subsequential functional blocks, which is another VPL form. While it was found that a GUI based on a VPL is beneficial for beginners, more geometrically complex structures can become extremely challenging to be designed, thus disrupting the intent in the case of an advanced design ([Saito et al., 2017](#)).

2.5 Research objectives

The primary aim of this thesis is to explore the use of F-rep for the geometric modeling of heterogeneous cellular structures, addressing the existing research gap in this area. The motivation for using F-rep lies in its ability to seamlessly represent complex geometry and topology, making it a promising candidate for modeling heterogeneous cellular structures that require variation in geometric parameters other than thickness. Additionally, there is a lack of open-source solutions for modeling these complex structures, which further motivates the development of novel techniques.

This chapter provided a comprehensive literature review on existing geometric modeling techniques, focusing on their application to cellular structures. It also identified the research

gap in modeling heterogeneous cellular structures with varied geometric parameters beyond thickness. The properties and advantages of F-rep as a geometric modeling technique have been investigated. Based on the performed review, the following research objectives have been identified to achieve the set goal:

1. Develop a deep understanding of the geometric, topological, and mechanical characteristics of heterogeneous cellular structures, which will inform the development of F-rep-based modeling techniques and enable the generation of high-quality models.
2. Propose an innovative F-rep-based modeling framework for designing and representing heterogeneous cellular structures, addressing the challenges and limitations of existing techniques while leveraging the strengths of F-rep and supporting the variety of diverse geometric parameters.
3. Develop efficient algorithms and open-source software tools that support the proposed F-rep-based modeling framework, considering computational efficiency, memory consumption, scalability, and interoperability with other modeling techniques and engineering tools.
4. Evaluate the performance of the proposed F-rep-based modeling framework in terms of computational efficiency and adaptability through a series of case studies involving the design and analysis of heterogeneous cellular structures with varied geometric parameters.
5. Generate high-quality meshes suitable for FEA and CFD simulations from the F-rep models of heterogeneous cellular structures.
6. Provide guidelines and best practices for using F-rep in the design and analysis of

heterogeneous cellular structures with diverse geometric parameters based on the insights gained from the case studies and the developed framework.

Chapter 3

Proposed geometric modeling framework

All hope abandon, ye who enter in.

Dante Alighieri (1265 – 1321), INFERNO

In this chapter, a novel geometric modeling framework will be introduced to suggest an architecture that is to address the research gap identified in Chapter 2.

As described in Section 2.1.4, F-rep modeling methods require real-valued mathematical functions to describe the geometry of a solid body. Such a definition of geometry provides significant design freedom since any shape can be defined by a mathematical function or interpolating one (Savchenko et al., 1995; Letov et al., 2021). However, utilizing such design freedom can prove challenging because defining the functions is difficult and tedious for an engineering designer. This challenge is usually solved by utilizing simpler interpolations for the functions that define the geometry (Savchenko et al., 1995; Yam et al., 2006). Such approximations, however, result in a solid model that is not of the original design. An approximated model often implies a geometry that does not reach all the goals set for the

product before the conceptual design process (Hsu and Liu, 2000; Letov et al., 2021).

In this research, instead of defining a complex set of functions that define the geometry, the focus was placed on providing tools to define these functions more straightforwardly. The proposed method, referred to as lattice-function representation (LF-rep), implements a single-function approach with the function depending on parameters necessary for modeling a heterogeneous cellular structure. Moreover, parameters themselves are proposed to be controlled by functions. First, such an approach supports design freedom by allowing the variation of lattice parameters such as the beam or node diameter, surface thickness, etc. Secondly, this approach can potentially allow the modeling of hierarchical cellular structures since lattice-defining functions can be nested inside a higher-tier function. This proposed approach expands the conventional F-rep approach to be better suited for modeling heterogeneous cellular structures. Instead of a single function $F(\mathbf{X})$ that defines the solid model, it is proposed to split this function into two: one function that defines the shape of a unit cell and another one that defines the geometric parameters of that topology. Thus, this special case of the conventional F-rep model defined by Equation 2.2 is defined in this work as

$$F(\mathbf{X}) = (P \circ T)(\mathbf{X}) \geq 0, \quad (3.1)$$

where T defines the topology of the cellular structure, and P defines the parameters of the topology. Figure 3.1 illustrates the heterogeneous cellular structure mapping process. Note that the order of the composition in Equation 3.1 matters since the parameters are different for different topologies.

This approach allows the modeling of highly complex solids. In this research, the

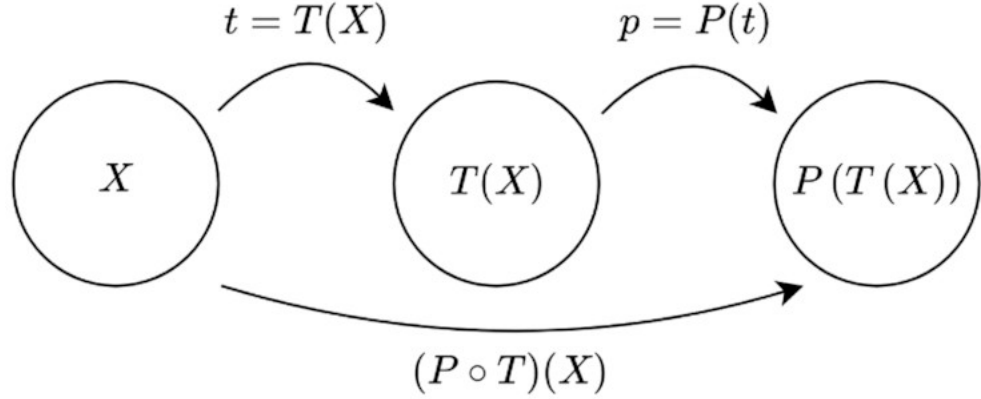


Figure 3.1 The sequential mapping of the function T that defines the topology and the function P that defines the geometric parameters of a heterogeneous cellular structure (Letov and Zhao, 2022)

complexity of a solid body \mathbb{S} defined by

$$\mathbb{S} := \{\mathbf{X} | F(\mathbf{X}) \geq 0\}, \quad (3.2)$$

which is considered to correlate with the genus of its bounding surface $\partial\mathbb{S}$ defined by

$$\partial\mathbb{S} := \overline{\mathbb{S}} \cap \overline{(\mathbf{X} - \mathbb{S})} = \{\mathbf{X} | F(\mathbf{X}) = 0\}, \quad (3.3)$$

which is essentially an oriented 2-manifold M_g^2 of a finite genus g . Here, $\overline{\mathbb{S}}$ is the closure of \mathbb{S} and $\overline{(\mathbf{X} - \mathbb{S})}$ is the closure of the complement of \mathbb{S} . The complexity of a cellular structure is often estimated by its genus g since it correlates with the amount of non-trivial curvatures in the corresponding solid model (Feng et al., 2018; Letov and Zhao, 2021). For example, a single simple cubic unit cell $\mathbb{U}_{\text{cubic}}$ of a cellular structure in Fig. 2.9 has genus $g = 5$ since it is homeomorphic to M_5^2 or a 5-torus \mathbb{T}^5 :

$$\mathbb{U}_{\text{cubic}} \cong \mathbb{T}^5 = S^1 \times S^1 \times S^1 \times S^1 \times S^1, \quad (3.4)$$

where S^1 is a circle. The complexity of a solid torus \mathbb{T}_S – the most simplistic solid body with a single hole – is proportional to $g = 1$ of the torus $\mathbb{T} \cong M_1^2$. Gyroid cellular structures can be of different varieties with the genus of at least $g = 5$ ([Góźdż and Holyst, 1996](#)).

The proposed framework should allow union operations between solids, such that

$$\mathbb{S} = \bigcup_{i=1}^n \mathbb{S}_i, \quad (3.5)$$

where n is the total number of solids and \mathbb{S}_i is the i -th solid. In the case of trivial union, the transition between topologies can become abrupt and the border between topologies might not be smooth unless there is a perfect match of nodes. The topology transition in cellular structures is a topic of interest in heterogeneous cellular structure research and has been implemented previously in several works ([Yang et al., 2015a](#)). In particular, the transition between two surface-based topologies invokes the most challenges ([Kim and Yoo, 2020](#)).

The rest of this section discusses the proposed LF-rep approach in detail. Section 3.1 introduces the proposed geometric description T to represent cellular topologies. Section 3.2 describes the proposed approach for the variation of geometric parameters P in a non-linear manner. Section 3.3 delves into the design of cellular structures with multiple topologies, showcasing the versatility of the proposed method. In Section 3.4, stochastic cellular structures are explored, highlighting the ability of the proposed approach to generate random and unique configurations. Lastly, Section 3.5 presents conformal cellular structures, demonstrating how the proposed method can adapt to complex and varying surface geometries.

3.1 Functional definition of cellular topologies

The LF-rep framework is developed in such a way that it supports both beam-based and surface-based topologies. The topology is proposed to be defined by its skeleton, which is defined by the function TT . Sections 3.1.1 and 3.1.2 describe how the LF-rep approach can be used to model beam-based and TPMS-based topologies, respectively.

3.1.1 Beam-based topologies

Since the methodology described in this work is proposed to be based on LF-rep, functions need to be defined for the common topologies. A skeleton of a beam-based topology can be defined by a set of lines that are defined in $x, y, z \in [0, u]$, where u is the size of a unit cell.

As an example of how a beam-based topology can be defined, consider a BCC topology sketched in Fig. 3.2 with eight nodes in every vertex of a cube and one more node in the center of the cube. The skeletal frame for this topology can be defined as follows:

$$T(\mathbf{X}) : \begin{cases} \frac{x}{a} = \frac{y}{b} = \frac{z}{c}, \\ \frac{x-a}{-a} = \frac{y}{b} = \frac{z}{c}, \\ \frac{x}{a} = \frac{y}{b} = \frac{z-c}{-c}, \\ \frac{x-a}{-a} = \frac{y}{b} = \frac{z-c}{-c} \end{cases} \quad \text{for } x \in [0, a], y \in [0, b], z \in [0, c], \quad (3.6)$$

where a, b , and c are sides of a cuboid unit cell. In the case of a cubic unit cell, $a = b = c$. After defining the skeletal frame, a cross-section with varying parameters can be assigned to the frame. The cross-section itself can be defined by function $\Delta(\mathbf{X}_c)$, where $\mathbf{X}_c \subset \mathbb{R}^2$ is the coordinate space local to the cross-section plane. For example:

1. A cylindrical beam can be defined by a cross-section which can be defined as

$$\Delta(x_c, y_c) : x_c^2 + y_c^2 = R_c^2, \quad (3.7)$$

where $x_c, y_c \in \mathbb{R}^2$ are Cartesian coordinates local to the cross-section plane and R_c is the radius of the circular cross-section.

2. A beam with a square cross-section can be defined as

$$\Delta(x_c, y_c) : |x_c + y_c| + |x_c - y_c| = \delta, \quad (3.8)$$

where $x_c, y_c \in \mathbb{R}^2$ are Cartesian coordinates local to the cross-section plane and δ is the side of the square cross-section.

3. A beam with a cross-section that has a shape of a square with rounded corners can be defined as

$$\Delta(x_c, y_c) : \max\left(|x| - \frac{\delta}{2} + \rho, 0\right)^2 + \max\left(|y| - \frac{\delta}{2} + \rho, 0\right)^2 = \rho_c, \quad (3.9)$$

where $x_c, y_c \in \mathbb{R}^2$ are Cartesian coordinates local to the cross-section plane, δ is the side of the rounded square, and ρ_c is its fillet radius. Note that Equation 3.9 converges to Equation 3.7 when $\rho_c \rightarrow \rho_{\max} = \delta/2$ and to Equation 3.8 when $\rho_c \rightarrow \rho_{\min} = 0$.

F-rep in the proposed work is proposed to allow control over these parameters, thus allowing change of topology parameters throughout the whole structure. For example, the diameter of beams within a cellular structure with the BCC topology can be controlled by the function P .

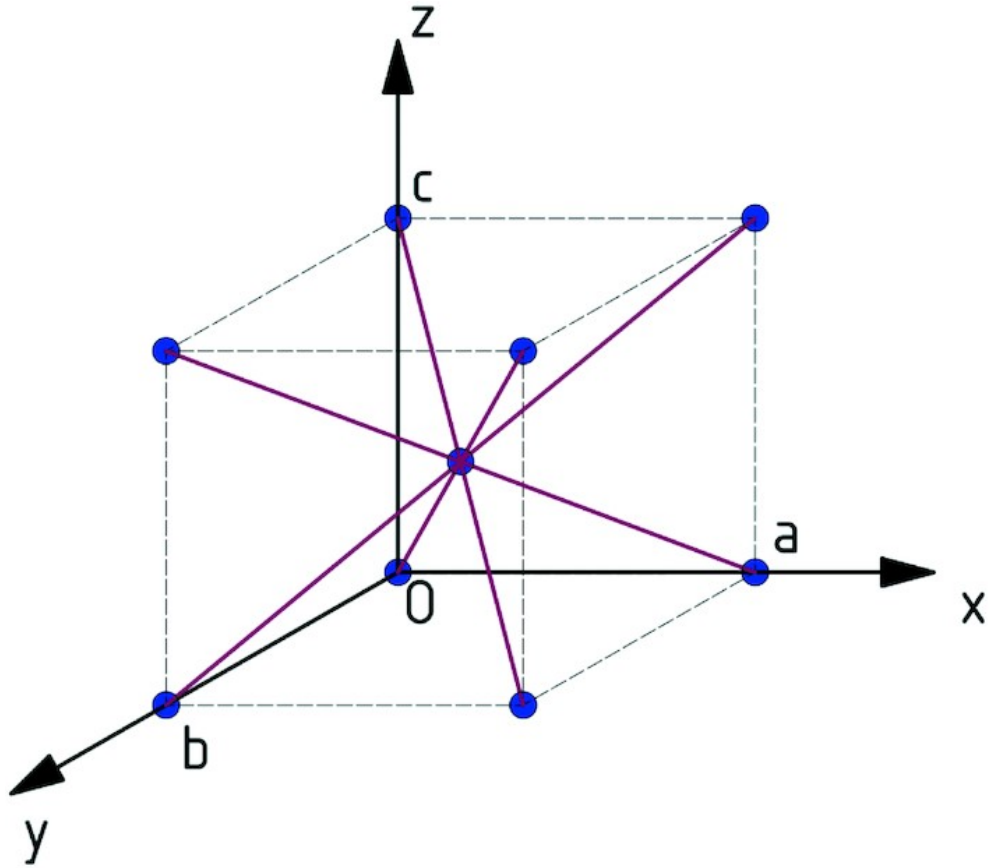


Figure 3.2 A BCC unit cell described by Equation 3.6 (Letov and Zhao, 2022)

For another example, consider a topology defined by

$$T(\mathbf{X}) : \left\{ \begin{array}{l} \left[\begin{array}{l} x \in \{0, u\}, z \in \{y, -y + u\}, \\ y \in \{0, u\}, z \in \{x, -x + u\}, \\ z \in \{0, u\}, y \in \{x, -x + u\}; \end{array} \right. \\ x, y, z \in [0, u], \end{array} \right. \quad (3.10)$$

where u is the side of the cubic unit cell, describes 12 straight line segments bounded by the cubic region $x, y, z \in [0, u]$ with each segment being from one vertex to the opposite

one within the same face of the cube. In this notation, $\alpha \in \{\beta, \gamma\}$ means a union of $\alpha = \beta$ and $\alpha = \gamma$. So, $x \in \{0, u\}$ means $x = 0$ and $x = u$. Equation (3.10) describes the skeletal graph of the face-centered cubic (FCC) topology, which is sketched in Fig. 3.3.

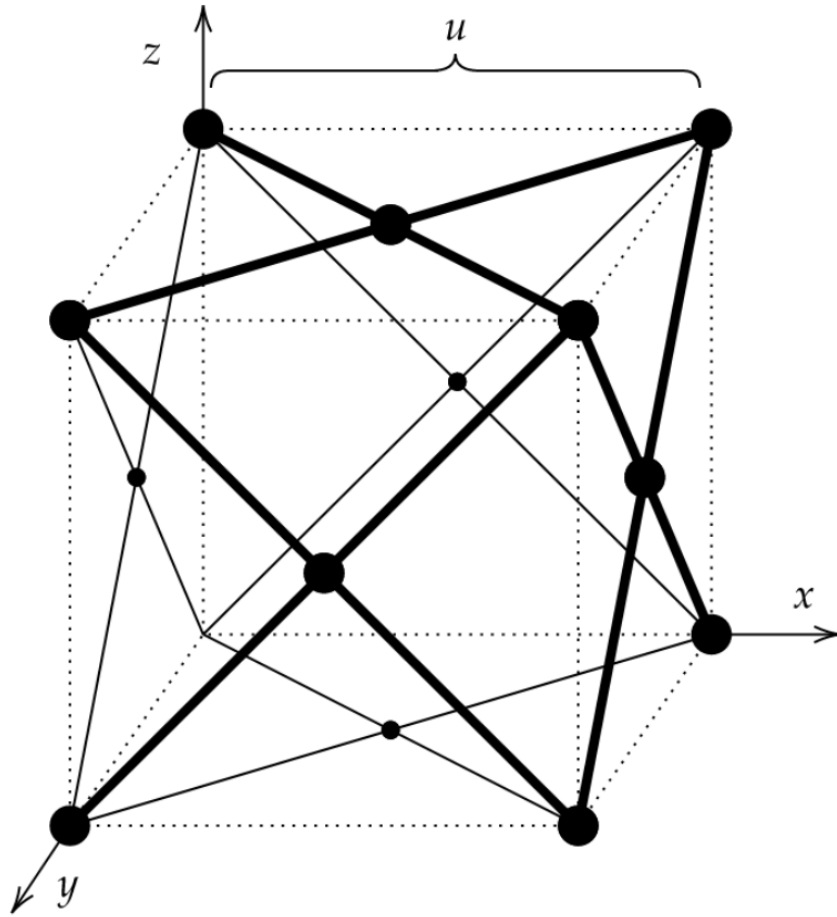


Figure 3.3 An FCC unit cell described by Equation 3.10. The thicker lines correspond to the beams located in the visible faces of the arbitrary cube with the side u . The edges of the arbitrary cube are represented as dotted lines. The nodes are represented as circles (Letov and Zhao, 2023a)

This way of defining skeletal graphs is based on LF-rep, which makes it different from original F-rep and the voxel-based method used in nTopology. LF-rep allows a more straightforward way of defining the thickness of topology by defining a variable within

the function (R_c for the circle Δ in the example in Equation 3.7). Furthermore, as will be described further, this approach allows variation of parameters other than thickness, thus further extending the design freedom.

Various cellular topologies were defined according to the LF-rep approach. Table 3.1 lists beam-based topologies inspired by the cubic crystal system and their topology-defining functions T . The topology-defining function T , in this case, is defined for $x, y, z \in [0, u]$. In Table 3.1, the unit cell is assumed to be cubic with the side u . The unit cells of these topologies are shown in Fig. 3.4. The notations of the form $x \in \{a, b\}$ that is used in this work denote the union of two parallel lines with $x = a$ and $x = b$. In other words,

$$x \in \{a, b\} \Leftrightarrow \neg[a, b] \cup (a, b). \quad (3.11)$$

Tables 3.2, 3.3, and 3.4 describe the diamond, rhombicuboctahedron, and truncated cube topologies, respectively. The rhombicuboctahedron and truncated cube topologies require an additional truncation parameter $\tau \in [0, 0.5u]$, which sets the size of truncation. These topologies are illustrated in Fig. 3.5.

3.1.2 Surface-based topologies

The LF-rep approach is proposed to be applied to the topologies based on TPMS. For TPMS-based cellular structures, the skeletal frame is equivalent to the TPMS itself described by a mathematical equation. Since the approximations of these equations are well-known, there is even more reason to rely on LF-rep to model TPMS-based cellular structures. For example, a gyroid surface illustrated in Fig. 3.6 is defined by its equation as follows:

$$T(\mathbf{X}) : \sin(x) \cos(y) + \sin(y) \cos(z) + \sin(z) \cos(x) = 0. \quad (3.12)$$

Table 3.1 Various beam-based topologies inspired by the cubic crystal system supported by the developed approach.

Topology	Topology defining function, T	Figure
Simple cubic	$\begin{cases} x \in \{0, u\}, y \in \{0, u\}, \\ y \in \{0, u\}, z \in \{0, u\}, \\ x \in \{0, u\}, z \in \{0, u\}. \end{cases}$	3.4a
BCC	$\begin{cases} x = y = z, \\ -x + u = y = z, \\ x = y = -z + u, \\ -x + u = y = -z + u. \end{cases}$	3.4b
S-FCC	$\begin{cases} x \in \{0, u\}, z \in \{y, -y + u\}, \\ y \in \{0, u\}, z \in \{x, -x + u\}. \end{cases}$	3.4c
FCC	$\text{S-FCC} \cup \begin{cases} z \in \{0, u\}, \\ y \in \{x, -x + u\}. \end{cases}$	3.4d
BCCz	$\text{BCC} \cup \begin{cases} x \in \{0, u\}, \\ y \in \{0, u\}. \end{cases}$	3.4e
FCCz	$\text{FCC} \cup \begin{cases} x \in \{0, u\}, \\ y \in \{0, u\}. \end{cases}$	3.4f
S-FCCz	$\text{S-FCCz} \cup \begin{cases} x \in \{0, u\}, \\ y \in \{0, u\}. \end{cases}$	3.4g
FBCC	$\text{BCC} \cup \text{FCC}.$	3.4h
S-FBCC	$\text{BCC} \cup \text{S-FCC}.$	3.4i
S-FBCCz	$\text{BCC} \cup \text{S-FCCz}.$	3.4j

Unlike beam-based topologies, TPMS-based topologies do not require its cross-section to be defined as a function Δ . Instead, only the thickness t of a solid body must be defined.

Table 3.5 covers functions T that define supported TPMS topologies. Note that T these surfaces are approximations of their exact form [Gandy and Klinowski \(2000\)](#). The unit cells of the TPMS topologies are shown in Fig. 3.7.

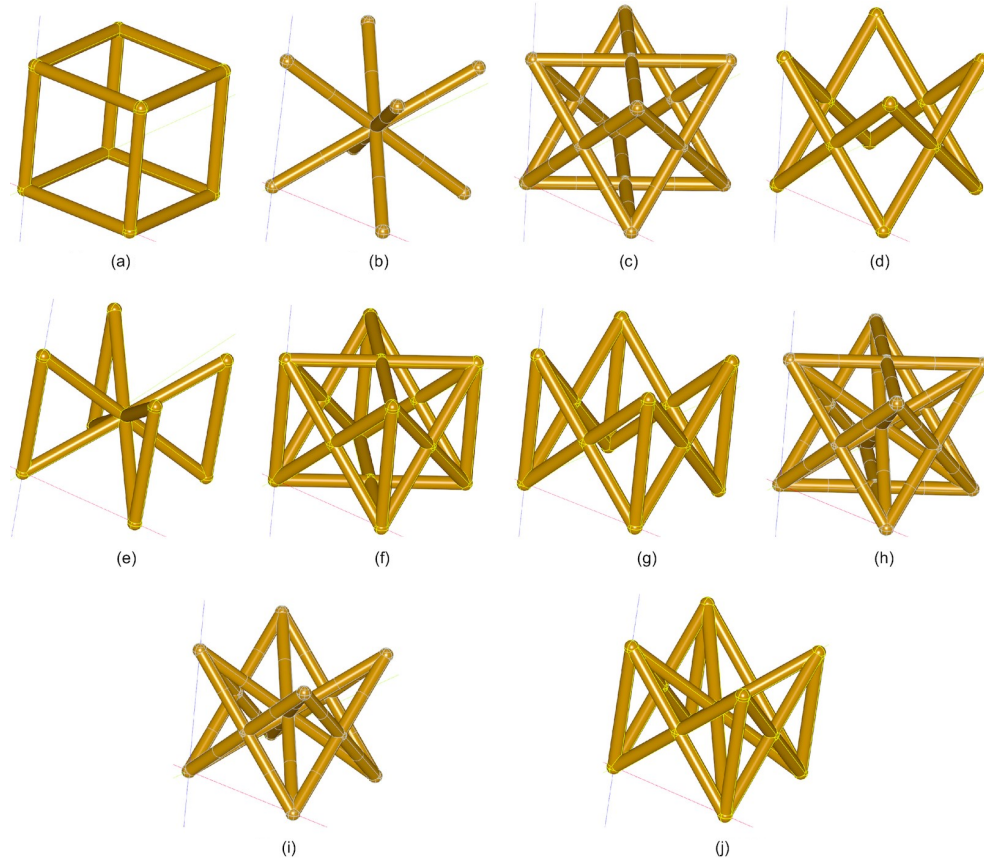


Figure 3.4 Various beam-based topologies inspired by the cubic crystal system supported by the developed approach: (a) simple cubic, (b) BCC, (c) FCC, (d) S-FCC, (e) BCCz, (f) FCCz, (g) S-FCCz, (h) FBCC, (i) S-FBCC, and (j) S-FBCCz ([Letov and Zhao, 2022](#))

The LF-rep approach allows the proposed framework not to be limited to beam-based topologies since the original F-rep allows the modeling of everything that can be defined with functions that define the geometry.

3.2 Functional variation of geometric parameters

As mentioned in Chapter 2, most existing approaches for modeling heterogeneous cellular structures permit control of the cellular structure thickness. This control is primarily

Table 3.2 The diamond topology supported by the developed approach.

Topology	Topology defining function, T	Figure
Diamond	<p>for $z \in [0, 0.25u]$:</p> $\begin{cases} -x + u = y = z, \\ x - 0.5u = -y + 0.5u = z, \\ -x + 0.5u = y - 0.5u = z, \\ x = -y + u = z; \end{cases}$ <p>for $z \in [0.25, 0.5u]$:</p> $\begin{cases} -x + 0.75u = -y + 0.25u = z - 0.25u, \\ x - 0.75u = y - 0.25u = z - 0.25u, \\ x - 0.25u = y - 0.75u = z - 0.25u, \\ -x + 0.25u = -y + 0.75u = z - 0.25u; \end{cases}$ <p>for $z \in [0.5, 0.75u]$:</p> $\begin{cases} -x + 0.5u = y = z - 0.5u, \\ x = -y + 0.5u = z - 0.5u, \\ -x + u = y - 0.25u = z - 0.5u, \\ x - 0.5u = -y + u = z - 0.5u; \end{cases}$ <p>for $z \in [0.75, u]$:</p> $\begin{cases} -x + 0.25u = -y + 0.25u = z - 0.75u, \\ x - 0.25u = y - 0.25u = z - 0.75u, \\ -x + 0.75u = -y + 0.75u = z - 0.75u, \\ x - 0.75u = y - 0.75u = z - 0.75u. \end{cases}$	3.5a

gradient-like, with the linear distribution of the thickness in a specified direction. The only exception among the reviewed methods is topology optimization. While topology optimization allows the generation of geometrically highly complex structures (Liu et al., 2021a), it has limited control from the user. Hence, it was decided to develop a less implicit modeling method not based on topology optimization but on the proposed LF-rep approach.

The LF-rep approach allows variation of various geometric parameters in different di-

Table 3.3 Rhombicuboctahedron topology supported by the developed approach.

Topology	Topology defining function, T	Figure
Rhombicuboctahedron	$\begin{cases} x \in \{\tau, u - \tau\}, \\ y \in \{\tau, u - \tau\}, \\ z \in \{\tau, u - \tau\}, \\ x \in \{\tau, u - \tau\}, y \in \{0, u\}, z \in [\tau, u - \tau]; \\ x \in \{0, u\}, y \in \{\tau, u - \tau\}, z \in [\tau, u - \tau]; \\ x \in \{\tau, u - \tau\}, z \in \{0, u\}, y \in [\tau, u - \tau]; \\ x \in \{0, u\}, z \in \{\tau, u - \tau\}, y \in [\tau, u - \tau]; \\ y \in \{\tau, u - \tau\}, z \in \{0, u\}, x \in [\tau, u - \tau]; \\ y \in \{0, u\}, z \in \{\tau, u - \tau\}, x \in [\tau, u - \tau]; \\ z \in \{\tau, u - \tau\}, \end{cases} \begin{cases} -y + \tau = z, \\ -y - u + \tau = z, \\ y = z - u + \tau, \\ -y + u = z - u + \tau; \\ x = z - u + \tau, \\ -x + u = z - u + \tau, \\ -x + \tau = z, \\ x - u + \tau = z; \\ -x + \tau = y, \\ x - u + \tau = y, \\ x = y - u + \tau, \\ x - u + \tau = -y + u; \\ -x + \tau = y, \\ x - u + \tau = y, \\ x = y - u + \tau, \\ x - u + \tau = -y + u. \end{cases}$	3.5b

rections and is not limited to the linear distribution of the cellular structure parameters. This variation is enabled by introducing the function P , which controls the parameters. For example, $P(\mathbf{X} : t(z))$, where $t : \mathbb{I} \mapsto \mathbb{R}_+$ is the thickness of the cellular structure, and \mathbb{I} is a unit interval $[0, 1] \subset \mathbb{R}$. The LF-rep approach allows setting thickness t as a distribution defined by any mathematical function. Here, the thickness can be either the beam or the

Table 3.4 Truncated cube topology supported by the developed approach.

Topology	Topology defining function, T	Figure
Truncated cube	$\begin{cases} x \in \{0, u\}, \\ y \in \{0, u\}, \\ z \in \{0, u\}, \\ x \in [t, u-t], \\ y \in [t, u-t], \\ z \in [t, u-t], \end{cases} \begin{cases} -y + t = z, \\ y - u + t = z, \\ y = z - u + t, \\ -y + u = z - u + t; \\ -x + t = z, \\ x - u + t = z, \\ x = z - u + t, \\ x - u + t = -z + u; \\ -x + t = y, \\ x - u + t = y, \\ x = y - u + t, \\ -x + u = y - u + t; \\ x \in \{0, u\}, \\ z \in \{0, u\}; \\ x \in \{0, u\}, \\ z \in \{0, u\}; \\ x \in \{0, u\}, \\ y \in \{0, u\}. \end{cases}$	3.5c

surface thickness, depending on function T , which describes the topology. Several use cases of varying $P(\mathbf{X}) : t(z)$ are presented in Chapter 4.

Apart from the cellular structure thickness, other geometric parameters can be regulated using the LF-rep method. Examples of these parameters encompass the radius ρ_c of the fillet of the square beam with rounded corners as described in Equation 3.9. Another example is the truncation parameter τ in the rhombicuboctahedron and the truncated cube topologies. Both topologies converge to simple cubic with $\tau_{\min} = 0$ (0%). The

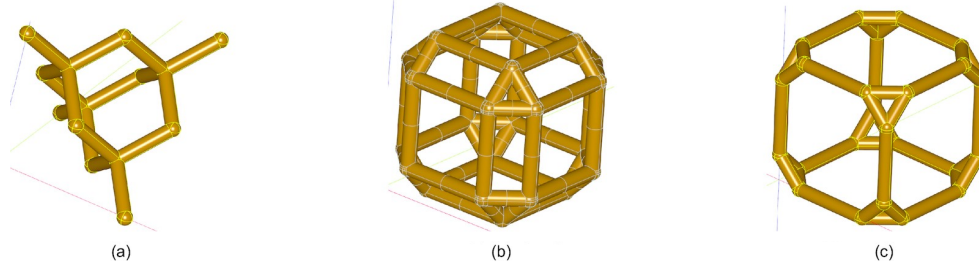


Figure 3.5 Additional beam-based topologies supported by the developed approach: (a) diamond, (b) rhombicuboctahedron, and (c) truncated cube (Letov and Zhao, 2022)

Table 3.5 Various TPMS-based topologies supported by the developed approach.

Topology	Topology defining function, T	Figure
Gyroid	$\sin x \cos y + \sin y \cos z + \sin z \cos x = 0$	3.7a
Schwarz P surface	$\cos x + \cos y + \cos z = 0$	3.7b
Schwarz D surface	$\cos x \cos y \cos z - \sin x \sin y \sin z = 0$	3.7c

rhombicuboctahedron topology converges to the octahedron topology with $\tau_{\max} = u/2$ (100%). The truncated cube topology converges to the cuboctahedron topology with $\tau_{\max} = u/2$ (100%). The truncation is an example of a parameter that is not commonly controlled in existing modeling tools such as Autodesk Netfabb and nTopology. Support for such control increases modeling capabilities and allows the design of cellular structures with desirable topology transition.

The LF-rep method has the potential to bolster current cellular structure modeling tools, introducing an additional F-rep tool to alter geometric parameters, extending beyond just the cellular structure thickness.

As an example, consider a heterogeneous cellular structure based on the Schwarz P

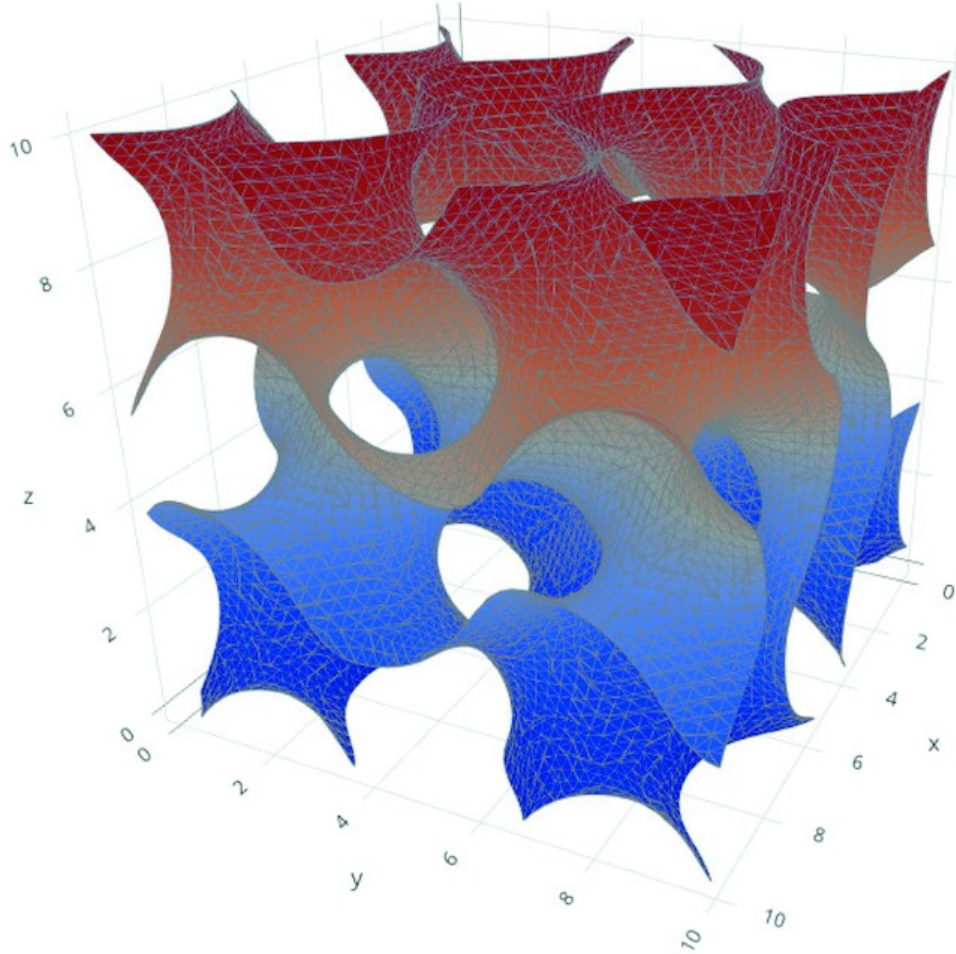


Figure 3.6 A gyroid surface described by Equation 3.12 (Letov and Zhao, 2022)

surface defined according to the proposed method. Let the thickness to linearly change from 0.1 mm to 7.0 mm along the z -axis. The Schwarz P surface itself is defined by its skeletal graph

$$T(\mathbf{X}) : \cos(x) + \cos(y) + \cos(z) = 0, \quad (3.13)$$

which is a TPMS with zero thickness t (Michielsen and Stavenga, 2008).

F-rep can be overly complicated when used in engineering design as a modeling tool, as it requires expertise in both design and mathematics. To simplify and adjust F-rep to

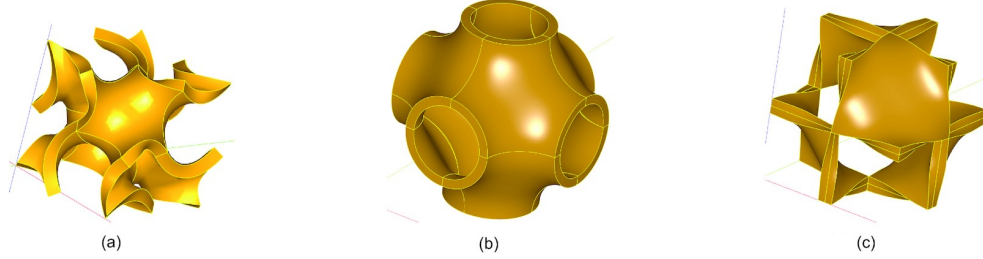


Figure 3.7 Various TPMS-based topologies supported by the developed approach: (a) gyroid, (b) Schwarz P surface, and (c) Schwarz D surface ([Letov and Zhao, 2022](#))

the AM needs, the solid model, which is based on a skeletal graph, can be obtained by an additional function specifically developed for this topology. For example, for the Schwarz P surface topology, this additional function appears as a single function with multiple parameters in it:

$$\text{Schwarz lattice}(\text{size}(\mathbb{U}), N_x, N_y, N_z, P(\mathbf{X})), \quad (3.14)$$

where $\text{size}(\mathbb{U}) = 10$ mm is the size of the unit cell, N_x , N_y , and N_z are the numbers of unit cells in x , y , and z directions, respectively, and $P(\mathbf{X})$ is the function that controls the thickness of the TPMS-based structure, thus enabling setting $t > 0$ and construction of solids based on surfaces. $P(\mathbf{X})$ in this case, corresponds to

$$P(\mathbf{X}) : t(z) = 6.9z + 0.1, \quad (3.15)$$

where t is the thickness of the cellular structure, and $z \in [0, 1]$ is the variable corresponding to the z -axis. Note that since $z \in [0, 1]$, it has to be mapped to the actual coordinate $z_a \in [1, N_z]$ with $z_a \in \mathbb{N}_+$. This distribution is illustrated in Fig. 3.8.

To exploit the F-rep representation in a practical context, individuals would require a blend of geometric understanding, familiarity with the mathematical principles underlying functional representation, and proficiency in computational design tools ([Pasko et al.,](#)

1995). The major challenge is the interplay of mathematical complexity and design intent; one has to discern the mathematical constructs and how they influence the final design output (Li et al., 2020c). However, with advances in computational methods and software interfaces, there is potential for automation (Munaux, 2004). Reverse engineering, in this context, would involve interpreting an existing design in terms of its functional representation, which is a non-trivial task (Pasko et al., 2001). The primary challenges would stem from the inherent complexity of translating intricate geometric features into concise functional descriptions while ensuring the uniqueness of representation (Kou and Tan, 2007). Additionally, tackling ambiguities in design details, and ensuring that the function-derived design adheres to the original intent, poses a significant challenge (Pasko et al., 1995).

For a more detailed implementation of the approach, please refer to Section 4.2.

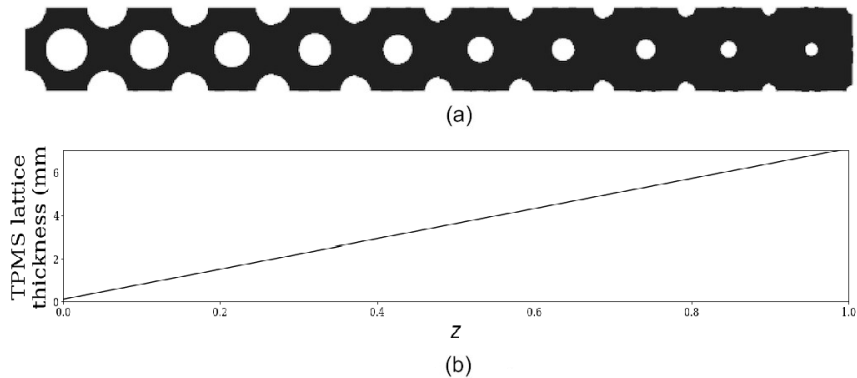


Figure 3.8 (a) A side view on a single column of a heterogeneous cellular structure with Schwarz P topology with linearly varying thickness in the z -direction, and (b) the linear function P that corresponds to the thickness of the TPMS-based structure vs. the z coordinate (Letov and Zhao, 2022)

3.3 Cellular structures with multiple topologies

A cellular structure with multiple homogeneous regions is an example of a heterogeneous cellular structure. Different topologies have different mechanical properties in different

directions ([Li et al., 2020a](#)). Assigning various topologies to different regions of the same structure ensures the variation of mechanical properties. This effect is often utilized in design for additive manufacturing (DFAM) ([Liu et al., 2020b](#)). For example, topology optimization can often identify the optimal topology for each cellular structure unit cell depending on the loading conditions ([Hu et al., 2021; Wei et al., 2022](#)). Figure 3.9 illustrates an example of a cellular structure with topologies selected based on a topology optimization algorithm.

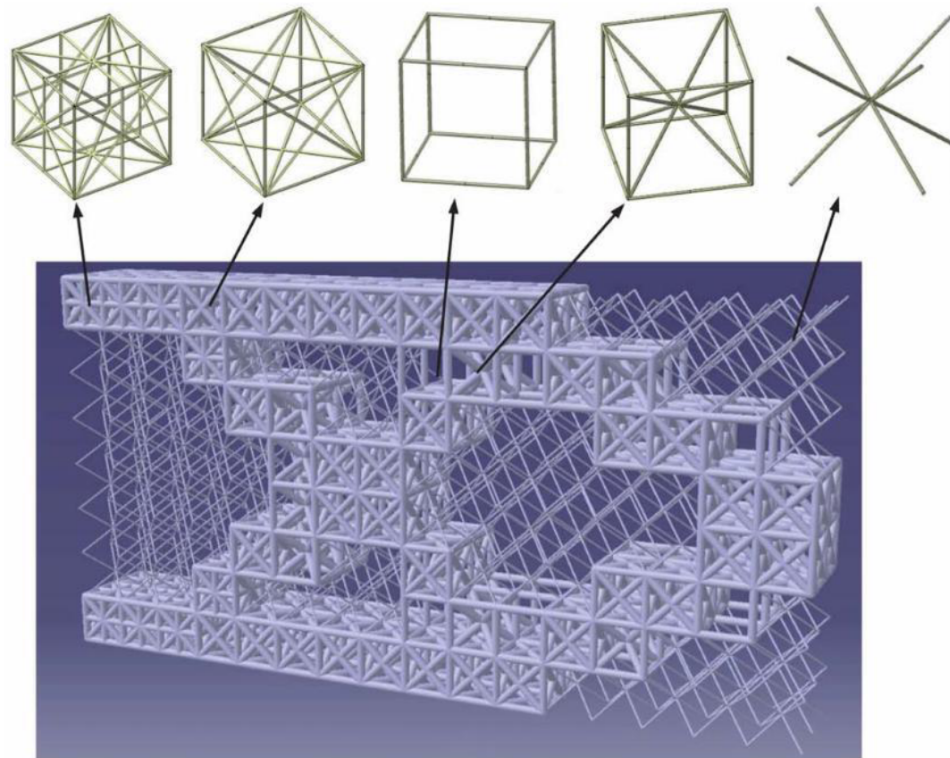


Figure 3.9 An example of a cellular structure with multiple topologies that are inspired by topology optimization ([Liu et al., 2020b](#))

The topic of topology transition in cellular structures is not a new one ([Leonardi et al., 2019](#)). Geometric modeling of transition between areas with different topologies within the same cellular structure is particularly interesting in research on this topic. A smooth

transition between topologies that are arbitrarily oriented between each other finds its application in, for example, the design of bone implants (Lu et al., 2020). Trabecular bone has multiple porous microstructures oriented depending on the direction in which the load is commonly applied to the bone. The bone regions subject to the same type of load possess similar mechanical properties, which are achieved by a seemingly randomized natural cellular structure with arbitrarily oriented beams.

The rest of this section describes the proposed LF-rep geometric modeling strategies to support the generation of cellular structures with multiple beam-based and surface-based topologies in Sections 3.3.1 and 3.3.2, respectively.

3.3.1 Beam-based cellular structures with multiple topologies

In beam-based topologies, the connectivity issue arises when there is no well-defined physical connection between the beams of two neighboring topologies. The connectivity issue affects the quality of the solid model of the cellular structure and its manufacturability. The LF-rep approach focuses on addressing these challenges, providing a robust framework for beam-based cellular structures. Figure 3.10 sketches a scheme of a cellular structure with multiple topologies with connectivity issues.

The crystallography cubic crystal system inspires a substantial number of beam-based topologies due to their ability to reinforce the structure in specific directions (Maskery et al., 2017). These topologies include simple cubic, body-centered cubic (BCC), and face-centered cubic (FCC), as well as variations of these topologies such as self-supporting FCC without horizontal beams (S-FCC), BCC with additional four z -direction oriented beams (BCCz), FCC with additional four z -direction oriented beams (FCCz), S-FCCz, face- and body-centered cubic (FBCC), S-FBCC, and S-FBCCz (Letov and Zhao, 2022). These topologies can be combined within a cellular structure without connectivity issues, given

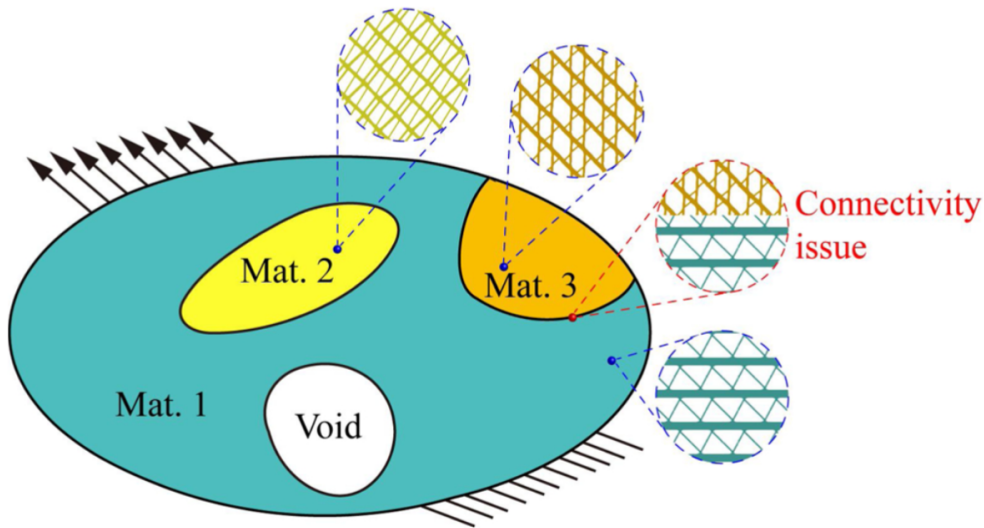


Figure 3.10 A schematic of a cellular structure with multiple topologies (Liu et al., 2020a)

the parallel translation of unit cells within it.

All the topologies inspired by the metal crystal structure listed above share the same cubic shape of their unit cell and at least four common nodes. Thus, the connectivity of these topologies can be efficiently achieved.

However, countless other beam-based topologies that are not inspired by crystallography exist. Among the topologies extensively used in AM are the diamond, rhombicuboctahedron, truncated cube, and truncated cuboctahedron topologies. All of these, except for the diamond topology, can generally parallel transition from one to another without significant connectivity issues. The diamond topology is not plane symmetrical, i.e., it cannot be obtained by mirroring a subset of that topology about a plane. This effect limits the application of the diamond topology in cellular structures with multiple topologies (Letov and Zhao, 2023a).

The transition of unit cells with different topologies is not limited to parallel. For example, assigning BCC and FCC topologies oriented in different directions in different

regions of the same cellular structure has proven mimicking of the crystal structure damage-resisting properties (Pham et al., 2019). The connectivity issue, in this case, is often mitigated by introducing additional beams between the unmatched nodes in the transition plane for support (Lertthanasarn et al., 2021). However, these additional beams in the transition region can affect the mechanical properties that arise in it, thus making the outcome of the design process less predictable. In particular, it has been found that the mechanical properties in homogeneous cellular structures are easily predictable by various techniques such as the homogenization technique (Somnic and Jo, 2022). On the contrary, the connectivity region between various topologies is greatly affected by the geometric properties of the transition region, which is more difficult to predict if stochastic (Wang et al., 2015).

Connectivity of beam-based topologies by the transition plane

The proposed LF-rep approach can support a special case of topology transition at certain angles. It is proposed to define the transition between the beam-based topologies by a transition plane. Since it is proposed to utilize a framework based on F-rep, this transition plane ought to be defined as a function.

Consider two topologies, the skeletal graphs T_1 and T_2 , of which are known. The transition plane \mathcal{P} between them is a plane of the scalar form

$$\mathcal{P}(\mathbf{X}) : a_t(x - x_{0t}) + b_t(y - y_{0t}) + c_t(z - z_{0t}) = 0, \quad (3.16)$$

where a_t , b_t , and c_t are the components of the normal vector $\vec{n}_t = (a_t, b_t, c_t)$ of the transition plane, x_{0t} , y_{0t} , and z_{0t} are the coordinates of an arbitrary point on \mathcal{P} . In this case, the skeletal graph of the cellular structure with the two topologies that are separated by a

transition plane \mathcal{P} can be described as

$$T(\mathbf{X}) = \begin{cases} \{T_1(\mathbf{X})|\mathcal{P} < 0\}, \\ \{T_2(\mathbf{X})|\mathcal{P} > 0\}, \\ \{(T_1 \cup T_2)(\mathbf{X})|\mathcal{P} = 0\}, \end{cases} \quad (3.17)$$

or, in a general case,

$$T(\mathbf{X}) = \begin{cases} \{T_i(\mathbf{X})|\mathcal{P}_{ij} < 0\} \\ \{T_j(\mathbf{X})|\mathcal{P}_{ij} > 0\} \\ \{(T_i \cup T_j)(\mathbf{X})|\mathcal{P}_{ij} = 0\} \end{cases} \quad (3.18)$$

$$\forall i, j \in [1, \dots, N],$$

where \mathcal{P}_{ij} is a transition plane between topologies T_i and T_j , N is the total number of regions with different topologies. Note that $\mathcal{P}_{ij} = -\mathcal{P}_{ji}$ is assumed to account for the change of the direction of a normal vector for each corresponding transition plane.

For example, consider a cellular structure consisting of two topologies T_1 and T_2 oriented as sketched in Fig. 3.11. Let T_1 be a beam-based topology with a cubic unit cell with the side u_1 . Let the transition plane \mathcal{P} between them be defined as follows:

$$\mathcal{P}(\mathbf{X}) : x + z - pu_1 = 0, \quad (3.19)$$

where u_1 is the side of the cubic unit cell with the T_1 topology and p is the number of unit cells between the origin and the transition plane along the x -axis. In this case, the normal vector \vec{n}_t of the transition plane \mathcal{P} forms 45° with the positive direction of the x -axis. The T_2 topology has a cuboid shape with the dimensions of u_2 , u_1 , and u_2 in the x_2 , y_2 , and z_2 directions, respectively, where $u_2 = u_1/\sqrt{2}$. $\mathbf{X}_2 = (x_2, y_2, z_2)^\top$ is obtained by the

Euclidean plane transformation of rotation as $\mathbf{X}_2 = R\mathbf{X}_1 = R\mathbf{X}$ where R is the rotation matrix defined as

$$R = \frac{\sqrt{2}}{2} \begin{bmatrix} 1 & 0 & 1 \\ 0 & \sqrt{2} & 0 \\ -1 & 0 & 1 \end{bmatrix}. \quad (3.20)$$

Note that the additional translation matrix is optional since T_2 is not defined for $\mathcal{P} < 0$.

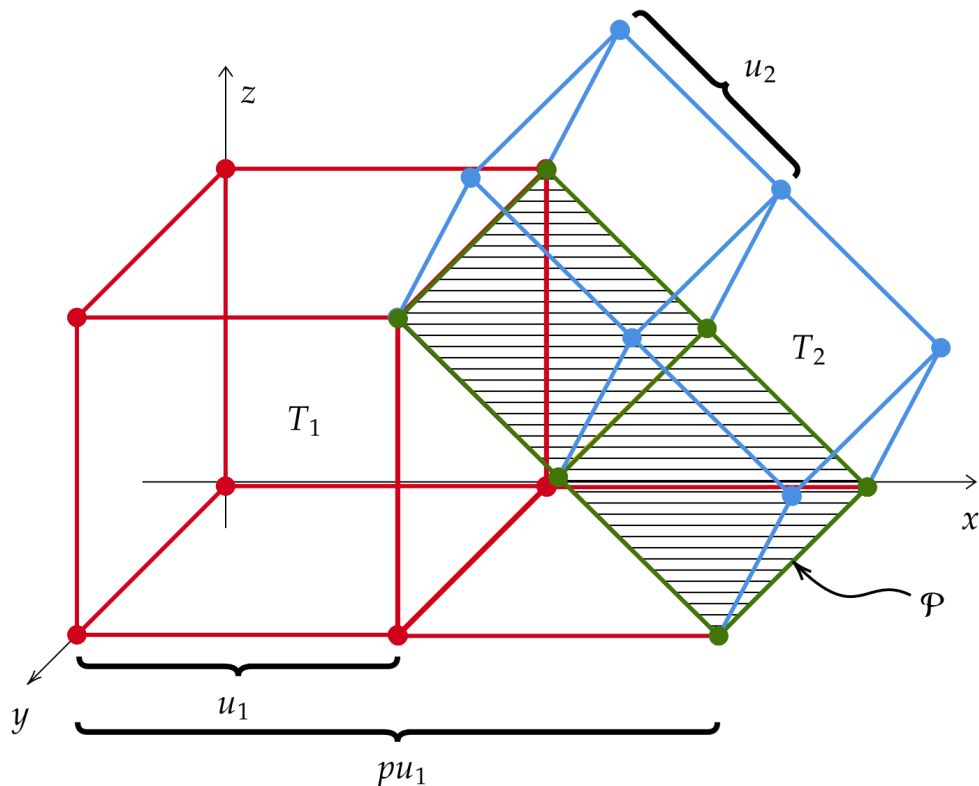


Figure 3.11 A diagram of two topologies transitioning in a plane (Letov and Zhao, 2023a)

Controllable truncation as a means to achieve topology transition

As mentioned in Section 3.2, some topologies have an optional truncation parameter required to fully define their skeletal graph T . Using the proposed LF-rep approach, it's

possible to utilize this feature effectively. For example, the rhombicuboctahedron and the truncated cube can have an additional truncation parameter τ that can be defined by the function P that defines geometric parameters within the LF-rep framework.

The strict definition of many truncated polyhedrons assumes that every edge has an equal length. This traditional notion of truncation is prevalent in designs like truncated polyhedrons. However, leveraging the flexibility offered by LF-rep, this work steps away from such strict definitions. Consider a skeletal graph T of the truncated cube topology with the unit cell size u sketched in Fig. 3.12. The skeletal graph is defined according to the F-rep principles (Letov and Zhao, 2022) in Table 3.4. There, the first three subsystems of equations correspond to the line segments that define the truncated faces, and the other three subsystems of equations correspond to the edges of the cube.

The truncated cube, if defined as an Archimedean solid, assumes that τ is defined in such a way that every edge has an equal length. Thus

$$u = 2\tau + \sqrt{2}\tau \quad (3.21)$$

or

$$\tau = \frac{u}{2 + \sqrt{2}}. \quad (3.22)$$

However, the LF-rep approach broadens this definition, assuming that truncation can span any real value in the range $\tau \in [0, u/2]$, or to put it plainly, between 0% and 100%.

Observe that in the two extreme cases when the value of τ takes 0 or $u/2$, the equation provided in Table 3.4 that defines the truncated cube illustrated in Fig. 3.12, it converges

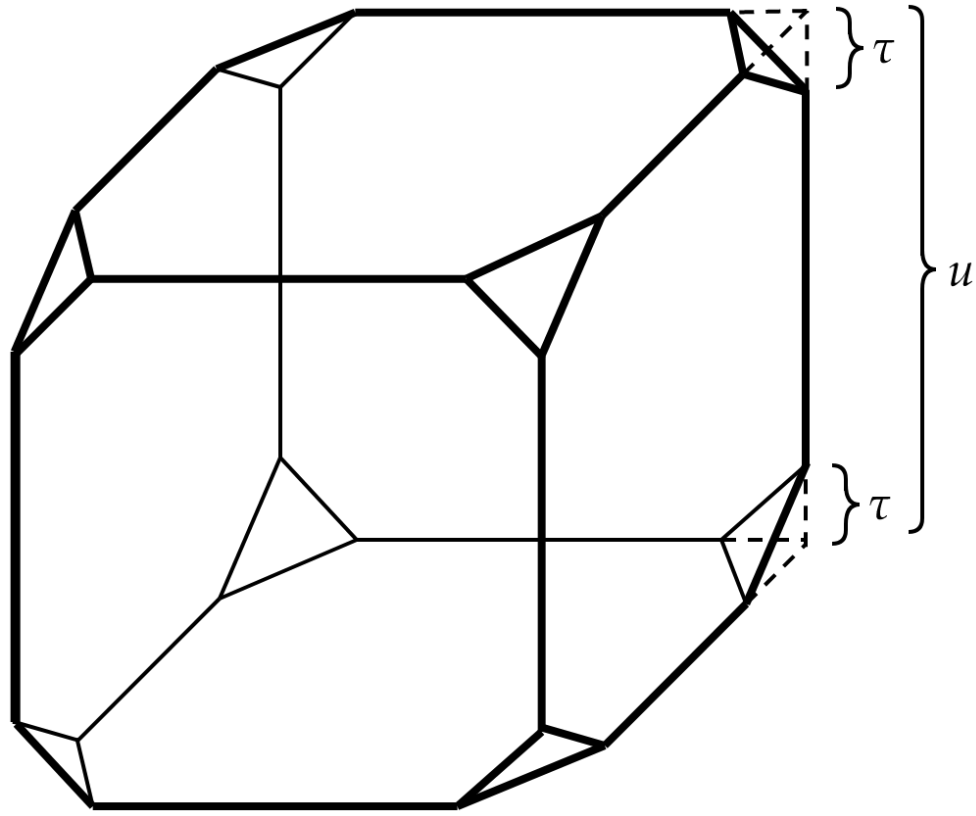


Figure 3.12 A skeletal graph of the truncated cube topology with the unit cell size u and the truncation τ (Letov and Zhao, 2023a)

to the simple cubic topology that is defined as

$$T(\mathbf{X}) : \begin{cases} x \in \{0, u\}, y \in \{0, u\}, \\ y \in \{0, u\}, z \in \{0, u\}, \\ x \in \{0, u\}, z \in \{0, u\} \end{cases} \quad (3.23)$$

and to the cuboctahedron topology, respectively. This effect is known as the *complete quasitruncation*. Equation 3.23 is defined on $x, y, z \in [0, u]$.

The LF-rep methodology similarly applies to the rhombicuboctahedron topology. In its two extreme complete quasitruncation cases, where the value of τ takes 0 or $u/2$, the

rhombicuboctahedron topology converges to the simple cubic topology and the octahedron topology, respectively.

By interpreting the truncation τ as a variable instead of a constant, LF-rep enables the transition from one topology T_1 to another T_2 by defining the function P that defines the geometric parameters. Note that the skeletal graph differs for any two truncation values $\tau \in [0, u/2]$. This effect blurs the differences between defining the geometric parameters with the function P and defining the topology with the function T .

For a more detailed explanation of the implementation of the proposed approach and examples of generated models of cellular structures, please refer to Section 4.3.1.

3.3.2 Surface-based cellular structures with multiple topologies

Ensuring a smooth topology transition without defects is crucial for surface-based cellular structures with multiple topologies. Many works assume a homogenized model, neglecting the properties of the transition region, leading to negative effects on mechanical properties (Feng et al., 2022; Ren et al., 2021). Achieving a balance between quality and performance is challenging, often resulting in high computation times and reduced model quality due to defects (Qureshi et al., 2021). Current topology optimization methods are limited, as they typically only optimize lattice thickness, which may not fully capture a topology's complexity (Letov and Zhao, 2022). Designing multi-topology surface-based cellular structures is challenging and has received limited attention in the research community. The process requires seamless transitions between different TPMS-based topologies while considering geometry, material properties, and performance requirements, with geometric modeling supporting the design process.

It is proposed to generate a skeletal graph between two surface-based topologies to create a smooth surface from the resulting points. Skeletal graphs can be useful in this

context as they represent the underlying connectivity of the cellular structure and can guide the interpolation process between different topologies.

For example, consider two topologies T_1 and T_2 shown in Fig. 3.13 separated by the gap δ . Let x be an axis directed from T_1 to T_2 perpendicular to their surfaces. Let T_1^+ be the outer face of the T_1 unit cell with the normal vector oriented with the x -axis, and T_2^- be the outer face of the T_2 unit cell with the normal vector oriented against the x -axis. Let ∂T_1^+ and ∂T_2^- be the contour curves corresponding to the cross-section of topologies in the planes T_1^+ and T_2^- , respectively. The transition region δ between T_1 and T_2 is proposed to be obtained by interpolating the missing geometry between the contour curves ∂T_1^+ and ∂T_2^- , guided by the corresponding skeletal graphs of the topologies.

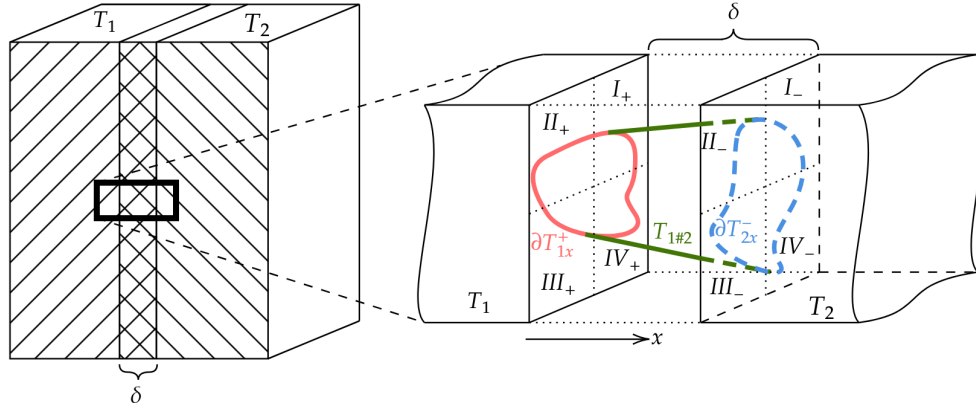


Figure 3.13 The transition region $T_{1\#2}$ in the gap δ between topologies T_1 and T_2

It is essential to mention that ∂T_1^+ and ∂T_2^- are not necessarily closed curves. For example, the cross-section of a face of the Schwarz P unit cell topology is a closed circular shape. However, the proposed approach is supposed to cover cases where the unit cells are not necessarily whole. For example, four differently oriented open curves represent a cross-section of half of the Schwarz P surface unit cell. Therefore, $T_{1\#2}$ can be a union of disconnected surfaces. It has been shown that the interpolated connection between two solid

bodies defined with surfaces may not be trivial and can result in visual artifacts (Cohen-Or et al., 1998). It is proposed to mitigate this effect by splitting topology faces T_1^+ and T_2^- into quarters, considering that the origin is located at the centroid of the faces. Let I_+ , II_+ , III_+ , and IV_+ denote the quarters on the T_1^+ face, or positive quarters, and I_- , II_- , III_- , and IV_- denote the quarters on the T_2^- face, or the negative quarters. It is proposed to connect curve sections in positive quarters to their respective sections in negative quarters. This approach considers $T_{1\#2}$ a skeletal graph derived from the two neighboring graphs.

This method assumes that T_1 and T_2 are tessellated regularly and $\partial T_1^+ \parallel \partial T_2^-$. Enabling the support of irregular tessellations is proposed for future work.

For a more detailed explanation of the implementation of the proposed approach and examples of generated models of cellular structures, please refer to Section 4.3.2.

3.4 Stochastic cellular structures

Stochastic cellular structures can be fully defined using three design parameters: connectivity, relative density, and beam thickness (Kechagias et al., 2022). A visual representation of stochastic cellular structures with varying design parameters is shown in Fig. 3.14 to illustrate how these parameters affect the overall structure. Connectivity is a porosity regulator and a key factor for the mechanical behavior of the structure. By controlling the design parameters of a cellular structure, such as beam thickness or cell size, foam-like structures with stiffness that varies throughout the part can be created (Hossain et al., 2021). Cellular structures can be designed using stochastic approaches, like Voronoi tessellation and Delaunay triangulation, to generate complex and irregular geometries (Savio et al., 2018; Zheng et al., 2021). Voronoi diagrams allow for space partitioning into cells, while Delaunay triangulations enable the creation of a network of interconnected nodes and

struts. These approaches can be combined with graph representations to efficiently model and analyze stochastic cellular structures ([Zheng et al., 2021](#)).

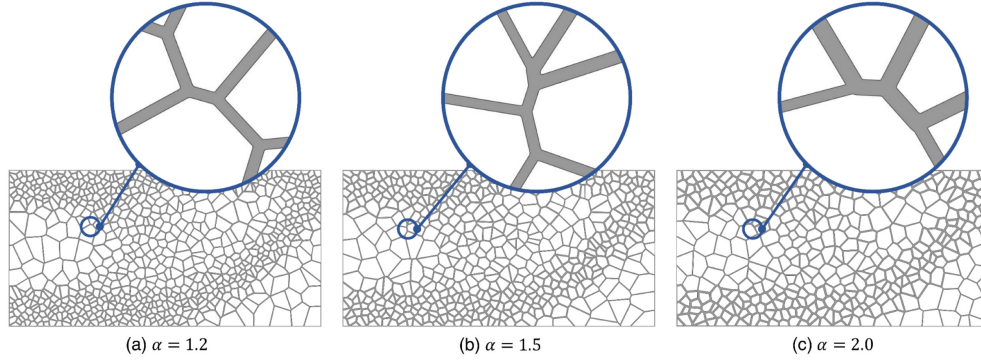


Figure 3.14 Voronoi cellular structures with various α which defines the ratio between the maximal and minimal beam thicknesses ([Do et al., 2021](#))

In this research, it is proposed to modify the original beam-based cellular structure modeling approach and adjust it for a stochastic case, incorporating skeletal graphs to represent the topology. As seen in Equation 3.1, defining the topology T is required in LF-rep first. T is a skeletal graph of lines of zero thickness. T is defined for a unit cell, and then P is applied to set its geometric properties, such as the beam thickness.

Beam-based unit cells in the original approach are defined as equations of line segments. Stochastic cellular structures, such as the Voronoi structure, have no unit cell. Therefore, T must define the skeletal graph of the whole structure. It is proposed to consider T as a 3D graph structure of edges that are connected at vertices, thereby representing the skeletal graph. Let Γ be a 3D graph consisting of n vertices, denoted as $w_1, \dots, w_i, \dots, w_j, \dots, w_n$, and m edges, represented as $\epsilon_{1,2}, \dots, \epsilon_{i,j}, \dots, \epsilon_{m-1,m}$, where $i \neq j$. Consider an arbitrary edge $\epsilon_{i,j}$ between vertices $w_i = (x_i, y_i, z_i)$ and $w_j = (x_j, y_j, z_j)$, which are shown in Fig. 3.15. Then, each edge can be defined in parametric form as

$$\epsilon_{i,j}(\alpha) = w_i + \alpha(w_j - w_i) \quad (3.24)$$

for $0 \leq \alpha \leq 1$, or

$$\epsilon_{i,j}(\mathbf{X}) : \frac{x - x_i}{x_j} = \frac{y - y_i}{y_j} = \frac{z - z_i}{z_j}. \quad (3.25)$$

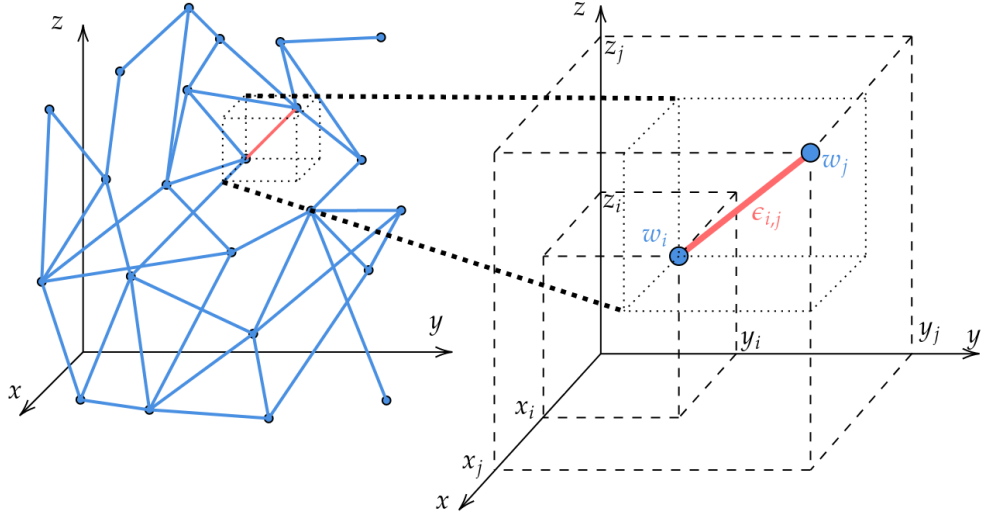


Figure 3.15 The edge $\epsilon_{i,j}$ between vertices w_i and w_j of a graph Γ

Consider that the edge $\epsilon_{i,j}(\mathbf{X})$ is nonexistent, or $\epsilon_{i,j}(\mathbf{X}) = \emptyset$, if vertices w_i and w_j are not connected in Γ or $i = j$. In this case, T is defined for the whole cellular structure as a union of all edges:

$$T(\mathbf{X}) = \bigcup_{i=1}^n \bigcup_{j=1}^m \epsilon_{i,j}(\mathbf{X}). \quad (3.26)$$

Voronoi cellular structures are commonly used in design for AM (DFAM) when the structure must be stochastic [Do et al. \(2021\)](#). The seeds of the Voronoi tessellation are considered to be uniformly distributed within the design space \mathbf{X} according to a specific distribution, such as a Poisson disk sampling. This work proposes to identify the edges of a Voronoi cellular structure by tracing the edges after applying the radial growth from its seeds ([Kim et al., 2005](#)). In this approach, since Voronoi edges are conic, they can be

described by a rational quadratic Bézier curve

$$B(\alpha) = \frac{\omega_0(1-\alpha)^2 p_0 + 2\omega_1(1-\alpha)\alpha p_1 + \omega_2\alpha^2 p_2}{\omega_0(1-\alpha)^2 + 2\omega_1(1-\alpha)\alpha + \omega_2\alpha^2}, \quad (3.27)$$

where p_0 , p_1 , and p_2 are the control points, and ω_0 , ω_1 , and ω_2 are their corresponding weights. The Bézier curve converges to a straight line by fitting tangent spheres between any three neighboring spheres with Voronoi seeds as their center. The complexity of this algorithm is $O(n)$ (Kim et al., 2005).

3.5 Conformal cellular structures

This subsection delves into the geometric modeling of conformal cellular structures using the LF-rep approach. It emphasizes the importance of skeletal graphs in representing a topology that conforms to a given surface or volume.

Geometric modeling plays a critical role in designing conformal cellular structures that adhere to the shape of a surface. Various methods have been proposed in the literature to support the efficient design and fabrication of such structures. However, these methods have disadvantages and limitations, which need to be addressed to improve their applicability.

This section is divided into two to discuss different aspects of conformality. In Section 3.5.1, the proposed method for generating cellular structures that conform to the boundary surfaces of an object is discussed. This ensures that the cellular structure precisely follows the surface geometry of the object, allowing for better control over structural properties and aesthetics. Subsection 3.5.2 delves into the proposed method for the generation of cellular structures that conform to the internal volumetric boundaries of an object. This is particularly useful for creating structures with varying material distribution or density, which can result in more efficient use of materials and improved performance in specific

applications. Both surface and volume conformality approaches are essential in the design of complex and functional cellular structures.

3.5.1 Surface conformality

The proposed LF-rep method to conform a cellular structure to a surface is achieved by transforming the design space \mathbf{X} to another design space \mathbf{X}_Φ that is mapped to an arbitrary surface Φ . In this context, the skeletal graph plays a crucial role in defining the topology of the cellular structure while adhering to the surface conformality constraints.

The transformation $\mathcal{N} : \mathbf{X} \rightarrow \mathbf{X}_\Phi$ might not be affine, and \mathcal{N} might not be a vector between points in \mathbb{R}^3 . This is because the surface's intrinsic geometry determines the conformal map, and the edges of a polyhedron have no geometric significance in this context, even when the metric arises from an embedding in \mathbb{R}^3 (Crane, 2020). The skeletal graph representation of the cellular structure enables the preservation of the topology while accommodating the complex geometric transformations required to achieve surface conformality. Figure 3.16 illustrates this transformation.

In the LF-rep framework, Φ is considered to be a middle plane of the cellular structure, and η is collinear with the normal unit vector \vec{n}_Φ of Φ . Let h be the thickness of the cellular structure that conforms to the surface Φ . The skeletal graph is then used to create a cellular structure that conforms to the surface Φ , maintaining the thickness h and the intended geometric properties, as follows. The furthest equidistant surfaces Φ_+ and Φ_- from the middle plane Φ will be positioned at $h/2$ from it in the directions of \vec{n}_Φ and $-\vec{n}_\Phi$, respectively. Constructing the equidistant surfaces Φ_+ and Φ_- is not always trivial (Vyshnepolsky et al., 2022). If Φ is defined in parametric form $\vec{\Phi}(p, q)$, then the

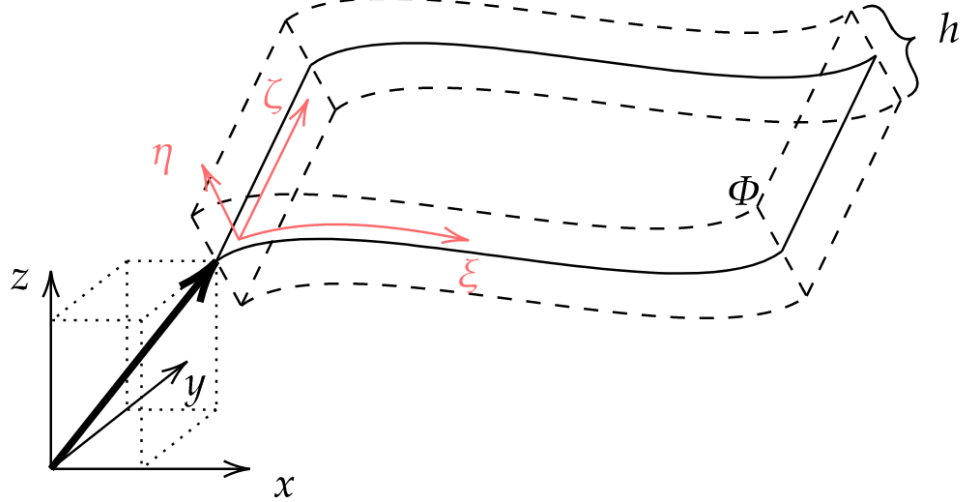


Figure 3.16 A transformation of the design space $\mathcal{N} : \mathbf{X} = (x, y, z) \rightarrow \mathbf{X}_\Phi = (\xi, \zeta, \eta)$ where \mathbf{X}_Φ is Cartesian with respect to the surface Φ . The skeletal graph of the cellular structure is used to maintain the topology while achieving surface conformality. Φ is considered the middle surface of the cellular structure that infills the volume with the thickness h .

vector \vec{n}_Φ can be found as

$$\vec{n}_\Phi = \frac{\left(\frac{\partial \vec{\Phi}}{\partial p}(p, q) \right) \times \left(\frac{\partial \vec{\Phi}}{\partial q}(p, q) \right)}{\left| \left(\frac{\partial \vec{\Phi}}{\partial p}(p, q) \right) \times \left(\frac{\partial \vec{\Phi}}{\partial q}(p, q) \right) \right|}. \quad (3.28)$$

After finding \vec{n}_Φ , the surfaces Φ_- and Φ_+ can be obtained numerically by offsetting every point of Φ by $\pm h \vec{n}_\Phi / 2$. This numerical approach is ensured by obtaining an equation for a line passing along \vec{n}_Φ and solving this equation as a system of two equations with the Euclidian distance

$$(x - x_\Phi)^2 + (y - y_\Phi)^2 + (z - z_\Phi)^2 = \left(\frac{h}{2} \right)^2, \quad (3.29)$$

where (x_Φ, y_Φ, z_Φ) is the offsetted point. Note that in the general case (x_Φ, y_Φ, z_Φ) will have two solutions for $h \vec{n}_\Phi / 2$ and $-h \vec{n}_\Phi / 2$. By leveraging the skeletal graph representation, it is possible to effectively conform the cellular structure to the surface while preserving the

structural topology and achieving surface conformality.

The proposed method for surface conformality using skeletal graphs paves the way for future research to improve support for non-Cartesian \mathbf{X}_Φ and consider more complex conformal mapping scenarios. The skeletal graph representation provides a powerful and flexible approach to achieving surface conformality while maintaining the intricate topological features of the cellular structure.

3.5.2 Volume conformality

In this work, through the LF-rep approach, it is proposed to extend the functionality of the approach by allowing \mathbf{X} to be limited to $\mathbf{X}_f \subset \mathbf{X} \subset \mathbb{R}^3$ while employing the skeletal graph representation to preserve the topology of the cellular structure.

Given a volume V that the cellular structure should uniformly infill, a skeletal graph $T = (W_T, E_T)$ can be used to define the connectivity and geometric properties of the structure, ensuring that it conforms to the intended volume. Here, W_T represents the vertices of the graph, and E_T represents the edges that connect the vertices. The skeletal graph can be mathematically described in a general form as follows:

$$T = (W_T, E_T) = \left\{ \begin{array}{l} w_i \in \mathbb{R}^3 \mid i = 1, 2, \dots, n_w; \\ \epsilon_{ij} = (w_i, w_j) \mid i, j = 1, 2, \dots, n_w; i \neq j \end{array} \right\}, \quad (3.30)$$

where n_w is the number of vertices in the graph, and ϵ_{ij} denotes an edge connecting vertices w_i and w_j .

Employing a skeletal graph makes it possible to create a more stable structure with better mechanical properties, as it ensures that the structure is more evenly loaded, reducing the likelihood of stress concentrations and failure points. A mathematical representation

of the cellular structure's uniformity can be expressed as follows:

$$\mathcal{U}(W) = \sum_{\epsilon_{ij} \in E_T} \frac{1}{|E_T|} \left| \frac{\partial W}{\partial \epsilon_{ij}} \right|, \quad (3.31)$$

where $\mathcal{U}(W)$ represents the uniformity of the cellular structure within the volume W and $\frac{\partial W}{\partial \epsilon_{ij}}$ denotes the change in the volume due to a change in edge ϵ_{ij} .

However, such an approach can result in an abrupt cut of beams in cellular structures. To address this issue, it is proposed to introduce the net-skin method shown in Fig. 3.17 to cellular structures, which incorporates the skeletal graph representation. A net-skin is applied to a cellular structure to mitigate the adverse effects of trimming ([Aremu et al., 2017](#)).

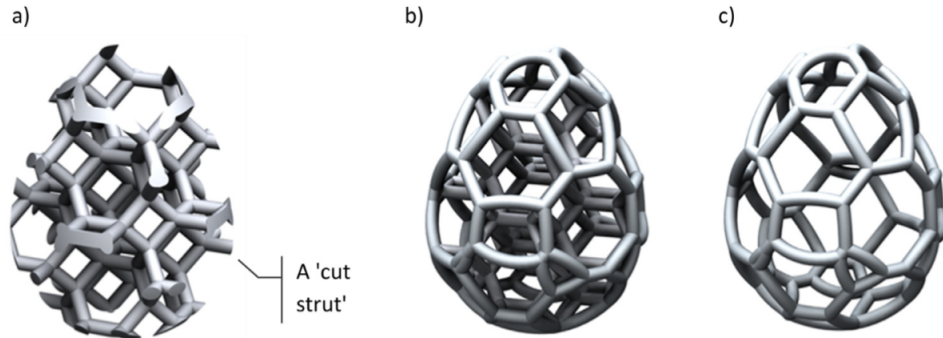


Figure 3.17 (a) A trimmed cellular structure based on the skeletal graph, (b) the cellular structure with a net-skin, and (c) the net-skin ([Aremu et al., 2017](#))

The net-skin method is useful for creating conformal cellular structures with complex geometries and can be used to optimize the structure's mechanical properties. This method is particularly useful for creating structures with non-uniform strut orientations, connectivity, and sizes, which can significantly affect the mechanical properties of the structure ([Aremu et al., 2017](#)).

Chapter 4

Implementation

We are stuck with technology when what we
really want is just stuff that works.

Douglas Adams (1952 – 2001),

THE SALMON OF DOUBT

For the implementation of the proposed LF-rep approach, it was decided to use Open CASCADE Technology (OCCT), the most widely used and well-documented open-source GMK ([Yuan and Zhang, 2008](#); [Banovic et al., 2018](#)). Developing the software prototype in the C++ programming language, which is the native programming language of OCCT, can undoubtedly prove to be useful in the long run for geometric modeling applications, which is confirmed by extensive use of C++ in every major existing CAD software ([Li et al., 2011](#); [Golovanov, 2014](#)). However, for prototyping purposes, it was decided to develop a minimal viable product (MVP) that would be faster to create and easier to iterate for further improvements ([Ries, 2011](#); [Lenarduzzi and Taibi, 2016](#)). For this purpose, it was decided to build the software prototype based on CadQuery ([Urbanczyk et al., 2021a](#)) as the modeling tool and CQ-editor ([Urbanczyk et al., 2021b](#)) as the GUI shell, both licensed

under a permissive license and written in Python. CadQuery introduces parametrization methods built on top of OCCT, which are critical for the proposed work. Moreover, OCCT and CadQuery are cross-platform, meaning that the developed prototype has no limitation in terms of an OS that it can be used on.

The development was focused only on the implementation of the methodology itself. The LF-rep methodology is implemented in a Python library, which describes all the geometry and constraints, and works together with CadQuery. The GUI is inherited from CQ-editor with an ability to import the developed library from within the CQ-editor inline code editor. The GUI also includes the 3D CAD viewer capable of rendering the resulting solid models with the OCCT GMK.

It is proposed that to generate CAD files via the LF-rep methodology, users need to provide several input parameters that define the desired cellular structure characteristics. These parameters are critical for customizing the generated cellular structures to meet the specific design requirements and constraints. The user input parameters include:

1. **Unit cell type:** Users need to select the desired unit cell type for the cellular structure, such as FCC, BCC, or gyroid. This selection will determine the overall topology and mechanical properties of the generated structure.
2. **Unit cell size:** Users must define the size of the unit cell, which will determine the dimensions of the entire cellular structure. This parameter can be adjusted to control the density and porosity of the generated structure. Note that a unit cell is not necessarily cubic.
3. **Domain dimensions:** Users need to provide the dimensions of the design domain, which will define the overall size of the cellular structure. This parameter is essential to ensure that the generated structure fits within the desired space or conforms to

specific design constraints.

4. **Geometric parameter types:** Users must choose the types of geometric parameters they wish to vary in the cellular structure. These parameters can include thickness, truncation, beam cross-section, and others. By varying these parameters, users can customize the cellular structure to achieve specific design goals or meet specific performance requirements.
5. **Parameter values:** Users need to provide the values for the chosen geometric parameters. These values can be constant or controlled by functions. For example, users can specify a constant thickness for the entire cellular structure or define a function that varies the thickness across the structure based on spatial coordinates or other input parameters. By controlling the values of these geometric parameters, users can fine-tune the performance and behavior of the cellular structure to meet their design objectives.

After providing these input parameters, the LF-rep methodology will generate the CAD files for the cellular structure, which can then be visualized and further processed.

This chapter delves into the practical application of the proposed geometric modeling methods discussed in Chapter 3. This chapter begins with Section 4.1, which introduces the functional definition of cellular topologies, covering both beam-based and surface-based topologies. Section 4.2 focuses on the implementation of the functional variation of geometric parameters, detailing how these parameters can be varied to create complex cellular structures. Section 4.3 discusses the implementation of the proposed approach to model cellular structures with multiple topologies. Section 4.4 explores the implementation of the proposed approach to model stochastic cellular structures and their application to surface-based cellular structures with multiple topologies. Conformal cellular structures are ad-

dressed in Section 4.5, which elaborates on both surface and volume conformality. Section 4.6 introduces LatticeQuery, a computational tool developed to support the proposed geometric modeling methods, including its architecture and usage. Section 4.7 evaluates the computational performance of the proposed methods, providing insights into the efficiency and effectiveness of the implementation. Finally, Section 4.8 provides a summary of this chapter.

4.1 Functional definition of cellular topologies

The implementation's first step is defining skeletal graphs of topologies. The implementation approaches differ between the beam-based and TPMS-based topologies. However, in both cases, a function T that defines the topology is required to be determined. The theoretical concepts implemented in this section have been introduced in Section 3.1.

4.1.1 Beam-based topologies

For the beam-based topologies, the topologies are defined by the positions of nodes and the line segments between them accordingly to each specific topology. The lines and nodes allow immediate obtaining of the function T as a union of equations for multiple straight lines.

Figure 3.4 illustrates beam-based topologies inspired by the cubic crystal system in crystallography that the developed software prototype can model, which includes: simple cubic (Fig. 3.4a), BCC (Fig. 3.4b), and FCC (Fig. 3.4c). Several varieties of these topologies are supported as well, such as self-supporting FCC without horizontal beams (S-FCC; Fig. 3.4d), BCC with additional four z -direction oriented beams (BCCz; Fig. 3.4e), FCC with additional four z -direction oriented beams (FCCz; Fig. 3.4e), S-FCCz (Fig. 3.4f), face-

and body-centered cubic (FBCC; Fig. 3.4h), S-FBCC (Fig. 3.4i), and S-FBCCz (Fig. 3.4j). All topologies shown in Fig. 3.4 have the cell size $u = 10\text{mm}$ and have a 1mm beam diameter and 1.1mm node diameter.

Figure 3.5 illustrates other supported beam-based topologies such as diamond (Fig. 3.5a), rhombicuboctahedron (Fig. 3.5b), and truncated cube (Fig. 3.5c). All topologies shown in Fig. 3.5 have the cell size $u = 10\text{ mm}$ and have 1.0 mm beam diameter and 1.6 mm node diameter. The truncation τ for the rhombicuboctahedron and the truncated cube topologies in Fig. 3.5 is 40%.

The beam-based topologies are common in design for AM ([Panesar et al., 2018](#)), but the process of their definition is based on F-rep in this work. These topologies were defined in the software prototype while following the object-oriented programming (OOP) principles which are crucial for any CAD ([Stroustrup, 1988](#); [Warman, 1990](#)). In particular, certain features are repeated across topologies, such as, for example, vertical z -oriented beams in simple cubic and BCCz topologies. These features were made into separate classes reused in other topologies. In the proposed work, OOP enables simple for the end-user modular definition of topologies and allows the end-user to define custom topologies. As a result, the number of topologies possible to be modeled is not limited by the ones illustrated in Fig. 3.4.

The geometric modeling of beam-based topologies is implemented as follows. A shape that defines the beam cross-section is defined. For example, in Fig. 3.4 and Fig. 3.5, the shape of the cross-section is set to be a circle. In the case of the beam-based topologies, the skeletal graph is generated as a wireframe made of the instances of the `TopoDS_Wire` class from OCCT. The wires are then subject to the sweep operation, which is described by the `BRepPrimAPI_MakeSweep` class in OCCT, which generates a solid model based on the wireframe, cross-section, and thickness, and is declared as shown in Listing. 1.

```

1 class BRepPrimAPI_MakeSweep : public BRepBuilderAPI_MakeShape
2 {
3     public:
4         DEFINE_STANDARD_ALLOC
5         //! Returns the TopoDS Shape of the bottom of the sweep.
6         Standard_EXPORT virtual TopoDS_Shape FirstShape() = 0;
7         //! Returns the TopoDS Shape of the top of the sweep.
8         Standard_EXPORT virtual TopoDS_Shape LastShape() = 0;
9     protected:
10    private:
11 };

```

Listing 1: The sweep operation class declared in OCCT that is used to implement wireframe modeling

Special attention was dedicated to the ability to model the nodes of the beam-based topologies. Nodes are critical components that allow a smooth transition between each unit cell and enable better manufacturability of such cellular structures.

4.1.2 Surface-based topologies

For the TPMS-based topologies, array programming with the NumPy library is used ([Harris et al., 2020](#)). In particular, NumPy allows the creation of linear spaces x , y , and z and uses them as variables for any function. Moreover, NumPy shows extremely high performance when dealing with large arrays of periodic data, which is natural in the geometric modeling of cellular structures since they are arrays themselves. Thus, NumPy opens the possibility of implementing subdivision surfaces to model TPMS structures. To achieve the effect of subdivision surfaces, several sample points are taken from each octant of a unit cell of a TPMS topology based on an implicit function that defines it. It has been found that 18 points per octant (144 points per unit cell) are sufficient to accurately represent the TPMS topologies supported by this approach. These points are used for modeling NURBS

and surfaces of the skeletal graph based on them. A modeling optimization process was designed to model only an octant of a unit cell and translate it seven times afterward to obtain an entire TPMS unit cell. This optimization is seen as visible boundaries between each octant of the unit cell in Fig. 3.7. The mirroring results are then united and considered a single solid model by Open CASCADE, even though a boundary remains. The definition of an octant rather than an entire unit cell is solely an optimization technique that works behind the scene of the application. Such an optimization technique decreases the number of subdivision iterations and thus mitigates a key disadvantage of subdivision surfaces mentioned in Section 2.1.1. Afterward, the resulting surfaces need to be converted into solid objects. The solidification is made possible by the implementation of the `BRepOffsetAPI_MakeFilling` class from OCCT, which allows the generation of a solid object by offset from the NURBS surface and which is shown in Listing 2. This offset is one-directional in this class. Thus, to generate a surface-based solid object with a thickness t , two solid models are generated from a single surface: one with the $t/2$ offset and another with the $-t/2$ offset. This approach ensures that the surface is in the middle of the desired solid model.

Figure 3.7a, Fig. 3.7b, and Fig. 3.7c illustrate the gyroid, the Schwarz ‘primitive’ (P) surface, and the Schwarz ‘diamond’ (D) surface topologies, respectively, modeled with the LF-rep approach. Table 3.5 covers the topology defining functions T for these topologies. The illustrated unit cells have the size $u = 20$ mm and the thickness $t = 20$ mm. Note that visible boundaries exist between each TPMS-based unit cell octant. This effect appears due to the object-oriented programming (OOP) optimization mentioned above. This optimization technique models only one octant and utilizes it to build the rest of the unit cell.

```

1 class BRepOffsetAPI_MakeFilling : public BRepBuilderAPI_MakeShape
2 {
3 public:
4     DEFINE_STANDARD_ALLOC
5     Standard_EXPORT BRepOffsetAPI_MakeFilling(const Standard_Integer Degree =
6         ↳ 3, const Standard_Integer NbPtsOnCur = 15, const Standard_Integer NbIter
7         ↳ = 2, const Standard_Boolean Anisotropie = Standard_False, const
8         ↳ Standard_Real Tol2d = 0.00001, const Standard_Real Tol3d = 0.0001, const
9         ↳ Standard_Real TolAng = 0.01, const Standard_Real TolCurv = 0.1, const
10        ↳ Standard_Integer MaxDeg = 8, const Standard_Integer MaxSegments = 9);
11     /*
12      The class includes more tolerance constants and data storage methods that
13      are available in the OCCT source code.
14     */
15 protected:
16 private:
17     BRepFill_Filling myFilling;
18 };

```

Listing 2: The surface offset operation class declared in OCCT that is used to implement surface-based cellular structures

4.2 Functional variation of geometric parameters

The next step of the implementation is to transform the obtained skeletal graph into a solid body by adding thickness. The beam-based topologies are solidified by defining a cross-section of the beam and its further application to each line segment that forms the beam. The TPMS-based topologies are solidified by utilizing the ability of OCCT to model solid bodies by B-rep offset. Considering that the thickness of a TPMS-based unit cell of a cellular structure is set to be t , a $t/2$ offset in both normal directions must be applied to the NURBS surface that forms the skeletal graph of the topology.

As for the implementation of the variation of geometric parameters of a cellular structure, linear spaces generated by NumPy are used as an input to any arbitrary function that

defines the distribution of the parameters.

As an example of the implementation, consider a heterogeneous cellular structure based on the Schwarz P that is described by Equation 3.14 and with the thickness distribution changing linearly and described by Equation 3.15. Let the unit cell size be set to 20 mm, and the lattice size to $10 \times 10 \times 10$. The resulting solid model is a heterogeneous Schwarz P cellular structure with varying thicknesses, illustrated in Fig. 4.1.

$P(\mathbf{X})$ is not limited to being linear as in Equation 3.15. For example, consider a BCC cellular structure with the size of $N_x = 20$, $N_y = 6$, and $N_z = 6$ with the beam diameter controlled by the parabolic function:

$$P(\mathbf{X}) : D(x) = -4D_{\max}(x - 0.5)^2 + D_{\max} + D_{\min}, \quad (4.1)$$

where D is the diameter of a beam of the BCC cellular structure, and D_{\min} and D_{\max} are the cellular structure's minimal and maximal diameters, respectively. This function was chosen as an example since it is symmetrical around $x = 0.5$. $D_{\min} = 1$ mm and $D_{\max} = 6$ mm were selected for this example. The resulting BCC structure is illustrated in Fig. 4.2. The cellular structure's beam diameter varies along the z -axis, which follows the parabolic function in Equation 4.1. Observe that the node diameter varies since it is also a parameter a function can control, and the process is virtually the same. In this example, the node diameter was chosen to be 10% larger than the beam diameter.

Non-linear variation of geometric parameters of cellular structures is not present in other existing tools, such as Autodesk Netfabb, which are limited to a linear change of parameters.

Figure 4.3 provides one more visual comparison between the parameter-defining function P and the resulting solid model. In this example, the thickness of the TPMS-based cellular

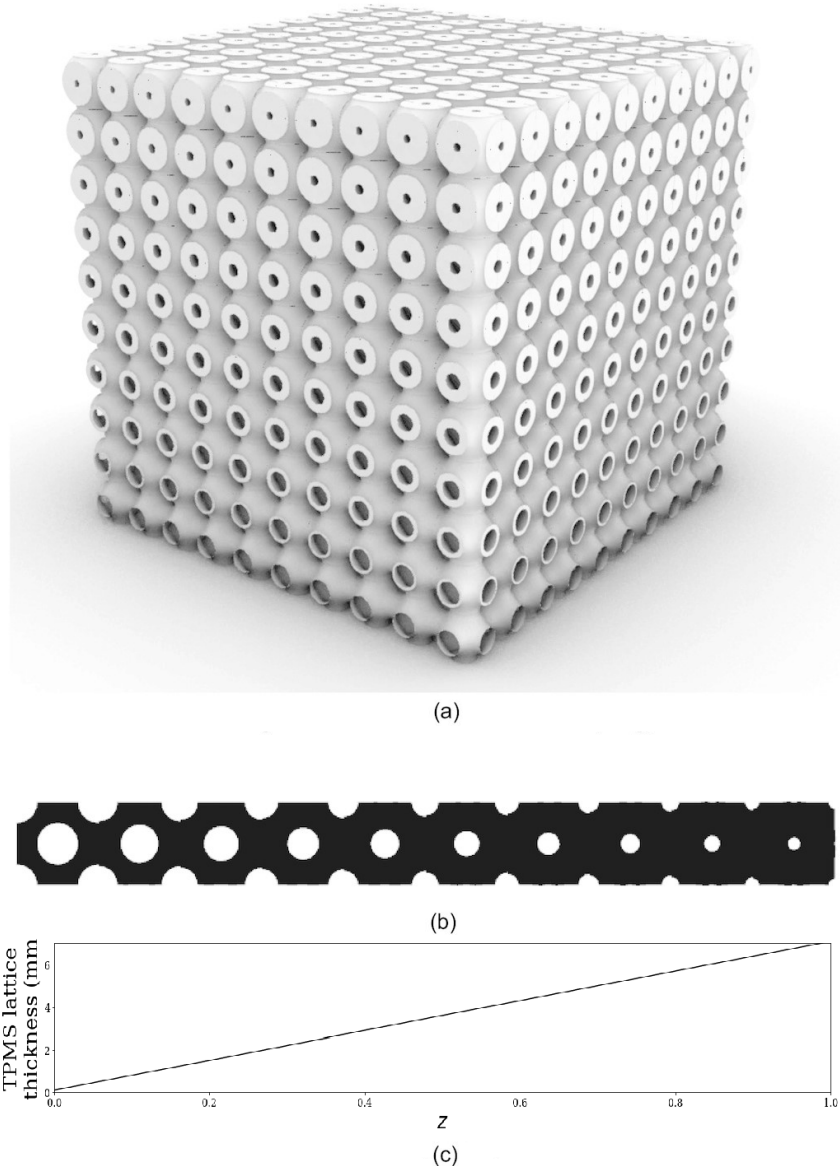


Figure 4.1 (a) An isometric view on a heterogeneous cellular structure with Schwarz P topology with linearly varying thickness generated with the proposed approach, (b) a side view on its single column in the z -direction, and (c) the linear function P that corresponds to the thickness of the TPMS-based structure vs. the z coordinate (Letov and Zhao, 2022)

structure is controlled by the sine function:

$$P(\mathbf{X}) : t(z) = 3 \sin(6\pi x) + 4, \quad (4.2)$$

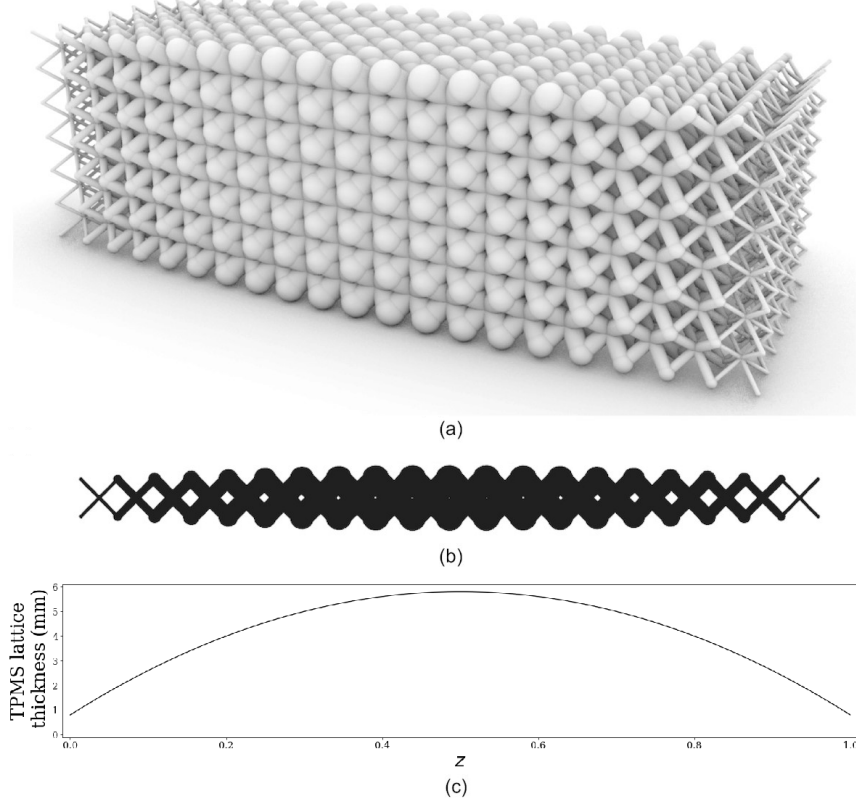


Figure 4.2 (a) An isometric view on a heterogeneous cellular structure with BCC topology with non-linearly varying thickness generated with the proposed approach, (b) a side view on its single column in the x -direction, and (c) the parabolic function P that corresponds to the thickness of the TPMS-based structure vs. the x coordinate ([Letov and Zhao, 2022](#))

so that the thickness varies in the range $t \in [1.0, 7.0]$. The size of the cellular structure is $N_x = 10$, $N_y = 10$, and $N_z = 20$.

A single cellular structure can have several geometric parameters varying in different directions. Consider the heterogeneous cellular structure illustrated in Fig. 4.4, which is modeled with the developed software prototype. This cellular structure has an FCC topology and has its beam size t decreasing along the y -axis linearly from 2.0 mm to 0.5 mm. However, the shape of the cross-section of the beam changes along the z -axis, which is uncommon in existing cellular modeling tools. In this case, the beam cross-

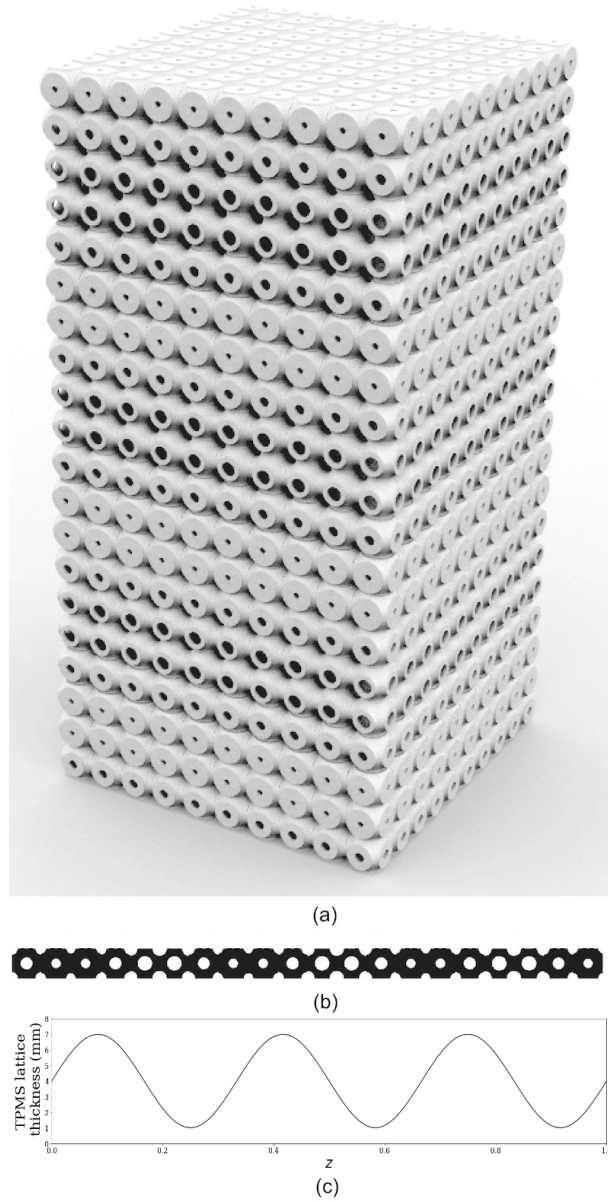


Figure 4.3 (a) An isometric view on a heterogeneous cellular structure with Schwarz P topology with non-linearly varying thickness generated with the proposed approach, (b) a side view on its single column in the z -direction, and (c) the sine function P that corresponds to the thickness of the TPMS-based structure vs. the z coordinate ([Letov and Zhao, 2022](#))

section's general shape is a square with the side length t and with vertices rounded with a fillet of the radius ρ_c as sketched in Fig. 4.5a. For this cellular structure, ρ_c is set to increase

linearly from $0.2t$ to $0.5t$. Note that $\rho_c = 0.5t$ is the extreme case in which the shape of the cross-section converges to a circle, as sketched in Fig. 4.5b. Such a transition between the two different beam cross-sections can be applied in, for example, AM of bone implants. It has been shown that the area moment of inertia of a beam cross-section can be used to indicate the mandible stiffness of the implant patient (Hansson and Ekestubbe, 2004). Control over the beam cross-section and, by the extent, of the area moment of inertia can enhance the AM of bone implants that feel more natural to the patient and have a lesser chance of being rejected by the body.

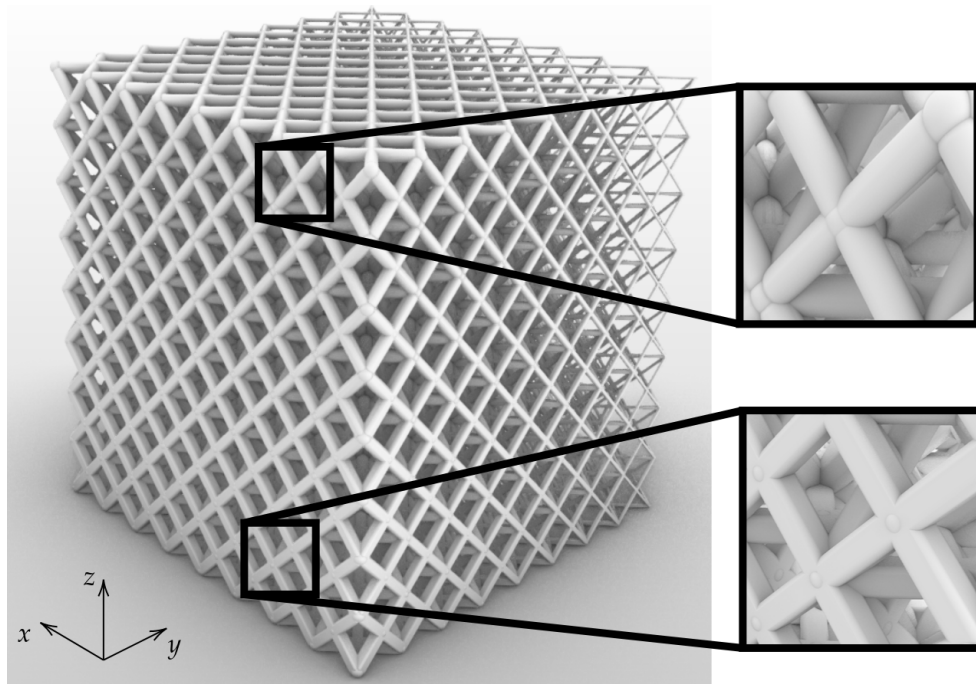


Figure 4.4 A heterogeneous cellular structure with the FCC topology with varying thickness and beam cross-section (Letov and Zhao, 2022)

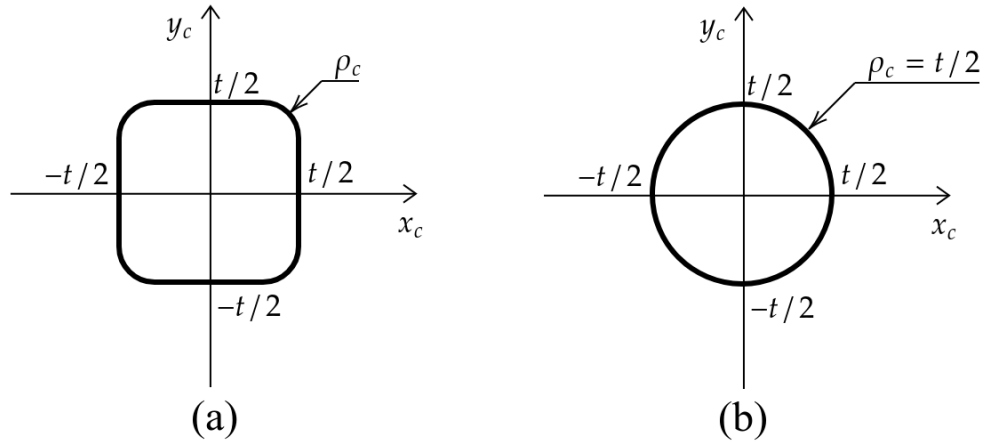


Figure 4.5 Cross-sections of a beam in shapes of (a) a square with rounded corners and (b) a circle ([Letov and Zhao, 2022](#))

4.3 Cellular structures with multiple topologies

This section discusses the implementation of the proposed method for the geometric modeling of cellular structures with multiple topologies. The ability to transition between different topologies within a single cellular structure enables the creation of heterogeneous cellular structures with tailored mechanical properties, paving the way for novel and innovative engineering solutions. Two main approaches for achieving topology transitions are discussed in this section – connectivity of beam-based topologies by the transition plane and controllable truncation – as well as the method of surface-based cellular structures with multiple topologies. Throughout this section, detailed examples are provided to demonstrate the versatility and potential of these approaches in various scenarios.

4.3.1 Beam-based cellular structures with multiple topologies

This subsection delves into the intricacies of beam-based cellular structures with multiple topologies, highlighting the methods and techniques employed to seamlessly transition between distinct topologies within a single cellular structure. By leveraging the transi-

tion plane concept, the connectivity of beam-based topologies is explored. Additionally, controllable truncation is introduced as an alternative approach to facilitate topology transitions, examining its application in cellular structures based on truncated polyhedrons. This discussion provides valuable insights into the design and implementation of heterogeneous cellular structures with beam-based topologies, offering a foundation for advanced applications in various fields.

Connectivity of beam-based topologies by the transition plane

As described in Section 3.3, it is possible to achieve the transition of topology T_1 into topology T_2 by defining the transition plane \mathcal{P} with an arbitrary position and orientation. This also enables support for non-cubic unit cells as one of the topologies may have the form of a cuboid.

As an example of such topology transition, consider a heterogeneous cellular structure with a total size of $37.5 \times 37.5 \times 37.5$ mm³, which consists of topologies T_1 and T_2 . Let T_1 and T_2 transition in the transition plane \mathcal{P} defined as

$$\mathcal{P}(\mathbf{X}) : x + z - 37.5 = 0, \quad (4.3)$$

so that the normal vector of \mathcal{P} forms 45° with the positive direction of the x -axis. Let the topology T_1 correspond to the cubic FCC with the unit cell size of $u_1 = 3.75$ mm, and the topology T_2 correspond to the cuboid BCC with the transition plane. Figure 4.6 illustrates the transition in detail. In this case, $u_2 = u_1/\sqrt{2} = 2.66$ mm.

According to the framework, after the definition of the topology T , the geometric parameters P are needed to be defined. The beams of the topologies in Fig. 4.6 are set to have the diameter $d = 0.7$ mm, and the node diameter is set to $D = 0.75$ mm.

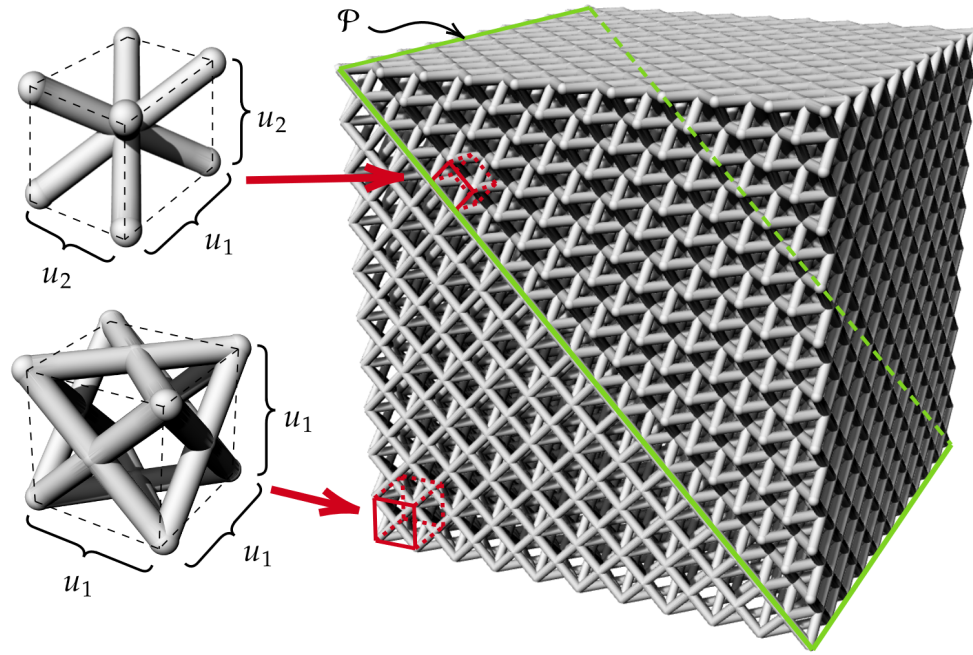


Figure 4.6 The transition between the FCC topology with the cubic unit cell to the BCC topology with the cuboid unit cell along the transition plane \mathcal{P} . Note that the BCC topology is rotated 45° (Letov and Zhao, 2023a)

Controllable truncation as a means to achieve topology transition

It is possible to achieve the topology transition T by controlling other geometric parameters P , such as the truncation τ of topologies that are based on the truncated polyhedrons. This can be done by defining $P(\mathbf{X}) : \tau(\mathbf{X})$.

Consider a $10 \times 10 \times 10$ cellular structure with the truncated cube topology with the unit cell size $u = 10$ mm as an example of such topology transition. Let the truncation τ of the truncated cube topology linearly change from $\tau_{\min} = 0$ (0%) to $\tau_{\max} = u/2 = 5$ mm (100%), i.e.

$$P(\mathbf{X}) : \tau(z) = z, \quad (4.4)$$

where $z \in [0, 1]$ is the variable corresponding to the z -axis. In this approach, $z \in [0, 1]$ is mapped to the actual coordinate $z_a \in [1, N_z]$ with $z_a \in \mathbb{N}^+$. The beam diameter is set

to 1 mm, and the node diameter is set to 1.05 mm. The resulting heterogeneous cellular structure is illustrated in Fig. 4.7. Note that at $z = 0$, the topology T described in Table 3.4 converges to the simple cubic topology defined by Equation (3.23), and at $z = 1$ it converges to the cuboctahedron topology. The approach allows simultaneous control over different geometric parameters in different directions. In this example, the beam thickness is an additional parameter that linearly increases from 0.5 mm on the left and 5.0 mm on the right, similar to the truncation. Note that the cellular structure nodes have a diameter larger than the diameter of the beams and is set to increase linearly from 0.55 mm to 5.5 mm.

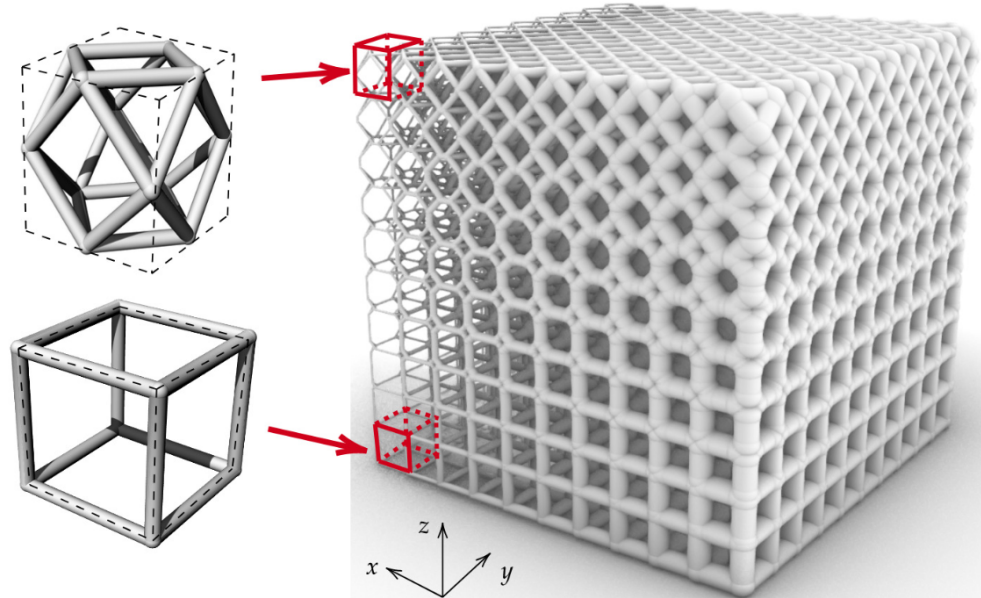


Figure 4.7 A heterogeneous cellular structure with the topology based on a truncated cube with the truncation parameter τ varying along the z -axis. The topology converges to the simple cubic at the bottom, and the cuboctahedron topology shifted to half of the unit cell size at the top. The thickness of the beams is linearly varying along the x -axis (Letov and Zhao, 2023a)

The truncation can be one of the potential output parameters of a topology optimization algorithm. For example, different regions of the cellular structure can be assigned a different

truncation depending on whether the region is subject to bending-, compression-, or tension loads (Alghamdi et al., 2020). Additionally, since the control over the truncation allows a smooth and continuous transition between topologies, this approach can find its application in lattice embedding (Sanders et al., 2021).

Another example of a topology that can support the truncation-based topology transition is the rhombicuboctahedron topology. Consider a $10 \times 10 \times 10$ cellular structure with the rhombicuboctahedron topology and unit cell size $u = 10$ mm. Let the truncation τ of the rhombicuboctahedron topology linearly change similarly to the previous example according to Equation (4.4). Similarly, the beam diameter is set to increase linearly from left to right. The resulting heterogeneous cellular structure is illustrated in Fig. 4.8. Note that at $z = 0$, the topology T described converges to the simple cubic topology defined, and at $z = 1$, it converges to the octahedron topology.

4.3.2 Surface-based cellular structures with multiple topologies

The method for topology transition introduced in Section 3.3.2 aims to fill a gap δ between surface-based structures. It is proposed to fill the gap between unit cells with topologies T_1 and T_2 by a quasi topology $T_{1\#2}$. A unit cell with the topology $T_{1\#2}$ retrieves the boundary curves from its neighboring topologies T_1 and T_2 . Similarly to the original work, the proposed approach models $T_{1\#2}$ by generating a skeletal graph in a wireframe form and applying thickness and other geometric parameters using the function P . For example, a wireframe surface between a gyroid and a Schwarz P topologies is sketched in Fig. 4.9.

The method described in Section 4.1.2 models TPMS structures by modeling one octant of a unit cell and tessellating to reuse objects and classes according to the OOP method for optimization purposes (Stroustrup, 1988). This means that the conventional approach of modeling one octant and tessellating it would not be suitable for transitional unit cells.

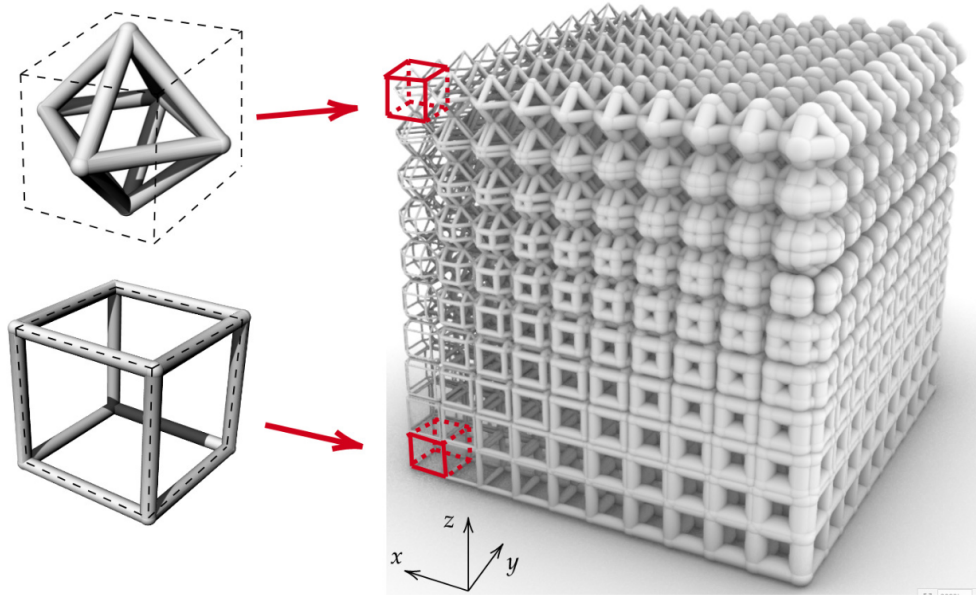


Figure 4.8 A heterogeneous cellular structure with the topology based on a rhombicuboctahedron with the truncation parameter τ varying along the z -axis. The topology converges to the simple cubic at the bottom and the octahedron topology at the top. The thickness of the beams is linearly varying along the x -axis (Letov and Zhao, 2023a)

Furthermore, as mentioned in Section 3.3.2, the boundary curves ∂T_1^+ and ∂T_2^- are not necessarily closed. Therefore, a simple loft CAD feature between ∂T_1^+ and ∂T_2^- is insufficient for addressing general non-trivial cases since a loft feature must exist between closed loops only (Park et al., 2019). Figure 4.10 illustrates the transition between the gyroid and Schwarz P topologies simultaneously with the variation of the structure thickness in a different direction.

4.4 Stochastic cellular structure

In this work, SciPy [Virtanen et al. \(2020\)](#), a Python library well-suited for numerical operations with graphs, is utilized to implement the skeletal graphs of stochastic cellular structures, enabling the modeling of Voronoi cellular structures [Gostick \(2017\)](#); [Fischman](#)

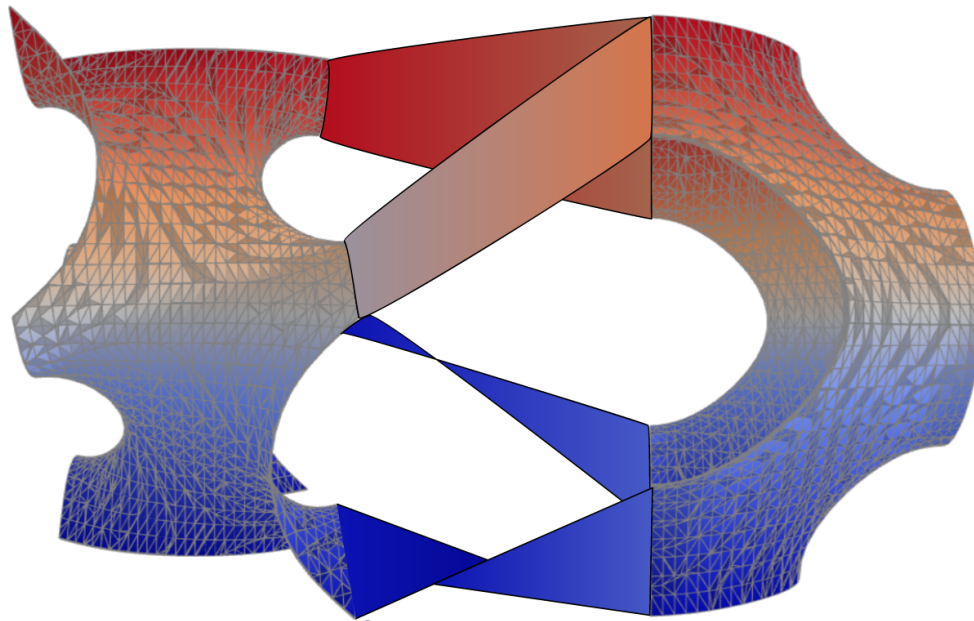


Figure 4.9 A wireframe transition between skeletal graphs of a gyroid and a Schwarz P topologies

et al. (2022). SciPy allows generating a defined number of Voronoi seeds and their Voronoi cells in 3D. To model stochastic structures, users need to provide parameters such as the number of Voronoi seeds, desired lattice thickness, and the boundary of the object to be filled. LatticeQuery and SciPy are Python libraries and can be implemented together for stochastic cellular structure modeling.

SciPy can compute the edges between the neighboring Voronoi cells and provide their coordinates. This data can then be used to generate equations of line segments that can be fed into LatticeQuery. These equations form the topology-defining function T , and then the parameter-defining function P can be used to apply other properties, such as the thickness. Figure 4.11 shows a Voronoi cellular structure that infills the volume of a human femur bone imported in the STL file format. Figure 4.12 illustrates stochastic Voronoi structures modeled with LF-rep that conform to random polyhedrons.

As mentioned in Section 3.4, the graph representation of a cellular structure is beneficial

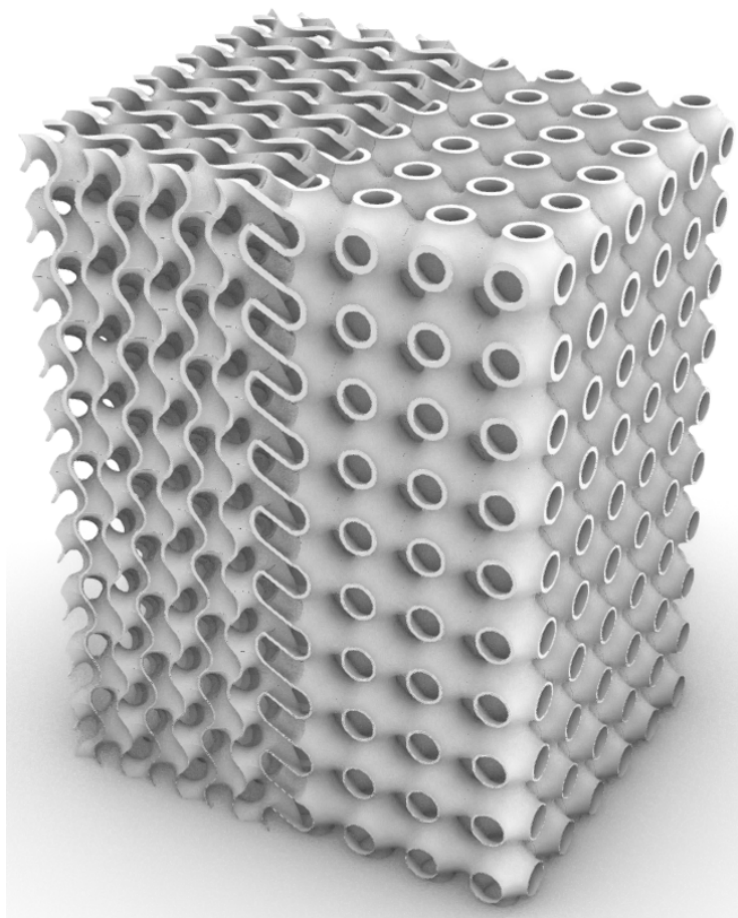


Figure 4.10 Surface-based cellular structure transition between the gyroid and Schwarz P topologies. The thickness of the structure varies vertically.

to estimating its mechanical and physical properties. It is proposed for future research that the graph representation is included as metadata with the geometry itself within a CAD file format.

4.5 Conformal cellular structures

In this section, the intricacies of implementing conformal cellular structures are discussed, focusing specifically on surface and volume conformality aspects that are discussed in Sec-

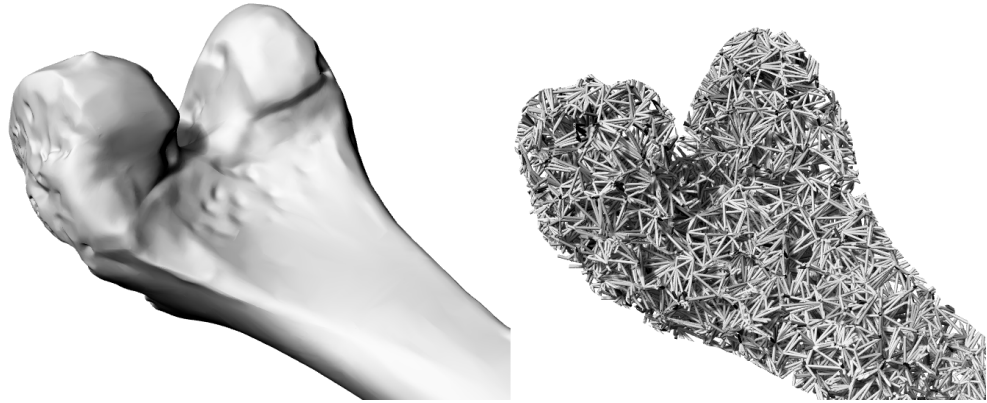


Figure 4.11 A stochastic Voronoi infill of a human femur bone

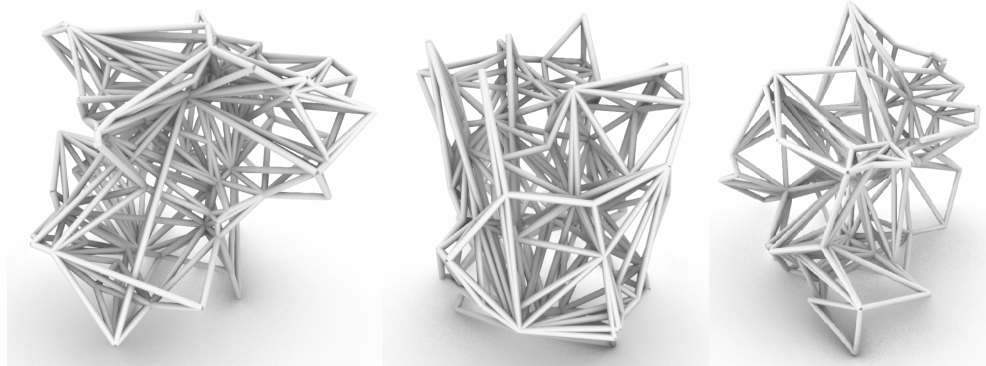


Figure 4.12 Stochastic Voronoi structures that conform to random polyhedrons

tion 4.5.1 and Section 4.5.2, respectively. These two subsections provide a detailed examination of the practical application of the proposed LF-rep approach for designing conformal cellular structures with defined surface and volume properties. By shedding light on the implementation process and its implications, this section demonstrates the versatility and effectiveness of the proposed approach in handling the complexities of conformal cellular structures, thus paving the way for enhanced design and performance in various industrial applications.

4.5.1 Surface conformality

The method described in Section 3.5.1 is implemented in a software prototype by incorporating NumPy (Harris et al., 2020) numerical operations in it. For example, consider a simple cubic topology that conforms to a surface defined by the equation

$$\Phi(\mathbf{X}) : y = \frac{5 \sin(x)}{x} \text{ for } x \in [-25, 25], z \in [0, 15]. \quad (4.5)$$

The function P is defined to control the beam thickness t as

$$P(\mathbf{X}) : t(x) = 0.125 + |0.025x|. \quad (4.6)$$

Let $N_x = 18$, $N_y = 5$, and $N_z = 2$ be the numbers of unit cells along the x -, y -, and z -axes, respectively. Let one layer of unit cells along y be of the normal distance $h/2 = 2$ mm. The method requires the normal vector field defined for $\Phi(\mathbf{X})$. The normal vector field can be obtained by rotating the tangent vector by $\pi/2$ and normalizing it. The tangent vector can be obtained by calculating the derivative of Φ , which is equivalent to the slope of the tangent line at any point on the curve:

$$k = \frac{\partial \Phi(\mathbf{X})}{\partial x} = \frac{x \cos(x) - \sin(x)}{x^2}. \quad (4.7)$$

The furthest equidistant surfaces Φ_+ and Φ_- from the middle plane Φ are numerically obtained from the slope of the normal line, which is the negative reciprocal of the tangent line's slope, or

$$-\frac{1}{k} = -\frac{x^2}{\sin(x) - x \cos(x)}. \quad (4.8)$$

Afterward, the normal line equation with the normal distance $h/2 = 2$ mm can be obtained. For all $(x_k, y_k, z_k) \in \Phi(\mathbf{X})$, the corresponding points of the equidistant surfaces Φ_+ and Φ_- can be derived from the Euclidian distance and the normal line equation as a solution of

$$\begin{cases} (x - x_k)^2 + (y - y_k)^2 = \left(\frac{h}{2}\right)^2, \\ y - y_k = \frac{1}{k}(x - x_k), \end{cases} \quad (4.9)$$

which, in this case, results in

$$x = \frac{2B \pm \sqrt{(2B)^2 - 4AC}}{2A}, \quad (4.10)$$

where $A = 1 + \frac{1}{k^2}$, $B = x_k + \frac{x_k}{k^2}$, $C = x_k^2 + \left(\frac{x_k}{k}\right)^2 - \left(\frac{h}{2}\right)^2$. The two solutions correspond to Φ_i and Φ_+ since they are both equidistant to Φ . The resulting structure of this example is shown in Fig. 4.13.

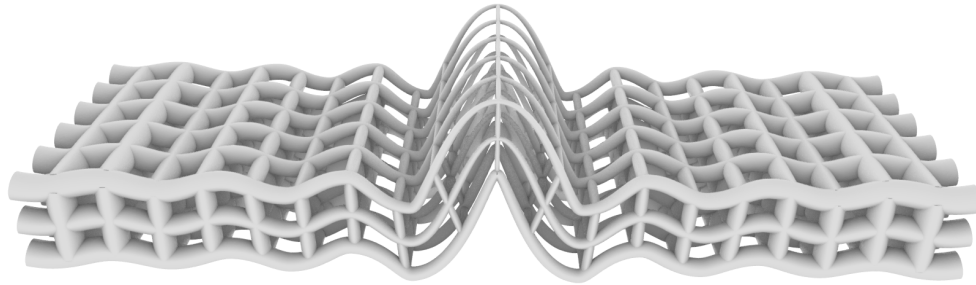


Figure 4.13 A cellular structure with varying thickness conforming to a surface

4.5.2 Volume conformality

As mentioned in Section 4.4, the initial step involves generating a cellular structure that fills the desired volume using NumPy. The volume can be set as an imported STL file.

Once the structure is generated, the trimming is commenced by identifying the vertices and their corresponding trimmed edges that lie on the boundary of the STL file. This allows us to have better control over the edges that will be included in the final cellular structure.

Next, a sweep method from the OCCT GMK is introduced to connect points of the graph more efficiently and precisely. By utilizing the sweep function, smooth connections between the trimmed edges and the boundary of the STL file can be created, resulting in a more conformal representation of the volume. This also aids in mitigating the edge-trimming effect by ensuring that the edges of the graph are connected seamlessly to the boundary of the volume.

By refining the volume conformality implementation, a better representation of the cellular structure within the desired volume can be achieved, paving the way for improved performance and reliability in various applications. Figure 4.11 demonstrates the improved conformal stochastic structure that fills the volume of a human femur bone imported in the STL file format.

Similarly to Intralattice, the proposed approach allows the modeling of conformal cellular structures. Intralattice allows the modeling of conformal cellular structures by transforming the coordinate system to a different one, such as the example illustrated in Fig. 2.18. However, in this case, the cellular structure density decreases further away from the wheel's axle. This cellular structure is homogeneous in cylindrical coordinates as radius ρ , angle ϕ , and z -axis remain constant for each unit cell. In Cartesian coordinates, $x = \rho \cos(\phi)$ and $y = \rho \sin(\phi)$ cannot remain constant. Moreover, the torsional shear stress increases linearly with ρ (Hartog, 1977). The proposed approach allows increasing the beam thickness in the ρ -direction so that the cellular structure becomes heterogeneous even in cylindrical coordinates, as seen in Fig. 4.14, thus illustrating a possible example of a real-world application.

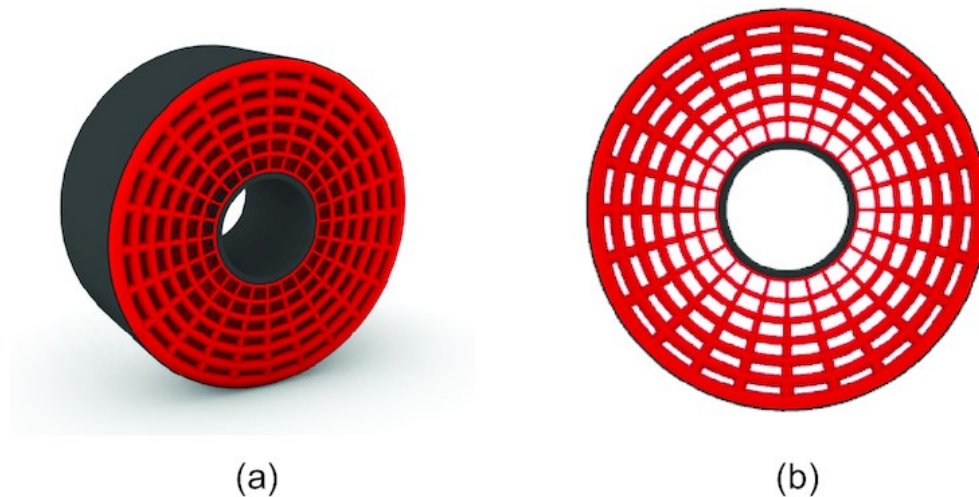


Figure 4.14 (a) An isometric and (b) a profile view on a conformal heterogeneous cellular tire design modeled with the beam thickness increase further away from the wheel axle ([Letov and Zhao, 2022](#))

4.6 LatticeQuery – the implemented FOSS tool

The LatticeQuery library was developed to be used from within CQ-editor ([Urbanczyk et al., 2021a](#)) – an inline editor with a CAD viewer developed for CadQuery. The organization of the methodology is presented in this section. The software is developed to make it modular and easily extendable, as well as simple to use.

This section presents the architecture (Section 4.6.1) and usage (Section 4.6.2) of the LatticeQuery library, which allows for the generation and manipulation of cellular structures.

4.6.1 Architecture

The inline editor is used to provide commands to the LatticeQuery library. LatticeQuery uses parametric methods from CadQuery to access the low-level functionality of OCCT and to generate a cellular structure according to the user commands. CadQuery can send status messages from OCCT to the traceback status menu. The resulting geometry is then

presented in the CAD viewer and can be exported in a CAD file via the object menu. OCCT supports exports in STL and STEP file formats. The software architecture is illustrated in Fig. 4.15.

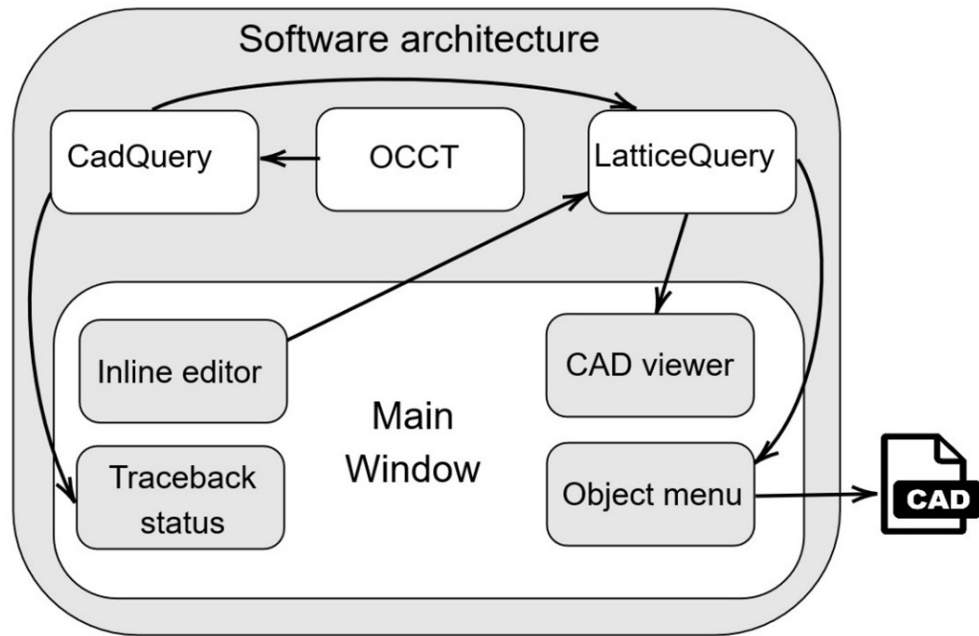


Figure 4.15 The high-level software architecture of the LatticeQuery library (Letov and Zhao, 2023b)

The library uses the OCCT instructions provided by CadQuery to generate the geometry of the predefined topologies, which can be called from the inline editor. Several standard functions are shared between the topologies. These functions include the generation of the design space subdivided for all unit cells, the generation of beams by two points, and the cross-section parameters. The library architecture is presented in Fig. 4.16.

Figure 4.17 demonstrates the main window of the software prototype, which utilizes LatticeQuery. The resulting library is published under a permissive license and is accessible as a FOSS (Letov, 2022). Releasing software as a FOSS is an advantage compared to existing commercial solutions since the total cost of ownership is minimized (Shaikh and

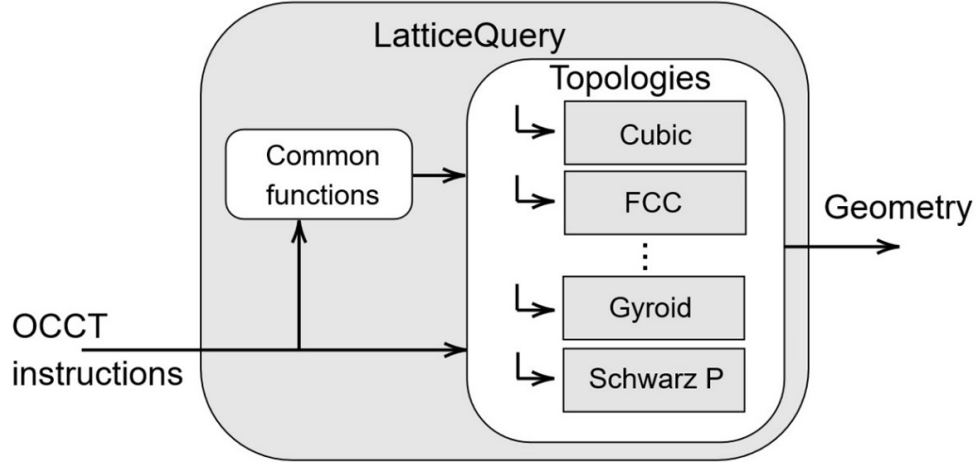


Figure 4.16 The low-level software architecture of the LatticeQuery library (Letov and Zhao, 2023b)

Cornford, 2011), and enthusiasts can introduce further advancements into the software.

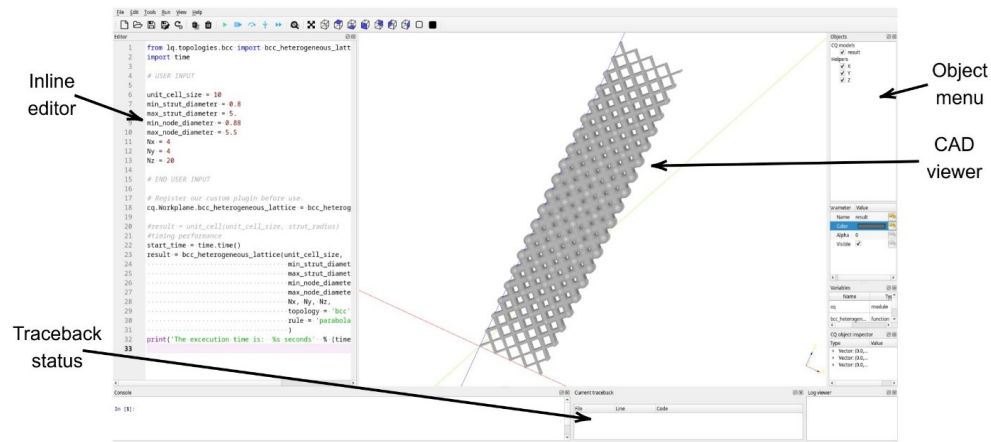


Figure 4.17 The main window of the software prototype that embeds LatticeQuery (Letov and Zhao, 2023b)

4.6.2 Usage

As an example of the application of the algorithm, consider the BCC heterogeneous cellular structure that is shown in Fig. 4.17, which is modeled with LatticeQuery. The

```

1 from lq.topologies.bcc import bcc_heterogeneous_lattice
2 # USER INPUT
3 unit_cell_size = 10.0
4 min_strut_diameter = 0.8
5 max_strut_diameter = 5.0
6 min_node_diameter = 0.88
7 max_node_diameter = 5.5
8 Nx = 4
9 Ny = 4
10 Nz = 20
11 # END USER INPUT
12 # Register the custom plugin before use.
13 cq.Workplane.bcc_heterogeneous_lattice = bcc_heterogeneous_lattice
14 result = bcc_heterogeneous_lattice(unit_cell_size, min_strut_diameter,
   ↳ max_strut_diameter, min_node_diameter, max_node_diameter, Nx, Ny, Nz,
   ↳ topology = 'bcc', rule = 'parabola')

```

Listing 3: The programming script that models the heterogeneous cellular structure illustrated in Fig. 4.17

input parameters remain the same as in the example presented in Fig. 4.2. The solid model can be obtained with the programming script shown in Listing 3.

In this case, the minimum and maximum values of the beam diameter are specified. Note that the lattice nodes are represented as spheres with their diameter following a similar parabolic distribution. The topology is set to BCC, with other possible variations of the BCC topology being BCCz, S-BCC, and S-BCCz.

Another example of generating a heterogeneous Schwarz P cellular structure shown in Fig. 4.1 is presented in Listing 4.

Multiple more documented examples, as well as the installation manual, are present in the open repository of LatticeQuery ([Letov, 2022](#)).

```

1 from parfunlib.topologies.schwartz import schwartz_p_heterogeneous_lattice
2 cq.Workplane.schwartz_p_heterogeneous_lattice =
3     schwartz_p_heterogeneous_lattice
4 # BEGIN USER INPUT
5 unit_cell_size = 4
6
7 Nx = 10
8 Ny = 10
9 Nz = 10
10 min_thickness = 0.1
11 max_thickness = 7
# END USER INPUT
schwartz = schwartz_p_heterogeneous_lattice(unit_cell_size, min_thickness,
                                              max_thickness, Nx, Ny, Nz)

```

Listing 4: The programming script that models the heterogeneous cellular structure illustrated in Fig. 4.1

4.7 Computational performance

The developed software prototype was tested on a machine equipped with the AMD Ryzen™, 7 3700X CPU with 3.20 GHz clock rate, the NVIDIA® GeForce® RTX 2070 Super GPU with 8 GB of memory, 16 GB of RAM, a solid-state drive, and the ArchLinux OS. The mesh precision was set to 0.1mm. CadQuery and, by extension, the developed software prototype allow changing the mesh precision in the settings. The performance of the software prototype of the proposed approach is listed in Table 4.1. The generation time for the beam-based cellular structures was discovered to be 1.843 s per unit cell on average (as a result of all topologies tested once with 0.1 mm precision). The results for the TPMS-based cellular structure are 6.453 s per unit cell on average. Note that the difference in computational efficiency of the geometric modeling of homogeneous and heterogeneous cellular structures is negligible. This is because this work focuses mainly on

modeling heterogeneous cellular structures, and homogeneous cellular structures lie outside the scope of this thesis. These results align with the expectations considering that optimization techniques such as GPU acceleration are not yet introduced to the software prototype. Furthermore, the algorithm complexity is identical to traversing a 3D matrix of the size N , which is $O(N^3)$ ([Cohen-Or and Kaufman, 1997](#)).

Table 4.1 The performance metrics of the modeling with the proposed approach.

Topology	Number of unit cells	Figure	CPU usage range	GPU usage range	RAM usage	Generation time
Schwarz P	1000	Figure 4.1	65.5–104.0%	388–406 MB	2.7%	122.70 min
BCC	720	Figure 4.2	36.8–101.0%	344–452 MB	1.7%	23.20 min
Schwarz P	2000	Figure 4.3	54.7–105.3%	390–533 MB	2.2%	121.30 min

The resulting model can be saved as an STL file and as a STEP file. The STL and STEP export is made possible by the support of STL and STEP by Open CASCADE. Notably, FLatt Pack and MSLattice do not support export to STEP. The STEP file format is rarely used in AM itself but can be used as an input for a CAE simulation in software such as Ansys ([ANSYS Inc., 2014](#)).

The output STL files were successfully imported into slicing tools such as Ultimaker Cura ([Ultimaker BV., 2013](#)) and Preform ([Formlabs Inc., 2019](#)). As a potential future feature, a pivot from ASCII STL to binary STL could be made to decrease the size of the output files. CadQuery supports only ASCII STL files, but Open CASCADE supports binary STL files. Thus, further optimization will focus on building a different method for CadQuery to export binary STL files. Also, as of now, LF-rep is packed into an importable library, but no significant effort has been made to provide a proper GUI for the proposed

method. While this was deemed acceptable for the scope of this work to provide a proof of concept, it can be more appealing for the actual designers of cellular structures to have a proper GUI.

While the performance of the developed software prototype is suitable for an MVP, for future improvements, it is essential to consider an enhanced geometric modeling approach with access to the low-level GMK functionality ([Xu, 2009](#)). It might involve developing a novel GMK to enable functionality not provided by Open CASCADE. However, the development of a GMK is outside the scope of the proposed MVP, as a GMK is often developed by a substantial team of mathematicians and programmers over several years ([Golovanov, 2014](#)). At the same time, having a GMK highly tuned to the scope of the proposed work does not solve the immediate problem of modeling heterogeneous cellular structures.

It is also noticeable that the software prototype does not make much use of the GPU and almost solely relies on the CPU. Appropriate utilization of the GPU is crucial for a geometric modeling tool operating with cellular structures, as GPUs are generally better suited for dealing with large amounts of parallel tasks. Specific changes must be made to the GPU utilization process to make the modeling process more efficient. GPU accelerated rendering of volumetric data with geometric modeling tools that utilize sparse voxel octrees, such as OpenVDB ([Academy Software Foundation, 2012](#)), is particularly of interest for future research. Such GPU acceleration could potentially facilitate the creation of an agile concurrent cellular structure design tool by minimizing the time needed for rendering ([Cordero et al., 2020](#)).

There is evidence that considering the bio-inspired nature of cellular structures in general, the geometric modeling approach suitable for their generation could utilize bio-inspired algorithms as well ([Letov and Zhao, 2021](#)).

The manufacturability of a cellular structure is also an important aspect to consider

when analyzing the resulting models ([Zhang and Zhao, 2022](#)). The manufacturability check is run on the resulting STL models using the Preform 3D printing software ([Formlabs Inc., 2019](#)).

It was decided to run the manufacturability checks for the transition plane connectivity similar to the example shown in Fig. 4.6 with all combinations of topologies inspired by the crystal metal structure and that are listed in Fig. 3.4. Also, the same manufacturability checks have been performed for the truncation-based topology transition. The basic manufacturability checks within the software have been successfully passed.

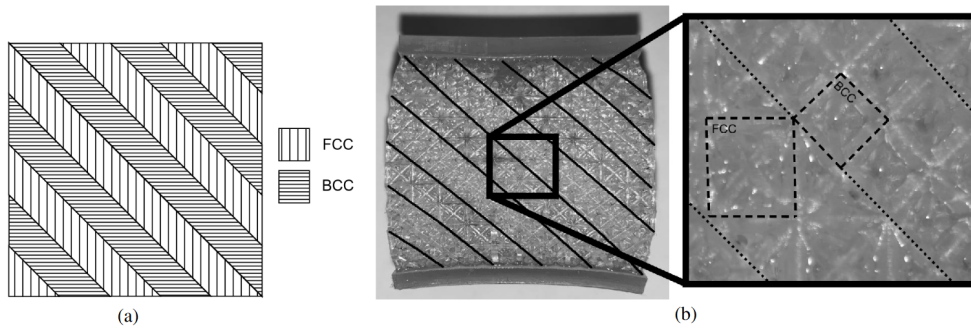


Figure 4.18 A use-case showing the cellular structure transition with the proposed approach: (a) The orientation of topologies for the manufacturability performance test and (b) the resulting print with a zoomed-in view on the topology transition region. In the zoomed-in view, the transition planes are marked with dotted lines, and the instances of the FCC and BCC unit cells are marked with dashed lines ([Letov and Zhao, 2023a](#)).

Moreover, a case with multiple transitions of topologies was decided to be manufactured with the Formlabs Form 2 stereolithography 3D printer ([Formlabs Inc., 2018](#)). Stereolithography 3D printers allow highly accurate AM with a smooth finish ([Bhattacharjee et al., 2018](#)). The material was chosen to be Formlabs Elastic 50A ([Formlabs Inc., 2020b](#)). It was decided to have 5 layers of FCC and 5 layers of BCC, each with an equal layer thickness and oriented at 45° to the horizontal plane as illustrated in Fig. 4.18a. The FCC unit cell is cubic, and its size is set to $u_1 = 3.75$ mm. The BCC unit cell is cuboid, and according to the

framework described in Section 3.3.1 and Fig. 3.11, its smaller side is $u_2 = u_1/\sqrt{2} \approx 2.65$ mm. The beam diameter for both topologies is set to $d = 0.7$ mm, and the node diameter is set to $D = 0.75$ mm. Additional 3.75 mm thick plates were added at the bottom and top of the cellular structure to support it during the AM process. The resulting print is illustrated in Fig. 4.18b. Note that one of the plates is bent in an arc, and its shrinkage can be explained by the residual stress occurring during the print, as this plate was attached to the printing platform (Milovanović et al., 2018).

4.8 Implementation summary

This chapter presented the implementation details of the proposed approach for modeling and generating cellular structures for AM. After discussing the software environment, programming languages, and libraries used to develop the framework, the key steps in the process were described, including unit cell creation and variation of geometric parameters.

The chapter highlighted important algorithms and techniques employed to achieve the desired results. These include the choice of unit cell types, the implementation of different topologies, and the application of design requirements. Furthermore, the generation of heterogeneous structures was explained.

Additionally, the solid model post-processing and validation steps were discussed, such as mesh generation and model preparation for AM. Finally, the versatility and adaptability of the implemented framework were showcased by demonstrating various modeled cellular structures.

This comprehensive implementation lays a solid foundation for the case studies presented in Chapter 5, which will demonstrate the practical applications and effectiveness of the proposed approach in creating a diverse range of cellular structures for AM.

Chapter 5

Case studies

To succeed, planning alone is insufficient. One must improvise as well.

Isaac Asimov (1920 – 1992), FOUNDATION

This chapter presents a series of real-world examples to demonstrate the application of the LF-rep geometric modeling approach to various scenarios. These case studies showcase the versatility and effectiveness of the method in addressing different challenges in cellular structure modeling. Some of these case studies are based on published research, while others present novel applications of the methodology. Each case study provides insights into the unique aspects of the modeling process, highlighting the advantages and potential improvements of the proposed approach. These case studies provide the practical implications of the geometric modeling technique and its potential impact on cellular structure design.

This chapter demonstrates the practical application of the proposed geometric modeling methods through two real-world examples. Section 5.1 explores the geometric modeling of cellular structures to estimate their flow and thermal characteristics. This section delves

into the geometric, flow, and thermal properties of cellular structures, reviews existing experimental results, outlines the methods employed, and presents the results obtained. In Section 5.2, the focus shifts to a multifunctional non-pneumatic tire design, showcasing the versatility of the proposed methods. This section covers the ideation and conceptual design process and presents the results achieved in creating an innovative tire design using the geometric modeling techniques discussed in earlier chapters. These case studies serve to illustrate the practical implications and potential benefits of the proposed methods in real-life applications. Section 5.3 contains visual examples of the cellular structures created with the methodology discussed in this thesis.

5.1 Geometric modeling of cellular structures to estimate their flow and thermal characteristics

This section highlights a case study on the flow and thermal characteristics of non-stochastic strut-based and surface-based cellular structures in the aerospace sector (Sarabhai et al., 2023). With the advent of AM (Blakey-Milner et al., 2021), the aerospace industry has shown increased interest in producing geometrically complex parts, such as cellular structures. Lattice structures, consisting of repeating geometric patterns of unit cells, offer lightweight and high thermal properties (Xu et al., 2021), making them suitable for aerospace applications.

However, limited information is available regarding the flow and thermal properties of cellular structures. While the mechanical properties have been extensively studied (Köhnen et al., 2018), a systematic investigation of the effects of different topologies on flow and thermal properties is still lacking. This case study aims to comprehensively analyze the flow and heat transfer in periodic 3D cellular structures with topologies based on struts

and TPMS.

The case study involves the geometric modeling of cellular structures and CFD simulation to model the flow continuum in a gas turbine context. The findings are intended to serve as a guideline for selecting cellular structure topologies based on desired operating and manufacturing conditions for a gas turbine. It is important to note that the study only considers the influence of geometry on the structural analysis of various topologies and does not address material selection for cellular structure design.

5.1.1 Geometric, flow, and thermal properties of cellular structures

This section provides a comprehensive overview of the properties and characteristics of lattice structures, focusing on their geometric properties. The relative density ρ' of a cellular structure is a crucial factor for comparing different topologies, as two different lattice structures can often be compared if they have the same relative density (Bai et al., 2019). Other important properties are used to compare cellular structures, such as porosity ϕ and apparent porosity ϕ_{AP} (Ashby, 2006).

Various strut-based and surface-based lattice topologies are inspired by cubic crystal structures, including primitive (simple cubic), BCC, FCC, octahedron, and octet-truss topologies. The additional z -oriented struts in BCCz and FCCz topologies transform the normally bending-dominated BCC and FCC into stretch-dominated topologies (Leary et al., 2018).

The available surface area of the topology per unit actual volume of the solid body A_L/V_S ratio is important in analyzing the geometry of cellular structures. This ratio is proposed to be used to compare the thermal properties of different topologies, as surface area plays a vital role in heat transfer rate through any structure (Letov and Zhao, 2021).

The flow and thermal properties of cellular structures are analyzed to understand the

heat transfer in various topologies. Heat transfer is typically quantified by estimating the system's heat transfer coefficient h , with the heat transfer rate Q being a function of the available surface area in contact A_L ([Park et al., 2022b](#)):

$$Q = hA_L\Delta T, \quad (5.1)$$

where ΔT is the temperature difference between the solid surface and the surrounding fluid. TPMS topologies, such as gyroid and Schwarz D, have been found to provide a large surface area, allowing for increased convection and conduction ([Jones et al., 2022](#)).

The Reynolds number Re is an essential characteristic of fluid flow, allowing for the comparison of the ratio of inertial forces to viscous forces in different flows. Minimizing pressure losses ΔP within gas turbines is vital in the aerospace and automotive industries. The Darcy–Weisbach equation defines pressure loss and can be used to analyze the Darcy friction factor f , estimating pressure loss and flow properties. The equation is

$$\Delta P = f \frac{L}{d} \frac{\rho_f \hat{v}^2}{2}, \quad (5.2)$$

where L is the characteristic length of the pipe, d is the hydraulic diameter, \hat{v} is the mean flow velocity of the fluid, and ρ_f is the fluid density. All these parameters, except for f , do not depend on the topology of the cellular structure.

The A_L/V_S ratio is proposed to be used to understand and compare the thermal performance of lattice structures. It is proposed to study its effect on heat transfer in this case study.

5.1.2 Existing experimental results

This case study also examines existing experimental results from the literature on heat transfer in cellular structures. The flow and thermal properties of surface-based cellular structures, especially in gas turbine applications, have generally been understudied compared to strut-based topologies (Deng et al., 2021). The literature analyzes different cellular structures' flow and thermal properties by varying input parameters. Strut-based cellular structures are typically analyzed through CFD simulations, while surface-based structures are more commonly analyzed in real experimental setups (Guo et al., 2022).

Surface-based cellular structures are more complex geometrically, making meshing, discretization, and CFD analysis more challenging (Catchpole-Smith et al., 2019). The study aims to compare the results obtained for strut-based cellular structures with similar simulation results from the literature and compare surface-based cellular structures with actual experimental results.

During the literature review, a list of cellular structure topologies was gathered and the data was filtered to obtain the frequency of different topologies studied for mechanical and thermal performance. This data is plotted in Fig. 5.1. BCC is the most common topology encountered in the reviewed works. Cellular structures were found to be primarily used in the aerospace industry sector (53.65% of analyzed works), followed by the biomechanics sector (27.05%).

The top 90% of the lattice structures (colored dark in Fig. 5.1) were selected for further study of their flow and thermal characteristics, including both strut-based and surface-based structures. Section 5.1.3 explains the modeling of these lattice structures.

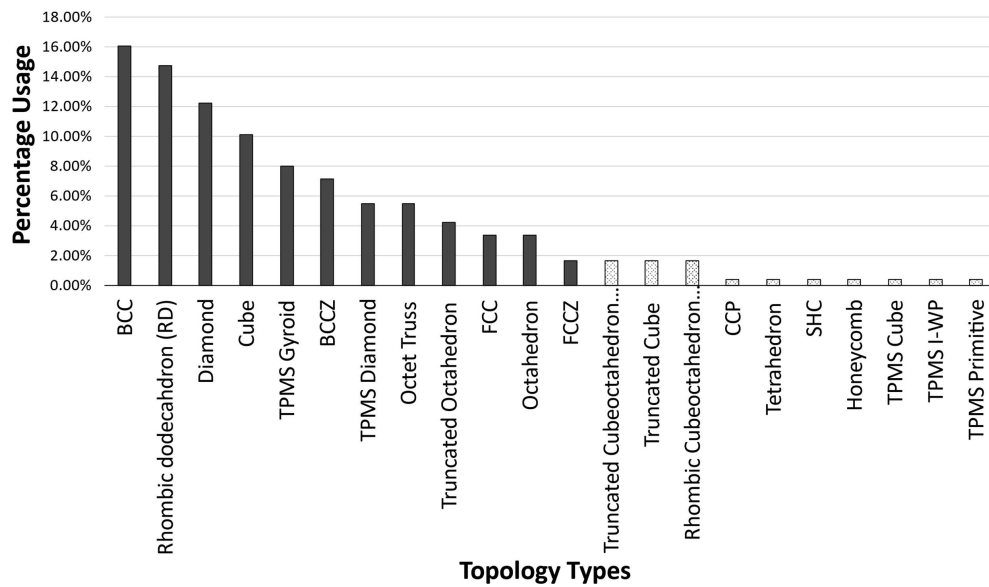


Figure 5.1 The statistics on the use of different topologies in the literature (Sarabhai et al., 2023)

5.1.3 Methods

This section examines the methods used for geometric modeling, mesh generation, and simulations of cellular structures in the case study. The selected topologies include strut-based topologies (primitive, BCC, BCCz, FCC, FCCz, octahedron, and octet-truss) and surface-based topologies (TPMS gyroid and Schwarz D). These topologies represent the top 90% cellular structures investigated in the literature.

Geometric modeling starts by defining the geometric parameters of the chosen topologies. Average dimensions were extracted from the literature: average strut thickness (1.10 mm), average thickness for surface-based lattices (1.37 mm), and average porosity (87%).

For strut-based cellular structures, Siemens NX ([Siemens Digital Industries Software, 2023a](#)) and Simcenter STAR-CCM+ ([Siemens Digital Industries Software, 2023b](#)) were used for geometric modeling and surface repair of CAD models, respectively. Unit-cell size u was set to 10 mm, and the thickness range was 1.0 mm, 1.5 mm, and 2.0 mm. Geometric

models of 21 cellular structures were generated.

Surface-based cellular structures, such as TPMS, are defined by equations and cannot be easily modeled with conventional CAD software. Approximate implicit mathematical functions define TPMS topologies, so the F-rep method proposed in this thesis was used for geometric modeling ([Letov and Zhao, 2022](#)). Gyroid and Schwarz D topologies were modeled with LatticeQuery ([Letov, 2022](#)).

In this case study, simulations are conducted to investigate the flow and thermal properties of cellular structures. A cylindrical computational flow domain with a cellular structure network of $3 \times 3 \times 9 = 81$ unit cells is chosen. Three strut diameters or thicknesses are analyzed: 1.0 mm, 1.5 mm, and 2.0 mm. The nomenclature used is the name of the topology, followed by the strut thickness (e.g., BCC1, FCC1.5, and BCCZ2).

Meshing or discretization is carried out with three regions of different mesh densities. The tetrahedral mesh is chosen for its easy generation and compatibility with most FEA simulation software packages ([Zhang et al., 2020](#)). A mesh convergence study is performed and is discussed in Section [5.1.4](#).

Siemens Energy Canada Limited provided boundary conditions, and three different values of the Reynolds number Re were used to represent different turbulent intensities. The Mach number was set to $Ma < 0.3$ for the inlet velocity. It was assumed that air is a dry, perfect gas, and the $k - \omega$ shear stress transport (SST) model was applied for turbulence ([Al-Waked and Behnia, 2004](#)). Eddy viscosity was added to model energy conservation more realistically.

81 simulations analyzed seven strut-based and two surface-based topologies with three thicknesses and three turbulent intensity settings. The convective heat transfer coefficient and friction factor were calculated and compared to a standard flow channel. Detailed simulation results are discussed in the following section.

5.1.4 Results

This section presents the results obtained from the design to the simulation phase. The simulation setting is presented in Fig. 5.2. The sensitivity analysis determined the optimal plane for measuring output parameters at 55 mm. The mesh convergence study resulted in an average base/element size of 0.4 mm with 9 832 216 elements, as seen in Fig. 2.3.

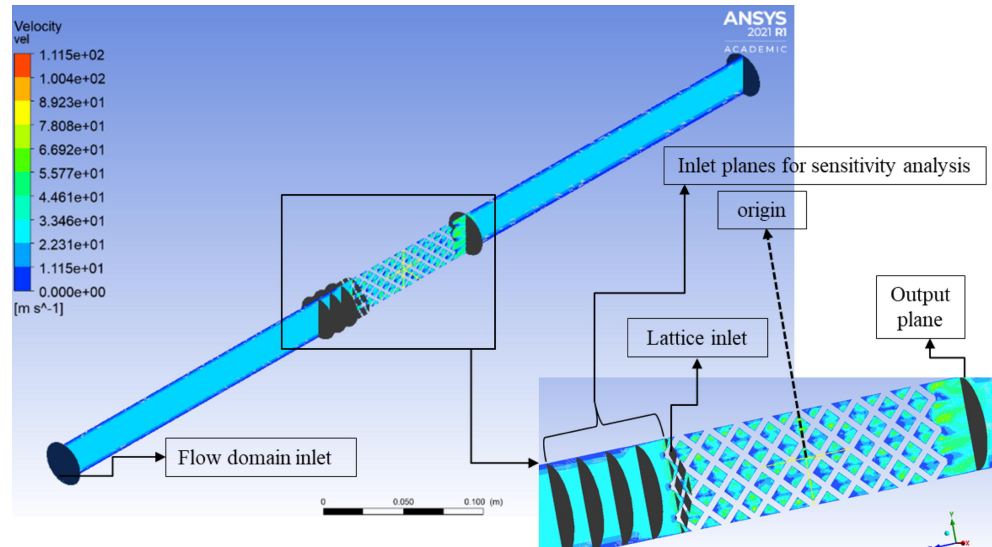


Figure 5.2 The simulation setting and planes chosen for sensitivity analysis (Sarabhai et al., 2023)

The apparent porosity ϕ_{AP} and A_L/V_S ratio of cellular structures were investigated, revealing that as the apparent porosity increases, A_L/V_S decreases (Fig. 5.3). The heat transfer rate Q was found to increase close to linearly with the surface area of the lattice, as expected from Equation 5.2 (Fig. 5.4). Note that the heat transfer rate Q here was divided by the temperature difference between gas and solid ΔT since Equation 5.1 can be rearranged such that the vertical axis can be considered the heat transfer coefficient h multiplied by the surface area A_L of the entire lattice.

Flow and thermal properties charts such as the one in Fig. 5.5 were created to visualize the correlation between flow and thermal properties. Inspired by the Ashby plotting

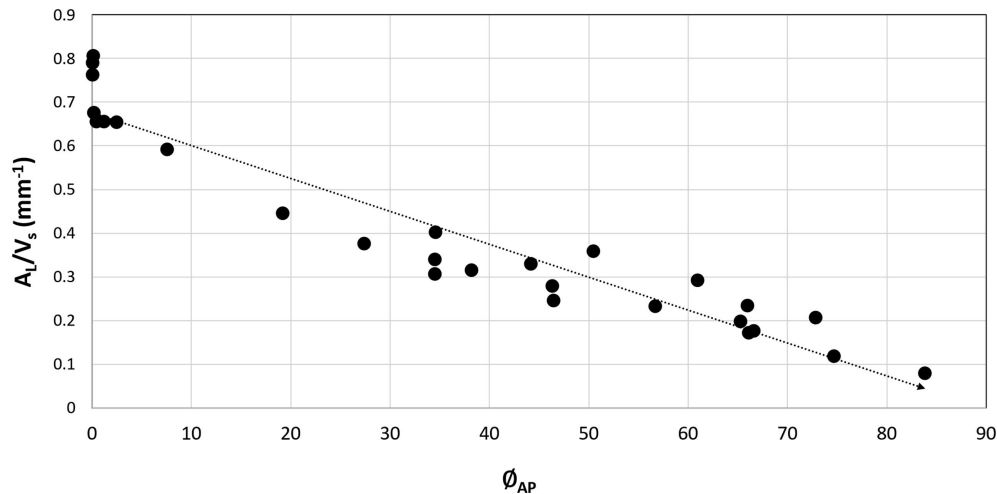


Figure 5.3 A_L/V_s ratio vs. ϕ_{AP} of strut-based and surface-based cellular structures ([Sarabhai et al., 2023](#))

method ([Ashby, 2006](#)), these charts help design engineers choose the best-suited structures for specific operating conditions, especially at high Reynolds numbers when obtaining experimental data is costly. Here, f_0 is the friction factor of a similar and hydraulically smooth channel which correlates with the Reynolds number Re . As a result, the friction factor ratio f/f_0 is used to compare the friction factor of various structures.

This case study investigated the thermal and flow behavior of strut- and surface-based cellular structures for gas turbine design. The friction factor ratio f/f_0 is found to be highest for TPMS-based topologies with a 2.0 mm thickness in laminar flow and the octet-truss topology with a 2.0 mm thickness in turbulent and highly turbulent flows. The results validate that gyroid TPMS structures perform better than Schwarz D TPMS structures ([Li et al., 2022b](#)).

The airflow path is found to be an important parameter in investigating the friction factor values of cellular structures. Flow characteristics suggest that aligning struts or holes in the direction of the airflow path can reduce pressure loss. The general trend of the heat transfer coefficient h increasing with the Reynolds number Re is consistent with

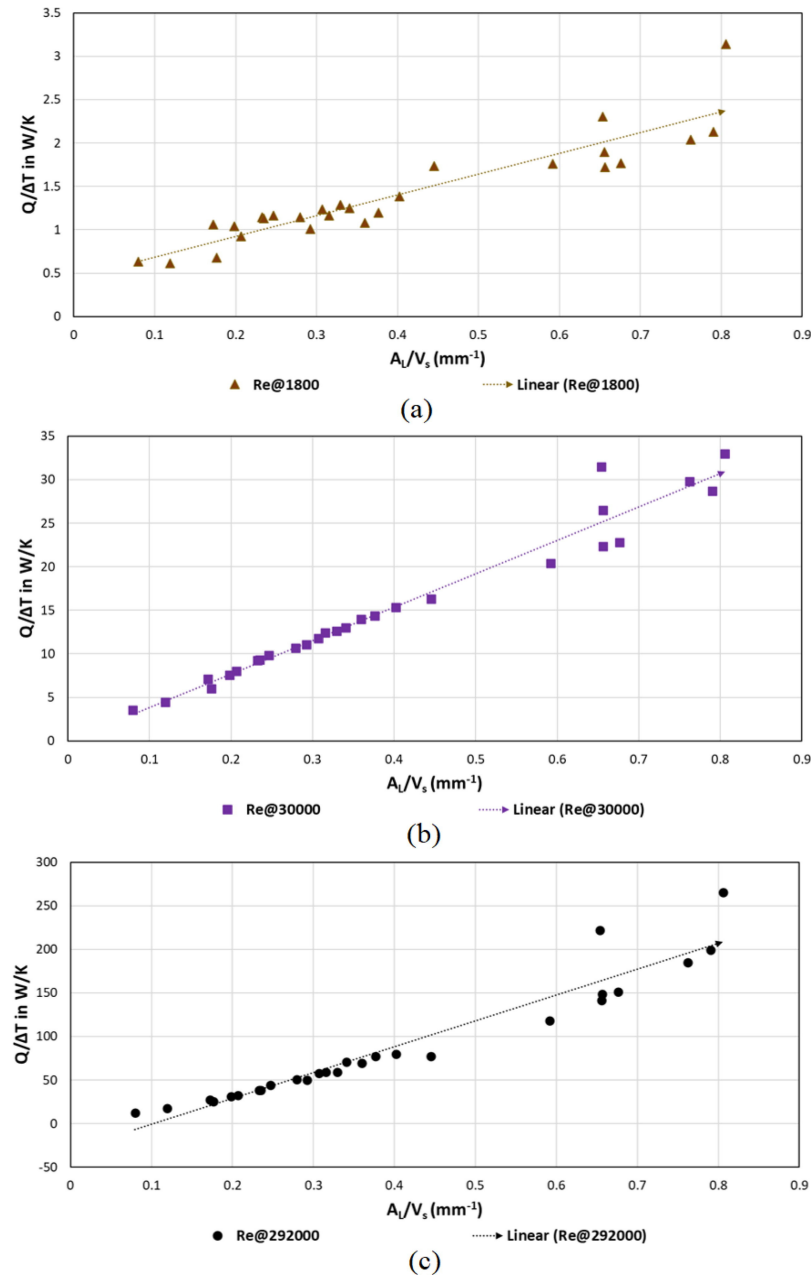


Figure 5.4 Dependency of the heat transfer variation $Q/\Delta T$ on the available surface area per unit total volume A_L/V_s for (a) $Re = 1.8 \cdot 10^3$, (b) $Re = 30.0 \cdot 10^3$, and (c) $Re = 292.0 \cdot 10^3$ (Sarabhai et al., 2023)

experimental findings (Soloveva et al., 2022).

The obtained flow and thermal properties charts aid in selecting lattice structure topo-

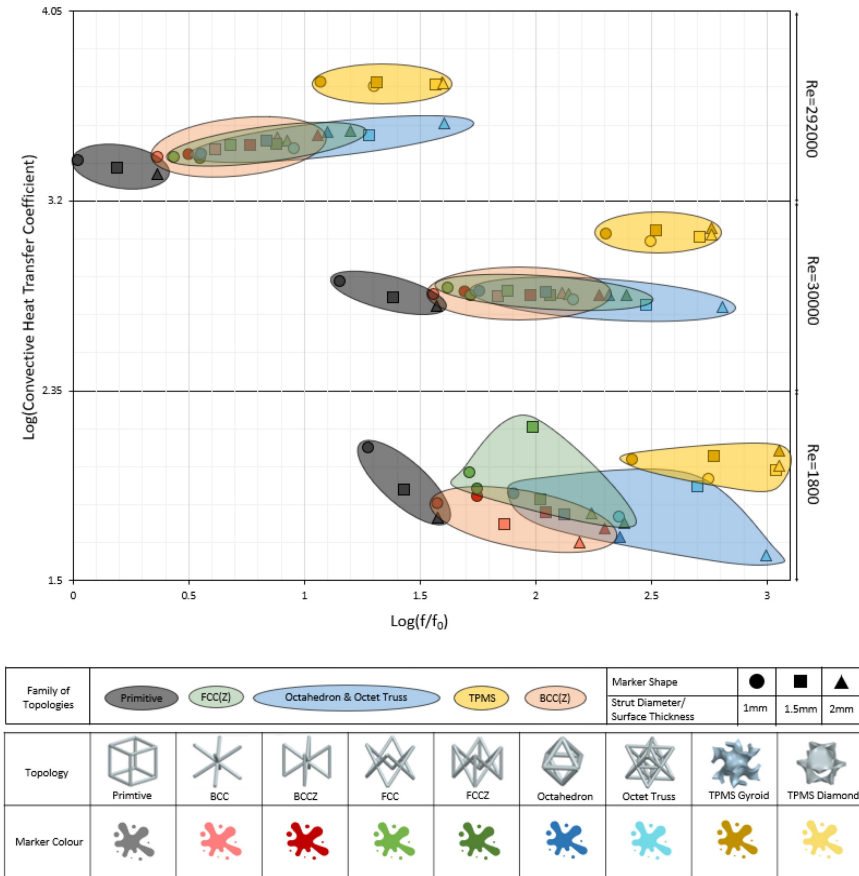


Figure 5.5 A flow and thermal property chart illustrating the distribution of the heat transfer coefficient h and the friction factor ratio f/f_0 for various Reynolds numbers, topologies, and thicknesses (Sarabhai et al., 2023)

gies for specific operating conditions and agree with the work of Catchpole-Smith (2019). The study concludes that the gyroid topology is a superior choice among surface-based lattice structures, while FCC and FCCz structures are better among strut-based structures.

This case study showcases that the loop from design to CFD simulation can be closed with the proposed approach.

5.2 Multifunctional non-pneumatic tire design

5.2.1 Ideation and conceptual design

A new bio-inspired non-pneumatic multifunctional tire design is developed using the Domain Integrated Design (DID) method ([Velivila et al., 2021](#)) in this case study. Figure 5.6 shows the multi-functional non-pneumatic tire design schematic sketch. The outer surface of the tire is inspired by snakeskin for effective friction management. Two different designs for the internal structure of the tire are chosen, both inspired by nature for impact resistance: one by the beak of a great spotted woodpecker (*Dendrocopos major*), and the other by the peel of pomelo (*Citrus maxima*). Woodpecker's beak has a varying porosity starting from 30% at the tire interface, 65% in the middle, and 30% at the central region of the tire ([Wang et al., 2013](#)). Pomelo peel has a varying porosity of 40% at the tire interface, followed by 50% in the middle and 30% at the central region ([Zhang et al., 2019](#)). To evaluate the impact resistance of tires, it is necessary to understand the interaction of the tire and pavement. The tires do not have line contact with the pavement; instead, has a patch. It is observed that in a pneumatic tire, the patch is in the form of an ellipse; for a non-pneumatic tire, the patch is in the form of a rectangle ([Kim et al., 2013](#)). The modeling and analysis are performed on patches and not the entire tire. The modeling and analysis of snake-inspired texture are not performed. This case study aims to validate the meta-level parameter for selecting the correct biological analogy and solving the convergent evolution problem.

Several cellular topologies can be modeled to approximate the original conceptual design. One of the topologies most closely resembling the intended design is the Schwarz P surface topology. Geometric modeling is a critical factor affecting a conceptual design's success, such as the novel tire design proposed in this case study ([Letov and Zhao, 2022](#)).

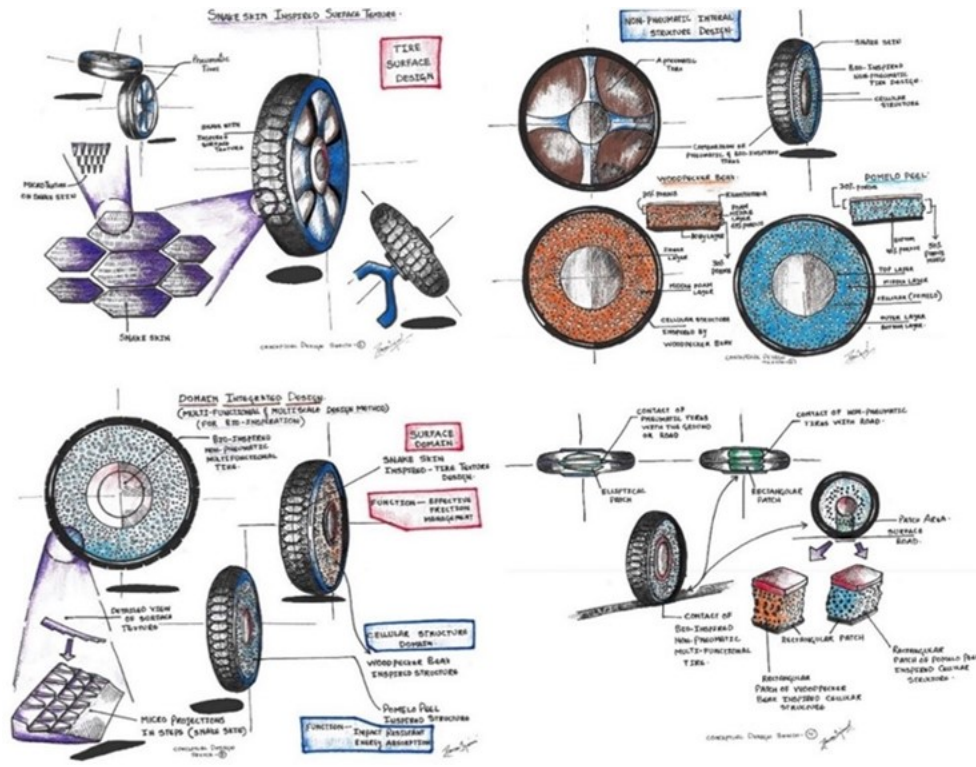


Figure 5.6 The initial conceptual designs that were produced in the ideation process (Velivila et al., 2023)

The cellular structure modeling approach proposed in this thesis was decided to use in this study. This approach allows the geometric modeling of cellular structures based on TPMS with varying parameters. This framework has been incorporated into the open-source software LatticeQuery. From the industrial analogs of tires, it was found that the tire radius is commonly chosen to be $R = 203$ mm. Since only the point of contact between the tire and the road surface actively participates in the wheel locomotion, a single column in the radial direction can be chosen for the finite element modeling (FEM) simulation. The column for both proposed designs has three regions with different porosities, sketched in Fig. 5.7. In this sketch, O is the location of the tire axis, and r_I , r_{II} , and r_{III} signify the upper limits of regions I, II, and III, respectively. The three regions are assigned different porosities to

represent the natural analogs closely. For the woodpecker-inspired design, the porosities ϕ_w in regions I, II, and III are $\phi_{wI} = \phi_{wIII} = 30\%$, $\phi_{wII} = 65\%$. For the pomelo-inspired design, the porosities $\phi_{pI} = 40\%$, $\phi_{pII} = 50\%$, $\phi_{pIII} = 30\%$. The column should fit a significant amount of unit cells of the lattice. Thus, it was decided to use the base unit cell size of $u = 3.98$ mm. Woodpeckers are known to have the porous region corresponding to region II elongated in the load direction. Thus, it was decided to have unit cells in the woodpecker region II elongated by 50% in the r -direction.

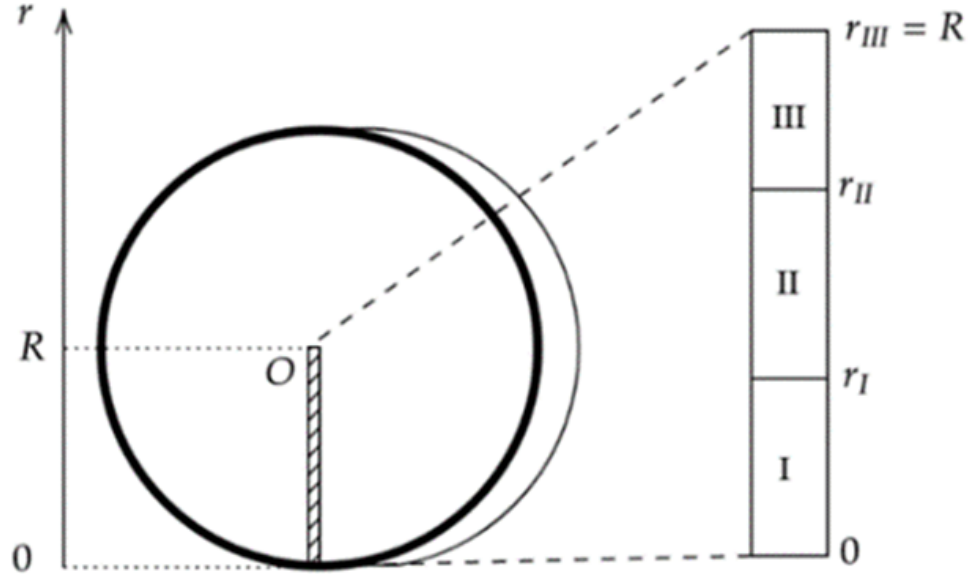


Figure 5.7 A single column is split into three regions with different porosities (Velivila et al., 2023)

LatticeQuery supports setting variable thickness t in a specific direction, not the porosity ϕ . However, the geometric properties of the Schwarz P surface have been studied well in literature (Gandy and Klinowski, 2000), and these findings were used to estimate its porosity based on thickness t as

$$\phi = 1 - \rho' = 1 - \frac{At}{V} = 1 - \frac{K(1/4)t}{16K(3/4)u}, \quad (5.3)$$

where ρ' is the relative density of the lattice, $V = u^3$ is the volume of the cubic unit cell, $A = \frac{K(1/4)t}{16K(3/4)u}$ is the surface area of the Schwarz P surface, and K denotes a complete elliptic integral of the first kind. The 3D print plugin for the Blender computer graphics software ([Blender Foundation, 2016](#)) validated the lattice thickness, which provided a proper estimate of the volume ([Froehlich et al., 2021](#)). It was found that the porosity $\phi_{wI} = \phi_{wIII} = \phi_{pI} = 30\%$ can be ensured by $t = 1.34$ mm; $\phi_{wII} = 65\%$ by $t = 0.61$ mm; $\phi_{pII} = 50\%$ by $t = 0.89$ mm; and $\phi_{pIII} = 40\%$ by $t = 1.10$ mm.

5.2.2 Results

The STL mesh was decided to be simulated with FEM in Abaqus Standard Edition 2021 ([Dassault Systèmes SE, 2023](#)). A contact patch of the tire is commonly subject to loads of $2 \cdot 10^3$ N ([Persson, 2010](#)). Since only one column is analysed, it is sufficient to spread this load across $45 \times 11 = 495$ unit cells, resulting in a 4 N load per column. The safety factor for the load on the tire is estimated at 1.125 ([Pal Singh, 2010](#)), resulting in a 4.5 N load per column. Elongation was found to be one of the key characteristics that are used to analyze the effectiveness of a tire ([Ratrou and Mahmoud, 2006](#)). Rigid polyurethane was chosen as the material for the simulation. Figure 5.8a and Fig. 5.8b illustrate the result of the FEM simulation for single columns corresponding to the woodpecker- and pomelo-inspired designs, respectively. The maximum values of the magnitude of elongation are 84.77 and 91.20 for the woodpecker- and pomelo-inspired designs, respectively. These values are significantly lower than the estimated elongation at break, which is estimated to be over 200 ([Faizah et al., 2019](#)). Note that the region I directly contacts the road surface in both cases is the most elongated one. This effect was expected in the conceptual design phase and motivated to provide region I with lower Porosity than the other two regions. Lower porosity results in a higher material interaction area and, thus, lower the

deformation.

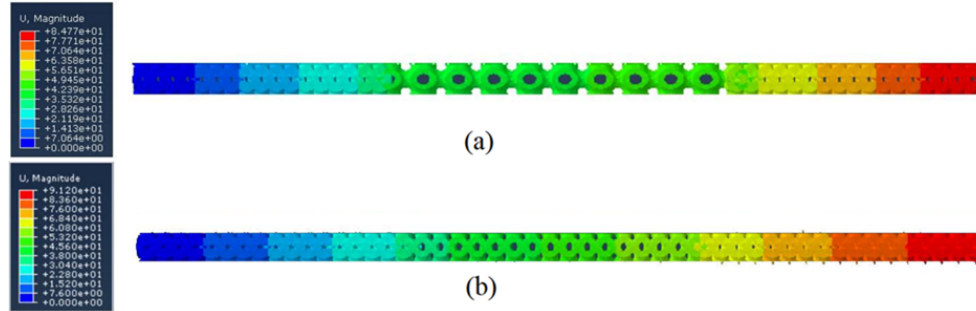


Figure 5.8 The simulation results show the magnitude of elongation for (a) the woodpecker- and (b) the pomelo-inspired tire designs (Velivila et al., 2023)

It is evident that the woodpecker's beak has a low porosity in the region I, which is in direct contact with the road, has a higher interaction area, and thus has a low deformation. This simulation validates the initial hypothesis to select the features with a higher Interaction area and low Porosity for the applications involving adsorption/absorption functions.

The analysis is performed to validate the meta-level parameter “interaction area” proposed for selecting biological analogy in the DID method. Two use cases of novel tire designs were conceptually designed, modeled with LatticeQuery, and simulated with Abaqus. The concepts covered in this work are an example of multifunctional design. The obtained results confirm the initial hypothesis derived from the DID methodology, that is, to select the biological analogy with a significant interaction area for the applications of adsorption/absorption.

This case study showcases that the loop from design to FEA simulation can be closed with the proposed approach.

5.3 Printed cellular structures modeled with the proposed approach

This section presents a collection of figures showcasing the versatility and potential applications of the proposed approach in creating various cellular structures. Distinct case studies will be examined, highlighting the diverse topologies used in the modeling process.

Figure 5.9a features a cellular structure with an FCC topology. This topology is rotated 45 degrees relative to the horizontal plane, resulting in a unique configuration. The material used for this print is the Ti-6Al-4V alloy, known for its excellent mechanical properties and biocompatibility. This example demonstrates the potential of the approach for creating complex and customized cellular structures in metal AM.

Figure 5.9b highlights a gyroid cellular structure known for its intricate geometry. This example further showcases the versatility and potential applications of the proposed approach in designing and fabricating unique cellular structures. The Formlabs Form 2 ([Formlabs Inc., 2018](#)) SLA 3D printer, and BioMed Amber Resin ([Formlabs Inc., 2020a](#)) were used for printing this and further structures of this section, emphasizing the compatibility of the proposed approach with a range of materials and 3D printing technologies.

Figure 5.9c showcases an airless tire concept designed using a heterogeneous simple cubic topology. Its solid model is shown previously in Fig. 4.14. The thickness of the lattice structure increases towards the outer edge, providing enhanced support and durability in the tire's contact area.

Figure 5.9d presents a cellular structure with varying thickness that conforms to a given surface. Its solid model is shown previously in Fig. 4.13. This structure showcases the adaptability and flexibility of the proposed approach in creating custom designs tailored to specific applications.

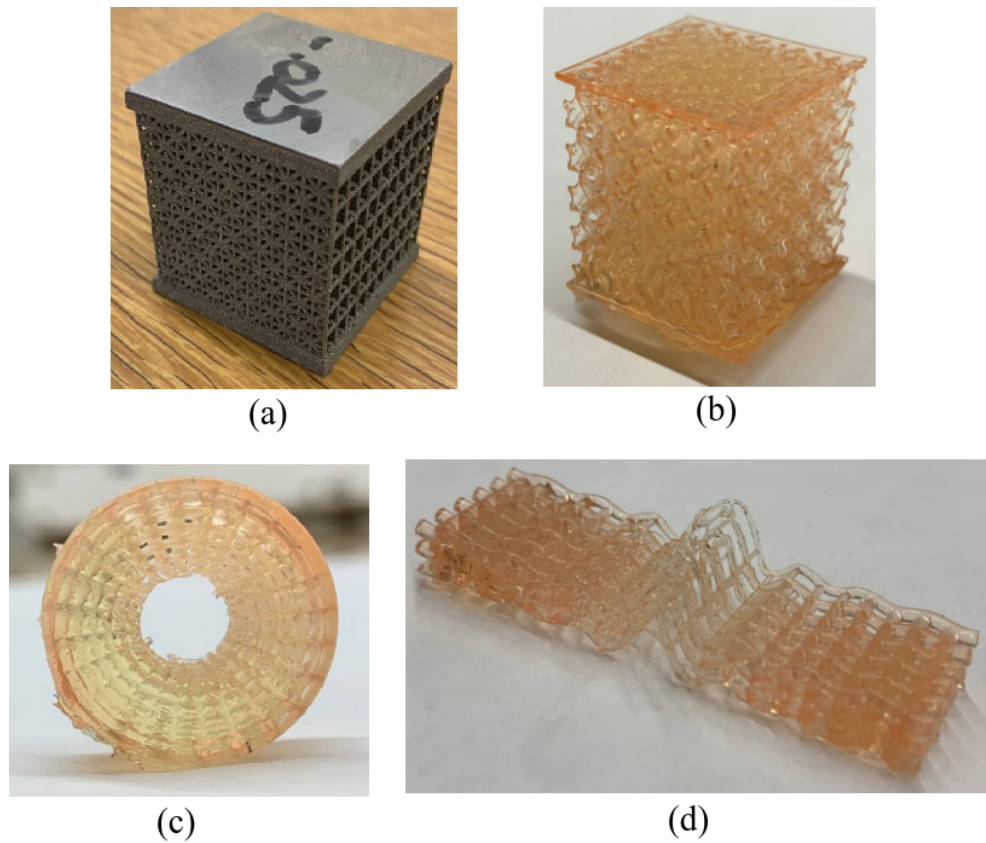


Figure 5.9 Diverse cellular structures created using the proposed approach: (a) Rotated FCC topology in Ti-6Al-4V alloy, (b) Gyroid cellular structure, (c) Heterogeneous tire concept with simple cubic topology and increasing thickness towards the outer edge, and (d) Cellular structure with varying thickness conforming to a surface. All structures except (a) are printed with Formlabs BioMed Amber Resin ([Formlabs Inc., 2020a](#)) using the Formlabs Form 2 ([Formlabs Inc., 2018](#)) SLA 3D printer.

While the main aim of the showcased structures in this section is to validate the printability and design versatility of the proposed LF-rep approach, some of these printed samples underwent physical testing to assess their mechanical performance and validate the theoretical underpinnings.

One such physical analysis was performed on the FCC topology rotated 45 degrees, shown in Figure 5.9a. This structure was subjected to compression testing to evaluate

its load-bearing capacity and mechanical response. It was compared with another printed sample in Figure 4.18 to validate the premise that varying topologies can influence the overall stiffness and structural behavior of the cellular design.

It is worth noting that while detailed and extensive physical studies on all printed artifacts were not performed, the above test serves as a preliminary validation of the capability of LF-rep in achieving desired mechanical behaviors through informed topology choices. Future studies can delve deeper into comprehensively testing and characterizing these cellular structures to draw more definitive conclusions about their real-world performance.

This case study showcases that the loop from design to fabrication and testing can be closed with the proposed approach.

Chapter 6

Conclusion and future directions

Never say goodbye because goodbye means
going away and going away means forgetting.

James Matthew Barrie (1860 – 1937),

PETER PAN

This thesis presented a geometric modeling approach based on F-rep, referred to as lattice-function representation (LF-rep), and expanded the freedom of designing heterogeneous cellular structures capable of creating stochastic, conformal, and multi-topology configurations. The LF-rep approach allows the geometric modeling of stochastic structures by generating random parameters within certain bounds, ensuring the desired degree of randomness. For conformal structures, the method adapts the cellular topology to conform to the underlying surface geometry, thereby enabling more efficient and seamless integration with the overall design. Additionally, the approach is capable of infilling a predefined volume. The approach enables the combination of multiple topologies within a single structure, providing designers with greater flexibility in tailoring the properties of the cellular material. Functionally controllable topology parameters such as thickness

(for TPMS) and beam diameter (for beam-based cellular structures) can be modeled and controlled by the proposed approach. A novel approach for transforming a topology from one to another, which is based on the variation of geometric parameters, has been proposed and implemented in a software prototype. Several use cases of topology transition by the variation of the truncation parameter have been covered. The proposed method was implemented in a software prototype and tested.

The integration in the design loop is proposed to be achieved by providing access and guidance to the design community and to a list of manufacturers utilizing which utilize cellular structures. The aerospace sector is one of the industry sectors that heavily relies on lightweight structures with unique thermophysical properties and is thus proposed as a potential venue for exploration. The tool is released as a documented FOSS and should enhance the user experience and foster further agile development.

For future research, improvements to the software prototype are proposed. These improvements include computational optimization based on the results obtained in Section 4.7, providing a proper GUI for using the tool, and other enhancements. GPU optimization could enhance the design experience and be a step forward to collaborative cellular structure design. A proper GUI would allow LF-rep to be integrated into a generic design workflow with the most immediate goal of collecting user feedback. This feedback can then improve the GUI and enhance the software's performance. Such functionality would enable higher design freedom.

The diamond beam-based cellular structure is an example of a beam-based topology that does not have conventional nodes at the edges of its cubic unit cell. Moreover, the properties of such cellular structures depend on the orientation of the unit cells. It is proposed to investigate the application of the proposed approach to this topology. The software prototype that embeds the proposed approach has been developed according to

the object-oriented programming principles, which enables the further extension of the framework.

The current version of the LatticeQuery software has a single-document interface. At the same time, many modern CAD software packages possess a multi-document interface (MDI) that allows simultaneously operating with multiple tabs of documents. It is proposed to switch to the MDI for future versions of LatticeQuery.

Future work is also proposed to focus on supporting multi-scale hierarchical cellular structures with the LF-rep approach.

Potential applications of LF-rep for enhancing topology optimization techniques are proposed to be investigated for future research.

Bibliography

- Aage, N., E. Andreassen, B. S. Lazarov, and O. Sigmund, 2017: Giga-voxel computational morphogenesis for structural design. *Nature*, **550** (7674), 84–86, doi:[10.1038/nature23911](https://doi.org/10.1038/nature23911).
- Abueidda, D. W., M. Bakir, R. K. A. Al-Rub, J. S. Bergström, N. A. Sobh, and I. Jasiuk, 2017: Mechanical properties of 3D printed polymeric cellular materials with triply periodic minimal surface architectures. *Materials & Design*, **122**, 255–267, doi:[10.1016/j.matdes.2017.03.018](https://doi.org/10.1016/j.matdes.2017.03.018).
- Academy Software Foundation, 2012: OpenVDB. URL <https://www.openvdb.org>, [Online; accessed March 15, 2023].
- Adalsteinsson, D., and J. A. Sethian, 1995: A fast level set method for propagating interfaces. *Journal of computational physics*, **118** (2), 269–277, doi:[10.1006/jcph.1995.1098](https://doi.org/10.1006/jcph.1995.1098).
- Adzhiev, V., and Coauthors, 2020: HyperFun: News. URL <https://hyperfun.org/hyperfun/main>, [Online; accessed June 28, 2022].
- Agugiaro, G., F. Remondino, G. Girardi, J. v. Schwerin, H. Richards-Rissetto, and R. d. Amicis, 2011: A web-based interactive tool for multi-resolution 3D models of a Maya archaeological site. *International Archives of the Photogrammetry, Remote Sensing and Spatial Information Science*, **XXXVIII-5/W16**, 23–30, doi:[10.5194/isprsarchives-XXXVIII-5-W16-23-2011](https://doi.org/10.5194/isprsarchives-XXXVIII-5-W16-23-2011).
- Al-Ketan, O., and R. K. Abu Al-Rub, 2021: MSLattice: A free software for generating uniform and graded lattices based on triply periodic minimal surfaces. *Material Design & Processing Communications*, **3** (6), e205, doi:[10.1002/mdp2.205](https://doi.org/10.1002/mdp2.205).
- Al-Waked, R., and M. Behnia, 2004: The performance of natural draft dry cooling towers under crosswind: CFD study. *International journal of energy research*, **28** (2), 147–161, doi:[10.1002/er.958](https://doi.org/10.1002/er.958).
- Alghamdi, A., T. Maconachie, D. Downing, M. Brandt, M. Qian, and M. Leary, 2020: Effect of additive manufactured lattice defects on mechanical properties: an automated

- method for the enhancement of lattice geometry. *The International Journal of Advanced Manufacturing Technology*, **108** (3), 957–971, doi:[Optimal and continuous multilattice embedding](#).
- Alkebsi, E. A. A., H. Ameddah, T. Outtas, and A. Almutawakel, 2021: Design of graded lattice structures in turbine blades using topology optimization. *International Journal of Computer Integrated Manufacturing*, **34** (4), 370–384, doi:[10.1080/0951192X.2021.1872106](#).
- Alsheghri, A., N. Reznikov, N. Piché, M. D. McKee, F. Tamimi, and J. Song, 2021: Optimization of 3D network topology for bioinspired design of stiff and lightweight bone-like structures. *Materials Science and Engineering: C*, **123**, 112010, doi:[10.1016/j.msec.2021.112010](#).
- An, X., and H. Fan, 2016: Hybrid design and energy absorption of luffa-sponge-like hierarchical cellular structures. *Materials & Design*, **106**, 247–257, doi:[10.1016/j.matdes.2016.05.110](#).
- ANSYS Inc., 2014: Ansys – Engineering simulation software. URL <https://www.ansys.com>, [Online; accessed March 17, 2023].
- Antolin, P., A. Buffa, and M. Martinelli, 2019: Isogeometric analysis on V-reps: first results. *Computer Methods in Applied Mechanics and Engineering*, **355**, 976–1002, doi:[10.1016/j.cma.2019.07.015](#).
- Arabnejad Khanoki, S., and D. Pasini, 2012: Multiscale design and multiobjective optimization of orthopedic hip implants with functionally graded cellular material. *Journal of Biomechanical Engineering*, **134** (3), 031004, doi:[10.1115/1.4006115](#).
- Aremu, A. O., J. Brennan-Craddock, A. Panesar, I. Ashcroft, R. J. Hague, R. D. Wildman, and C. Tuck, 2017: A voxel-based method of constructing and skinning conformal and functionally graded lattice structures suitable for additive manufacturing. *Additive Manufacturing*, **13**, 1–13, doi:[10.1016/j.addma.2016.10.006](#).
- Ashby, M. F., 2006: The properties of foams and lattices. *Philosophical Transactions of the Royal Society A: Mathematical, Physical and Engineering Sciences*, **364** (1838), 15–30, doi:[10.1098/rsta.2005.1678](#).
- Ashby, N., W. Brittin, W. Love, and W. Wyss, 1975: Brachistochrone with coulomb friction. *American Journal of Physics*, **43** (10), 902–906, doi:[10.1119/1.9976](#).
- Ashgriz, N., and J. Mostaghimi, 2002: *An introduction to computational fluid dynamics*, chap. 24, 401–410. 1st ed., McGraw-Hill Education, New York, NY, USA.

- ASTM F2792-12, 2021: Standard Terminology for Additive Manufacturing Technologies. Standard, ASTM International, West Conshohocken, PA, USA, 1–3 pp. URL <https://www.astm.org/f2792-12.html>.
- Autodesk Inc., 2017: Fusion 360 with Netfabb. URL <https://www.autodesk.com/products/netfabb/overview>, [Online; accessed March 15, 2023].
- Azarov, A. V., F. K. Antonov, M. V. Golubev, A. R. Khaziev, and S. A. Ushanov, 2019: Composite 3D printing for the small size unmanned aerial vehicle structure. *Composites Part B: Engineering*, **169**, 157–163, doi:[10.1016/j.compositesb.2019.03.073](https://doi.org/10.1016/j.compositesb.2019.03.073).
- Bai, L., C. Yi, X. Chen, Y. Sun, and J. Zhang, 2019: Effective design of the graded strut of BCC lattice structure for improving mechanical properties. *Materials*, **12 (13)**, 2192, doi:[10.3390/ma12132192](https://doi.org/10.3390/ma12132192).
- Bajaj, M., B. Cole, and D. Zwemer, 2016: Architecture to geometry – integrating system models with mechanical design. *AIAA SPACE 2016*, 5470, doi:[10.2514/6.2016-5470](https://doi.org/10.2514/6.2016-5470).
- Balzannikov, M., V. Alpatov, I. Kholopov, A. Saharov, and A. Lukin, 2016: Usage of spatial lattice metal structures as roofing for mechanical equipment rooms of hydroelectric power stations. *XV International Conference “Topical Problems of Architecture, Civil Engineering, Energy Efficiency and Ecology”*, Tyumen, Russia, EDP Sciences, Vol. 73, 01012, doi:[10.1051/matecconf/20167301012](https://doi.org/10.1051/matecconf/20167301012).
- Banovic, M., O. Mykhaskiv, S. Auriemma, A. Walther, H. Legrand, and J.-D. Müller, 2018: Algorithmic differentiation of the Open CASCADE Technology CAD kernel and its coupling with an adjoint CFD solver. *Optimization Methods and Software*, **33 (4-6)**, 813–828, doi:[10.1080/10556788.2018.1431235](https://doi.org/10.1080/10556788.2018.1431235).
- Bar-Cohen, Y., 2005: *Biomimetics: biologically inspired technologies*. CRC press, Boca Raton, FL, USA, 552 pp., doi:[10.1201/9780849331633](https://doi.org/10.1201/9780849331633).
- Batty, C., F. Bertails, and R. Bridson, 2007: A fast variational framework for accurate solid-fluid coupling. *ACM Transactions on Graphics (TOG)*, **26 (3)**, 100–es, doi:[10.1145/1276377.1276502](https://doi.org/10.1145/1276377.1276502).
- Bazilevs, Y., V. M. Calo, J. A. Cottrell, J. A. Evans, T. J. R. Hughes, S. Lipton, M. A. Scott, and T. W. Sederberg, 2010: Isogeometric analysis using T-splines. *Computer methods in applied mechanics and engineering*, **199 (5-8)**, 229–263, doi:[10.1016/j.cma.2009.02.036](https://doi.org/10.1016/j.cma.2009.02.036).
- Becker, H., V. Hwang, M. J. Kannwischer, B.-Y. Yang, and S.-Y. Yang, 2021: Neon NTT: faster Dilithium, Kyber, and Saber on Cortex-A72 and Apple M1. *Cryptology ePrint Archive, Paper 2021/986*, 1–38, URL <https://eprint.iacr.org/2021/986>.

- Ben Makhlouf, A., B. Louhichi, M. A. Mahjoub, and D. Deneux, 2019: Reconstruction of a CAD model from the deformed mesh using B-spline surfaces. *International Journal of Computer Integrated Manufacturing*, **32** (7), 669–681, doi:[10.1080/0951192X.2019.1599442](https://doi.org/10.1080/0951192X.2019.1599442).
- Bendsøe, M. P., and O. Sigmund, 2013: *Topology optimization: theory, methods, and applications*. 2nd ed., Springer Science & Business Media, Berlin, Germany, 370 pp., doi:[10.1007/978-3-662-05086-6](https://doi.org/10.1007/978-3-662-05086-6).
- Benyus, J. M., 1997: *Biomimicry: Innovation inspired by nature*. William Morrow, New York, NY, USA.
- Bhattacharjee, N., C. Parra-Cabrera, Y. T. Kim, A. P. Kuo, and A. Folch, 2018: Desktop-stereolithography 3D-printing of a poly (dimethylsiloxane)-based material with sylgard-184 properties. *Advanced materials*, **30** (22), 1800 001, doi:[10.1002/adma.201800001](https://doi.org/10.1002/adma.201800001).
- Bikas, H., P. Stavropoulos, and G. Chryssolouris, 2016: Additive manufacturing methods and modelling approaches: a critical review. *The International Journal of Advanced Manufacturing Technology*, **83** (1-4), 389–405, doi:[10.1007/s00170-015-7576-2](https://doi.org/10.1007/s00170-015-7576-2).
- Blakey-Milner, B., and Coauthors, 2021: Metal additive manufacturing in aerospace: A review. *Materials & Design*, **209**, 110 008, doi:[10.1016/j.matdes.2021.110008](https://doi.org/10.1016/j.matdes.2021.110008).
- Blender Foundation, 2016: Home of the Blender project – Free and Open 3D Creation Software. URL <https://www.blender.org/>, [Online; accessed April 22, 2023].
- Bloomenthal, J., C. Bajaj, J. Blinn, M.-P. Cani, B. Wyvill, A. Rockwood, and G. Wyvill, 1997: *Introduction to implicit surfaces*. Morgan Kaufmann, San Francisco, CA, USA.
- Boender, E., W. F. Bronsvoort, and F. H. Post, 1994: Finite-element mesh generation from constructive-solid-geometry models. *Computer-Aided Design*, **26** (5), 379–392, doi:[10.1016/0010-4485\(94\)90025-6](https://doi.org/10.1016/0010-4485(94)90025-6).
- Bonabeau, E., M. Dorigo, and G. Theraulaz, 1999: *Swarm intelligence: from natural to artificial systems*. 1, Oxford university press, New York, NY, USA, 293 pp., doi:[10.1093/oso/9780195131581.001.0001](https://doi.org/10.1093/oso/9780195131581.001.0001).
- Borrman, A., T. H. Kolbe, A. Donaubauer, H. Steuer, J. R. Jubierre, and M. Flurl, 2015: Multi-scale geometric-semantic modeling of shield tunnels for GIS and BIM applications. *Computer-Aided Civil and Infrastructure Engineering*, **30** (4), 263–281, doi:[10.1111/mice.12090](https://doi.org/10.1111/mice.12090).
- Botsch, M., and L. Kobbelt, 2004: A remeshing approach to multiresolution modeling. *Proceedings of the 2004 Eurographics/ACM SIGGRAPH symposium on Geometry processing*, Nice, France, 185–192, doi:[10.1145/1057432.1057457](https://doi.org/10.1145/1057432.1057457).

- Brasseur, V. M. V., 2018: *Forge Your Future with Open Source: Build Your Skills. Build Your Network. Build the Future of Technology.* Pragmatic Bookshelf, Raleigh, NC, USA, 224 pp.
- Braun, P., M. Sliwinski, J. Hinckeldeyn, and J. Kreutzfeldt, 2021: Challenges of CAD conversion to 3D development environments with respect to kinematic dependencies. *Proceedings of The 61st SIMS Conference on Simulation and Modelling SIMS 2020*, Oulu, Finland, 215–221, doi:[10.3384/ecp20176215](https://doi.org/10.3384/ecp20176215).
- Bronstein, M. M., J. Bruna, Y. LeCun, A. Szlam, and P. Vandergheynst, 2017: Geometric deep learning: going beyond Euclidean data. *IEEE Signal Processing Magazine*, **34** (4), 18–42, doi:[10.1109/MSP.2017.2693418](https://doi.org/10.1109/MSP.2017.2693418).
- Brunet, P., C. Hoffmann, and D. Roller, 2000: *CAD Tools and Algorithms for Product Design*. 1st ed., Springer Science & Business Media, Berlin, Germany, 165–177 pp., doi:[10.1007/978-3-662-04123-9](https://doi.org/10.1007/978-3-662-04123-9).
- Burkhart, D., B. Hamann, and G. Umlauf, 2010: Iso-geometric finite element analysis based on Catmull-Clark subdivision solids. *Eurographics Symposium on Geometry Processing 2010*, Lausanne, Switzerland, Wiley Online Library, Vol. 29, 1575–1584, doi:[10.1111/j.1467-8659.2010.01766.x](https://doi.org/10.1111/j.1467-8659.2010.01766.x).
- C3D Labs, 2020: C3D. Developer Manual. URL https://c3dlabs.com/source/documents/en/2020-09-C3D_Manual_English.pdf, [Online; accessed March 9, 2023], 553 pp.
- Catchpole-Smith, S., 2019: Laser powder bed fusion of lattice structures for thermomechanical applications. Ph.D. thesis, University of Nottingham, Nottingham, UK, URL <http://eprints.nottingham.ac.uk/60244>.
- Catchpole-Smith, S., R. Sélo, A. Davis, I. Ashcroft, C. Tuck, and A. Clare, 2019: Thermal conductivity of TPMS lattice structures manufactured via laser powder bed fusion. *Additive Manufacturing*, **30**, 100 846, doi:[10.1016/j.addma.2019.100846](https://doi.org/10.1016/j.addma.2019.100846).
- Catmull, E., and J. Clark, 1978: Recursively generated B-spline surfaces on arbitrary topological meshes. *Computer-aided design*, **10** (6), 350–355, doi:[10.1016/0010-4485\(78\)90110-0](https://doi.org/10.1016/0010-4485(78)90110-0).
- Cazzani, A., M. Malagù, and E. Turco, 2016: Isogeometric analysis: a powerful numerical tool for the elastic analysis of historical masonry arches. *Continuum Mechanics and thermodynamics*, **28**, 139–156, doi:[10.1007/s00161-014-0409-y](https://doi.org/10.1007/s00161-014-0409-y).
- Chen, F., C. Dokken, T. A. Grandine, and G. Morin, 2017: Geometric modelling, interoperability and new challenges (Dagstuhl Seminar 17221). *Dagstuhl Reports*, Dagstuhl, Germany, Schloss Dagstuhl-Leibniz-Zentrum für Informatik, Vol. 7, 140–168, doi:[10.4230/DagRep.7.5.140](https://doi.org/10.4230/DagRep.7.5.140).

- Chen, H., and J. Bishop, 1997: Delaunay triangulation for curved surfaces. *Meshing Roundtable*, 115–127.
- Chu, C., G. Graf, and D. W. Rosen, 2008: Design for additive manufacturing of cellular structures. *Computer-Aided Design and Applications*, **5** (5), 686–696, doi:[10.3722/cadaps.2008.686-696](https://doi.org/10.3722/cadaps.2008.686-696).
- Cohen-Or, D., and A. Kaufman, 1997: 3D line voxelization and connectivity control. *IEEE Computer Graphics and Applications*, **17** (6), 80–87, doi:[10.1109/38.626973](https://doi.org/10.1109/38.626973).
- Cohen-Or, D., A. Solomovic, and D. Levin, 1998: Three-dimensional distance field metamorphosis. *ACM Transactions on Graphics (TOG)*, **17** (2), 116–141, doi:[10.1145/274363.274366](https://doi.org/10.1145/274363.274366).
- Cordero, S. S., C. Fortin, and R. Vingerhoeds, 2020: Concurrent conceptual design sequencing for MBSE of complex systems through design structure matrices. *Proceedings of the Design Society: DESIGN Conference*, Dubrovnik, Croatia, Cambridge University Press, Vol. 1, 2375–2384, doi:[0.1017/dsd.2020.96](https://doi.org/10.1017/dsd.2020.96).
- Cottrell, J. A., T. J. Hughes, and Y. Bazilevs, 2009: *Isogeometric analysis: toward integration of CAD and FEA*. John Wiley & Sons, Singapore, 360 pp., doi:[10.1002/9780470749081](https://doi.org/10.1002/9780470749081).
- Crane, K., 2020: Conformal geometry of simplicial surfaces. *Proceedings of Symposia in Applied Mathematics*, San Diego, CA, USA, Vol. 76, 52–102, doi:[10.1090/psapm/076](https://doi.org/10.1090/psapm/076).
- Cutanda, V., P. Møller Juhl, and F. Jacobsen, 2001: On the modeling of narrow gaps using the standard boundary element method. *The Journal of the Acoustical Society of America*, **109** (4), 1296–1303, doi:[10.1121/1.1350399](https://doi.org/10.1121/1.1350399).
- Dassault Systèmes SE, 2006: SOLIDWORKS. URL <https://www.solidworks.com>, [Online; accessed March 4, 2023].
- Dassault Systèmes SE, 2020: SOLIDWORKS and SW Data Management System Requirements. URL <https://www.solidworks.com/support/system-requirements>, [Online; accessed March 5, 2023].
- Dassault Systèmes SE, 2023: Abaqus – Mechanical and Civil Engineering Simulation. URL <https://www.3ds.com/products-services/simulia/products/abaqus>, [Online; accessed April 22, 2023].
- Davidson, S., 2009: Grasshopper – Algorithmic modeling for Rhino. URL <https://www.grasshopper3d.com>, [Online; accessed March 15, 2023].

- De Berg, M., O. Cheong, M. Van Kreveld, and M. Overmars, 2008: *Computational geometry: introduction*, chap. 1, 1–17. Springer-Verlag, Berlin, Germany, doi:[10.1007/978-3-540-77974-2_1](https://doi.org/10.1007/978-3-540-77974-2_1).
- Deng, H., J. Zhao, and C. Wang, 2021: Leaf vein-inspired bionic design method for heat exchanger infilled with graded lattice structure. *Aerospace*, **8** (9), 237, doi:[10.3390/aerospace8090237](https://doi.org/10.3390/aerospace8090237).
- DeRose, T., M. Kass, and T. Truong, 1998: Subdivision surfaces in character animation. *Proceedings of the 25th annual conference on Computer graphics and interactive techniques*, New York, NY, USA, 85–94, doi:[10.1145/280814.280826](https://doi.org/10.1145/280814.280826).
- Dimas, L. S., and M. J. Buehler, 2014: Modeling and additive manufacturing of bio-inspired composites with tunable fracture mechanical properties. *Soft Matter*, **10** (25), 4436–4442, doi:[10.1039/C3SM52890A](https://doi.org/10.1039/C3SM52890A).
- Do, Q. T., C. H. P. Nguyen, and Y. Choi, 2021: Homogenization-based optimum design of additively manufactured Voronoi cellular structures. *Additive Manufacturing*, **45**, 102057, doi:[10.1016/j.addma.2021.102057](https://doi.org/10.1016/j.addma.2021.102057).
- Dong, G., Y. Tang, and Y. F. Zhao, 2017: A survey of modeling of lattice structures fabricated by additive manufacturing. *Journal of Mechanical Design*, **139** (10), doi:[10.1115/1.4037305](https://doi.org/10.1115/1.4037305).
- Doo, D., and M. Sabin, 1978: Behaviour of recursive division surfaces near extraordinary points. *Computer-Aided Design*, **10** (6), 356–360, doi:[10.1016/0010-4485\(78\)90111-2](https://doi.org/10.1016/0010-4485(78)90111-2).
- Dorigo, M., M. Birattari, and T. Stutzle, 2006: Ant colony optimization. *IEEE Computational Intelligence Magazine*, **1** (4), 28–39, doi:[10.1109/MCI.2006.329691](https://doi.org/10.1109/MCI.2006.329691).
- Doubrovski, E. L., E. Y. Tsai, D. Dikovsky, J. M. Geraedts, H. Herr, and N. Oxman, 2015: Voxel-based fabrication through material property mapping: A design method for bitmap printing. *Computer-Aided Design*, **60**, 3–13, doi:[10.1016/j.cad.2014.05.010](https://doi.org/10.1016/j.cad.2014.05.010).
- ECR Labs, 2018: Dendro. URL <https://www.ecrlabs.com/dendro>, [Online; accessed March 15, 2023].
- Edalat, A., and A. Lieutier, 2002: Foundation of a computable solid modeling. *Theoretical Computer Science*, **284** (2002), 3119–345, doi:[10.1016/S0304-3975\(01\)00091-3](https://doi.org/10.1016/S0304-3975(01)00091-3).
- Edgar, J., and S. Tint, 2015: Additive manufacturing technologies: 3D printing, rapid prototyping, and direct digital manufacturing. *Johnson Matthey Technology Review*, **59** (3), 193–198, doi:[10.1595/205651315X688406](https://doi.org/10.1595/205651315X688406).

- Eggli, L., C.-y. Hsu, B. D. Bruederlin, and G. Elber, 1997: Inferring 3D models from freehand sketches and constraints. *Computer-Aided Design*, **29** (2), 101–112, doi:[10.1016/S0010-4485\(96\)00039-5](https://doi.org/10.1016/S0010-4485(96)00039-5).
- F EQUALS F LLC., 2019: f=f: Crystallon. URL <http://fequalsf.blogspot.com/p/crystallon.html>, [Online; accessed March 15, 2023].
- Faizah, R., H. Priyosulistyo, and A. Aminullah, 2019: The properties of waste rubber tires in increasing the damping of masonry wall structure. *IOP Conference Series: Materials Science and Engineering*, Jakarta, Indonesia, IOP Publishing, Vol. 650, 012041, doi:[10.1088/1757-899X/650/1/012041](https://doi.org/10.1088/1757-899X/650/1/012041).
- Fang, J., G. Sun, N. Qiu, G. P. Steven, and Q. Li, 2017: Topology optimization of multi-cell tubes under out-of-plane crushing using a modified artificial bee colony algorithm. *Journal of Mechanical Design*, **139** (7), 071403, doi:[10.1115/1.4036561](https://doi.org/10.1115/1.4036561).
- Fantini, M., M. Curto, and F. De Crescenzo, 2016: A method to design biomimetic scaffolds for bone tissue engineering based on Voronoi lattices. *Virtual and Physical Prototyping*, **11** (2), 77–90, doi:[10.1080/17452759.2016.1172301](https://doi.org/10.1080/17452759.2016.1172301).
- Federle, W., M. Riehle, A. S. Curtis, and R. J. Full, 2002: An integrative study of insect adhesion: mechanics and wet adhesion of pretarsal pads in ants. *Integrative and Comparative Biology*, **42** (6), 1100–1106, doi:[10.1093/icb/42.6.1100](https://doi.org/10.1093/icb/42.6.1100).
- Felbrich, B., G. Jahn, C. Newnham, and A. Menges, 2018: Self-organizing maps for intuitive gesture-based geometric modelling in augmented reality. *2018 IEEE international conference on artificial intelligence and virtual reality (AIVR)*, Taichung, China, IEEE, 61–67, doi:[10.1109/AIVR.2018.00016](https://doi.org/10.1109/AIVR.2018.00016).
- Feng, J., J. Fu, Z. Lin, C. Shang, and B. Li, 2018: A review of the design methods of complex topology structures for 3D printing. *Visual Computing for Industry, Biomedicine, and Art*, **1** (1), 1–16, doi:[10.1186/s42492-018-0004-3](https://doi.org/10.1186/s42492-018-0004-3).
- Feng, Y., T. Huang, Y. Gong, and P. Jia, 2022: Stiffness optimization design for TPMS architected cellular materials. *Materials & Design*, **222**, 111078, doi:[10.1016/j.matdes.2022.111078](https://doi.org/10.1016/j.matdes.2022.111078).
- Fischman, S., and Coauthors, 2022: Non-invasive scoring of cellular atypia in keratinocyte cancers in 3D LC-OCT images using Deep Learning. *Scientific reports*, **12** (1), 481, doi:[10.1038/s41598-021-04395-1](https://doi.org/10.1038/s41598-021-04395-1).
- Floreano, D., and C. Mattiussi, 2023: *Bio-inspired artificial intelligence: theories, methods, and technologies*. MIT press, Cambridge, MA, USA, 674 pp.

- Formlabs Inc., 2018: Form 2: Affordable Desktop SLA 3D Printer. URL <https://formlabs.com/3d-printers/form-2>, [Online; accessed April 12, 2023].
- Formlabs Inc., 2019: Preform 3D printing software: Prepare your models for printing. URL <https://formlabs.com/software>, [Online; accessed March 17, 2023].
- Formlabs Inc., 2020a: BioMed Amber. Biocompatible Photopolymer Resin for Formlabs SLA Printers. Tech. rep., Fromlabs, Somerville, MA, USA, 1–2 pp. URL <https://formlabs-media.formlabs.com/datasheets/2001403-TDS-ENUS-0.pdf>.
- Formlabs Inc., 2020b: Material data sheet. Elastic 50A. URL <https://formlabs-media.formlabs.com/datasheets/2001420-TDS-ENUS-0.pdf>, [Online; accessed April 22, 2023].
- Fortin, C., G. McSorley, D. Knoll, A. Golkar, and R. Tsykunova, 2017: Study of data structures and tools for the concurrent conceptual design of complex space systems. *Product Lifecycle Management and the Industry of the Future: 14th IFIP WG 5.1 International Conference, PLM 2017*, IFIP Advances in Information and Communication Technology, Seville, Spain, Springer, Vol. 53, 601–611, doi:[10.1007/978-3-319-72905-3_53](https://doi.org/10.1007/978-3-319-72905-3_53).
- Froehlich, J. J., N. Rajewsky, and C. Y. Ewald, 2021: Estimation of *C. elegans* cell-and tissue volumes. *microPublication Biology*, **2021**, doi:[10.17912/micropub.biology.000345](https://doi.org/10.17912/micropub.biology.000345).
- Frulloni, E., J. M. Kenny, P. Conti, and L. Torre, 2007: Experimental study and finite element analysis of the elastic instability of composite lattice structures for aeronautic applications. *Composite structures*, **78** (4), 519–528, doi:[10.1016/j.compstruct.2005.11.013](https://doi.org/10.1016/j.compstruct.2005.11.013).
- Fuchs, R., V. Welker, and J. Hornegger, 2010: Non-convex polyhedral volume of interest selection. *Computerized medical imaging and graphics*, **34** (2), 105–113, doi:[10.1016/j.compmedimag.2009.07.002](https://doi.org/10.1016/j.compmedimag.2009.07.002).
- Gandy, P. J. F., and J. Klinowski, 2000: Exact computation of the triply periodic Schwarz P minimal surface. *Chemical Physics Letters*, **314** (5-6), 543–551, doi:[10.1016/S0009-2614\(99\)01000-3](https://doi.org/10.1016/S0009-2614(99)01000-3).
- Gao, Z., H. Wang, N. Letov, Y. F. Zhao, X. Zhang, Y. Wu, C. L. A. Leung, and H. Wang, 2023: Data-driven design of biometric composite metamaterials with extremely recoverable and ultrahigh specific energy absorption. *Composites Part B: Engineering*, **251**, 110 468, doi:[10.1016/j.compositesb.2022.110468](https://doi.org/10.1016/j.compositesb.2022.110468).
- García-Dominguez, A., J. Claver, and M. A. Sebastián, 2020: Optimization methodology for additive manufacturing of customized parts by fused deposition modeling (FDM). application to a shoe heel. *Polymers*, **12** (9), 2119, doi:[10.3390/polym12092119](https://doi.org/10.3390/polym12092119).
- Gardan, Y., 2014: *Mathematics and CAD: Numerical Methods for CAD*. 1st ed., MIT Press, Cambridge, MA, USA, 170 pp.

- Garinis, D., M. Dinulović, and B. Rašuo, 2012: Dynamic analysis of modified composite helicopter blade. *FME Transactions*, **40** (2), 63–68, URL <https://scindeks.ceon.rs/article.aspx?artid=1451-20921202063G>.
- Gavryushkina, M., 2021: The potential and problems of volumetric 3D modeling in archaeological stratigraphic analysis: A case study from Chlorakas-Palloures, Cyprus. *Digital Applications in Archaeology and Cultural Heritage*, **21**, e00184, doi:[10.1016/j.daach.2021.e00184](https://doi.org/10.1016/j.daach.2021.e00184).
- Gen3D Ltd., 2019: Sulis AM software. URL <https://gen3d.com/software>, [Online; accessed March 15, 2023].
- Ghavidel, A., S. R. Mousavi, and M. Rashki, 2018: The effect of FEM mesh density on the failure probability analysis of structures. *KSCE Journal of Civil Engineering*, **22**, 2370–2383, doi:[10.1007/s12205-017-1437-5](https://doi.org/10.1007/s12205-017-1437-5).
- Gibson, L. J., 2012: The hierarchical structure and mechanics of plant materials. *Journal of the royal society interface*, **9** (76), 2749–2766, doi:[10.1098/rsif.2012.0341](https://doi.org/10.1098/rsif.2012.0341).
- Gillebaart, T., A. van Zuijlen, and H. Bijl, 2016: Radial basis function mesh deformation including surface orthogonality. *54th AIAA Aerospace Sciences Meeting*, San Diego, CA, USA, American Institute of Aeronautics and Astronautics, 1674, doi:[10.2514/6.2016-1674](https://doi.org/10.2514/6.2016-1674).
- Gobert, C., E. W. Reutzel, J. Petrich, A. R. Nassar, and S. Phoha, 2018: Application of supervised machine learning for defect detection during metallic powder bed fusion additive manufacturing using high resolution imaging. *Additive Manufacturing*, **21**, 517–528, doi:[10.1016/j.addma.2018.04.005](https://doi.org/10.1016/j.addma.2018.04.005).
- Golovanov, N., 2014: *Geometric MOdeling*. CreateSpace Independent Publishing Platform, Scotts Valley, CA, USA, 344 pp.
- Gómez-Gálvez, P., and Coauthors, 2018: Scutoids are a geometrical solution to three-dimensional packing of epithelia. *Nature communications*, **9** (1), 2960, doi:[10.1038/s41467-018-05376-1](https://doi.org/10.1038/s41467-018-05376-1).
- Gostick, J. T., 2017: Versatile and efficient pore network extraction method using marker-based watershed segmentation. *Physical Review E*, **96** (2), 023307, doi:[10.1103/PhysRevLett.118.021043](https://doi.org/10.1103/PhysRevLett.118.021043).
- Góźdź, W., and R. Holyst, 1996: High genus periodic gyroid surfaces of nonpositive gaussian curvature. *Physical review letters*, **76** (15), 2726, doi:[10.1103/PhysRevLett.76.2726](https://doi.org/10.1103/PhysRevLett.76.2726).

- Guo, X., J. Ding, X. Li, S. Qu, X. Song, J. Y. H. Fuh, W. F. Lu, and W. Zhai, 2022: Enhancement in the mechanical behaviour of a Schwarz Primitive periodic minimal surface lattice structure design. *International Journal of Mechanical Sciences*, **216**, 106977, doi:[10.1016/j.ijmecsci.2021.106977](https://doi.org/10.1016/j.ijmecsci.2021.106977).
- Hahmann, S., G.-P. Bonneau, S. Barbier, G. Elber, and H. Hagen, 2012: Volume-preserving FFD for programmable graphics hardware. *The Visual Computer*, **28**, 231–245, doi:[10.1007/s00371-011-0608-5](https://doi.org/10.1007/s00371-011-0608-5).
- Haimes, R., and M. Drela, 2012: On the construction of aircraft conceptual geometry for high-fidelity analysis and design. *50th AIAA Aerospace sciences meeting including the new horizons forum and aerospace exposition*, Nashville, TN, USA, 683, doi:[10.2514/6.2012-683](https://doi.org/10.2514/6.2012-683).
- Halstead, M., M. Kass, and T. DeRose, 1993: Efficient, fair interpolation using Catmull-Clark surfaces. *Proceedings of the 20th annual conference on Computer graphics and interactive techniques*, Anaheim, CA, USA, 35–44, doi:[10.1145/166117.166121](https://doi.org/10.1145/166117.166121).
- Hamelin, R. D., D. D. Walden, and M. E. Krueger, 2010: 4.4.2 INCOSE systems engineering handbook v3.2: Improving the process for SE practitioners. *INCOSE International Symposium*, Chicago, IL, USA, Wiley Online Library, Vol. 20, 532–541, doi:[10.1002/j.2334-5837.2010.tb01087.x](https://doi.org/10.1002/j.2334-5837.2010.tb01087.x).
- Hamri, O., J.-C. Léon, F. Giannini, and B. Falcidieno, 2010: Software environment for CAD/CAE integration. *Advances in Engineering Software*, **41** (10-11), 1211–1222, doi:[10.1016/j.advengsoft.2010.07.003](https://doi.org/10.1016/j.advengsoft.2010.07.003).
- Hancock, M. J., K. Sekeroglu, and M. C. Demirel, 2012: Bioinspired directional surfaces for adhesion, wetting, and transport. *Advanced functional materials*, **22** (11), 2223–2234, doi:[10.1002/adfm.201103017](https://doi.org/10.1002/adfm.201103017).
- Hansson, S., and A. Ekstubbe, 2004: Area moments of inertia as a measure of the mandible stiffness of the implant patient. *Clinical Oral Implants Research*, **15** (4), 450–458, doi:[10.1111/j.1600-0501.2004.01021.x](https://doi.org/10.1111/j.1600-0501.2004.01021.x).
- Harris, C. R., and Coauthors, 2020: Array programming with NumPy. *Nature*, **585** (7825), 357–362, doi:[10.1038/s41586-020-2649-2](https://doi.org/10.1038/s41586-020-2649-2).
- Hartog, D., 1977: *Strength of materials*. Dover Publications, Inc., New York, NY, USA, 342 pp.
- Hatcher, A., 2001: *Algebraic Topology*. 1st ed., Cambridge University Press, Cambridge, MA, USA, 556 pp.

- He, T., L. Hong, A. Kaufman, A. Varshney, and S. Wang, 1995: Voxel based object simplification. *Proceedings Visualization'95*, Atlanta, GA, USA, IEEE, 296–303, doi:[10.1109/VISUAL.1995.485142](https://doi.org/10.1109/VISUAL.1995.485142).
- Hedayati, R., M. Sadighi, M. Mohammadi-Aghdam, and A. Zadpoor, 2016: Mechanical properties of regular porous biomaterials made from truncated cube repeating unit cells: Analytical solutions and computational models. *Materials Science and Engineering: C*, **60**, 163–183, doi:[10.1016/j.msec.2015.11.001](https://doi.org/10.1016/j.msec.2015.11.001).
- Hirt, C. W., and B. D. Nichols, 1981: Volume of fluid (VOF) method for the dynamics of free boundaries. *Journal of computational physics*, **39** (1), 201–225, doi:[10.1016/0021-9991\(81\)90145-5](https://doi.org/10.1016/0021-9991(81)90145-5).
- Hossain, U., S. Ghouse, K. Nai, and J. R. Jeffers, 2021: Controlling and testing anisotropy in additively manufactured stochastic structures. *Additive Manufacturing*, **39**, 101849, doi:[10.1016/j.addma.2021.101849](https://doi.org/10.1016/j.addma.2021.101849).
- Hsu, W., and B. Liu, 2000: Conceptual design: issues and challenges. *Computer-aided design*, **14** (32), 849–850, doi:[10.1016/S0010-4485\(00\)00074-9](https://doi.org/10.1016/S0010-4485(00)00074-9).
- Hu, J., Y. Luo, and S. Liu, 2021: Two-scale concurrent topology optimization method of hierarchical structures with self-connected multiple lattice-material domains. *Composite Structures*, **272**, 114224, doi:[10.1016/j.compstruct.2021.114224](https://doi.org/10.1016/j.compstruct.2021.114224).
- Huang, J., S. Y. Chiam, H. H. Tan, S. Wang, and W. K. Chim, 2010: Fabrication of silicon nanowires with precise diameter control using metal nanodot arrays as a hard mask blocking material in chemical etching. *Chemistry of Materials*, **22** (13), 4111–4116, doi:[10.1021/cm101121c](https://doi.org/10.1021/cm101121c).
- Hughes, T. J. R., J. A. Cottrell, and Y. Bazilevs, 2005: Isogeometric analysis: CAD, finite elements, NURBS, exact geometry and mesh refinement. *Computer methods in applied mechanics and engineering*, **194** (39-41), 4135–4195, doi:[10.1016/j.cma.2004.10.008](https://doi.org/10.1016/j.cma.2004.10.008).
- Ivakhnenko, A. G., and V. G. Lapa, 1967: *Cybernetics and forecasting techniques*, Vol. 8. American Elsevier Publishing Company, New York, NY, USA, 168 pp.
- Jared, B. H., M. A. Aguiló, L. L. Beghini, B. L. Boyce, B. W. Clark, A. Cook, B. J. Kaehr, and J. Robbins, 2017: Additive manufacturing: Toward holistic design. *Scripta Materialia*, **135**, 141–147, doi:[10.1016/j.scriptamat.2017.02.029](https://doi.org/10.1016/j.scriptamat.2017.02.029).
- Javaid, M., A. Haleem, and L. Kumar, 2019: Current status and applications of 3D scanning in dentistry. *Clinical Epidemiology and Global Health*, **7** (2), 228–233, doi:[10.1016/j.cegh.2018.07.005](https://doi.org/10.1016/j.cegh.2018.07.005).

- Jihong, Z., Z. Han, W. Chuang, Z. Lu, Y. Shangqin, and W. Zhang, 2021: A review of topology optimization for additive manufacturing: Status and challenges. *Chinese Journal of Aeronautics*, **34** (1), 91–110, doi:[10.1016/j.cja.2020.09.020](https://doi.org/10.1016/j.cja.2020.09.020).
- Jones, A., M. Leary, S. Bateman, and M. Easton, 2022: Parametric design and evaluation of TPMS-like cellular solids. *Materials & Design*, **221**, 110908, doi:[10.1016/j.matdes.2022.110908](https://doi.org/10.1016/j.matdes.2022.110908).
- Jones, A. C., L. Gu, C. M. Sorrels, D. H. Sherman, and W. H. Gerwick, 2009: New tricks from ancient algae: natural products biosynthesis in marine cyanobacteria. *Current Opinion in Chemical Biology*, **13** (2), 216–223, doi:[10.1016/j.cbpa.2009.02.019](https://doi.org/10.1016/j.cbpa.2009.02.019).
- Junk, S., and C. Kuen, 2016: Review of open source and freeware CAD systems for use with 3D-printing. *Procedia CIRP*, **50**, 430–435, doi:[10.1016/j.procir.2016.04.174](https://doi.org/10.1016/j.procir.2016.04.174).
- Kamaci, N., and Y. Altunbasak, 2003: Performance comparison of the emerging h. 264 video coding standard with the existing standards. *2003 International Conference on Multimedia and Expo. ICME'03. Proceedings (Cat. No. 03TH8698)*, Baltimore, MD, USA, IEEE, Vol. 1, I–345, doi:[10.1109/ICME.2003.1220925](https://doi.org/10.1109/ICME.2003.1220925).
- Katopodes, N. D., 2018: *Free-surface flow: computational methods*. Butterworth-Heinemann, Oxford, UK, 879 pp., doi:[10.1016/C2017-0-00542-6](https://doi.org/10.1016/C2017-0-00542-6).
- Kauker, D., M. Falk, G. Reina, A. Ynnerman, and T. Ertl, 2016: VoxLink – combining sparse volumetric data and geometry for efficient rendering. *Computational Visual Media*, **2**, 45–56, doi:[10.1007/s41095-016-0034-8](https://doi.org/10.1007/s41095-016-0034-8).
- Kechagias, S., R. N. Oosterbeek, M. J. Munford, S. Ghouse, and J. R. Jeffers, 2022: Controlling the mechanical behaviour of stochastic lattice structures: The key role of nodal connectivity. *Additive Manufacturing*, **54**, 102730, doi:[10.1016/j.addma.2022.102730](https://doi.org/10.1016/j.addma.2022.102730).
- Kedward, L., C. B. Allen, and T. C. S. Rendall, 2017: Efficient and exact mesh deformation using multiscale RBF interpolation. *Journal of Computational Physics*, **345**, 732–751, doi:[10.1016/j.jcp.2017.05.042](https://doi.org/10.1016/j.jcp.2017.05.042).
- Kerrick, D., 2011: From wood to composite materials: The evolution of the rotor blade. URL <https://helicoptermaintenancemagazine.com/article/wood-composite-materials-evolution-rotor-blade>, [Online; accessed March 4, 2023].
- Kim, D.-S., Y. Cho, and D. Kim, 2005: Euclidean Voronoi diagram of 3D balls and its computation via tracing edges. *Computer-Aided Design*, **37** (13), 1412–1424, doi:[10.1016/j.cad.2005.02.013](https://doi.org/10.1016/j.cad.2005.02.013).

- Kim, J., and D.-J. Yoo, 2020: 3D printed compact heat exchangers with mathematically defined core structures. *Journal of Computational Design and Engineering*, **7** (4), 527–550, doi:[10.1093/jcde/qwaa032](https://doi.org/10.1093/jcde/qwaa032).
- Kim, K., J. Ju, and D. M. Kim, 2013: Static contact behaviors of a non-pneumatic tire with hexagonal lattice spokes. *SAE International Journal of Passenger Cars-Mechanical Systems*, **6** (2013-01-9117), 1518–1527, doi:[10.4271/2013-01-9117](https://doi.org/10.4271/2013-01-9117).
- Kloft, H., L. P. Schmitz, C. Müller, V. Laghi, N. Babovic, and A. Baghdadi, 2023: Experimental application of robotic wire-and-arc additive manufacturing technique for strengthening the I-beam profiles. *Buildings*, **13** (2), 366, doi:[10.3390/buildings13020366](https://doi.org/10.3390/buildings13020366).
- Köhnen, P., C. Haase, J. Bültmann, S. Ziegler, J. H. Schleifenbaum, and W. Bleck, 2018: Mechanical properties and deformation behavior of additively manufactured lattice structures of stainless steel. *Materials & Design*, **145**, 205–217, doi:[10.1016/j.matdes.2018.02.062](https://doi.org/10.1016/j.matdes.2018.02.062).
- Koltunov, S. S., and M. N. Koroleva, 2021: Monitoring and decision support system for traffic safety on bridges. *CEUR Workshop Proceedings*, Kolomna, Russia, 111–119, URL <https://ceur-ws.org/Vol-2965/paper13.pdf>.
- Kou, X., and S. T. Tan, 2007: Heterogeneous object modeling: A review. *Computer-Aided Design*, **39** (4), 284–301, doi:[10.1016/j.cad.2006.12.007](https://doi.org/10.1016/j.cad.2006.12.007).
- Kucewicz, M., P. Baranowski, J. Małachowski, A. Popławski, and P. Płatek, 2018: Modelling, and characterization of 3D printed cellular structures. *Materials & Design*, **142**, 177–189, doi:[10.1016/j.matdes.2018.01.028](https://doi.org/10.1016/j.matdes.2018.01.028).
- Kurtz, A., 2009: Intra—lattice. URL <http://www.intralattice.com>, [Online; accessed March 14, 2023].
- Laine, S., and T. Karras, 2010: Efficient sparse voxel octrees. *Proceedings of the 2010 ACM SIGGRAPH symposium on Interactive 3D Graphics and Games*, **17** (8), 1051–4651, doi:[10.1109/TVCG.2010.240](https://doi.org/10.1109/TVCG.2010.240).
- Leary, M., and Coauthors, 2018: Inconel 625 lattice structures manufactured by selective laser melting (SLM): Mechanical properties, deformation and failure modes. *Materials & Design*, **157**, 179–199, doi:[10.1016/j.matdes.2018.06.010](https://doi.org/10.1016/j.matdes.2018.06.010).
- Lee, S. H., and K. Lee, 2001: Partial entity structure: a compact non-manifold boundary representation based on partial topological entities. *Proceedings of the sixth ACM symposium on Solid modeling and applications*, Ann Arbor, MI, USA, 159–170, doi:[10.1145/376957.376976](https://doi.org/10.1145/376957.376976).

- Lenarduzzi, V., and D. Taibi, 2016: MVP explained: a systematic mapping study on the definitions of minimal viable product. *2016 42th Euromicro Conference on Software Engineering and Advanced Applications (SEAA)*, IEEE, Limassol, Cyprus, 112–119, doi:[10.1109/SEAA.2016.56](https://doi.org/10.1109/SEAA.2016.56).
- Leonardi, F., S. Graziosi, R. Casati, F. Tamburrino, and M. Bordegoni, 2019: Additive manufacturing of heterogeneous lattice structures: An experimental exploration. *Proceedings of the Design Society: International Conference on Engineering Design*, Delft, Netherlands, Cambridge University Press, Vol. 1, 669–678, doi:[10.1017/dsi.2019.71](https://doi.org/10.1017/dsi.2019.71).
- Lertthanasarn, J., C. Liu, and M.-S. Pham, 2021: Influence of the base material on the mechanical behaviors of polycrystal-like meta-crystals. *Journal of Micromechanics and Molecular Physics*, 2150004, doi:[10.1142/S2424913021500041](https://doi.org/10.1142/S2424913021500041).
- Letov, N., 2018: Integrating 3D solid modeling for conceptual concurrent design. M.S. thesis, Skolkovo Institute of Science and Technology, 105 pp., Moscow, Russia, URL https://www.researchgate.net/publication/369190543_Integrating_Concurrent_Conceptual_Systems_Design_with_3D_Modeling.
- Letov, N., 2022: jalovisko/LatticeQuery: (0.1LQ). Zenodo, [Repository], doi:[10.5281/zenodo.6959068](https://doi.org/10.5281/zenodo.6959068).
- Letov, N., P. T. Velivila, S. Sun, and Y. F. Zhao, 2021: Challenges and opportunities in geometric modeling of complex bio-inspired three-dimensional objects designed for additive manufacturing. *Journal of Mechanical Design*, **143** (12), 121 705, doi:[10.1115/1.4051720](https://doi.org/10.1115/1.4051720).
- Letov, N., and Y. F. Zhao, 2021: Volumetric cells: A framework for a bio-inspired geometric modelling method to support heterogeneous lattice structures. *Proceedings of the Design Society: DESIGN Conference*, Dubrovnik, Croatia, Cambridge University Press, Vol. 1, 295–304, doi:[10.1017/dsd.2020.164](https://doi.org/10.1017/dsd.2020.164).
- Letov, N., and Y. F. Zhao, 2022: A geometric modelling framework to support the design of heterogeneous lattice structures with non-linearly varying geometry. *Journal of Computational Design and Engineering*, **9** (5), 1565–1584, doi:[10.1093/jcde/qwac076](https://doi.org/10.1093/jcde/qwac076).
- Letov, N., and Y. F. Zhao, 2023a: Beam-based lattice topology transition with function representation. *Journal of Mechanical Design*, **145** (1), 011 704, doi:[10.1115/1.4055950](https://doi.org/10.1115/1.4055950).
- Letov, N., and Y. F. Zhao, 2023b: Geometric modelling of heterogeneous lattice structures through function representation with LatticeQuery. *Proceedings of the Design Society: International Conference on Engineering Design (ICED23)*, Bordeaux, France, Cambridge University Press, Vol. 3, 2045–2054, doi:[10.1017/pds.2023.205](https://doi.org/10.1017/pds.2023.205).

- Li, C., H. Lei, Z. Zhang, X. Zhang, H. Zhou, P. Wang, and D. Fang, 2020a: Architecture design of periodic truss-lattice cells for additive manufacturing. *Additive Manufacturing*, **34**, 101 172, doi:[10.1016/j.addma.2020.101172](https://doi.org/10.1016/j.addma.2020.101172).
- Li, H., and Coauthors, 2022a: Assessing the effects of Kampo medicine on human skin texture and microcirculation. *Artificial Life and Robotics*, **27** (1), 64–69, doi:[10.1007/s10015-022-00736-z](https://doi.org/10.1007/s10015-022-00736-z).
- Li, J., Y. Liu, H. Ling, W. Guo, and G. He, 2011: Development of solid-based modeling system for surface micromachined MEMS. *2011 3rd International Conference on Computer Research and Development*, IEEE, Shanghai, China, 297–301, doi:[10.1109/ICCRD.2011.5764136](https://doi.org/10.1109/ICCRD.2011.5764136).
- Li, L., C. Guo, Y. Chen, and Y. Chen, 2020b: Optimization design of lightweight structure inspired by glass sponges (porifera, hexacinellida) and its mechanical properties. *Bioinspiration & Biomimetics*, **15** (3), 036 006, doi:[10.1088/1748-3190/ab6ca9](https://doi.org/10.1088/1748-3190/ab6ca9).
- Li, S., H. Bai, R. F. Shepherd, and H. Zhao, 2019: Bio-inspired design and additive manufacturing of soft materials, machines, robots, and haptic interfaces. *Angewandte Chemie International Edition*, **58** (33), 11 182–11 204, doi:[10.1002/anie.201813402](https://doi.org/10.1002/anie.201813402).
- Li, W., W. Li, and Z. Yu, 2022b: Heat transfer enhancement of water-cooled triply periodic minimal surface heat exchangers. *Applied Thermal Engineering*, **217**, 119 198, doi:[10.1016/j.applthermaleng.2022.119198](https://doi.org/10.1016/j.applthermaleng.2022.119198).
- Li, Y., and Coauthors, 2020c: A review on functionally graded materials and structures via additive manufacturing: from multi-scale design to versatile functional properties. *Advanced Materials Technologies*, **5** (6), 1900 981, doi:[10.1002/admt.201900981](https://doi.org/10.1002/admt.201900981).
- Liu, C., Z. Du, W. Zhang, Y. Zhu, and X. Guo, 2017: Additive manufacturing-oriented design of graded lattice structures through explicit topology optimization. *Journal of Applied Mechanics*, **84** (8), doi:[10.1115/1.4036941](https://doi.org/10.1115/1.4036941).
- Liu, J., J. Yan, and H. Yu, 2021a: Stress-constrained topology optimization for material extrusion polymer additive manufacturing. *Journal of Computational Design and Engineering*, **8** (3), 979–993, doi:[10.1093/jcde/qwab028](https://doi.org/10.1093/jcde/qwab028).
- Liu, J., and Coauthors, 2018: Current and future trends in topology optimization for additive manufacturing. *Structural and multidisciplinary optimization*, **57**, 2457–2483, doi:[10.1007/s00158-018-1994-3](https://doi.org/10.1007/s00158-018-1994-3).
- Liu, K., M. Cao, A. Fujishima, and L. Jiang, 2014: Bio-inspired titanium dioxide materials with special wettability and their applications. *Chemical reviews*, **114** (19), 10 044–10 094, doi:[10.1021/cr4006796](https://doi.org/10.1021/cr4006796).

- Liu, P., Z. Kang, and Y. Luo, 2020a: Two-scale concurrent topology optimization of lattice structures with connectable microstructures. *Additive Manufacturing*, **36**, 101427, doi:[10.1016/j.addma.2020.101427](https://doi.org/10.1016/j.addma.2020.101427).
- Liu, T., S. Guessasma, J. Zhu, and W. Zhang, 2019: Designing cellular structures for additive manufacturing using Voronoi-Monte Carlo approach. *Polymers*, **11** (7), 1158, doi:[10.3390/polym11071158](https://doi.org/10.3390/polym11071158).
- Liu, Y., H. Yang, Y. F. Zhao, and G. Zheng, 2022: A heterogeneous lattice structure modeling technique supported by multiquadric radial basis function networks. *Journal of Computational Design and Engineering*, **9** (1), 68–81, doi:[10.1093/jcde/qwab069](https://doi.org/10.1093/jcde/qwab069).
- Liu, Y., G. Zheng, N. Letov, and Y. F. Zhao, 2021b: A survey of modeling and optimization methods for multi-scale heterogeneous lattice structures. *Journal of Mechanical Design*, **143** (4), 040803, doi:[10.1115/1.4047917](https://doi.org/10.1115/1.4047917).
- Liu, Y., S. Zhuo, Y. Xiao, G. Zheng, G. Dong, and Y. F. Zhao, 2020b: Rapid modeling and design optimization of multi-topology lattice structure based on unit-cell library. *Journal of Mechanical Design*, **142** (9), 091705, doi:[10.1115/1.4046812](https://doi.org/10.1115/1.4046812).
- Loh, G. H., E. Pei, D. Harrison, and M. D. Monzón, 2018: An overview of functionally graded additive manufacturing. *Additive Manufacturing*, **23**, 34–44, doi:[10.1016/j.addma.2018.06.023](https://doi.org/10.1016/j.addma.2018.06.023).
- Loh, Q. L., and C. Choong, 2013: Three-dimensional scaffolds for tissue engineering applications: role of porosity and pore size. *Tissue Engineering Part B: Reviews*, **19** (6), 485–502, doi:[10.1089/ten.teb.2012.0437](https://doi.org/10.1089/ten.teb.2012.0437).
- Loop, C. T., 1987: Smooth subdivision surfaces based on triangles. M.S. thesis, University of Utah, 74 pp., Salt Lake City, UT, USA, URL <https://charlesloop.com/thesis.pdf>.
- Lorensen, W. E., and H. E. Cline, 1987: Marching cubes: A high resolution 3D surface construction algorithm. *ACM SIGGRAPH Computer Graphics*, **21** (4), 163–169, doi:[10.1145/37402.37422](https://doi.org/10.1145/37402.37422).
- Lu, Y., L. Cheng, Z. Yang, J. Li, and H. Zhu, 2020: Relationship between the morphological, mechanical and permeability properties of porous bone scaffolds and the underlying microstructure. *PloS one*, **15** (9), e0238471, doi:[10.1371/journal.pone.0238471](https://doi.org/10.1371/journal.pone.0238471).
- Luebke, D., M. Reddy, J. D. Cohen, A. Varshney, B. Watson, and R. Huebner, 2003: *Level of detail for 3D graphics*. 1st ed., Morgan Kaufmann, San Francisco, CA, USA, 416 pp.
- Lutfi, M., 2018: The effect of gravitational field on brachistochrone problem. *Journal of Physics: Conference Series*, IOP Publishing, Vol. 1028, 012060, doi:[10.1088/1742-6596/1028/1/012060](https://doi.org/10.1088/1742-6596/1028/1/012060).

- Marcus, R. C., 2017: Level-of-detail independent voxel-based surface approximations. M.S. thesis, Utrecht University, 49 pp., Utrecht, Netherlands, URL <https://studenttheses.uu.nl/handle/20.500.12932/25769>.
- Marshall, W. F., 2011: Origins of cellular geometry. *BMC biology*, **9**, 1–9, doi:[10.1186/1741-7007-9-57](https://doi.org/10.1186/1741-7007-9-57).
- Martin, W., E. Cohen, R. Fish, and P. Shirley, 2000: Practical ray tracing of trimmed NURBS surfaces. *Journal of Graphics Tools*, **5** (1), 27–52, doi:[10.1080/10867651.2000.10487519](https://doi.org/10.1080/10867651.2000.10487519).
- Martínez, J., J. Dumas, and S. Lefebvre, 2016: Procedural voronoi foams for additive manufacturing. *ACM Transactions on Graphics (TOG)*, **35** (4), 1–12, doi:[10.1145/2897824.2925922](https://doi.org/10.1145/2897824.2925922).
- Maskery, I., A. Hussey, A. Panesar, A. Aremu, C. Tuck, I. Ashcroft, and R. Hague, 2017: An investigation into reinforced and functionally graded lattice structures. *Journal of Cellular Plastics*, **53** (2), 151–165, doi:[10.1177/0021955X16639035](https://doi.org/10.1177/0021955X16639035).
- Maskery, I., L. Parry, D. Padrao, R. Hague, and I. Ashcroft, 2022: FLatt Pack: A research-focussed lattice design program. *Additive Manufacturing*, **49**, 102510, doi:[10.1016/j.addma.2021.102510](https://doi.org/10.1016/j.addma.2021.102510).
- Massarwi, F., P. Antolin, and G. Elber, 2019: Volumetric untrimming: Precise decomposition of trimmed trivariate into tensor products. *Computer Aided Geometric Design*, **71**, 1–15, doi:[10.1016/j.cagd.2019.04.005](https://doi.org/10.1016/j.cagd.2019.04.005).
- Massarwi, F., and G. Elber, 2016: A B-spline based framework for volumetric object modeling. *Computer-Aided Design*, **78**, 36–47, doi:[10.1016/j.cad.2016.05.003](https://doi.org/10.1016/j.cad.2016.05.003).
- Materialise NV., 2012: Materialise Mimics – 3D medical image processing software. URL <https://www.materialise.com/en/medical/mimics-innovation-suite/mimics>, [Online; accessed March 15, 2023].
- Mathur, A., M. Pirron, and D. Zufferey, 2020: Interactive programming for parametric CAD. *Computer Graphics Forum*, Wiley Online Library, Vol. 39, 408–425, doi:[10.1111/cgf.14046](https://doi.org/10.1111/cgf.14046).
- Matlack, K. H., A. Bauhofer, S. Krödel, A. Palermo, and C. Daraio, 2016: Composite 3D-printed metastructures for low-frequency and broadband vibration absorption. *Proceedings of the National Academy of Sciences*, **113** (30), 8386–8390, doi:[10.1073/pnas.1600171113](https://doi.org/10.1073/pnas.1600171113).

- McGregor, M., S. Patel, S. McLachlin, and M. Vlasea, 2021: Architectural bone parameters and the relationship to titanium lattice design for powder bed fusion additive manufacturing. *Additive Manufacturing*, **47**, 102273, doi:[10.1016/j.addma.2021.102273](https://doi.org/10.1016/j.addma.2021.102273).
- Mensch, T. E., E. A. Delesky, R. W. Learsch, K. E. Foster, S. K. Yeturu, W. V. Srubar, and G. Miyake, 2021: Mechanical evaluation of 3D printed biomimetic non-Euclidean saddle geometries mimicking the mantis shrimp. *Bioinspiration & biomimetics*, **16** (5), 056002, doi:[10.1088/1748-3190/ac0a33](https://doi.org/10.1088/1748-3190/ac0a33).
- Menshenin, Y., D. Knoll, Y. Brovar, and C. Fortin, 2020: Analysis of MBSE/PLM integration: From conceptual design to detailed design. *Product Lifecycle Management Enabling Smart X: 17th IFIP WG 5.1 International Conference, PLM 2020*, Rapperswil, Switzerland, Springer, Vol. 593, 593–603, doi:[10.1007/978-3-030-62807-9_47](https://doi.org/10.1007/978-3-030-62807-9_47).
- Michielsen, K., and D. G. Stavenga, 2008: Gyroid cuticular structures in butterfly wing scales: biological photonic crystals. *Journal of The Royal Society Interface*, **5** (18), 85–94, doi:[10.1098/rsif.2007.1065](https://doi.org/10.1098/rsif.2007.1065).
- Milbradt, P., and T. Pick, 2008: Polytope finite elements. *International Journal for Numerical Methods in Engineering*, **73** (12), 1811–1835, doi:[10.1002/nme.2149](https://doi.org/10.1002/nme.2149).
- Milovanović, A., M. Milošević, G. Mladenović, B. Likozar, K. Čolić, and N. Mitrović, 2018: Experimental dimensional accuracy analysis of reformer prototype model produced by FDM and SLA 3D printing technology. *Experimental and numerical investigations in materials science and engineering*, N. Mitrović, M. Milošević, and G. Mladenović, Eds., Vol. 54, Springer, Cham, Switzerland, 84–95, doi:[10.1007/978-3-319-99620-2_7](https://doi.org/10.1007/978-3-319-99620-2_7).
- Minc, N., D. Burgess, and F. Chang, 2011: Influence of cell geometry on division-plane positioning. *Cell*, **144** (3), 414–426, doi:[10.1016/j.cell.2011.01.016](https://doi.org/10.1016/j.cell.2011.01.016).
- Moffett, M., M. W. Fazio, and L. Wodehouse, 2003: *A world history of architecture*. 3rd ed., Laurence King Publishing, London, United Kingdom, 592 pp.
- Mohammadi, K., M. R. Movahhedy, I. Shishkovsky, and R. Hedayati, 2020: Hybrid anisotropic pentamode mechanical metamaterial produced by additive manufacturing technique. *Applied Physics Letters*, **117** (6), 061901, doi:[10.1063/5.0014167](https://doi.org/10.1063/5.0014167).
- Munaux, O., 2004: CAD interface and framework for curve optimisation applications. Ph.D. thesis, Cranfield University, 299 pp., Cranfield, UK, URL <https://dspace.lib.cranfield.ac.uk/handle/1826/835>.
- Newman, T. S., and H. Yi, 2006: A survey of the marching cubes algorithm. *Computers & Graphics*, **30** (5), 854–879, doi:[10.1016/j.cag.2006.07.021](https://doi.org/10.1016/j.cag.2006.07.021).

- Nguyen, C. H. P., Y. Kim, Q. T. Do, and Y. Choi, 2021: Implicit-based computer-aided design for additively manufactured functionally graded cellular structures. *Journal of Computational Design and Engineering*, **8** (3), 813–823, doi:[10.1093/jcde/qwab016](https://doi.org/10.1093/jcde/qwab016).
- Nooruddin, F. S., and G. Turk, 2003: Simplification and repair of polygonal models using volumetric techniques. *IEEE Transactions on Visualization and Computer Graphics*, **9** (2), 191–205, doi:[10.1109/TVCG.2003.1196006](https://doi.org/10.1109/TVCG.2003.1196006).
- nTopology, Inc., 2017: Next generation engineering design software. URL <https://ntopology.com>, [Online; accessed March 15, 2023].
- Object Research Systems, 2018: Dragonfly – 3D visualization and analysis solution for scientific and industrial data. URL <https://www.theobjects.com/dragonfly>, [Online; accessed March 15, 2023].
- Open Cascade S.A.S.U., 2018: Open CASCADE Technology – Open Cascade. URL <https://www.opencascade.com/open-cascade-technology>, [Online; accessed March 10, 2023].
- Pal Singh, R., 2010: Structural performance analysis of formula SAE car. *Jurnal Mekanikal*, **31** (2), 46–61, URL <https://jurnalmekanikal.utm.my/index.php/jurnalmekanikal/article/view/102>.
- Panda, B. N., 2015: Design and development of cellular structure for additive manufacturing. Ph.D. thesis, National Institute of Technology Rourkela, 58 pp., Rourkela, India, URL <http://ethesis.nitrkl.ac.in/6928>.
- Panesar, A., M. Abdi, D. Hickman, and I. Ashcroft, 2018: Strategies for functionally graded lattice structures derived using topology optimisation for additive manufacturing. *Additive Manufacturing*, **19**, 81–94, doi:[10.1016/j.addma.2017.11.008](https://doi.org/10.1016/j.addma.2017.11.008).
- Park, J. M., B. C. Lee, S. W. Chae, and K. Y. Kwon, 2019: Surface reconstruction from FE mesh model. *Journal of Computational Design and Engineering*, **6** (2), 197–208, doi:[10.1016/j.jcde.2018.05.004](https://doi.org/10.1016/j.jcde.2018.05.004).
- Park, J. W., H. Park, J. H. Kim, H. M. Kim, C. H. Yoo, and H. G. Kang, 2022a: Fabrication of a lattice structure with periodic open pores through three-dimensional printing for bone ingrowth. *Scientific Reports*, **12** (1), 17 223, doi:[10.1038/s41598-022-22292-z](https://doi.org/10.1038/s41598-022-22292-z).
- Park, K.-M., K.-S. Min, and Y.-S. Roh, 2022b: Design optimization of lattice structures under compression: study of unit cell types and cell arrangements. *Materials*, **15** (1), 97, doi:[10.3390/ma15010097](https://doi.org/10.3390/ma15010097).
- Pasko, A., and V. Adzhiev, 2004: Function-based shape modeling: mathematical framework and specialized language. *Lecture notes in computer science*, **2930**, 132–160, doi:[10.1007/978-3-540-24616-9_9](https://doi.org/10.1007/978-3-540-24616-9_9).

- Pasko, A., V. Adzhiev, R. Cartwright, E. Fausett, A. Ossipov, and V. Savchenko, 1999: HyperFun project: a framework for collaborative multidimensional F-rep modeling. *Eurographics/ACM SIGGRAPH Workshop Implicit Surfaces' 99*, Bordeaux, France, Workshop Implicit Surfaces 1999, 59–69.
- Pasko, A., V. Adzhiev, A. Sourin, and V. Savchenko, 1995: Function representation in geometric modeling: concepts, implementation and applications. *The visual computer*, **11**, 429–446, doi:[10.1007/BF02464333](https://doi.org/10.1007/BF02464333).
- Pasko, A., O. Fryazinov, T. Vilbrandt, P.-A. Fayolle, and V. Adzhiev, 2011: Procedural function-based modelling of volumetric microstructures. *Graphical Models*, **73** (5), 165–181, doi:[10.1016/j.gmod.2011.03.001](https://doi.org/10.1016/j.gmod.2011.03.001).
- Pasko, G., A. Pasko, C. Vilbrandt, and T. Ikeda, 2001: Virtual Shikki and Sazaedo: shape modeling in digital preservation of Japanese lacquer ware and temples. *Proceedings Spring Conference on Computer Graphics*, Budmerice, Slovakia, IEEE, 147–154, doi:[10.1109/SCCG.2001.945349](https://doi.org/10.1109/SCCG.2001.945349).
- Persson, B. N. J., 2010: Rubber friction and tire dynamics. *Journal of Physics: Condensed Matter*, **23** (1), 015003, doi:[10.1088/0953-8984/23/1/015003](https://doi.org/10.1088/0953-8984/23/1/015003).
- Peters, J., and U. Reif, 1997: The simplest subdivision scheme for smoothing polyhedra. *ACM Transactions on Graphics (TOG)*, **16** (4), 420–431, doi:[10.1145/263834.263851](https://doi.org/10.1145/263834.263851).
- Pham, M.-S., C. Liu, I. Todd, and J. Lertthanasarn, 2019: Damage-tolerant architected materials inspired by crystal microstructure. *Nature*, **565** (7739), 305–311, doi:[10.1038/s41586-018-0850-3](https://doi.org/10.1038/s41586-018-0850-3).
- Qureshi, Z. A., S. A. B. Al Omari, E. Elnajjar, F. Mahmoud, O. Al-Ketan, and R. A. Al-Rub, 2021: Thermal characterization of 3D-printed lattices based on triply periodic minimal surfaces embedded with organic phase change material. *Case Studies in Thermal Engineering*, **27**, 101315, doi:[10.1016/j.matdes.2019.108137](https://doi.org/10.1016/j.matdes.2019.108137).
- Raja, F., 2019: Evaluation of properties of triply periodic minimal surface structures using ANSYS. M.S. thesis, Arizona State University, 129 pp., Tempe, AZ, USA, URL <https://hdl.handle.net/2286/R.I.53888>.
- Ratnout, N. T., and I. A. Mahmoud, 2006: Adequacy of the tensile/elongation test as a quality control criterion for vehicle tires. *Polymer testing*, **25** (5), 588–596, doi:[10.1016/j.polymertesting.2006.01.017](https://doi.org/10.1016/j.polymertesting.2006.01.017).
- Raviv, A., and G. Elber, 2001: Interactive direct rendering of trivariate B-spline scalar functions. *IEEE Transactions on Visualization and Computer Graphics*, **7** (2), 109–119, doi:[10.1109/2945.928164](https://doi.org/10.1109/2945.928164).

- Rawson, S. D., L. Margetts, J. K. Wong, and S. H. Cartmell, 2015: Sutured tendon repair; a multi-scale finite element model. *Biomechanics and modeling in mechanobiology*, **14** (1), 123–133, doi:[10.1007/s10237-014-0593-5](https://doi.org/10.1007/s10237-014-0593-5).
- Ren, F., and Coauthors, 2021: Transition boundaries and stiffness optimal design for multi-TPMS lattices. *Materials & Design*, **210**, 110 062, doi:[10.1016/j.matdes.2021.110062](https://doi.org/10.1016/j.matdes.2021.110062).
- Reznikov, N., and Coauthors, 2020: Altered topological blueprint of trabecular bone associates with skeletal pathology in humans. *Bone Reports*, **12**, 100 264, doi:[10.1016/j.bonr.2020.100264](https://doi.org/10.1016/j.bonr.2020.100264).
- Ries, E., 2011: *The Lean Startup: How Today's Entrepreneurs Use Continuous Innovation to Create Radically Successful Businesses* LK. First edit ed., Crown Business, New York (NY), United States, 320 pp.
- Ritter, F., T. Boskamp, A. Homeyer, H. Laue, M. Schwier, F. Link, and H.-O. Peitgen, 2011: Medical image analysis. *IEEE pulse*, **2** (6), 60–70, doi:[10.1109/MPUL.2011.942929](https://doi.org/10.1109/MPUL.2011.942929).
- Robert McNeel & Associates, 2020a: Rhino – Rhinoceros 3D. URL <https://www.rhino3d.com>, [Online; accessed March 4, 2023].
- Robert McNeel & Associates, 2020b: System Requirements. URL <https://www.rhino3d.com/6/system-requirements>, [Online; accessed March 5, 2023].
- Roettger, S., S. Guthe, D. Weiskopf, T. Ertl, and W. Strasser, 2003: Smart hardware-accelerated volume rendering. *VisSym*, Grenoble, France, Vol. 3, 231–238, doi:[10.2312/VisSym/VisSym03/231-238](https://doi.org/10.2312/VisSym/VisSym03/231-238).
- Rogers, D. F., 2001: *An introduction to NURBS: with historical perspective*. Morgan Kaufmann, San Diego, CA, USA, 324 pp., doi:[10.1016/B978-1-55860-669-2.X5000-3](https://doi.org/10.1016/B978-1-55860-669-2.X5000-3).
- Rom, M., and K.-H. Brakhage, 2011: Volume mesh generation for numerical flow simulations using Catmull-Clark and surface approximation methods. *Proceedings of the 20th International Meshing Round Table*, Institut für Geometrie und Praktische Mathematik Aachen, Germany, Paris, France, 1–20, URL <https://publications.rwth-aachen.de/record/225535>.
- Rosen, D. W., 2007: Computer-aided design for additive manufacturing of cellular structures. *Computer-Aided Design and Applications*, **4** (5), 585–594, doi:[10.1080/16864360.2007.10738493](https://doi.org/10.1080/16864360.2007.10738493).
- Rosenthal, S., S. Platt, R. Hölker-Jäger, S. Gies, S. Kleszczynski, A. E. Tekkaya, and G. Witt, 2019: Forming properties of additively manufactured monolithic Hastelloy X sheets. *Materials Science and Engineering: A*, **753**, 300–316, doi:[10.1016/j.msea.2019.03.035](https://doi.org/10.1016/j.msea.2019.03.035).

- Rossignac, J. R., and A. A. Requicha, 1986: Offsetting operations in solid modelling. *Computer Aided Geometric Design*, **3** (2), 129–148, doi:[10.1016/0167-8396\(86\)90017-8](https://doi.org/10.1016/0167-8396(86)90017-8).
- Sacks, M. S., A. Khalighi, B. Rego, S. Ayoub, and A. Drach, 2017: On the need for multi-scale geometric modelling of the mitral heart valve. *Healthcare Technology Letters*, **4** (5), 150, doi:[10.1049/htl.2017.0076](https://doi.org/10.1049/htl.2017.0076).
- Saito, D., H. Washizaki, and Y. Fukazawa, 2017: Comparison of text-based and visual-based programming input methods for first-time learners. *Journal of Information Technology Education: Research*, **16** (1), 209–226, doi:[10.28945/3775](https://doi.org/10.28945/3775).
- Sánchez-Reyes, J., 1995: Quasinonparametric surfaces. *Computer-aided design*, **27** (4), 263–275, doi:[10.1016/0010-4485\(95\)91136-9](https://doi.org/10.1016/0010-4485(95)91136-9).
- Sanders, E., A. Pereira, and G. Paulino, 2021: Optimal and continuous multilattice embedding. *Science Advances*, **7** (16), eabf4838, doi:[10.1126/sciadv.abf4838](https://doi.org/10.1126/sciadv.abf4838).
- Sarabhai, S., N. Letov, M. Kibsey, F. Sanchez, and Y. F. Zhao, 2023: Understanding the flow and thermal characteristics of non-stochastic strut-based and surface-based lattice structures. *Materials & Design*, **227**, 111787, doi:[10.1016/j.matdes.2023.111787](https://doi.org/10.1016/j.matdes.2023.111787).
- Sasaki, Y., M. Takezawa, S. Kim, H. Kawaharada, and T. Maekawa, 2017: Adaptive direct slicing of volumetric attribute data represented by trivariate B-spline functions. *The International Journal of Advanced Manufacturing Technology*, **91**, 1791–1807, doi:[10.1007/s00170-016-9800-0](https://doi.org/10.1007/s00170-016-9800-0).
- Savchenko, V. V., A. A. Pasko, O. G. Okunev, and T. L. Kunii, 1995: Function representation of solids reconstructed from scattered surface points and contours. **14** (4), 181–188, doi:[10.1111/1467-8659.1440181](https://doi.org/10.1111/1467-8659.1440181).
- Savio, G., R. Meneghelli, and G. Concheri, 2017: Optimization of lattice structures for additive manufacturing technologies. *Advances on Mechanics, Design Engineering and Manufacturing: Proceedings of the International Joint Conference on Mechanics, Design Engineering & Advanced Manufacturing (JCM 2016)*, 14-16 September, 2016, Catania, Italy, Springer, 213–222, doi:[10.1007/978-3-319-45781-9_22](https://doi.org/10.1007/978-3-319-45781-9_22).
- Savio, G., S. Rosso, R. Meneghelli, G. Concheri, and Coauthors, 2018: Geometric modeling of cellular materials for additive manufacturing in biomedical field: a review. *Applied bionics and biomechanics*, **2018**, 1654782, doi:[10.1155/2018/1654782](https://doi.org/10.1155/2018/1654782).
- Schmick, M., and P. I. Bastiaens, 2014: The interdependence of membrane shape and cellular signal processing. *Cell*, **156** (6), 1132–1138, doi:[10.1016/j.cell.2014.02.007](https://doi.org/10.1016/j.cell.2014.02.007).

- Schmidt, R., R. Wüchner, and K.-U. Bletzinger, 2012: Isogeometric analysis of trimmed NURBS geometries. *Computer Methods in Applied Mechanics and Engineering*, **241**, 93–111, doi:[10.1016/j.cma.2012.05.021](https://doi.org/10.1016/j.cma.2012.05.021).
- Schnitger Corporation, 2012: New Math. The Hidden Cost of Swapping CAD Kernels. URL <https://schnitgercorp.com/wp-content/uploads/2020/12/SchnitgerCorp-Hidden-Cost-of-Kernel-Change-2020.pdf>, [Online; accessed March 10, 2023], 11 pp.
- Schnös, F., D. Hartmann, B. Obst, and G. Glashagen, 2021: GPU accelerated voxel-based machining simulation. *The International Journal of Advanced Manufacturing Technology*, **115 (1-2)**, 275–289, doi:[10.1007/s00170-021-07001-w](https://doi.org/10.1007/s00170-021-07001-w).
- Schulz, H., 2009: Polyhedral approximation and practical convex hull algorithm for certain classes of voxel sets. *Discrete applied mathematics*, **157 (16)**, 3485–3493, doi:[10.1016/j.dam.2009.04.008](https://doi.org/10.1016/j.dam.2009.04.008).
- Schumacher, C., B. Bickel, J. Rys, S. Marschner, C. Daraio, and M. Gross, 2015: Microstructures to control elasticity in 3D printing. *ACM Transactions on Graphics (Tog)*, **34 (4)**, 1–13, doi:[10.1145/2766926](https://doi.org/10.1145/2766926).
- Seemann, P., S. Fuhrmann, S. Guthe, F. Langguth, and M. Goesele, 2016: Simplification of multi-scale geometry using adaptive curvature fields. *arXiv preprint arXiv:1610.07368*, doi:[10.48550/arXiv.1610.07368](https://arxiv.org/abs/1610.07368).
- Shaikh, M., and T. Cornford, 2011: Total cost of ownership of open source software: a report for the UK Cabinet Office supported by OpenForum Europe. Tech. rep., UK Cabinet Office, London, UK. URL <http://eprints.lse.ac.uk/39826/>, accessed on 2023-04-02.
- Shapiro, V., 1994: Real functions for representation of rigid solids. *Computer Aided Geometric Design*, **11 (2)**, 153–175, doi:[10.1016/0167-8396\(94\)90030-2](https://doi.org/10.1016/0167-8396(94)90030-2).
- Shapiro, V., 2002: *Solid Modeling*, chap. 20, 473–518. 1st ed., Elsevier Science, Amsterdam, The Netherlands, doi:[10.1016/B978-044451104-1/50021-6](https://doi.org/10.1016/B978-044451104-1/50021-6).
- Shapiro, V., 2007: Semi-analytic geometry with R-functions. *ACTA numerica*, **16**, 239–303, doi:[10.1017/S096249290631001X](https://doi.org/10.1017/S096249290631001X).
- Shi, J., L. Zhu, L. Li, Z. Li, J. Yang, and X. Wang, 2018: A TPMS-based method for modeling porous scaffolds for bionic bone tissue engineering. *Scientific reports*, **8 (1)**, 7395, doi:[10.1038/s41598-018-25750-9](https://doi.org/10.1038/s41598-018-25750-9).

- Siemens Digital Industries Software, 2018: Parasolid. Siemens Software. URL <https://www.plm.automation.siemens.com/global/en/products/plm-components/parasolid.html>, [Online; accessed March 10, 2023].
- Siemens Digital Industries Software, 2023a: NX software including CAD and CAM. URL <https://plm.sw.siemens.com/en-US/nx>, [Online; accessed April 28, 2023].
- Siemens Digital Industries Software, 2023b: Simcenter STAR-CCM+. URL <https://plm.sw.siemens.com/en-US/simcenter/fluids-thermal-simulation/star-ccm>, [Online; accessed April 28, 2023].
- Sigmund, O., 1997: On the design of compliant mechanisms using topology optimization. *Journal of Structural Mechanics*, **25** (4), 493–524, doi:[10.1080/08905459708945415](https://doi.org/10.1080/08905459708945415).
- Soloveva, O. V., S. A. Solovev, A. R. Talipova, R. Z. Shakurova, and D. L. Paluku, 2022: Study of heat transfer in models of FCC, BCC, SC and DEM porous structures with different porosities. *Journal of Physics: Conference Series*, Saint Petersburg, Russia, IOP Publishing, Vol. 2373, 022040, doi:[10.1088/1742-6596/2373/2/022040](https://doi.org/10.1088/1742-6596/2373/2/022040).
- Somnic, J., and B. W. Jo, 2022: Status and challenges in homogenization methods for lattice materials. *Materials*, **15** (2), 605, doi:[10.3390/ma15020605](https://doi.org/10.3390/ma15020605).
- Song, Y., and E. Cohen, 2019: Refinement for a hybrid boundary representation and its hybrid volume completion. *The SMAI journal of computational mathematics*, **5**, 3–25, doi:[10.5802/smai-jcm.49](https://doi.org/10.5802/smai-jcm.49).
- Song, Y., Z. Dai, Z. Wang, A. Ji, and S. N. Gorb, 2016: The synergy between the insect-inspired claws and adhesive pads increases the attachment ability on various rough surfaces. *Scientific Reports*, **6** (1), 26219, doi:[10.1038/srep26219](https://doi.org/10.1038/srep26219).
- Sourin, A., and A. Pasko, 1996: Function representation for sweeping by a moving solid. *IEEE Transactions on Visualization and Computer Graphics*, **2** (1), 11–18, doi:[10.1109/2945.489382](https://doi.org/10.1109/2945.489382).
- Stam, J., 1998: Exact evaluation of Catmull-Clark subdivision surfaces at arbitrary parameter values. *Proceedings of the 25th annual conference on Computer graphics and interactive techniques*, Orlando, FL, USA, 395–404, doi:[10.1145/280814.280945](https://doi.org/10.1145/280814.280945).
- Strand, R., 2004: Surface skeletons in grids with non-cubic voxels. *Proceedings of the 17th International Conference on Pattern Recognition, 2004. ICPR 2004.*, Cambridge, UK, IEEE, Vol. 1, 548–551, doi:[10.1109/ICPR.2004.1334195](https://doi.org/10.1109/ICPR.2004.1334195).
- Stratakis, E., and Coauthors, 2020: Laser engineering of biomimetic surfaces. *Materials Science and Engineering: R: Reports*, **141**, 100562, doi:[10.1016/j.mser.2020.100562](https://doi.org/10.1016/j.mser.2020.100562).

- Stroud, I., 2006: *Boundary Representation Modelling Techniques*. 1st ed., Springer London, London, UK, 788 pp., doi:[10.1007/978-1-84628-616-2](https://doi.org/10.1007/978-1-84628-616-2).
- Stroustrup, B., 1988: What is object-oriented programming? *IEEE software*, **5** (3), 10–20, doi:[10.1109/52.2020](https://doi.org/10.1109/52.2020).
- Tang, Y., G. Dong, and Y. F. Zhao, 2019: A hybrid geometric modeling method for lattice structures fabricated by additive manufacturing. *The International Journal of Advanced Manufacturing Technology*, **102**, 4011–4030, doi:[10.1007/s00170-019-03308-x](https://doi.org/10.1007/s00170-019-03308-x).
- Tang, Y., and Y. F. Zhao, 2016: A survey of the design methods for additive manufacturing to improve functional performance. *Rapid Prototyping Journal*, **22** (3), 569–590, doi:[10.1108/RPJ-01-2015-0011](https://doi.org/10.1108/RPJ-01-2015-0011).
- Taufik, M., and P. K. Jain, 2016: Additive manufacturing: Current scenario. *Proceedings of International Conference on: Advanced Production and Industrial Engineering-ICAPIE*, New Delhi, India, 380–386.
- Telea, A., and A. Jalba, 2011: Voxel-based assessment of printability of 3D shapes. *Mathematical Morphology and Its Applications to Image and Signal Processing: 10th International Symposium, ISMM 2011. Lecture Notes in Computer Science*, Springer, Berlin, Heidelberg, Verbania-Intra, Italy, Springer, Vol. 6671, 393–404, doi:[10.1007/978-3-642-21569-8_34](https://doi.org/10.1007/978-3-642-21569-8_34).
- Thane, J., 2007: Honeycomb. URL <https://flic.kr/p/2UHtEd>, [Online; accessed March 4, 2023].
- The MathWorks, Inc., 2008: MATLAB – MathWorks – MATLAB and Simulink. URL <https://www.mathworks.com/products/matlab.html>, [Online; accessed March 15, 2023].
- Ultimaker BV., 2013: Ultimaker Cura: Powerful, easy-to-use 3D printing software. URL <https://ultimaker.com/software/ultimaker-cura>, [Online; accessed March 17, 2023].
- Urbanczyk, A., and Coauthors, 2021a: CadQuery/cadquery: CadQuery 2.1. doi:[10.5281/zenodo.4498634](https://doi.org/10.5281/zenodo.4498634).
- Urbanczyk, A., and Coauthors, 2021b: CadQuery/CQ-editor: 0.2. doi:[10.5281/zenodo.4532367](https://doi.org/10.5281/zenodo.4532367).
- Ushakov, D. M., 2018: *Mathematics and CAD: Numerical Methods for CAD*. DMK Press, Moscow, Russia, 210 pp.
- Vaxman, A., M. Campen, O. Diamanti, D. Panozzo, D. Bommes, K. Hildebrandt, and M. Ben-Chen, 2016: Directional field synthesis, design, and processing. *Computer graphics forum*, Wiley Online Library, Vol. 35, 545–572, doi:[10.1111/cgf.12864](https://doi.org/10.1111/cgf.12864).

- Velivila, P. T., 2018: Masking materials and bio-inspired caps for chemical etching of dental implants. M.S. thesis, Politecnico di Milano, 81 pp., Milano, Italy, URL <http://hdl.handle.net/10589/143135>.
- Velivila, P. T., N. Letov, L. Kong, and Y. F. Zhao, 2023: A case study of multifunctional non-pneumatic tire design for the validation of meta-level design parameter in Domain Integrated Design (DID) method. *Proceedings of the Design Society: International Conference on Engineering Design (ICED23)*, Bordeaux, France, Cambridge University Press, Vol. 3, 39–48, doi:[10.1017/pds.2023.5](https://doi.org/10.1017/pds.2023.5).
- Velivila, P. T., N. Letov, Y. Liu, and Y. F. Zhao, 2021: Application of Domain Integrated Design methodology for bio-inspired design-a case study of suture pin design. *Proceedings of the Design Society: DESIGN Conference*, Dubrovnik, Croatia, Cambridge University Press, Vol. 1, 487–496, doi:[10.1017/pds.2021.49](https://doi.org/10.1017/pds.2021.49).
- Virtanen, P., and Coauthors, 2020: SciPy 1.0: fundamental algorithms for scientific computing in Python. *Nature Methods*, **17** (3), 261–272, doi:[10.1038/s41592-019-0686-2](https://doi.org/10.1038/s41592-019-0686-2).
- Vyshnepolsky, V. I., A. V. Efremov, and E. V. Zavarikhina, 2022: Modeling and study of properties of surfaces equidistant to a sphere and a plane. *Journal of Physics: Conference Series*, Chengdu, China, IOP Publishing, Vol. 2182, 012012, doi:[10.1088/1742-6596/2182/1/012012](https://doi.org/10.1088/1742-6596/2182/1/012012).
- Wang, H., Y. Chen, and D. W. Rosen, 2005: A hybrid geometric modeling method for large scale conformal cellular structures. *International Design Engineering Technical Conferences and Computers and Information in Engineering Conference*, Long Beach, CA, USA, Vol. 47403, 421–427, doi:[10.1115/DETC2005-85366](https://doi.org/10.1115/DETC2005-85366).
- Wang, L., and Coauthors, 2013: Biomechanism of impact resistance in the woodpecker's head and its application. *Science China Life Sciences*, **56**, 715–719, doi:[10.1007/s11427-013-4523-z](https://doi.org/10.1007/s11427-013-4523-z).
- Wang, P., F. Casadei, S. H. Kang, and K. Bertoldi, 2015: Locally resonant band gaps in periodic beam lattices by tuning connectivity. *Physical Review B*, **91** (2), 020103, doi:[10.1103/PhysRevB.91.020103](https://doi.org/10.1103/PhysRevB.91.020103).
- Wang, X., and X. Qian, 2014: An optimization approach for constructing trivariate B-spline solids. *Computer-Aided Design*, **46**, 179–191, doi:[10.1016/j.cad.2013.08.030](https://doi.org/10.1016/j.cad.2013.08.030).
- Wang, X., and Coauthors, 2016: Topological design and additive manufacturing of porous metals for bone scaffolds and orthopaedic implants: A review. *Biomaterials*, **83**, 127–141, doi:[10.1016/j.biomaterials.2016.01.012](https://doi.org/10.1016/j.biomaterials.2016.01.012).

- Wang, Z., and A. Y. Tamjani, 2022: Computational synthesis of large-scale three-dimensional heterogeneous lattice structures. *Aerospace Science and Technology*, **120**, 107 258, doi:[10.1016/j.ast.2021.107258](https://doi.org/10.1016/j.ast.2021.107258).
- Wang, Z., Y. Zhang, and A. Bernard, 2021: A constructive solid geometry-based generative design method for additive manufacturing. *Additive Manufacturing*, **41**, 101 952, doi:[10.1016/j.addma.2021.101952](https://doi.org/10.1016/j.addma.2021.101952).
- Warman, E., 1990: Object oriented programming and CAD. *Journal of Engineering Design*, **1** (1), 37–46, doi:[10.1080/09544829008901641](https://doi.org/10.1080/09544829008901641).
- Warren, J., and H. Weimer, 2002: *Subdivision methods for geometric design: A constructive approach*. 1st ed., Elsevier, Burlington, MA, USA, 320 pp., doi:[10.1016/B978-1-55860-446-9.X5000-5](https://doi.org/10.1016/B978-1-55860-446-9.X5000-5).
- Wassermann, B., N. Korshunova, S. Kollmannsberger, E. Rank, and G. Elber, 2020: Finite cell method for functionally graded materials based on V-models and homogenized microstructures. *Advanced Modeling and Simulation in Engineering Sciences*, **7** (1), 1–33, doi:[10.1186/s40323-020-00182-1](https://doi.org/10.1186/s40323-020-00182-1).
- Wei, N., H. Ye, X. Zhang, J. Li, and Y. Sui, 2022: Topology optimization for design of hybrid lattice structures with multiple microstructure configurations. *Acta Mechanica Solida Sinica*, 1–17, doi:[10.1007/s10338-021-00302-3](https://doi.org/10.1007/s10338-021-00302-3).
- Weiler, M., R. Westermann, C. Hansen, K. Zimmermann, and T. Ertl, 2000: Level-of-detail volume rendering via 3D textures. *Proceedings of the 2000 IEEE symposium on Volume visualization*, Salt Lake City, UTm USA, 7–13, doi:[10.1145/353888.353889](https://doi.org/10.1145/353888.353889).
- Weiskittel, A. R., J. A. Kershaw Jr, P. V. Hofmeyer, and R. S. Seymour, 2009: Species differences in total and vertical distribution of branch-and tree-level leaf area for the five primary conifer species in maine, usa. *Forest Ecology and Management*, **258** (7), 1695–1703, doi:[10.1016/j.foreco.2009.07.035](https://doi.org/10.1016/j.foreco.2009.07.035).
- Wen, L., J. C. Weaver, and G. V. Lauder, 2014: Biomimetic shark skin: design, fabrication and hydrodynamic function. *Journal of Experimental Biology*, **217** (10), 1656–1666, doi:[10.1242/jeb.097097](https://doi.org/10.1242/jeb.097097).
- Wohlers, T., and T. Gornet, 2014: History of additive manufacturing. *Wohlers report*, **24** (2016), 38.
- Wong, K. V., and A. Hernandez, 2012: A review of additive manufacturing. *International scholarly research notices*, **2012**, 208 760, doi:[10.5402/2012/208760](https://doi.org/10.5402/2012/208760).

- X. Gu, G., I. Su, S. Sharma, J. L. Voros, Z. Qin, and M. J. Buehler, 2016: Three-dimensional-printing of bio-inspired composites. *Journal of biomechanical engineering*, **138** (2), 021 006, doi:[10.1115/1.4032423](https://doi.org/10.1115/1.4032423).
- Xu, L., Q. Ruan, Q. Shen, L. Xi, J. Gao, and Y. Li, 2021: Optimization design of lattice structures in internal cooling channel with variable aspect ratio of gas turbine blade. *Energies*, **14** (13), 3954, doi:[10.3390/en14133954](https://doi.org/10.3390/en14133954).
- Xu, X., 2009: *Integrating Advanced Computer-Aided Design, Manufacturing, and Numerical Control: Principles and Implementations*. IGI Global, 1–31 pp., doi:[10.4018/978-1-59904-714-0](https://doi.org/10.4018/978-1-59904-714-0).
- Yam, Y., M. L. Wong, and P. Baranyi, 2006: Interpolation with function space representation of membership functions. *IEEE Transactions on Fuzzy Systems*, **14** (3), 398–411, doi:[10.1109/TFUZZ.2006.876332](https://doi.org/10.1109/TFUZZ.2006.876332).
- Yang, N., Y. Song, J. Huang, Y. Chen, and I. Maskery, 2021: Combinational design of heterogeneous lattices with hybrid region stiffness tuning for additive manufacturing. *Materials & Design*, **209**, 109 955, doi:[10.1016/j.matdes.2021.109955](https://doi.org/10.1016/j.matdes.2021.109955).
- Yang, N., Y. Tian, and D. Zhang, 2015a: Novel real function based method to construct heterogeneous porous scaffolds and additive manufacturing for use in medical engineering. *Medical engineering & physics*, **37** (11), 1037–1046, doi:[10.1016/j.medengphy.2015.08.006](https://doi.org/10.1016/j.medengphy.2015.08.006).
- Yang, S., Y. Tang, and Y. F. Zhao, 2015b: A new part consolidation method to embrace the design freedom of additive manufacturing. *Journal of Manufacturing Processeses*, **20**, 444–449, doi:[10.1016/j.jmapro.2015.06.024](https://doi.org/10.1016/j.jmapro.2015.06.024).
- Yang, S., and Y. F. Zhao, 2015: Additive manufacturing-enabled design theory and methodology: a critical review. *The International Journal of Advanced Manufacturing Technology*, **80** (1-4), 327–342, doi:[10.1007/s00170-015-6994-5](https://doi.org/10.1007/s00170-015-6994-5).
- Yang, X.-S., 2020: *Nature-inspired optimization algorithms*. 2nd ed., Academic Press, London, UK, 310 pp., doi:[10.1016/C2013-0-01368-0](https://doi.org/10.1016/C2013-0-01368-0).
- Yuan, G., and Y. Zhang, 2008: Development of 3D modeling platform based on Open CASCADE. *Journal of Engineering Graphics*, **4**.
- Zhang, C., J. Liu, Z. Yuan, S. Xu, B. Zou, L. Li, and Y. Ma, 2021: A novel lattice structure topology optimization method with extreme anisotropic lattice properties. *Journal of Computational Design and Engineering*, **8** (5), 1367–1390, doi:[10.1093/jcde/qwab051](https://doi.org/10.1093/jcde/qwab051).

- Zhang, H., S. Tang, H. Yue, K. Wu, Y. Zhu, C. Liu, B. Liang, and C. Li, 2020: Comparison of computational fluid dynamic simulation of a stirred tank with polyhedral and tetrahedral meshes. *Iranian Journal of Chemistry and Chemical Engineering*, **39** (4), 311–319, doi:[10.30492/ijcce.2019.34950](https://doi.org/10.30492/ijcce.2019.34950).
- Zhang, W., S. Yin, T. Yu, and J. Xu, 2019: Crushing resistance and energy absorption of pomelo peel inspired hierarchical honeycomb. *International Journal of Impact Engineering*, **125**, 163–172, doi:[10.1016/j.ijimpeng.2018.11.014](https://doi.org/10.1016/j.ijimpeng.2018.11.014).
- Zhang, X., and F. Liou, 2021: Chapter 1 – Introduction to additive manufacturing. *Additive Manufacturing*, J. Pou, A. Riveiro, and J. P. Davim, Eds., Handbooks in Advanced Manufacturing, Elsevier, 1–31, doi:[10.1016/B978-0-12-818411-0.00009-4](https://doi.org/10.1016/B978-0-12-818411-0.00009-4).
- Zhang, Y., and Y. F. Zhao, 2022: Hybrid sparse convolutional neural networks for predicting manufacturability of visual defects of laser powder bed fusion processes. *Journal of Manufacturing Systems*, **62**, 835–845, doi:[10.1016/j.jmsy.2021.07.002](https://doi.org/10.1016/j.jmsy.2021.07.002).
- Zheng, A., S. Bian, E. Chaudhry, J. Chang, H. Haron, L. You, and J. J. Zhang, 2021: Voronoi diagram and Monte-Carlo simulation based finite element optimization for cost-effective 3D printing. *Journal of Computational Science*, **50**, 101301, doi:[10.1016/j.jocs.2021.101301](https://doi.org/10.1016/j.jocs.2021.101301).
- Zheng, Y., 2019: *Bioinspired design of materials surfaces*. Elsevier, Amsterdam, Netherlands, 27–97 pp., doi:[10.1016/C2017-0-02152-3](https://doi.org/10.1016/C2017-0-02152-3).
- Zhong, Z., M. Rong, H. Lei, X. Chang, and L. Zhang, 2020: An efficient large-scale mesh deformation method based on MPI/OpenMP hybrid parallel radial basis function interpolation. *Chinese Journal of Aeronautics*, **33** (5), 1392–1404, doi:[10.1016/j.cja.2019.12.025](https://doi.org/10.1016/j.cja.2019.12.025).
- Zorin, D., P. Schröder, and W. Sweldens, 1997: Interactive multiresolution mesh editing. *Proceedings of the 24th annual conference on Computer graphics and interactive techniques*, Los Angeles, CA, USA, 259–268, doi:[10.1145/258734.258863](https://doi.org/10.1145/258734.258863).
- Zurlo, G., and L. Truskinovsky, 2017: Printing non-Euclidean solids. *Physical review letters*, **119** (4), 048 001, doi:[10.1103/PhysRevLett.119.048001](https://doi.org/10.1103/PhysRevLett.119.048001).

Appendices

Appendix A

Case study of a bio-inspired geometric modeling framework

Tiger got to hunt, bird got to fly;
Man got to sit and wonder ‘why, why, why?’
Tiger got to sleep, bird got to land;
Man got to tell himself he understand.

Kurt Vonnegut (1922 – 2007), CAT’s CRADLE

Bio-inspired algorithms have garnered significant attention in recent years due to their ability to mimic the efficient and adaptive processes found in nature (Bonabeau et al., 1999; Dorigo et al., 2006). In geometric modeling, these algorithms offer a novel approach to tackling complex problems, leveraging the inherent flexibility and robustness of biological systems (Floreano and Mattiussi, 2023). The motivation behind using bio-inspired algorithms in geometric modeling stems from the observation that natural systems often exhibit optimal or near-optimal solutions to problems they encounter, such as growth, adaptation, and structural organization (Benyus, 1997). This appendix is based on Letov and Zhao

([2021](#)), which introduces a 2D bio-inspired geometric modeling method. Additionally, this appendix scales this method to 3D and provides a performance comparison of the method.

The importance of using bio-inspired algorithms in geometric modeling lies in their potential to address the limitations of traditional methods. Conventional modeling techniques may struggle to cope with the increasing complexity and scale of modern geometric problems, often requiring significant computational resources and time ([Edgar and Tint, 2015](#)). On the other hand, bio-inspired algorithms can offer more efficient and adaptive solutions, taking advantage of the self-organizing and problem-solving capabilities observed in nature ([Yang, 2020](#)).

To evaluate the benefits and drawbacks of bio-inspired geometric modeling, one should examine an example of bio-inspired meshing ([Letov and Zhao, 2021](#)). Suppose there is a set \mathbb{S} that represents the geometric model of a structure, which can be mapped to a set of unit elements comprising it, or

$$\mathbb{S}(p) \mapsto v_1, \dots, v_n = \bigcup_{i=1}^n v_i, \quad (\text{A.1})$$

where p is a vector of lattice properties (e.g., topology type or material), and v_i for $i = 1, \dots, n$ is a set of unit elements corresponding to the geometric model \mathbb{S} . These unit elements are called volumetric cells and are depicted in Fig. A.1. \mathbb{S} is a 3D shape that is bounded by a finite genus g orientable 2-manifold M_g^2 , which is not necessarily convex. According to the complex cell theory, each volumetric cell is defined as a compact 3-manifold M_0^3 of genus $g = 0$. Thus, \mathbb{S} can be described as a 3D quotient space resulting from the quotient map attaching volumetric cells v_i by their boundaries ∂v_i^j , where ∂v_i^j denotes the j -th boundary

of the i -th volumetric cell. Mathematically, this can be expressed as:

$$\mathbb{S} := \bigcup_{i=1}^n \left(v_i / \bigcup_{j=1}^m \partial v_i^j \right) \subset \mathbb{R}^3. \quad (\text{A.2})$$

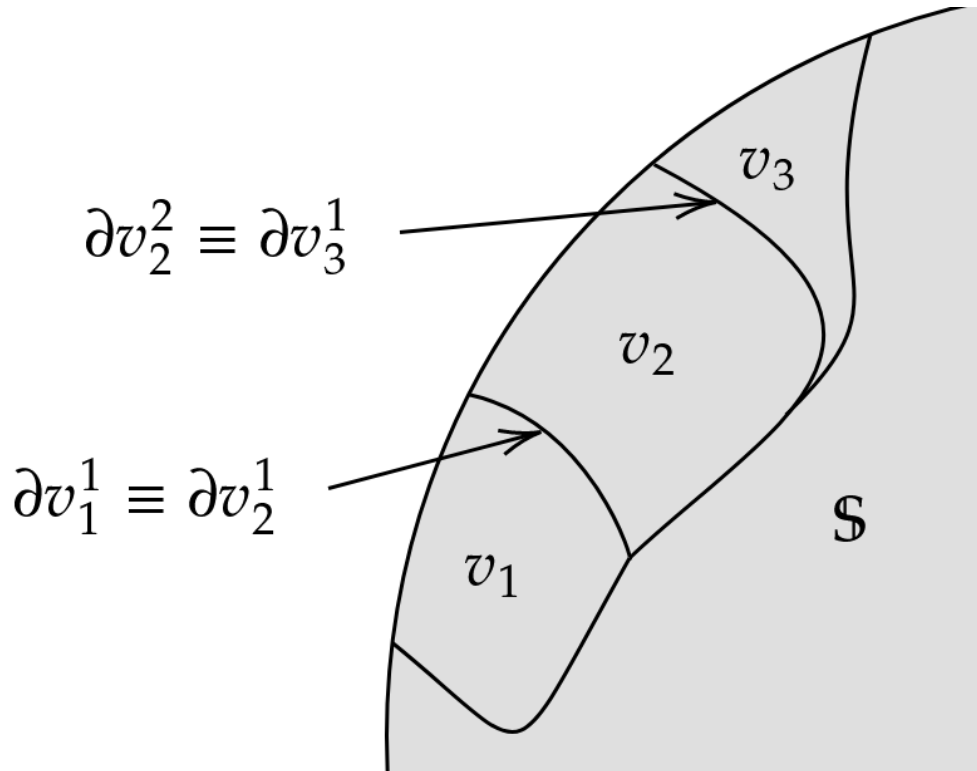


Figure A.1 Representation of the geometrical model \mathbb{S}

This framework is similar to other geometric modeling methods involving volumetric data discretization but with redefined constraints. Firstly, unlike voxels, volumetric cells v_i in this framework can vary in shape and size. Secondly, volumetric cells v_i are not necessarily convex, unlike volumetric mesh.

In this case study, two bio-inspired algorithms are presented and combined into a single algorithm.

A prevalent pattern in cell geometry formation is the long axis rule (LAR), as illustrated

in Fig. A.2. LAR specifies the cleavage plane as perpendicular to the longest axis, passing through the center of mass ([Minc et al., 2011](#)).

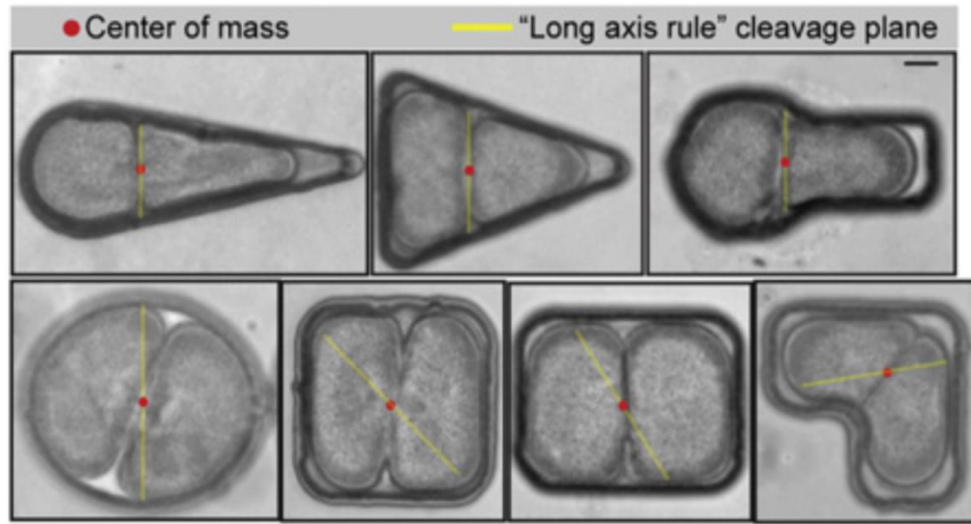


Figure A.2 The long axis rule observed in cell division process of the embryos of sea urchin (*Echinoidea*) ([Minc et al., 2011](#))

In this case study, a geometric modeling approach that uses LAR as its discretization technique base is described as follows:

1. Let $\partial\mathbb{S}$ be the boundary of a structure \mathbb{S} . Set $k = 1$. Set k_{\max} to be the maximum number of iterations. Let v_1^k be a volume cell that fills the space bounded by $\partial\mathbb{S}$.
2. Divide each volumetric cell v_l^k into two volumetric cells v_{2l-1}^{k+1} and v_{2l}^{k+1} by LAR as follows:
 - (a) For each v_l^k identify its centroid $c(\mathbf{X}) = \frac{\int \mathbf{X} F(\mathbf{X}) d\mathbf{X}}{\int F(\mathbf{X}) d\mathbf{X}}$ for all $\mathbf{X} = (x_1, x_2, x_3) \subset \mathbb{R}^3$ such that $F(\mathbf{X}) \geq 0$.
 - (b) Identify the long axis L .
 - (c) Identify the plane σ perpendicular to the long axis L .

- (d) Divide V_l^k into two volumetric cells v_{2l-1}^{k+1} and v_{2l}^{k+1} by the plane σ such that $v_{2l-1}^{k+1} \cap v_{2l}^{k+1} = \sigma$ and $v_{2l-1}^{k+1} \cup v_{2l}^{k+1} = V_l^k$.
3. Set $k \leftarrow k + 1$. If $k < k_{\max}$ go to Step 2.
 4. STOP.

Note that instead of the center of mass of a volumetric cell, its centroid is used, which is due to the fact that the material of the structure is omitted. Only geometric properties are taken into account. Note that LAR is not always followed in nature, as seen in the bottom row of Fig. A.2.

It has been observed in nature that cells tend to minimize their surface-to-volume ratio (SVR) (Schmick and Bastiaens, 2014). The 3D shape with the most optimal SVR in this sense is a sphere which also explains the blob-like shape of most cells. Sometimes, external geometrical constraints do not allow sphericity (Marshall, 2011). The external geometrical constraints result from the physical and environmental ones. In this case study, a geometric modeling approach that takes the S/V ratio as a base for its discretization technique is described as follows:

1. Define $\partial\mathbb{S}$ to be the boundary of a structure \mathbb{S} . Set $k = 1$. Set k_{\max} to be the maximum number of iterations. Let v_1^k be a single volume cell that fills the space bounded by $\partial\mathbb{S}$.
2. Define the volumetric cells v_{2l-1}^{k+1} and v_{2l}^{k+1} by minimizing S/V as follows:
 - (a) For v_{2l-1}^{k+1} and v_{2l}^{k+1} define their S/V functions as $R_{S/V1}(\mathbf{X}) = S_1(\mathbf{X})/V_1(\mathbf{X})$ and $R_{S/V2}(\mathbf{X}) = S_2(\mathbf{X})/V_2(\mathbf{X})$, respectively, where S_1 and S_2 are surfaces and V_1 and V_2 are volumes of v_{2l-1}^{k+1} and v_{2l}^{k+1} , respectively, both depending on cell division.

(b) Find the optimal division surface $D(\hat{\mathbf{X}})$ where $\hat{\mathbf{X}} = \arg \min_{\mathbf{X}} (R_{S/V1}(\mathbf{X}) + R_{S/V2}(\mathbf{X}))$

and set v_{2l-1}^{k+1} and v_{2l}^{k+1} such that $v_{2l-1}^{k+1} \cap v_{2l}^{k+1} = D(\hat{\mathbf{X}})$ and $v_{2l-1}^{k+1} \cup v_{2l}^{k+1} = v_l^k$.

Note that $D(\hat{\mathbf{X}})$ is not necessarily plane.

3. Set $k \leftarrow k + 1$. If $k < k_{\max}$ go to Step 2.

4. STOP.

Note that the minimization of $R_{S/V1}(\mathbf{X})$ and $R_{S/V2}(\mathbf{X})$ separately results in contradiction as $\min_x R_{S/V1}(\mathbf{X})$ and $\min_{\mathbf{X}} R_{S/V2}(\mathbf{X})$ produce values of $\hat{\mathbf{X}}$ such that either $v_{2l-1}^{k+1} = V_l^k$ or $v_{2l}^{k+1} = V_l^k$ while the minimization of $(R_{S/V1}(\mathbf{X}) + R_{S/V2}(\mathbf{X}))$ is performed in a balanced way with no contradiction of values of $\hat{\mathbf{X}}$.

In nature, there is no single algorithm that defines cell geometry. This case study analyzes a combined approach illustrated in Fig. A.3. The trade-off between the two algorithms is performed manually. The method is considered to be defined for each iteration of the division. Note that the LOD concept can be applied to the result of the combined approach by combining neighboring vertices of two adjacent volumetric cells and thus providing a modified version of the approach.

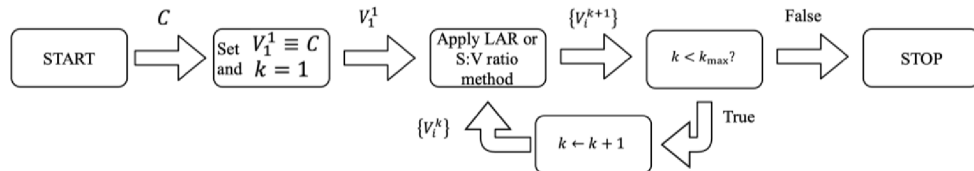


Figure A.3 The flowchart of the combined bio-inspired algorithm for geometric modeling (Letov and Zhao, 2021)

Two use cases are considered to verify the validity of the approach. For verification of the LAR method, a circular cross-section in Fig. A.4a and a square cross-section with a hole in the middle in Fig. A.5b are discretized into volumetric cells. The hole in the middle is added

as it is vital to consider a simple shape with a non-zero genus, as cellular structures have a high genus. Every resulting cell is convex at every iteration of the algorithm. A volumetric cell is divided into two by a plane. Moreover, LAR has a high level of inconsistency between each volumetric cell, and the variety of shapes is large.

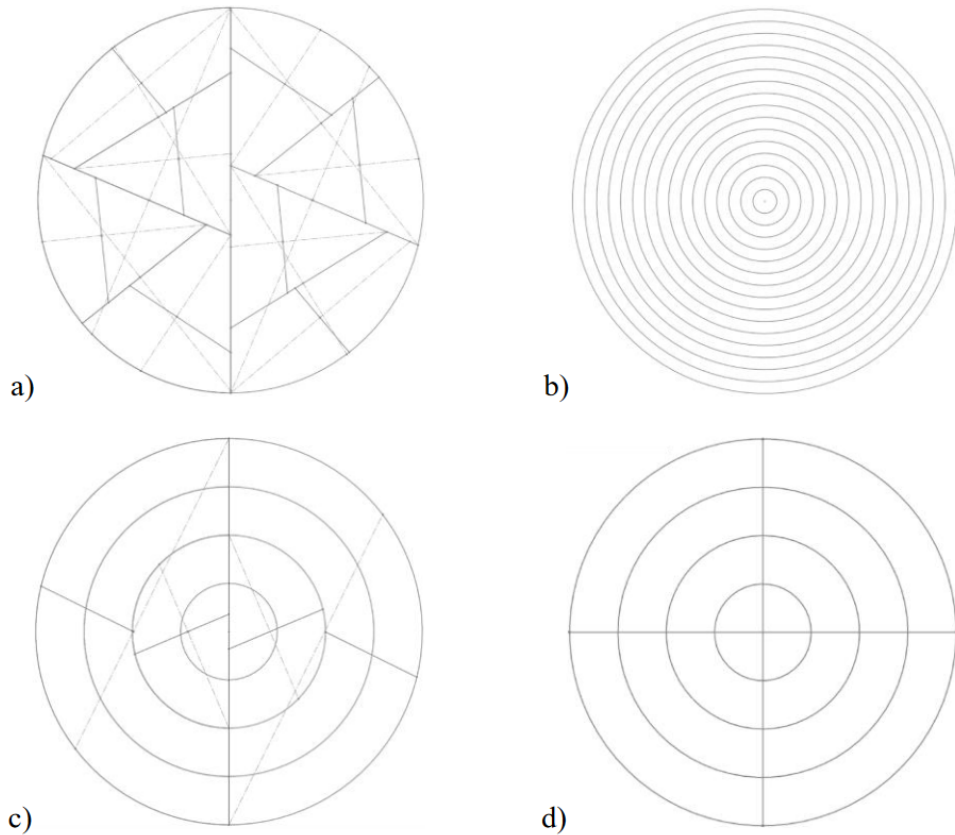


Figure A.4 (a) LAR, (b) the S/V ratio minimization, (c) the combined method, and (d) the modified combined algorithms applied as discretization methods to a circular cross-section for $k_{\max} = 4$ iterations. Long axes are shown as dotted lines ([Letov and Zhao, 2021](#)).

The verification of the S/V ratio method is performed similarly and shown in Fig. A.4b and Fig. A.5b. Consider the first iteration ($k = 1$) applied to the circular cross-section

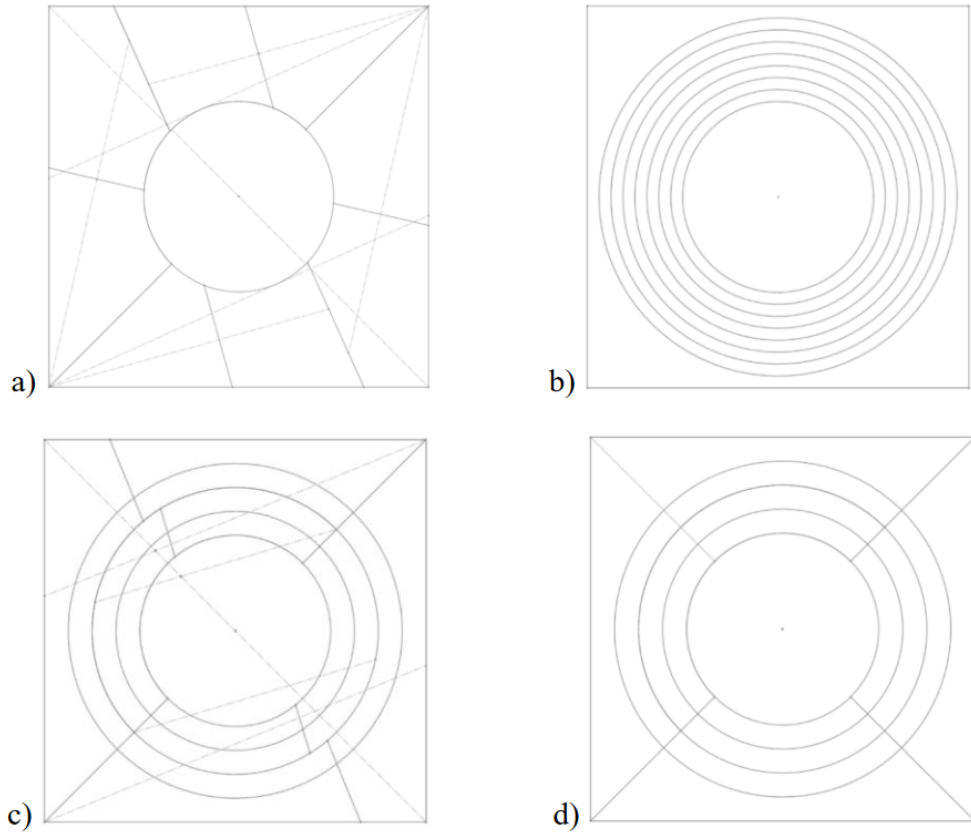


Figure A.5 (a) LAR, (b) the S/V ratio minimization, (c) the combined method, and (d) the modified combined algorithms applied as discretization methods to a square cross-section with a circular hole in its middle for $k_{\max} = 4$ iterations. Long axes are shown as dotted lines ([Letov and Zhao, 2021](#)).

with the set of S/V functions defined as

$$R_{S/V1} = \frac{2}{r} \text{ and } R_{S/V2} = \frac{2R + 2r}{R^2 - r^2} \text{ for } r \in [0, R]. \quad (\text{A.3})$$

Note that $\arg \min_r R_{S/V1} = R$ and $\arg \min_r R_{S/V2} = 0$. This result indicates that two optimized values of r contradict, while $\hat{r} = \arg \min_r (R_{S/V1} + R_{S/V2}) = R/2$ produces the first optimal division surface $D(\hat{r})$. However, the resulting volumetric cells do not fit the framework as they correspond to 2-manifolds of genus higher than 0.

In this case study, both the LAR and S/V ratio methods are combined manually and verified for $k_{\max} = 4$ with $k = \{1, 3\}$ corresponding to the LAR method and $k = \{2, 4\}$ corresponding to the S/V ratio method. The results are shown in Fig. A.4c and Fig. A.5c. Compared to volumetric mesh, volumetric cells obtained with this method are not necessarily convex. Volumetric cells discretize the model with similar unit cells but with different sizes compared to voxelized models. However, the inconsistency between volumetric cells remains from the LAR method. This method is modified according to the LOD concept by combining neighboring vertices of several pairs of adjacent volumetric cells as seen in Fig. A.4d and Fig. A.5d. This method provides a result similar to the unit cells used for stress analysis of cylindrical structures. The obtained unit cells appear similar to the results obtained by the iterative application of the signed distance function (Katopodes, 2018).

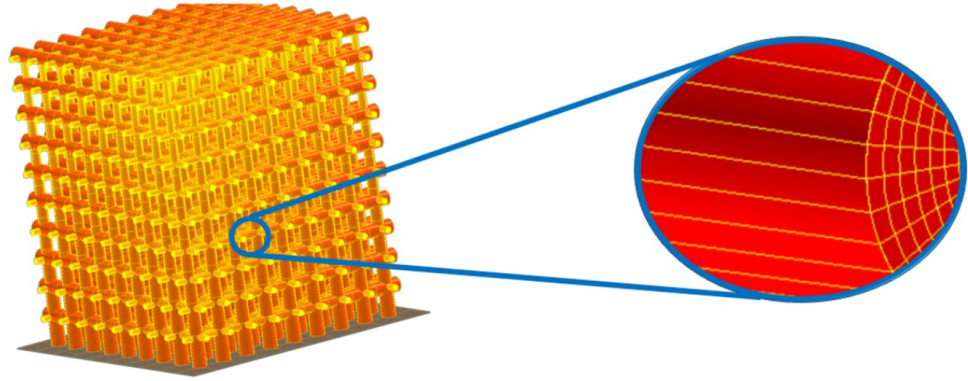


Figure A.6 A heterogeneous lattice structure with the graded beam thickness modeled with volumetric cells

Figure A.6 illustrates the implementation of the bio-inspired volumetric cells framework to a 3D case study of a heterogeneous lattice with a simple cubic topology. This implementation is achieved with the IRIT modeling environment introduced in Section 2.1.2. Table A.1 provides performance metrics of this approach. The modeling was performed on a machine equipped with the Nvidia RTX 2080 Ti GPU, the Intel Xeon Gold 6234 CPU, 64

Table A.1 Performance metrics comparing the voxel, Rhinoceros 3D, and volumetric cell models.

	RAM load	CPU load	GPU load	Size
Voxel model	2534 MB	19%	30%	125 MB
Rhinoceros 3D	911 MB	11%	16%	131 MB
Volumetric cells	913 MB	17%	27%	29 MB

GB of RAM, an SSD, and running the Manjaro Linux operating system (OS). Nevertheless, the further advancement of the bio-inspired modeling approach requires the development of a specialized GMK, which forms a whole separate direction of research.